Université de Montréal

Studies of the role of MAP kinase-activated protein kinase-5 (MK5) in reactive and reparative fibrosis in the murine heart

par

Sherin Ali Nawaito

Département de Pharmacologie et Physiologie, Faculté de Médecine

Thèse présentéeà la Faculté des études supérieures
en vue de l'obtention du grade de PhD
en Physiologie

Décembre, 2017

Université de Montréal
Faculté de Médecine

Cette thèse intitulée:

Studies of the role of MAP kinase-activated protein kinase-5 (MK5) in reactive and reparative fibrosis in the murine heart

Présentée par:

Sherin Ali Nawaito

A été évaluée par un jury composé des personnes suivantes:

Dr. René Cardinal
Président-rapporteur

Dr. Bruce Gordon Allen
Directeur de recherche

Dr. Guy Rousseau
Membre du jury

Dr. Ian M.C. Dixon
Examinateur externe

Dr. Denis Deblois
Représentant du doyen

Résumé

MK5 est une sérine/thréonine kinase, identifiée à l'origine comme une protéine kinase régulée/activée par p38 (PRAK), activée par les p38 MAPK et MAPK atypiques ERK3 et ERK4. Bien que MK5 soit exprimée dans le cœur, sa fonction physiologique commence seulement à être étudiée. Nous avons étudié les effets de la surcharge de pression chronique induite par la constriction aortique transversale (TAC) et les effets de l'infarctus du myocarde (IM) induit par la ligature permanente de l'artère coronaire descendante antérieure gauche (LADG) chez des souris hétérozygotes ($MK5^{+/-}$). Aussi, nous avons étudié *in vitro* le rôle de MK5 dans la fonction de fibroblaste cardiaque en utilisant des fibroblastes de génotype $MK5^{+/+}$, $MK5^{+/-}$, $MK5^{-/-}$ et des fibroblastes avec un knockdown de MK5 par *siRNA* (MK5-kd).

À l'âge de douze semaines, les souris $MK5^{+/-}$ étaient plus petites que les souris $MK5^{+/+}$. La fonction systolique était diminuée chez les souris $MK5^{+/-}$. Deux semaines après TAC, les poids cardiaque/longueur du tibia (PC/LT) ont augmenté de manière similaire et significative dans les 2 groupes.L'augmentation de l'ARNm du collagène de type 1α1 (COL1A1) $MK5^{+/+}$ était atténuée de manière significative chez les souris $MK5^{+/-}$. Huit semaines après TAC, PC/LT était significativement moins chez les souris TAC-$MK5^{+/-}$. La progression de l'hypertrophie était atténuée dans les cœurs $MK5^{+/-}$. L'immunoréactivité de MK5 a été détectée dans les fibroblastes cardiaques mais pas dans les myocytes.Ces données suggèrent que MK5 dans les fibroblastes cardiaques joue un rôle pro-fibrotique et pro-hypertrophique important dans le remodelage cardiaque pathologique.

Nous avons examiné l'effet de $MK5^{+/-}$ dans la fibrose réparatrice après un IM. Les taux de mortalité chez les 2 groupes avec LADGne différaient pas 7 jours suivant l'IM mais ilsétaient plus élevés chez les souris $MK5^{+/-}$ sur une période de 21 jours. La principale cause de décès était la rupture cardiaque. Les fonctions systolique et diastolique sont également altérées chez les 2 groupes avec LADG. La zone de cicatrice et le collagène dedans la cicatrice ont diminué dans les cœurs de $MK5^{+/-}$8 jours après l'IM.L'infiltration des cellules inflammatoires était similaire dans les deux groupes avec LADG. L'angiogenèse était significativement élevéedans la zone péri-infarctus de cœursduMK5$^{+/-}$.

Ces données suggèrent que MK5 peut jouer un rôle dans la régulation de la fonction des fibroblastes cardiaques. C'est pourquoi, nous avons examiné la mobilité et la prolifération du fibroblastes qui étaient diminuées chez les fibroblasts $MK5^{-/-}$. Le transcriptome pour les protéines impliquées dans le remodelage de la matrice extracellulaire différait selon le génotype des fibroblastes. La sécrétion de COL1A1 et fibronectine étaient significativement augmentée dans les fibroblastes $MK5^{-/-}$ et MK5-kd. La contraction du myofibroblaste a été diminuée dans les fibroblastes MK5-kd. Ces données suggèrent que MK5 est impliqué dans la régulation de multiples aspects de la fonction des fibroblasts cardiaques.

En conclusion, nous avons montré un rôle de MK5 dans le remodelage cardiaquepathologique ainsi qu'un rôle de MK5 dans la fonction des fibroblastes cardiaques.

Mots-clés : MK5/PRAK, hypertrophie cardiaque, fibroblaste, surcharge de pression chronique, fibrose réparatrice, infarctus du myocarde, matrice extracellulaire, p38 MAPK

Abstract

MK5 is a serine/threonine kinase, originally identified as a p38 Regulated/Activated Protein Kinase (PRAK), activated by p38 MAPK and the atypical MAPKs ERK3 and ERK4. Although MK5 is expressed in the heart, its physiological function is just beginning to be studied. Herein, we studied the effects of chronic pressure overload induced by transverse aortic constriction (TAC) and the effects of myocardial infarction (MI) induced by permanent ligation of the left anterior descending coronary artery (LADL) in heterozygous mice for a functional knockout of MK5 ($MK5^{+/-}$). We also studied the role of MK5 in cardiac fibroblast function and in extracellular remodeling in healthy heart *in vitro* using MK5 wild type ($MK5^{+/+}$), haplodeficient ($MK5^{+/-}$), deficient ($MK5^{-/-}$), and siRNA-mediated knockdown (MK5-kd) fibroblasts.

At twelve weeks of age, $MK5^{+/-}$ mice were smaller than age-matched wild-type littermates ($MK5^{+/+}$). Left ventricular end-diastolic diameter and systolic function were reduced in $MK5^{+/-}$ mice. Two weeks post-TAC, heart weight/tibia length ratios (HW/TL) were similarly and significantly increased in both $MK5^{+/+}$ and $MK5^{+/-}$ hearts. However, eight weeks post-TAC, HW/TL ratios were significantly lower in TAC-$MK5^{+/-}$ mice compared to TAC-$MK5^{+/+}$ mice. Thus, the progression of hypertrophy in response to chronic pressure overload was attenuated in $MK5^{+/-}$ hearts. Furthermore, two weeks of pressure overload induced increase in collagen type 1 α 1 (COL1A1) mRNA in $MK5^{+/+}$ mice and this increase was significantly attenuated in $MK5^{+/-}$ mice. As MK5 immunoreactivity was detected in cardiac fibroblasts but not myocytes, these findings suggest that MK5 within cardiac fibroblasts plays an important pro-fibrotic and pro-hypertrophic role in cardiac remodeling during chronic pressure overload.

We then examined the effect of reduced MK5 expression on reparative fibrosis following MI. Mortality rates for $MK5^{+/+}$ and $MK5^{+/-}$ did not differ significantly over seven days post-MI. In contrast, mortality was higher in $MK5^{+/-}$ mice over twenty-one days. Systolic and diastolic functions were similarly impaired in both $MK5^{+/+}$ and $MK5^{+/-}$ mice post-MI. Scar area and scar collagen content were reduced in $MK5^{+/-}$ hearts eight days post-MI. Inflammatory cell infiltration was similar in both ligated groups whereas angiogenesis was

significantly greater in the peri-infarct zone in LADL-MK5$^{+/-}$ hearts. These results suggest that MK5 may play a role in regulating cardiac fibroblast function.

Finally, we examined the effect of reduced MK5 expression on fibroblast function. Motility and proliferation were reduced in MK5$^{-/-}$ fibroblasts compared to MK5$^{+/+}$ and MK5$^{+/-}$ fibroblasts. The transcriptome for proteins involved in extracellular matrix remodeling (ECM) differed depending on fibroblast genotype. Similarly, collagen 1-α_1 and fibronectin secretion was increased in MK5$^{-/-}$ and MK5-kd fibroblasts compared with MK5$^{+/+}$. In addition, knocking down MK5 decreased myofibroblast contraction. Taken together, these data suggest that MK5 is involved in regulating multiple aspects of cardiac fibroblast function.

In conclusion, we have shown a role for MK5 in cardiac remodeling during chronic pressure overload and myocardial infarction. Moreover, we have demonstrated a role for MK5 in cardiac fibroblast function and extracellular matrix remodeling.

Keywords : MK5/PRAK,cardiac hypertrophy, fibroblast, chronic pressure overload, reparative fibrosis, myocardial infarction, extracellular matrix, p38MAPK

Table of contents

List of tables

Listoffigures

Introduction

Article -1

ARTICLE-2

ARTICLE-3

Listof abbreviations

α-MHC	α-myosin heavy chain
α-SMA	α-smooth muscle actin
β-MHC	β-myosin heavy chain
ACE	Angiotensin-converting enzyme
AD	Alzheimer's disease
AGEs	Advanced glycation end-products
AMPK	AMP-activated protein kinase
Ang-II	Angiotensin II
ANP	Atrial natriuretic peptitde
ATP	Adenosine triphosphate
AT1R	Angiotensin 1 receptor
BNP	B-type natriuretic peptide
CAMK	Calcium/calmodulin-dependent protein kinase
CD	Docking motif
CFs	Cardiac fibroblasts
COL1A1	Collagen type 1 alpha 1
CREB	cAMP- binding response element-binding protein
CTGF	Connective tissue growth factor
Cx	Connexin
DAMPs	Danger-associated molecular patterns
DDR-2	Discoidin domain receptor 2
DMBA	Dimethylbenzanthracene
DNA	Deoxyribonucleic acid
DUSP2	Dual specificity protein phosphatase 2
ECM	Extracellular matrix
EGCG	Epithelial –to-mesenchymal transition
EMT	Endothelial-to-mesenchymal transition
EndoMT	Epicardial-derived cells
EPDCs	Extracellular signal-regulated kinases
ERKs	Epigallocatechin gallate
ET-1	Endothelin 1
FAK	Focal adhesion kinase
FGF	Fibroblast growth factor
FN	Fibronectin
FSP-1	Fibroblast-specific protein 1
GAGs	Glycosaminoglycans

GAPDH	Glyceraldehyde 3-phosphate dehydrogenase
GPCR	G protein-coupled receptors
IGF2BP1	Insulin-like growth factor 2 binding protein
IHD	Ischemic heart disease
IL	Interleukin
I/R	Ischemia/reperfusion injury
HA	Hyaluronan
HAT	Histone acetyltransferase
HEK293	Human embryonic kidney 293
HMGB1	High mobility group box 1
HSP	Heat shock proteins
hTid-1$_s$	Human tumorous imaginal disc1$_s$Insulin-like growth factor 1
HUVECs	Human umbilical vein endothelial cells
IGF1	Insulin-like growth factor 1
JNK	c-jun amino-terminal kinases 1-3
KIM	Kinase-interacting motif
LADL	Ligation of left anterior descending coronary artery
LAP	Latency associated peptide
LDL	Low Density lipoproteins
LOX	Lysyl oxidases enzymes
LTBP	Latent TGF-β binding protein
LV	Left ventricular
M1	Proinflammatory type I macrophage
M2	Proreparative type II macrophage
MAPK	Mitogen activated protein kinase
MCP-1	Monocyte chemoattractant protein 1
MEFs	Mouse embryonic fibroblasts
MFG-E8	Milk fat globule-epidermal growth factor 8
MI	Myocardial infarction
miRNAs	MicroRNAs
MK5	Mitogen-activated protein kinase-activated protein kinase5
MMP	Matrix metalloproteinase
mPTP	Mitochondrial permeability transition pore
mRNA	Messenger RNA
MRTF	Myocardin-related transcription factor
mTOR	Mammalian target of rapamycin
NES	Nuclear export signal
NF	Nuclear factor

NLS	Nuclear localization signal
NLRs	Cytosolic nucleotide-binding oligomerization domain-like receptors
OMM	Outer mitochondrial membrane
PAI-1	Plasminogen activator inhibitor-1
PAKs	Group 1 p21-activated kinases
PDGFBB	Platelet derived growth factor-BB
PDGFR	Platelet derived growth factor receptor
PGs	Proteoglycans
PI3K	Phosphoinositide 3-kinase
PKA	Protien kinase A
PKC	Protein kinase C
PRAK	p38-regulated/activated protein kinase
PRRs	Pattern recognition receptors
RAAS	Renin angiotensin aldosterone system
RAGE	Receptor for advanced glycation end-products
Reg3β	Regenerating islet-derived 3 beta
revD	Reverse D motif
ROS	Reactive oxygen species
RNA	Ribonucleic acid
RSK	P90 ribosomal-S6-kinase
SAPK	Stress-activated protein kinase
SERCA2a	Sarcoplasmic/ endoplasmic reticulum $Ca^{(2+)}$ATPase 2a
SR	Sarcoplasmic reticulum
TAC	Transverse aortic constriction
TβRI	TGF-β receptor type 1
TβRII	TGF-β receptor type 2
Tcf21	Transcription factor 21
TGF-B	Transforming growth factor-β
Thr-182	Threonine residue 182
TIMPs	Tissue inhibitor of metalloproteinases
TLRs	Toll-like receptors
TNF-α	Tumor necrosis factor α
TSP	Thrombospondin
VEGF	Vascular endothelial growth factor
VSMC	Vascular smooth muscle cells

Dedication

To my late husband.

To my mother and father.

To my three little munchkins.

Acknowledgement

I would like to thank all the peoples that contribute to this work and make this thesis as it is.

Dr. Bruce Allen, my research supervisor, and advisor; I do not know where I can start. Thanks Bruce for providing me the opportunity to join your laboratory. I joined your laboratory like a baby who was crawling and you stood by me and still standing by me till I grew up and learned how to walk, run, and think. Without your precious continuous support, guidance, patience, and motivation, it would not be possible to conduct this research. The door of your office was always open whenever I had a trouble or a question about my research or writing; you were always available. Working with you, exposed me to a new way of thinking that gave me the opportunity to be a better thinker. I sincerely appreciate my experience in your laboratory. Bruce, you are not only a supervisor, you are also a friend to whom I can discuss life events and take his advice and who supported me in my critical events of my life "my husband death and my high-risk pregnancy". I will never forget your joke about all joined females candidates at your laboratory that got pregnant after "we will change the name of the lab from cellular biochemistry lab to fertility lab" ☺.

Beside my advisor, I would like to thank my members of the jury for this thesis: Dr. René Cardinal, Dr. Ian Dixon, and Dr. Guy Rousseau for accepting with interest to spend their time for reading and commenting on my work, for their insightful and valuable comments and I really appreciate them.

I am very grateful for the guidance and support of Dr. Angelo Calderone. I do appreciate your help. I would like to express my sincere gratitude to my laboratory members for all the fun we have had together, for being a family. I am thankful for all the help I got during my Ph.D. studies from my colleagues; Ana Branco, George Vaniotis, Clemence Merlen, Rahma Boulayah, Artak Tadevosyan, Dharmendra Dingar, Matthieu Ruiz and Rabah Dabouz. Special thanks to Pramod Sahadevan for always being so helpful, without your help; my project would not have gone smoothly as it did. You were always so kind, patient, smiley, hard worker. It is always inspiring working with you. Thank you, Fatiha Sahmi for all your help you did in order to finish this work. You were always being there for me at any time I

need help. You are a wonderful friend. Thanks, Bahira Hussein, it was a great pleasure to work with you. You were in my place completing animal's surgery when I was admitted to the hospital. You are an organized, attentive and smart girl. I greatly appreciate your help. I am also so grateful for Laurie Caland (trainee) and Joelle Trepanier (master student) that give me the chance to learn how to share my knowledge.

Also, I would like to thank my friend Nassiba Merabet for pushing me to keep going and for her psychological support and encouragement to finish this work, and for being with me in good as well as bad times.

I would like to acknowledge Maya Mamarbachi, Marc-Antoine Gillis, Karine Bouthillier and Robert Parent for all the technical help you supported me with. I would like also to thank Dr.Jean-Claude Tardif, Yanfen Shi and Danielle Gelinas for echocardiography support. Thanks, Marie-Elaine Clavet-Lanthier for your histological advice and troubleshooting.

I would like to thank the funding agencies, the Canadian Institutes of Health Research (CIHR), Heart and Stroke Foundation of Canada, and Montreal Heart Institute Foundation (FICM) for providing funds to accomplish my research project.

Last but not least, I would like to thank my mother Sohir for providing me with moral and physical support throughout my years of Ph.D. and through my thesis writing. I love you and I thank you for encouraging me to continue in my difficult times. Without your presence in my life, your warm, your caring about me and my kids, I would not achieve what I achieved today and this accomplishment would not have been possible.

1. Introduction

1.1 Left ventricular (LV) hypertrophy

The heart is made up of cardiomyocytes (muscle cells), non-myocytes (e.g. fibroblasts, endothelial cells, vascular smooth muscle cells, inflammatory cells), and the extracellular matrix. Cardiomyocytes account for only one third of the total cell number but 70-80% of the heart's mass [8, 11]. The fundamental contractile units of the cardiac myocyte are the sarcomeres, which are arranged into myofilaments comprising 'thin' actin and 'thick' myosin filaments. Myofilaments are, in turn, bundled into myofibrils. Cardiac myocytes are connected to each other via intercalated discs, which maintain cell-cell adhesion in order to transmit the contractile force between adjacent myocytes [8, 12]. In addition, cardiomyocytes may possess an intrinsic mechano-sensing mechanism, as their plasma membrane contains stretch sensitive ion channels as well as structural proteins (such as integrins) that couple the extracellular matrix (ECM) with the cytoskeleton, sarcomere, calcium handling proteins, and nucleus [8, 13, 14].

Cardiac hypertrophy refers to an increase in heart mass due to increased cardiomyocyte size [15, 16]. In response to an increase in load, cardiac growth is initiated by activation of signaling pathways, enhanced protein synthesis, changes in gene expression and contractile protein organization into sarcomeres (sarcomere assembly). The hypertrophic response is also associated with an increase in the release of autocrine and paracrine humoral factors such as angiotensin II (Ang II), insulin-like growth factor 1 (IGF1), transforming growth factor-β (TGF-β), and endothelin 1 (ET-1). These factors bind to receptors on cardiac cells, triggering the activation of intracellular signaling pathways, leading to hypertrophic growth of cardiomyocytes [8, 17]. Furthermore, in response to progressive or chronic increases in load (volume or pressure overload), cardiomyocytes undergo an initial compensatory hypertrophy to normalize wall stress and to maintain normal cardiovascular function; however, persistence of the increase in wall stress leads to decompensation associated with LV dilatation and contractile dysfunction promoting heart failure [8, 18].

Left ventricular hypertrophy can occur in healthy individuals as a physiological adaptation to physical exercise (athlete's heart), pregnancy (physiological), post-natal development of the heart until adulthood (developmental), or in disease as a pathologic response, which is either genetic or secondary to increased cardiac load (pathological) [15, 18, 19]. Both physiological and pathological cardiac hypertrophies have been subdivided into either *concentric* or *eccentric*

hypertrophy (Figure 1) depending on the type of overload, which has a great influence on sarcomere assembly, cardiac geometry, and re-expression of fetal genes. Pressure overload (e.g. hypertension, aortic stenosis) results in concentric hypertrophy that involves an increase in cardiac mass and in relative wall thickness, with reduced or unchanged chamber volume, due to the addition of sarcomeres in a parallel pattern resulting in an increase in cardiomyocytes width. In contrast, volume overload (e.g. aortic regurgitation, arteriovenous fistula) results in eccentric hypertrophy, which is characterized by an increase in both cardiac mass and chamber volume (dilated chambers) with normal, decreased, or increased relative wall thickness as a result of the addition of sarcomeres in series and hence increased myocyte length (Figure 1) [8, 20]. Pathological and physiological cardiac hypertrophies are accompanied by distinct structural and molecular phenotypes [8, 18].

1.1.1 Physiological cardiac hypertrophy

Physiological hypertrophy, resulting from pregnancy or exercise, is reversible and associated with enhanced or preserved cardiac function [18, 21].However, recent studies have demonstrated thatintense endurance exercise resulted inthe development of artial fibrosis and the induction of atrial dilatation and fibrillation(reviewed in[22]). In the case of athlete's heart, intense training results in an increase in LV mass, chamber enlargement, and proportional change in wall thickness that is considered a physiological adaptation. Depending on the type of training, the heart changes in shape: endurance exercise (e.g. running, swimming) increase venous return to heart leading to increase in volume overload and eccentric hypertrophy while isometric exercise (e.g. weight lifting) results in pressure overload and concentric hypertrophy [15]. At cellular and molecular levels, physiological cardiac hypertrophy is characterized by the induction of angiogenesis, absence of cardiac fibrosis and cardiomyocyte apoptosis, and a proper balance of increased glycolytic and fatty acid oxidation for generating ATP in the heart. Moreover, during physiological hypertrophy the fetal gene programme is not induced and genes encoding calcium-handling proteins (e.g. sarcoplasmic reticulum (SR) Ca^{2+}-ATPase 2a (SERCA2a)) remain unaffected [21]. Furthermore, smooth muscle α-actin, a marker of fibroblast to myofibroblast activation in pathological remodeling, is not detected in exercised rat hearts [21, 23]. Finally, in physiological hypertrophy there is an increase in myosin ATPase activity and enhanced contractility. Insulin-like growth factor 1 is considered to be the main initiator of physiological growth signaling and activates the

phosphoinositide 3-kinase [PI3K, (p110α)]-Akt pathway; however, other signaling pathways are also involved [8]. Although athlete's heart is a physiological condition, exercise can induce cardiac changes that not involve only the left ventricle, but all heart chambers such asatrial dilatation and arrythmias[22]. Long-term endurance exercise has been shown to induce myocardial damage, right ventriclar inflammation and fibrosisin athletes [24, 25]. In rat model of prolonged and vigorous exercise, the atria and right ventricle showed eccentric hypertrophy and diastolic dysfunction with atrial dilatation and fibrosis[26]. Moreover, excessive physiological hypertrophy may be accompanied with poor angiogenesis resulting in heart failure[27]. In conclusion, despite the beneficial effects of the exercise on the heart, a high exercise load was recently emerged as a potential cause of atrial fibrillation.

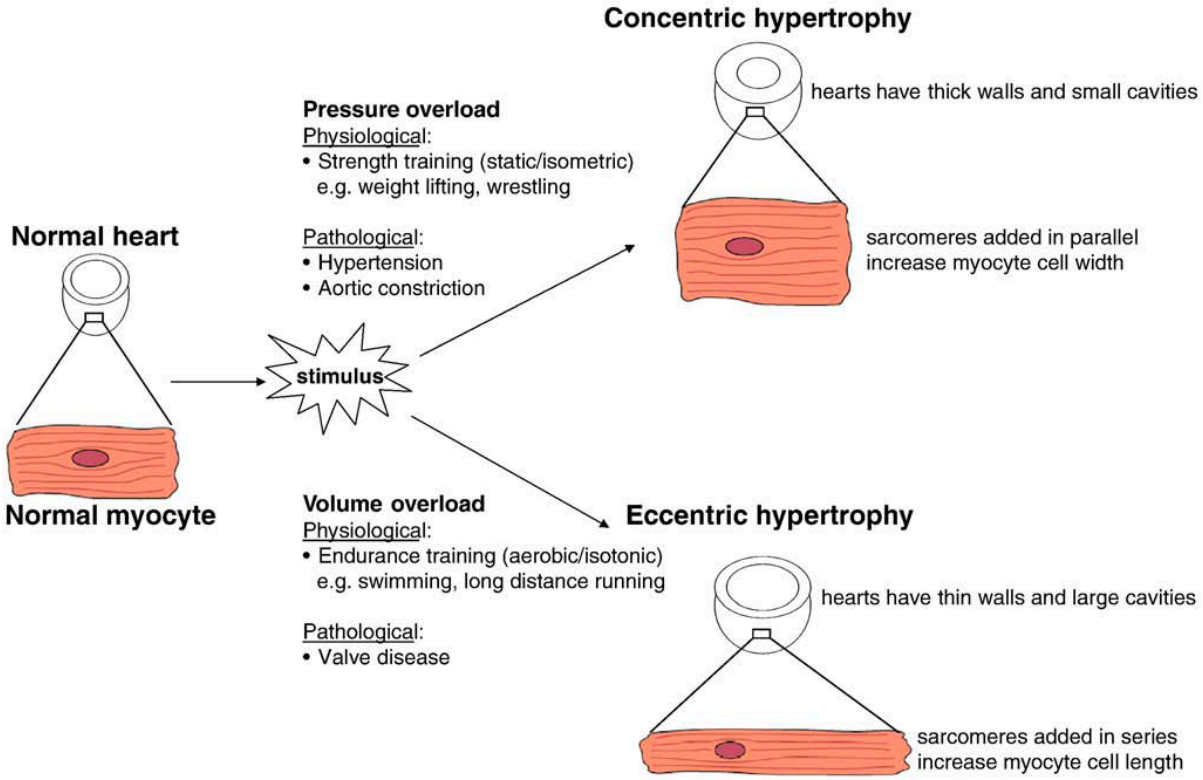

Figure 1. Diagram showing concentric and eccentric hypertrophy. Pressure overload produces LV wall thickness as sarcomeres are added in parallel without change in chamber volume resulting in concentric hypertrophy, while volume overload leads to an increase in cardiac mass along with increase in chamber volume due to addition of sarcomeres in series resulting in eccentric hypertrophy (adapted from Bernardo et al, 2010) [8].

1.1.2 Pathological cardiac hypertrophy

In contrast to physiological hypertrophy, pathological hypertrophy is induced by conditions such as hypertension, valve disease, myocardial infarction, coronary artery disease, genetic mutations, or diabetic cardiomyopathy that impose either pressure or volume overload on the heart. Remodeling caused by hypertension or myocardial infarction is a major risk factor for heart failure. Pathological growth is associated with cardiomyocyte apoptosis and necrosis, interstitial fibrosis, decreased systolic and diastolic function, and increased risk of heart failure and sudden death. Increased collagen deposition in the remodeling heart stiffens the ventricles resulting in impaired

contraction and relaxation, impairment of cardiomyocytes electrical coupling, and reduced capillary density. Each of these changes contribute to the transition to heart failure [8, 18]. Furthermore, the substrate profile of the hypertrophied myocardium for ATP production is also affected, as there is a shift from fatty acid oxidation to glucose metabolism [21]. In addition, an important molecular feature of pathological hypertrophy is the reactivation of the fetal gene programme. There is upregulation of atrial natriuretic peptide (ANP), B-type natriuretic peptide expression as well as the fetal isoforms of contractile proteins suchas skeletal α-actin and β-myosin heavy chain (β-MHC) that is accompanied by a decrease in expression of α-myosin heavy chain (α-MHC) and SERCA2a [8]. However, a retrospective study has found no correlation between fetal gene expression and increased heart weight, leading the authors to propose that increased fetal gene expression may be a protective rather than pathological response[28]. The increased expression of ANP and BNP prevent cardiac hypertrophy [29, 30]and fibrosis [31]. As the ATPase activity and contractile velocity for α-MHCare higher than those ofβ-MHC, the shift in expression of myosin heavy chain isoform represents an adaptive response to preserving energy despite the increased oxygen demand [32]. Reduced SERCA2a expression, which is responsible for calcium re-uptake into the sarcoplasmic reticulum, impedes cardiac relaxation [28]. Pathological cardiac hypertrophy is partly induced by humoral cardiovascular regulating factors such as angiotensin-II (Ang-II) and endothelin 1 that activate GTP-binding protein (G_q), resulting in cardiac hypertrophy. Overexpression of G_q resulted in cardiac hypertrophy and contractile dysfunction that lead to the induction of heart failure [33]. G_q regulate several intracellular signaling pathways including mitogen-activated protein kinase (MAPK) signaling cascades. Here we will focus on MAPK-activated protein kinase 5 (MK5) which is downstream of MAPK signaling pathway [8].

1.2 Myocardial infarction

1.2.1 Epidemiology, risk factors, and principal causes of myocardial infarction

Despite the reduction in rates of mortality and hospitalization for ischemic heart disease since the 1970s, it remains the principal cause of death and disability worldwide [34]. In developed countries, cardiovascular diseases are responsible for 38.5% of deaths in which coronary artery disease counts for 45% of all cardiovascular deaths [35]. Data from the Public Health Agency of Canada's Canadian Chronic Disease Surveillance System for the year 2012/2013 indicates that about 2.4 million Canadians aged 20 years and older have been diagnosed with ischemic heart disease (www.canada.ca). The prevalence of MI increases with age and more so in men than women [35]. There are multiple risk factors for cardiovascular disease, with hypertension being a principal risk factor. High blood levels of low density lipoproteins (LDLs) is considered as second risk factor, counting for 56% of ischemic cardiomyopathy worldwide. Moreover, smoking, physical inactivity, obesity and inappropriate diet constitute other risk factors for cardiovascular disease. Finally, diabetes is an important risk factor, as diabetic patients are 2 to 4 times more susceptible to develop cardiovascular insults [35].

Myocardial ischemia is a result of an imbalance between myocardial oxygen supply and demand [6]. The main cause of MI is coronary artery atherosclerosis [6]. Although even with more than 75% luminal narrowing there is no decrease in blood flow at rest, in response to increased myocardial demand (due to exercise, anemia, etc.), the atherosclerotic plaque impedes an increase in oxygen supply, causing the development of ischemia and angina pectoris. Plaque rupture is the most common cause of thrombosis [6]. In addition to atherosclerosis, there non-atherosclerotic forms of MI, such as coronary embolism, congenital anomaly of the coronary artery, increased myocardial oxygen demand, hematological troubles, and arteritis due to autoimmune or infectious diseases, which are less frequent [36].

1.2.2 Pathophysiology of MI

Myocardial infarction can occur as a result of partial or complete coronary artery occlusion. The myocardial zone supplied by the occluded coronary artery undergoes cessation of its blood supply, resulting in cardiomyocyte ischemia and death [37, 38]. If reperfusion fails to occur within less

than 15-20 minutes, large numbers of cardiomyocytes undergo necrosis and death in the ischemic zone [6]. This cardiomyocyte death triggers an acute inflammatory response that helps to clear the infarct of dead cells and matrix debris, promoting replacement of damaged tissue with a non-contractile collagen-based scar that maintains the structural integrity of the ventricular wall [37-39]. Moreover, this inflammatory response elicits ventricular remodeling that is associated with molecular and cellular changes in the ischemic zone, the border zone, and the non-ischemic zone, and it is manifested clinically as ventricular chamber dilatation, cardiac hypertrophy, modification of the three-dimensional structure of the heart from spherical to ellipsoidal shape, and deterioration of cardiac function [38, 39]. Ventricular remodeling may last for weeks or months, continuing until the tensile strength of the collagen scar is able to compensate for the increasing forces. This compensation is dependent on the size, location, and duration of the ischemia, the patency of the occluded artery, the presence of existing collaterals, and whether the ischemia is transmural or not [40].

Two phases of post-infarction remodeling have been determined; an early phase (within 72 hours) and a late phase (after 72 hours) [40]. The early phase involves the acute cardiomyocyte loss through apoptosis and necrosis, which triggers an inflammatory response, and contributes to infarct expansion resulting in wall thinning, ventricular dilatation, and ventricular rupture or aneurysm formation [38, 40]. The late phase of remodeling involves structural changes to the left ventricle, such as alterations in shape and compensatory hypertrophy of non-ischemic myocardium, to normalize cardiac function [38, 40]. However, if the wall stress is not normalized, progressive ventricular dilatation occurs, leading to deterioration of contractile function [40], ventricular arrhythmias, and heart failure [38].

1.2.3 Infarct healing following MI

As the myocardium has negligible endogenous regenerative capacity, loss of large numbers of cardiomyocytes leads to collagen-based scar formation. Following MI, many events occur in the ischemic zone that contribute to ventricular remodeling. The process of wound healing starts with necrosis and apoptosis of the damaged cardiomyocytes that initiates an inflammatory response (inflammatory phase), which is responsible for the clearance of dead cells and matrix debris from the infarcted region (≈ 3-4 days post MI in mice) [38-40]. Reparative fibrosis (reparative and proliferative phases) follows the inflammatory response, which helps in the recruitment of cardiac

fibroblasts from the non-infarcted area (≈ 7 days post MI in mice). Cardiac fibroblasts migrate into the infarcted area and become activated into myofibroblasts, which then proliferate and secrete collagen and other extracellular matrix proteins to form the mature scar (maturation phase) (Figure 2) [39]. Finally, successful scar formation is associated with neovascularization in the healing infarct, providing oxygen and nutrients to the reparative cells [39, 41].

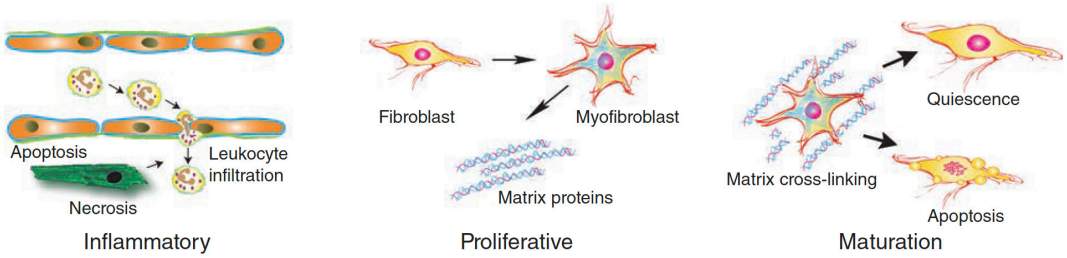

Figure 2. The phases of repair following myocardial infarction. Infarct repair is divided into three different, but overlapping phase: 1- the inflammatory phase; initiated by alarmins released by necrotic cardiomyocytes, serves to clear the infarct from dead cells and matrix debris. 2- the proliferative and reparative phase, associated with proinflammatory signaling suppression, fibroblasts activation into myofibroblast and deposition of extracellular matrix proteins. 3- the maturation phase, in which the extracellular matrix is cross-linked and fibroblasts become quiescent (adapted from Frangogiannis, 2015) [6].

1.2.3.1 Cardiomyocyte death via necrosis and apoptosis

Myocardial ischemia is a result of animbalance between oxygen supply and demand of the myocardium by the occluded coronary artery [6]. Prolonged coronary ischemia results in cardiomyocyte death via necrosis, apoptosis, and autophagy in the ischemic zone [42]. As the mammalian heart is incapable of producing sufficient amounts of energy to maintain cellular processes in an anaerobic environment, a constant supply of oxygen is essential for proper cardiac contractility and viability [38]. Occlusion of coronary artery results in reduced oxygen tension and ischemia of cardiomyocytes, which prevents oxidative phosphorylation, and decreases the

production of adenosine triphosphate (ATP), which is required to drive the Na^+/K^+-ATPase [38]. Decreased sodium-potassium pump activity results in the loss of sodium efflux and therefore water accumulation and cardiomyocytes swelling. Furthermore, this pump failure also leads to depletion of the intracellular potassium [38]. Moreover, within 10 seconds of occlusion, aerobic metabolism stops, ATP reserves are depleted, and lactic acid accumulates via anaerobic metabolism [6, 38]. In parallel, there is a progressive loss of cardiac contractility that is obvious within 1 minute of ischemia [38]. Minutes after the onset of ischemia, reversible ultrastructural modifications occur, in the form of depletion of glycogen reserves, distortion of the transverse tubular system, and cellular and mitochondrial swelling [38]. However, sustained ischemia with no reperfusion within 20-30 minutes results in irreversible cardiomyocyte injury in the subendocardial area, including sarcolemmal disruption and the presence of small amorphous densities in the mitochondria [6, 38]. The main mechanisms of cell death in the infarcted myocardium are necrosis and apoptosis [6]. Necrosis is a passive process characterized histologically by a loss of membrane integrity, cell swelling, karyolysis, vacuolar degeneration, and hypereosinophilia. Necrosis is defined by opening of the mitochondrial permeability transition pore (mPTP) in response to Ca^{2+} entry into the mitochondria, which encourages water influx, resulting in mitochondrial swelling and cardiomyocyte necrosis [6, 43]. Necrosis is first observed in the subendocardium followed by a "wavefront of necrosis" moving towards the subepicardium as the duration of ischemia increases [6, 44]. Within 24 hours of coronary occlusion, the necrotic phase is completed. Cardiomyocyte necrosis triggers an intense inflammatory response due to the release of 'danger' signals [6, 45]. In contrast to necrosis, apoptosis does not provoke inflammation [6]. Apoptosis is a programmed process that contributes to cardiomyocyte death through cell shrinkage, condensation of the chromatin and fragmentation of DNA into apoptotic bodies, and removal by phagocytes [6]. Apoptosis is induced by the binding of death ligands to cell surface death receptors and activation of mitochondrial signaling by permeabilization of the outer mitochondrial membrane (OMM). This permeabilization triggers the release of mitochondrial apoptogens into the cytoplasm causing apoptotic death [6, 46]. Furthermore, in response to ischemia, autophagy in cardiomyocytes is stimulated through an AMP-activated protein kinase (AMPK)-dependent pathway [6, 47]. Autophagy is a process by which unnecessary constituents of the cell are transported to lysosomes for degradation and provides energy and nutrients in response to stress. There is controversy on the role of autophagy in the infarcted myocardium; both protective and detrimental effects have been shown [6, 48, 49].

1.2.3.2 The inflammatory phase of infarct healing

In the infarcted heart, the inflammatory phase is characterized by an intense inflammatory response and immune cell infiltration that clears the wound from dead cells [42]. Cardiomyocyte death via necrosis results in the release of endogenous molecules "alarmins" that rapidly activate innate immune system by binding to pattern recognition receptors (PRRs) such as toll-like receptors (TLRs), receptor for advanced glycation end-products (RAGE) and cytosolic nucleotide-binding oligomerization domain-like receptors (NLRs). Alarmins act as "danger signals" initiating an intense, but transient, inflammatory reaction [6, 50, 51]. Alarmins belong to a large family of mediators known as danger-associated molecular patterns (DAMPs) including high mobility group box 1 (HMGB1), RNA, nucleotides, heat shock proteins (HSPs), members of the S100 family, and interleukin (IL)-1α[6, 42, 52]. The proinflammatory effects of HMGB1, one of the best characterized alarmins following myocardial ischemia, are mediated through activation of the RAGE signaling pathway [6, 53, 54]. Activation of the innate immune response is also initiated by damage to the extracellular matrix and release of matrix protein fragments such as hyaluronan and fibronectin fragments, which activate TLRs expressed on leukocytes [6, 52]. Moreover, activation of the complement system in the infarcted heart is involved in the inflammatory and immune responses by accentuating cardiomyocyte necrosis and promoting leukocyte recruitment in the injured myocardium [6, 55]. Furthermore, following myocardial infarction, there is generation of reactive oxygen species (ROS) that activate immune cells as the antioxidant defenses are overwhelmed [52]. ROS induce leukocyte infiltration and chemotaxis in the infarcted heart by upregulating chemokine and cytokine expression, promoting the expression of adhesion molecules such as P-selectin, and activating integrin adhesion receptors on leukocytes [6, 52]. Thus, activation of the innate immune system by alarmins activates nuclear factor (NF)-κB resulting in the activation of genes encoding cytokines, chemokines, and adhesion molecules [38, 39, 56-58]. NF-κB can also be activated by tumor necrosis factor α (TNFα), IL-1β, and ROS [38]. The proinflammatory cytokines IL-1β, IL-6 and TNFα promote synthesis of adhesion molecules and activation of leukocyte integrins, leading to extravasation of inflammatory cells into the infarct region [6, 52]. The release of proinflammatory chemokines such as monocyte chemoattractant protein 1 (MCP-1) lead to recruitment of leukocytes (neutrophils and monocytes) to the infarcted region in order to phagocytose the necrotic cells and ECM debris [6, 52]. In addition, activated macrophages release cytokines and growth factors, which

promote granulation tissue formation to replace damaged cells [38, 56].

Many cell types that are normally present in the heart (cardiomyocytes, vascular cells, and fibroblasts), as well as newly recruited immune cells, are involved in the postinfarction inflammatory response [6, 42, 52]. Dead and surviving cardiomyocytes play important roles in myocardial infarction. The release of alarmins from necrotic cardiomyocytes results in the activation of inflammatory signaling in fibroblasts, immune, and vascular cells, and the stimulation of the surviving cardiomyocytes in the infarct border zone to synthesize and secrete a variety of cytokines such as IL-6 [6, 59, 60]. Also, viable cardiomyocytes in the infarct border zone act as a barrier to protect the non-ischemic part of myocardium from the inflammatory injury, and they secrete Reg3β protein that mediates recruitment of macrophages involved in the clearance of neutrophil infiltrate and matrix preservation[61, 62]. Activated vascular endothelial cells promote neutrophil infiltration and leucocyte extravasation into the infarcted area, by the expression of adhesion molecules on their surface, promoting their adhesion with circulating leucocytes [6, 42]. Moreover, activated endothelial cells act as a main source of proinflammatory chemokines [6, 63, 64]. Fibroblasts are the most abundant non-muscle cells, they remain quiescent in the absence of injury, and are suited as sentinel cells sensing myocardial injury to initiate the inflammatory response [6, 42, 65]. In contrast to cardiomyocytes, cardiac fibroblasts are more resistant to oxidative stress and less susceptible to ischemic injury [39, 66]. In response to cardiac injury (in the first 24-72 hours), fibroblasts are activated via DAMPs, ROS, IL-1, TNF-α, and oncostatin-Mand secrete inflammatory cytokines and chemokines and show matrix-degrading properties (Figure 3) [3, 6, 42]. A recent study by Nakaya *et al.* revealed a role of myofibroblasts in the phagocytosis of dead cells following MI [67]. Another study demonstrated a role of cardiac fibroblasts in the recruitment of monocytes and their differentiation to M1 or M2 macrophages [68]. In parallel, activation of fibroblasts by IL-1 promotes matrix metalloproteinase expression, inhibition of α-smooth muscle actin (α-SMA) expression, and delay fibroblast activation into myofibroblasts until the dead cells and ECM debris has been removed from the infarct (Figure 3) [42, 69].In addition, the normal adult myocardium contains small populations of resident macrophages, dendritic cells, and mast cells [52, 70, 71]. These mast cells contain preformed proinflammatory cytokines and, upon cardiac injury, they release their proinflammatory granules and initiate the inflammatory pathway [52, 72]. Neutrophils are the first leukocytes to infiltrate the myocardium, peaking within 24 hours of injury. Neutrophil

recruitment and migration to the site of injury is initiated by activation of the complement cascade as well as the release of chemokines and leukotrienes. Once recruited, neutrophils release proteolytic enzymes, thus contributing to the clearance of dead cells and ECM debris [6, 42]. Furthermore, proinflammatory Ly6C^{hi} monocytes and lymphocytes are recruited to the infarcted myocardium soon after neutrophil infiltration. At later stages of inflammation, anti-inflammatory monocytes are recruited, contributing to resolution of the inflammatory response post MI [42].

B-lymphocytes play a key role in mobilizing and activating Ly6C^{hi} monocytes following acute myocardial infarction [73]. Moreover, in the infarcted heart, monocytes have the ability to undergo phenotypic changes and give rise to mature macrophages in response to the dynamic alterations in cytokine expression. Macrophages are characterized by plasticity, they can differentiate to proinflammatory type I (M1) or anti-inflammatory or proreparative type II macrophages (M2). They contribute to wound healing in different ways: 1) clear the infarct of dead cells and matrix debris, 2) release cytokines and growth factor, thus regulating inflammatory cascade, 3) contribute to new blood vessel formation, and 4) release matrix metalloproteinases (MMPs) and their inhibitors. Thus, inflammatory cells play a significant role in ECM remodeling within the infarct [6].

The ECM not only serves as a structural support but also plays a pivotal role following cardiac injury by regulating the phenotype and the function of multiple cell types that are surrounded by matrix proteins. Ten minutes after coronary occlusion, interstitial MMPs are activated, resulting in the degradation and fragmentation of structural matrix proteins [6, 74]. These protein fragments are involved in leukocyte recruitment [6, 75]. Matrix degradation is accompanied by the deposition of a newly formed fibrin-based provisional matrix that creates a scaffold for infiltration, migration and proliferation of inflammatory and reparative cells [6, 76].

Many studies have targeted the inflammatory phase of myocardial infarction, as inflammation is thought to play a crucial role in proper myocardial healing [77]. Some studies have shown that cardiac rupture is due to an excessive inflammatory response through upregulation of MMP and the degradation of ECM after MI [78-80]. In contrast, Matsui *et al*. have suggested that reduction of the inflammatory response leads to impairment of the formation of granulation tissue, improper reparative response, and cardiac rupture [81]. However, clinical trials targeting the complement system and CD18 integrins in order to reduce the recruitment of leukocytes and their

cytotoxic effects in patients with myocardial infarction did not have the expected effects [6, 82-84]. Mortality and the composite end points of death, shock, or heart failure were unaffected by administration of a humanized-anti-C5 monoclonal antibody (pexelizumab) to patients with acute ST-elevation MI (STEMI) undergoing percutaneous transluminal coronary intervention [84]. Moreover, administration of a CD18 integrin receptor inhibitor in patients with acute MI prior to angioplasty did not reduce infarct size [82]. Thus, clinical trials revealed inhibiting the complement system provided no beneficial effect in the treatment of acute MI.

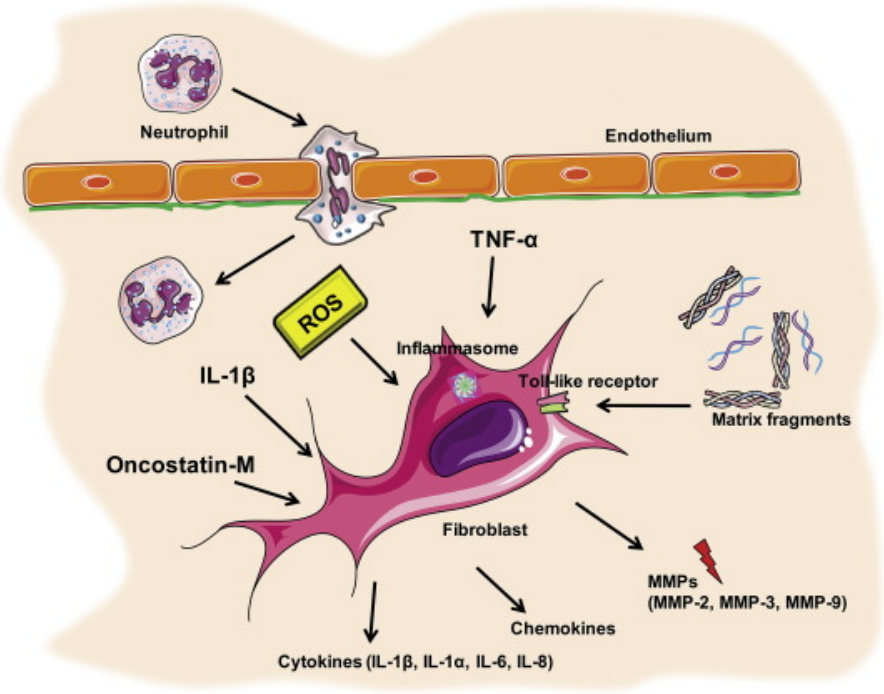

Figure 3. Resident cardiac fibroblasts in ischemic myocardiun contribute to inflammatory response after injury. Cardiac fibroblasts are sensors of cardiac injury. They are activated by ROS, proinflammatory cytokines (TNFα, IL-1β) and ECM fragments and acting as inflammatory cells. Activated fibroblasts initiate the inflammatory response and secrete cytokines, chemokines and matrix metalloproteinases (MMPs) promoting a matrix-degrading phenotype (adapted from Shinde and Frangogiannis, 2014) [3].

1.2.3.3 The proliferative and reparative phase of infarct healing (scar formation)

After the clearance of dead cells and matrix debris from the infarcted area, a transition from

the inflammatory to the proliferative and reparative phase is initiated by the activation of intracellular STOP signals that inhibit the inflammatory response and promote the formation of scar tissue and angiogenesis [41]. Neutrophils undergo apoptosis and release mediators such as annexin A1 and lactoferrin, which inhibit further neutrophil recruitment and secrete neutrophil gelatinase-associated lipocalin that promotes macrophages conversion into an M2 reparative phenotype [6, 42, 85]. M2 macrophages then phagocytose apoptotic neutrophils and secrete anti-inflammatory and profibrotic cytokines, such as IL-10 and TGF-β, and proresolving lipid mediatorsthat are produced from polyunsaturated fatty acid precursors including as lipoxins and resolvins. Lipoxins and resolvins in turn, inhibit neutrophil entry to the site of inflammation, but promote monocyte migration[6, 86]. TGF-β initially plays a role in inhibiting the inflammatory response by suppressing cytokine expression in the infarcted area. Then, later, TGF-β stimulates 1) the recruitment of cardiac fibroblasts from the non-ischemic region to the ischemic zone, 2) the activation of cardiac fibroblasts to myofibroblasts, 3) the synthesis and deposition of collagen types I and III and other ECM molecules that are necessary for scar formation, and 4) the synthesis of MMPs and tissue inhibitor of metalloproteinases (TIMPs) [37, 39, 87].

The replacement of the inflammatory infiltrate with granulation tissue is accompanied by an extensive angiogenic response, leading to the formation of neovessels that provide oxygen and nutrients to metabolically active mesenchymal cells in the healing myocardium [6, 56]. Early neovessels in the infarcted heart lack a pericyte coat, rendering them hyperpermeable and proinflammatory [6, 56, 88]. As a collagen-based scar is formed, maturation of the infarct vasculature occurs, playing a role in wound stabilization [6, 56, 88]. Matured neovessels acquire pericyte and smooth muscle cell coats, whereas uncoated endothelial cells undergo apoptosis. This mural coat decreases vascular permeability and the angiogenic potential of the vessels, thus contributing to stable scar formation. Platelet derived growth factor (PDGF)-BB-PDGFR-β signaling is involved in the interactions between mural cells and endothelial cells that results in vascular coating [6, 56, 89]. Inhibition of PDGFR-β in a mouse model of reperfused ischemia leads to defective vascular maturation, decreased collagen content in the infarcted heart, and uncontrolled inflammation [6, 56, 89]. Accordingly, pericyte coating plays an important role in suppressing granulation tissue formation after MI, promoting the resolution of inflammation, and scar stabilization [6, 56].

Dynamic alterations in the ECM is a characteristic of the proliferative phase of repair.

Phagocytosis of the matrix fragments is followed by formation of a fibrin- and fibronectin-based provisional matrix and deposition of matricellular proteins (macromolecules) [42, 90]. These macromolecules do not provide structural support, but bind to cell surface receptors, modifying cell-cell and cell-matrix interactions [42, 91]. Osteopontin, periostin, and thrombospondin (TSP) are examples of matricellular proteins that modulate fibroblast phenotype and growth factor signals [3, 91].

Scar formation is a result of reparative fibrosis that is considered as an important physiological response. The objective of reparative fibrosis is to maintain the structural integrity of the ischemic ventricle by replacing the necrosed cardiomyocytes with a collagen-based scar, thus preventing cardiac rupture and LV dilatation. However, if reparative fibrosis is altered, due to inadequate collagen deposition, decrease myofibroblast proliferation, or insufficient angiogenesis, scar formation will be impaired resulting in increased ventricular dilatation and adverse cardiac remodeling [37-39].

Many cell types are implicated in scar formation. Immune cells and vascular endothelial cells act indirectly by secreting fibrogenic mediators whereas fibroblasts act directly by producing ECM proteins [41]. Myofibroblasts play a central role in the proliferative phase of wound healing.

1.2.3.3.1 Myofibroblasts during the proliferative phase

The hallmarks of the proliferative phase of infarct healing are the expansion of cardiac fibroblasts, their activation into synthetic myofibroblast, and infiltration of the infarct border zone with activated myofibroblasts to facilitate scar formation [42, 92-94]. Myofibroblasts are abundant in the infarct region but not present in healthy myocardium [95] and their main characteristics include the expression of contractile proteins such as α-SMA and formation of contractile stress fibers, the synthesis and secretion of large amounts of extracellular matrix proteins such as type I and III fibrillar collagens, and a proliferative phenotype [3, 6, 41, 96, 97]. Early myofibroblasts (proto-myofibroblasts)do not express α-SMA but have stress fibers composed of cytoplasmic actin and focal adhesions, containing β- and γ-actin microfilaments, connected with nonmuscle myosin. They represent the intermediate cell type during fibroblast-myofibroblast transition, but whether they are present in infarcted myocardium remains unknown [3, 6, 98].

Resident cardiac fibroblasts are the main source of myofibroblasts in cardiac repair [99, 100].

Endothelial- and bone marrow-derived cells have also been proposed to be important sources of myofibroblasts in cardiac fibrosis [10, 95, 99, 101, 102]; however, recent studies by Kanisicak *et al.* and Nakaya *et al.* reported that resident fibroblasts are the only source of myofibroblasts in the heart [67, 103]. Thus, resident cardiac fibroblasts remain the major source of myofibroblasts.

Many pathways are involved in cardiac fibroblast activationinto myofibroblast in the infarct border zone (Figure 4) [99]. First, TGF-β is the main stimulus for cardiac fibrosis. There are three TGF-β isoforms: TGF-β1, TGF-β2, TGF-β3. TGF-β is synthesized by many cell types as an inactive "latent propeptide" form that is covalently bound to the latency associated peptide (LAP) [39]after release from cells. In the ECM, this inactive complex is bound by latent TGF-β binding protein (LTBP), which is essential for the secretion and storage of TGF-β. Latent TGF-β then becomes activated by proteolytic cleavage (MMP-2, MMP-9, and plasmin) and matricellular proteins such as thrombospondin (TSP)-1 [39, 104, 105]. Integrins also play a role in TGF-β activation by binding both the latent TGF-β complex and proteases, altering the conformation of the latent TGF-β complex and facilitating its proteolytic cleavage to active TGF-β [106]. Once released, activated TGF-β binds to its cell surface receptor type 2 (TβRII), which phosphorylates TGF-β receptor type 1 (TβRI), forming an active receptor complex that activates intracellular signaling through Smad proteins [39, 107]. Unphosphorylated R-Smad (Smad2 and Smad3) proteins exist primarily as monomers. After binding to the TGF-β receptor complex and phosphorylation, the activated R-Smads form homomers (homo-dimer and homo-trimer) and can also form heteromers (hetero-dimers) with each other. Thereafter, phosphorylated R-Smad form a hetero-oligomericcomplexes with CO-Smad (Smad 4) leadig to dimers or trimers, whichtranslocates to the nucleus to regulate the transcription of target genes [108-111]. Inhibitory Smad 7 binds to TβRI and both prevents phosphorylation of Smad 2 or Smad 3 and promotes TβRI degradation through proteosomal pathways [112]. TGF-β induces α-SMA transcription in fibroblasts via Smad3-mediated signaling [3, 99, 113], by promoting the translocation of myocardin-related transcription factor (MRTF)-A into the nucleus [3, 99, 114], and by activation of non-canonical pathways such as p38 mitogen-activated protein kinase (MAPK), thus inducing fibroblast activation[3, 115, 116]. Second, alterations in the matrix environment also modulate myofibroblast activation. Upregulation of the ED-A fibronectin splice variant in the infarcted heart [39, 117] induces TGF-β-mediated myofibroblast activation[3, 98, 118-120]. Moreover, deposition of collagen VI in the infarcted heart may promote

myofibroblast activation[3, 121]. Third, expression of proteoglycans such as syndecan 4 and integrins may be important for growth factor-mediated signal transduction in cardiac fibroblasts that leads to myofibroblast activation[3, 81]. Finally, mechanical stress directly stimulates α-SMA transcription in fibroblasts through Rho kinase and MAPK signaling in the presence of TGF-β [3, 99, 122-124]. Following cardiac injury, the structural integrity of the myocardium is disrupted, leading to exposure of fibroblasts to mechanical stress, which significantly contributes to their activation[3, 98, 99].

Neurohumoral pathways and several growth factors also play a role in fibroblast activation. Angiotensin II promotes ECM protein synthesis and stimulates fibroblast proliferation within the infarct via AT1 receptors. Some of the effects of angiotensin II in cardiac fibroblasts may be mediated through TGF-β activation [42, 125, 126]. Aldosterone also has strong profibrotic actions in the infarcted heart and promotes cardiac fibroblast proliferation [6, 42, 127]. Platelet derived growth factor (PDGF), fibroblast growth factor (FGF)-2, and the mast cell-derived proteases tryptase and chymase are potent fibrogenic mediators that are released in the infarcted heart and may be involved in stimulating fibroblasts proliferation and matrix deposition [3, 42, 128-130].

Activated myofibroblasts play a pivotal role in wound healing. Migration of myofibroblasts to the areas devoid of cardiomyocytes is crucial for scar formation. Although the molecular signals implicated in fibroblast migration remains unknown, growth factors such as TGF-β and FGF [113], leukotrienes [131], cytokines such as IL-1 [132]and chemokines such as monocyte chemoattractant protein (MCP)-1/CCL2 [133]may promote fibroblast migration to site of injury [3, 39]. The migration of fibroblasts through the matrix involves integrin activation, production of matrix-degrading proteases, and deposition of matricellular proteins into the cardiac matrix, favoring a "de-adhesive" state and thereby enhancing migration [3, 39, 91]. Inhibitory signals that reduce fibroblast migration are also activated in the infarcted heart in order to limit the excessive fibrotic response and induce wound contraction [3, 39, 63]. Moreover, myofibroblasts become highly proliferative [3, 95, 99, 134]. In addition, myofibroblasts possess contractile properties as they express high levels of contractile proteins such as α-SMA, vimentin, and focal adhesion proteins that allow scar contraction and reduce scar size by bringing wound margins closer after their perpendicular alignment to the wound rim, thus enabling effective wound healing [37, 135]. Myofibroblasts are the primary source of ECM proteins in the healing infarcted heart [3, 136, 137]. They synthesize and secrete large amounts of

structural ECM proteins, mainly fibrillar collagen types I and III that provide tensile strength, deposit matricellular proteins, and express MMPs and their inhibitors to promote scar formation, replace the areas of cardiomyocyte loss, and prevent cardiac rupture [3, 37, 95]. Unbalanced ECM remodeling may lead to either systolic dysfunction in response to LV dilatation due to inadequate strength of the myocardium or diastolic dysfunction due to heart stiffness resulting from excessive or prolonged ECM accumulation [37].

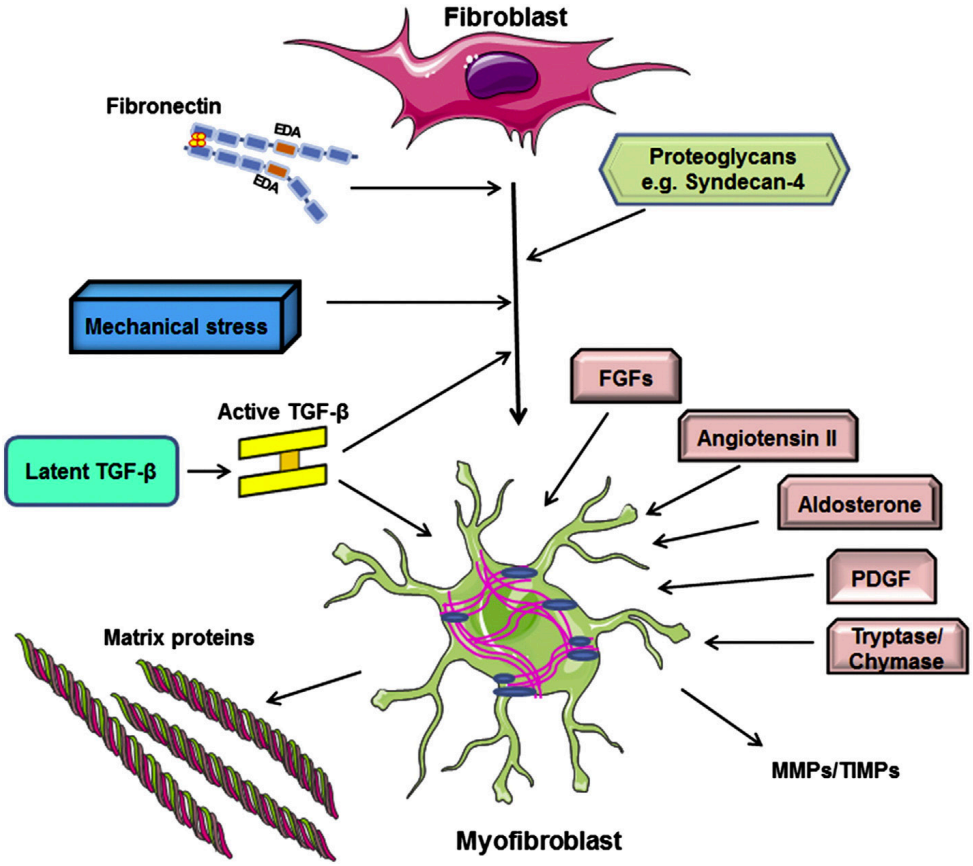

Figure 4. Activation of cardiac fibroblasts into myofibroblasts. Activation of TGF-β signalling pathway, expression of ED-A fibronectin splice variant, and the degradation of ECM that induce mechanical stress stimulate the activation of cardaic fibroblasts. Many growth factors such as angiotensin II, TGF-β, fibroblast growth factor (FGF), and platelet-derived growth factor (PDGF) stimulate synthesis of collagen and other ECM proteins by myofibroblasts. Finally, myofibroblasts secrete matrix metalloproteinases (MMPs) and tissue inhibitor of metalloproteinases (TIMPs) (adapted from Shinde and Frangogiannis, 2014) [3].

1.2.3.4 The maturation phase of infarct healing

The proliferative phase ends with the formation of collagen-based scar and is followed by the maturation phase of cardiac wound healing in which the myofibroblasts return to their quiescent state [6, 99]. Maturation of the scar is characterized by increased expression of lysyl-oxidase, which catalyzes matrix cross-linking, decreased expression of matricellular proteins, deactivation of the

reparative cells, inhibition of angiogenesis, and vascular regression [6, 88, 99, 138, 139]. The mechanism of scar maturation remains poorly understood. Apoptosis has been identified as a major mechanism for the elimination of most myofibroblasts from the mature scar [99, 140]. Depletion of growth factors, clearance of matricellular proteins, and activation of intracellular inhibitory STOP signals may deprive scar fibroblasts of key signals that promote their survival and activation, resulting in their deactivation and apoptosis [6, 99]. Moreover, alterations in matrix composition and the stable mechanical environment of the mature cross-linked scar may play a role in the deactivation of infarct myofibroblasts and their transition to quiescent state [3, 141]. However, myofibroblasts in the viable remodeling myocardium may become chronically activated in response to increased hemodynamic load and wall stress, which in turn may contribute to chronic chamber remodeling and ventricular dysfunction [39, 118].

1.2.4 Remote non-infarcted part of myocardium after MI

Following an MI, cardiomyocyte death in the infarcted heart leads to a sudden increase in LV filling pressure that induces a remodeling in both the infarct border zone and non-infarcted myocardium [40]. The remodeling of the non-infarct myocardium is an adaptive process that involves structural and functional modifications characterized by interstitial reactive fibrosis and cardiac hypertrophy [6, 40].

1.2.4.1 Reactive fibrosis

An imbalance in synthesis of ECM and/or inhibition of MMPs can lead to cardiac fibrosis. Two types of fibrosis have been identified: reparative and reactive fibrosis [142, 143]. Reparative (replacement) fibrosis is an essential physiological response intended to preserve the structural integrity of the heart by the deposition of collagen in the infarcted area resulting in scar formation to replace the dead cardiomyocytes [135, 137, 142, 143]. In contrast, reactive (interstitial) fibrosis is a pathologic response that occurs in the non-infarcted myocardial region, which impairs ventricular function and stiffens the ventricles as fibrillar collagen is deposited in intermuscular spaces and within the adventitia of intramyocardial coronary arteries and arterioles (perivascular fibrosis) [135, 142, 144]. Interstitial fibrosis can also alter the electrical conduction of cardiomyocytes by isolating them from one another with ECM proteins [142, 145]. Moreover, perivascular fibrosis can promote cardiomyocyte hypoxia by increasing the oxygen diffusion distance and decreasing coronary

capillary density [142, 146]. Thisdeposition of collagen is secondary to the release of many neurohumoral substances, such as angiotensin II and TGFβ-1, resulting in the activation of fibroblasts in non-infarcted regions that then synthesize and deposit collagen types I and III [135, 144, 147].

1.2.5 Pathophysiologic consequences of MI at the cellular level

Ischemicsystolic and diastolic dysfunctions are the noticeable functional consequences of MI. As action potentials and calcium transients are well maintained during the early stages of ischemia, ischemic systolic dysfunction is mainly linked to inhibition of contractile protein function as a result of intracellular acidosis, which reduces calcium binding to contractile proteins, and the inorganic phosphate that is produced from the breakdown of creatine phosphate reserves [6, 148, 149]. Diastolic dysfunction is caused by the production of metabolic products, such as lactate, leading to hyperosmolarity, increased interstitial water, and the reduction of ventricular compliance. In addition, there is impairment of relaxation in MI due to an energetic imbalance [6, 150]. Cardiomyocytes normally generate adenosine triphosphate (ATP) through oxidative phosphorylation whereas the ischemic heart employs anaerobic glycolysis to generate ATP from intracellular glycogen stores leading to rapid accumulation of lactate and intracellular acidosis, which in turn affects the rate of anaerobic glycolysis, resulting in marked reduction in ATP levels [6, 151]. ATP depletion leads to failure of sodium-potassium (Na^+/K^+) pump resulting in accumulation of Na^+ within the myocytes and depletion of their K^+ content. This ionic perturbations cause failure of cardiomyocyte repolarization resulting in conduction block and loss of excitability [6, 152]. In parallel, the cytosolic free calcium concentration (Ca^{2+}) is increased during ischemia. All these perturbations can result in an arrhythmogenic response [6].

1.2.6 Complications associated with MI

Rupture of the LV free wall is a drastic and fatal complication of MI, representing about 5-31% of post-MI-related deaths [153, 154]. Rupture may occur in the LV free wall, the interventricular septum, or the papillary muscles causing hemopericardium and cardiac tamponade, ventricular septal defect, and acute mitral regurgitation, respectively [6, 155]. In murine heart, cardiac rupture occurs 2-6 days post-MI in response to decreased tensile strength of the infarcted myocardium [155]. Several factors have been implicated in the induction of cardiac rupture, including a large

transmural infarct, excessive inflammatory response, increased MMP activity, and delayed reparative wound healing [6, 153, 156-158]. Infarct expansion and ventricular aneurysm, two possible consequences of adverse postinfarction remodeling, are more prominent in the apex and associated with higher rates of death [6, 159, 160]. In mouse models, infarct expansion is characterized by decreased infarct volume, as the scar undergoes maturation and contraction, and not by the progressive increase in the infarct size [6, 161]whereas ventricular aneurysm is an area of the infarcted LV wall that bulges with each contraction when a thinned area of noncontractile scar is stretched [6]. Another common complication of MI is cardiogenic shock, which represents a significant cause of early mortality following MI due to pump failure [6]. Moreover, pericardial disease is also common with acute MI, as in clinical studies the incidence of postinfarction pericarditis and pericardial effusion account for 7-41% and 43% of deaths post-MI, respectively [6, 162, 163]. Finally, ventricular arrhythmias are a major cause of mortality during both early and late phase post-MI. Several processes may explain the generation of arrhythmias. In the early phase, ischemia leads to ionic perturbations resulting in the creation of a pathophysiologic substrate that enhances arrhythmias. In the late phase, fibrosis forms inexcitable barriers and reentry circuits [6]. Furthermore, oxidative stress and neurohumoral, sympathetic, and activation of the renin angiotensin aldosterone system (RAAS) have been implicated in generation of arrhythmias [6, 164].

1.3 Cardiac (myo)fibroblasts

The heart consists of myocytes, vascular smooth muscle cells, endothelial cells, and fibroblasts. Cardiac fibroblasts (CFs) represent the most abundant cell in the mammalian heart [39, 99, 165]. Of the cells present in the myocardium, 90% are cardiomyocytes and CFs. In the human heart, CFs account for 60-70% of myocardial cells [95]; however, their distribution may vary according age, sex and species [39, 99]. In the adult murine heart, 56% of cells are myocytes while 27% are CFs [3, 166]. Cardiac fibroblasts are quiescent mesenchymal cells that are not terminally differentiated in the healthy heart [5]. They are flat, spindle shaped cells interspersed between cardiomyocytes in the interstitial and perivascular matrix and interconnected by gap junctions [167, 168]. In the heart, cardiac fibroblasts are the only interstitial cell type that has no basement membrane [10, 39]. To date, no specific protein marker solely expressed by fibroblasts has been identified. Various markers used to identify cardiac fibroblasts include vimentin, discoidin domain receptor 2 (DDR-2), fibroblast-specific protein 1 (FSP-1), and nestin [10, 39, 169, 170]. Moreover, it is known that the distinction between normal fibroblasts and activated cardiac myofibroblasts is based on the expression of contractile proteins such as α-SMA by myofibroblasts [10, 39, 169]. However, α-SMA is not a myofibroblast-specific marker. The morphology and the localization of site of lesion are also important determinants in the identification of cardiac myofibroblasts [39, 169].

1.3.1 Origin, development and activation

Two main sources of CFs have been described [95]. During development, most of the embryonic CFs originate from mesenchymal cells in the proepicardial organ [167, 171]. These cells migrate around the heart, forming the epicardium, providing epicardial-derived cells (EPDCs) through epithelial-to-mesenchymal transition (EMT), which then migrate into the myocardium and gradually differentiate into CFs [95, 165, 172-174]. Nevertheless, the presence of growth factors such as platelet derived growth factor (PDGF), fibroblast growth factor (FGF), and transforming growth factor (TGF) are essential for EMT [10, 95]. Progenitor stem cells present in the circulation or in the heart represent the second source of fibroblasts [95]. However, in response to cardiac injury, and in the presence of profibrotic stimuli, CFs have the ability to be activated into myofibroblasts, which are rarely present in the healthy myocardium [5, 65]. Myofibroblasts have a unique phenotype that distinguishes them from fibroblasts; they express α-SMA, are contractile, secrete and synthetizing

high amounts of ECM proteins, and are resistant to apoptosis [5]. Myofibroblasts can arise from various precursor cell types (Figure 5). In addition to resident fibroblasts, they can originate from epithelial cells through EMT, endothelial cells through endothelial-mesenchymal transition (EndoMT), vascular smooth muscle cells (VSMC), perivascular cells (pericytes), and bone marrow progenitor stem cells (fibrocytes and monocytes) [5, 175-179]. Moreover, Chang et al. showed that fibroblasts derived from skin at different anatomical sites displayed distinct and characteristic transcriptional patterns and comprise a diverse class of distinct differentiated cell types, suggesting heterogenity among fibroblasts in the same organ[180].The source of myofibroblasts in the heart remains controversial. Resident cardiac fibroblasts are considered the main source of myofibroblasts [41, 99, 100]. However, non-resident cells such as circulating bone marrow-derived cells (monocytes and fibrocytes), and endothelial cells have also been shown to be a source of myofibroblasts in models of infarcted and non-infarcted cardiac fibrosis [10, 95, 99, 101, 102]. Kanisicak *et al*. in 2016 have shown that myofibroblasts are derived mainly from resident fibroblasts and not from endothelial, immune or smooth muscle cells [103]. In a more recent study done by Nakaya *et al.* in 2017 they too reported that myofibroblasts originate from resident fibroblasts and EndoMT [67]. Similarly, Moore-Morris *et al.* in 2014 demonstrated that in response to pressure-overload, ≈ 95% of cardiac fibroblasts in adult ventricular murine myocardium originated from resident fibroblasts and are not of hematopoietic origin [181]. Thus, resident cardiac fibroblasts are currently thought to be the major source of myofibroblasts but this not excludes fibroblasts heterogenity in the heart.

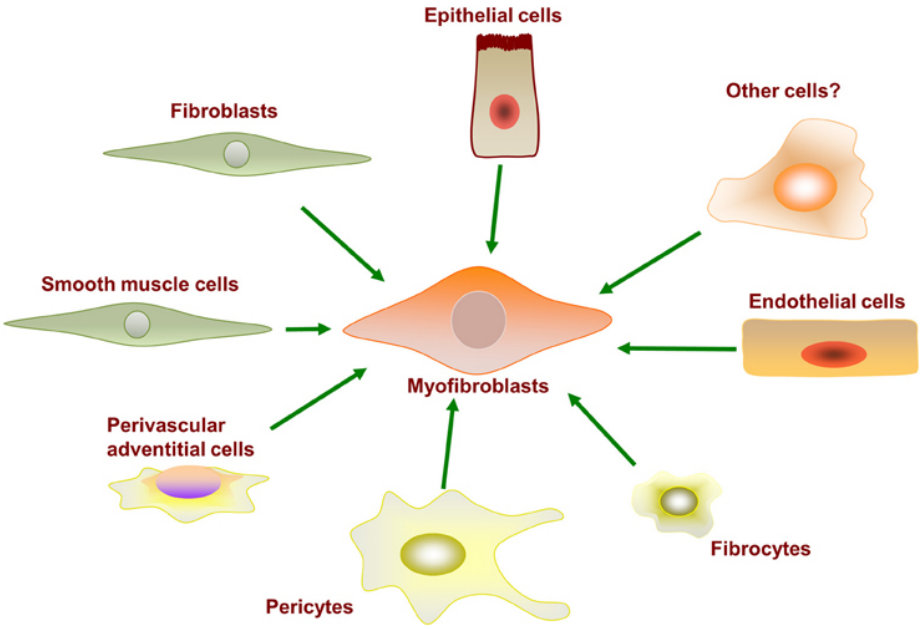

Figure 5. Myofibroblasts can originate from a variety of precursor cell types (adapted from Kendall and Feghali-Bostwick, 2014)[5]**.**

1.3.2 Normal function of CFs

Although the main primary function of CFs is the synthesis and degradation of the extracellular matrix, providing structure to the heart, and organizing the myocytes so that they may function, CFs also serve as sentinel cells that sense changes in their microenvironment (chemical, mechanical, structural and electrical signals) and respond to these changes in an appropriate manner (Figure 6) [65].

1.3.2.1 ECM production, maintenance, and reabsorption as well as cardiac homeostasis

CFs secrete all ECM constituents including the structural proteins, adhesion proteins, proteoglycans and glycosaminoglycans. On the other hand, they are also responsible for matrix degradation through production of degrading enzyme such as MMPs as well as their inhibitors, the tissue inhibitors of metalloproteinases (TIMPs) [5].

1.3.2.2 Production of bioactive molecules

Depending on the type of stimulus, CFs produce and secrete growth factors, cytokines, and

other signaling molecules that can regulate the function of nearby cells via autocrine/paracrine signaling networks [10, 37, 65]. The stimuli may be chemical factors, electrical signals, or stretch [65, 182, 183].

1.3.2.3 Cardiac vessel homeostasis

Cardiac fibroblasts stimulate angiogenesis (i.e., the formation of capillaries from pre-existing blood vessels) through production and secretion of fibroblast growth factor (FGF) and vascular endothelial growth factor (VEGF) (See Figure 2). In contrast, they can also produce and secrete anti-antiangiogenic factors such as platelet derived growth factor (PDGF) and connective tissue growth factor (CTGF) that inhibit angiogenesis [10, 184]. Moreover, MMPs and TIMPs produced by fibroblasts can activate or inhibit angiogenesis as MMPs degrade the ECM, leading to endothelial cell migration and sprouting [65, 185, 186]. Furthermore, for optimal vessel formation, direct interactions between fibroblasts and endothelial cells are needed [65, 187]. Hence, CFs contribute to maintaining appropriate cardiac vascularization.

1.3.2.4 Proliferation of cardiomyocytes

Cardiac fibroblasts regulate cardiomyocyte proliferation during development [188]. Cardiomyocytes are capable of proliferating slowly to maintain cardiac homeostasis [10, 189]. In addition, CFs secrete FGF and periostin that stimulate the proliferation of adult cardiomyocytes *in vitro* and *in vivo*; hence, it is possible that CFs contribute to cardiomyocyte proliferation during embryonic development and in the adult heart through paracrine signaling [10, 39, 169, 190, 191]. In addition, in response to cardiac injury CFs stimulate hypertrophy and fibrosis of the heart [169].

1.3.2.5 Electrophysiological function of cardiac fibroblasts

Connective tissue can serve as an electrical insulator [167]. Although CFs are non-excitable cells, they contribute both actively and passively to cardiac electrophysiology [10, 95, 167]. CFs are good conductors as they have a high membrane resistance [65, 167]. Moreover, electrical signals can be propagated between fibroblasts and myocytes via gap junctions in which fibroblasts act as a bridge that connects electrically isolated regions of myocytes, promoting the synchronization of contraction between individual myocytes [10, 65, 95, 169, 192]. In addition, CFs act as mechano-electrical transducers, as they express K^+, Na^+, and Ca^{++} channels that are activated by stretch [10, 193]. In

response to mechanical contraction of the myocardium, these ion channels open and depolarize the fibroblast membrane [10, 194, 195]. On the other hand, CFs can passively block the spread of electrical signals between myocytes via the production of ECM [10, 169, 196].

1.3.3 Fibroblast-myocyte coupling

One form of fibroblast-myocyte electrotonic coupling is through gap junctions [167, 197]. Another form of coupling is through tunneling nanotubes, which form long distance connections between myocytes and CFs [167, 198]. Furthermore, a recent study provided evidence that non-electrotonic coupling (non-gap junction) occurs in the myocardium, which involves cell-to-cell propagation of action potentials [167, 199]. Myocytes and fibroblasts can electrically interact through 3 known modes, which exist in both healthy and diseased hearts, depending on the arrangement of both cells in the heart. 1) "Zero-sided coupling" is the most common form, where CFs act as electrical insulators. Fibroblasts separate layers of connected myocytes without being electrically connected to them. 2) "Single-sided coupling", where a group of myocytes are electrically coupled to fibroblasts. 3) "Double-sided coupling", where fibroblasts act as short or long range conductors of electrical signals and have the ability to electrically couple myocytes that are separated [167, 200].

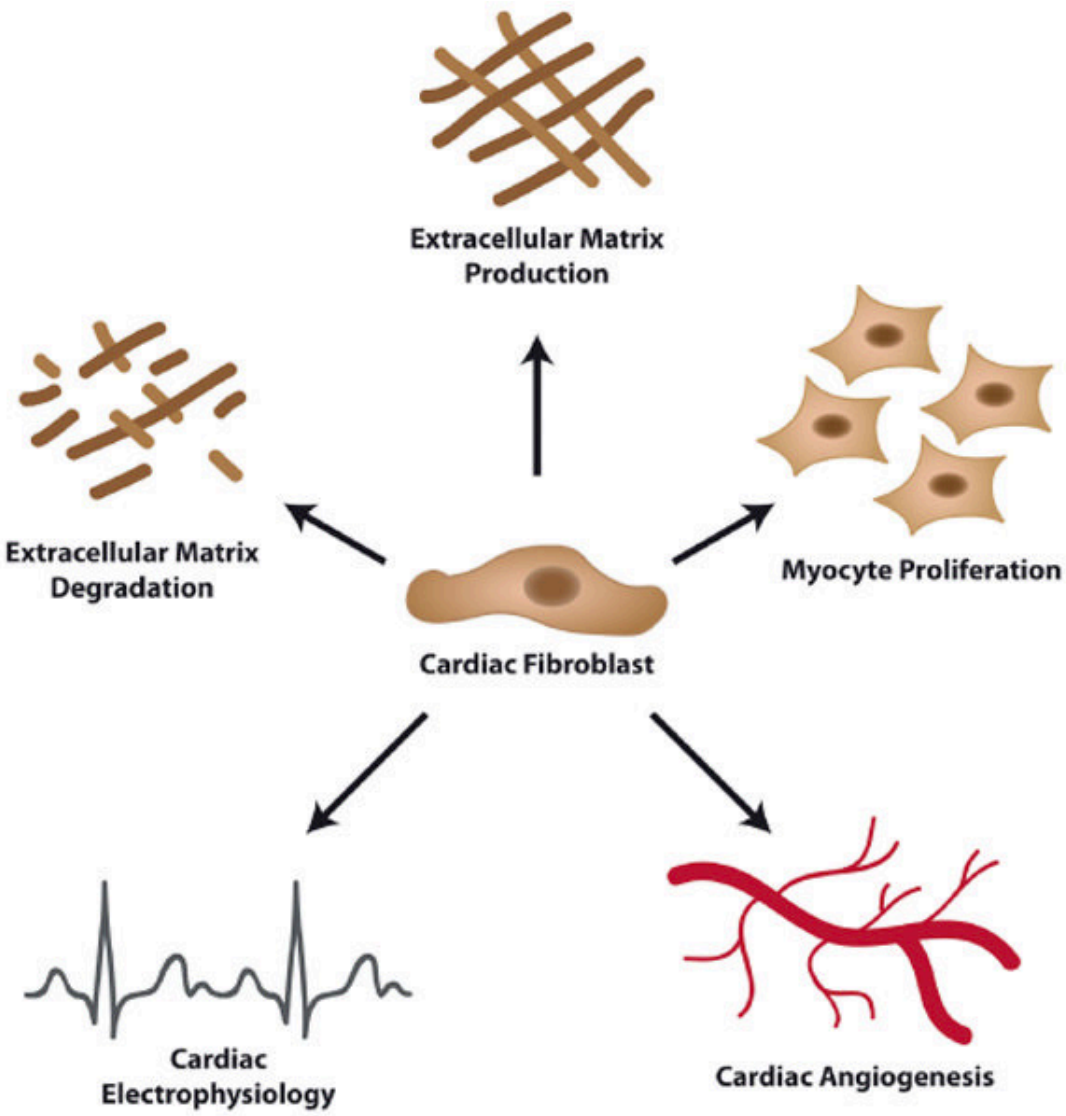

Figure 6. Functions of cardiac fibroblasts. The primary function of CFs is the secretion and degradation of the ECM, in addition to the secretion of growth factors and cytokines. In addition, CFs play a role in the proliferation of the cardiomyocytes, participate passively in cardiac electrophysiology, and contribute to cardiac angiogenesis (adapted from Krenning and Kalluri, 2010) [10].

1.3.4 Signalling in cardiac fibroblasts

Signalling mechanisms in CFs are divided into mechanical, chemical, and electrical.

1.3.4.1 Mechanical signalling

The cytoskeleton network is responsible for the transmission of forces between fibroblasts and the ECM [201]. Cardiac fibroblasts can act as sensor and responder to mechanical stimuli by affecting the release of growth factors, ECM proteins, and proteases as well as proliferating [201, 202]. Members of the integrin family play an important role in CF mechanosensing, as they facilitate fibroblast adhesion to the ECM and interact with a variety of extracellular ligands [201, 203]. Collagen, fibronectin, vitronectin and osteopontin are the primary ligands for CF integrins [201, 204]. Furthermore, mechanical activation of angiotensin II type 1 receptors *in vitro* and *in vivo*, without the participation of angiotensin II, modulates CFs cytoskeleton protein, MMPs and integrin β I signaling [201, 205]. In addition, stretch-activated channels and transient receptor potential (TRP) channels [201, 206]can affect ECM synthesis [201, 207].

1.3.4.2 Chemical signalling

Pro- or anti-inflammatory stimuli such as IL-Iβ, IL-6, and TNF-α, as well as pro-fibrotic stimuli such as TGF-β can induce CFs to secrete cytokines, growth factors, and other bioactive molecules, which can then act in a paracrine or autocrine manner [201]. IL-Iα, secreted by CFs, stimulates fibroblast proliferation, migration, collagen deposition [132, 201], MMPs expression, AT1R activation in CFs, as well as the release of cytokines (IL-6) and growth factors (tenascin C, CTGF) [201, 208]. Moreover, IL-6 is a bioactive molecule that plays a role in cell-cell interactions between endothelial cells, fibroblasts and cardiomyocytes [201, 209]. Angiotensin II, acting through AT1Rs on CFs, can modulate collagen expression and secretion [201, 210]. Finally, TGF-β secreted by CFs leads to the conversion of fibroblasts into myofibroblast [201, 211]in addition to its role in ECM synthesis, cell differentiation, proliferation, and migration [201, 212].

1.4 Cardiac extracellular matrix (ECM)

1.4.1 Cardiac ECM structure and function

The cardiac ECM is a non-cellular macromolecular network composed of structural, non-structural, and adhesion proteins in which cardiomyocytes, fibroblasts, vascular cells, and immune cells reside. The main constituents of the ECM are fiber-forming proteins (such as collagens), glycoproteins (such as fibronectin (FN)), proteoglycans (PGs), glycosaminoglycans (GAGs), and matricellular proteins. Comprising 80% and 20% of the total ECM, respectively, collagen types I and III are the most abundant and primary structural proteins in the cardiac ECM. Collagen I provides the myocardial tensile strength whereas collagen III provides distensibility. Matricellular proteins, on the other hand, are secreted locally and have non-structural roles. Fibronectin plays both structural and non-structural roles [213]. See Table 1 for the classification of cardiac ECM proteins.

The ECM also contains a variety of growth factors, cytokines, proteases (MMPs), and proteases inhibitors (TIMPs) that modulate cellular function and protease activity and hence regulate ECM biosynthesis and degradation [213]. Growth factors such as VEGF, FGF, and TGF-βare deposited within ECM through binding to fibrillar ECM molecules, to be released into the microenvironment following cardiac injury. When there is an increase in growth factor and cytokine activity stimulated by mechanical force or tissue injury, MMPs degrade and remodel the ECM. MMP activities are regulated by TIMPs to prevent excessive matrix breakdown [214].

The ECM has several functions. It forms an organizational structural framework for cardiomyocytes, thus maintaining the structural integrity and normal chamber geometry of the heart. It distributes mechanical forces throughout the myocardium and renders the myocardial wall stiff by providing scaffold and mechanical support for both myocytes and non-myocytes. It acts as an electrical barrier, separating the atria and the ventricles for proper cardiac contraction. It modulates cell motility, survival, and proliferation through its actions as a signal transducer for cell-cell communication [10, 213, 215]. In addition, the ECM serves as a reservoir for growth factors. Moreover, the ECM participates in biochemical signaling through direct interactions of ECM structural molecules with cell surface receptors [214].

Non-structural matricellular proteins are minimally expressed in normal adult hearts;

however, they are upregulated in response to cardiac injury and during development. Thus, they play an important role in cardiac pathophysiological conditions. They have a key role in signal transduction. While associating with growth factors, cytokines, and proteases, matricellular protein bind to structural ECM proteins and activate cell surface receptors. Furthermore, matricellular proteins promote the "de-adhesion" state of cells, activate survival signals through promoting an intermediate adhesive state, modulate cell migration, proliferation, and adhesion, and stimulate the expression of adaptation and repair genes [91].

Table 1. Classification of extracellular matrix (ECM) proteins

The cardiac ECM is a non- cellular macromolecular network that is divided into glycoproteins, proteoglycans, and glycosaminoglycans. Proteins (pink) such as collagen have a structural role, while matricellular proteins (yellow) serve nonstructural functions. Other proteins, such as fibronectin, serve both structural and nonstructural roles (purple). GAGs; glycosaminoglycan. (Modified from [1, 2]).

Cardiac Extracellular Matrix

Glycoproteins			GAGs	Proteoglycans			
Prototypical matricellular proteins	Fibers	Others	Hyaluronan	Intracellular	Cell Surface	Pericellular-Basment membrane	Extracellular
Thrombospondin, Tenascin, CNN family of proteins, Osteopontin, Periostin, Secreted protein acidic and rich in cysteine (SPARC)	Collagens, Elastins (not glycosylated)	Fibronectin, Laminin		Serglycin	Syndecan, Glypican	Perlecan, Agrin, Collagen types XV and XVIII	**Hyalectans:** Aggrecan, Versican, neurocan, Brevican **Small leucine-rich proteoglycans (SLRPs):** Class I Biglycan, Decorin, Asporin Class II Lumican, Fibromodulin, Proline/ arginine-rich end leucine-rich repeat protein (PRELP), Keratocan, Osteoadherin Class III Osteoglycin, Epiphycan, Opticin Class IV Nyctalopin, Tsukushi, Chondroadherin Class V Podocan, Podocan-like protein 1

ECM-cell interactions and signaling in normal heart

Myocytes and non-myocytes embedded in the ECM interact with matrix proteins through cell-surface receptors, such as integrin receptors and non-integrin receptors, including discoidin domain receptors (DDRs), cell surface PGs, and the hyaluronan (HA) receptor CD44, to ensuring

proper contractile synchrony and cardiomyocyte function [2, 213]. Integrin receptors are the main mediators of ECM-cell interactions. They bind to ECM components such as collagen, fibronectin, laminin, thrombospondin, tenascin-c, osteopontin, and periostin to form focal adhesions, thus linking the ECM to the cellular cytoskeleton. As integrins lack enzymatic activity, they must bind to downstream molecules such as calreticulin, focal adhesion kinase (FAK), and components of cytoskeleton to transmit their signals to numerous signaling pathways including the mitogen-activated protein kinases (MAPKs). Furthermore, non-integrin receptors such as proteoglycan CD44 play a crucial role in cell adhesion and movement by binding to types I and IV collagens [213]. Collagen and fibronectin, in turn, are the structural ECM proteins responsible for intercellular communication.

1.4.1.1 Collagen

1.4.1.1.1 Collagen structure and function

Collagens are the most abundant proteins in and the main structural constituents of the ECM. To date, more than 28 different collagen subtypes have been identified. They are classified into: fibrillar and network-forming collagens (types I, II, III, V, and XI), fibril-associated collagens with interrupted triple helices, membrane-associated collagens with interrupted triple helices, and multiple triple-helix domains and interruptions [216]. Among the most abundant in the heart are fibrillar collagen type I and type III, produced by fibroblasts and myofibroblasts, which together constitute about 90% of all collagen. Collagens are characterized by a right-handed triple helix formed by three polypeptides chains (α-chains) supercoiled around a central axis. Each of the three chains has the repeating structure Gly-Xaa-Yaa, where Xaa is frequently proline and Yaa is frequently hydroxyproline. Glycine, the smallest amino acid, should be present at every third residue along each chain toallow the α chains to wind together tightly into a triple helix. Proline contributes to the stability of the triple helical conformation [217]. The triple helix of type I collagen is formed by two identical α_1 (I)-chains and one α_2 (I)-chain (heterotrimer), whereas the collagen type III triple helix is a homotrimer of three α_1 (III)-chains. The formation of a stable trimer consists of three different domains: the C-propeptide that is involved in the initiation of triple helix formation, N-propeptide that could be involved in primary fibril diameters regulation, and the collagen triple helix flanked at either end by short non-helical telopeptides allowing collagen to form covalent

cross-links that are important for the mechanical integrity of the molecule and fibril formation [218].

In addition to collagen being the major structural element of the cardiac interstitium, it performs many other functions. Collagen acts as a supportive scaffold on which cardiomyocytes and coronary vessels reside. It connects both individual cardiac cells and muscle bundles, thus maintaining the structural integrity of the heart and providing the left ventricular chamber with the tensile strength and compliance that are keys factors of systolic and diastolic myocardial stiffness. In addition, collagen prevents ventricular rupture and aneurysm. Moreover, collagen plays a role in intracellular signal transduction by activating FAK and downstream signaling pathways, which are involved in cell proliferation and migration. Collagen also inhibits apoptosis *in vitro* via a β1 integrin-dependent pathway. Finally, collagen is involved in proper contraction of the myocardium by helping in the transmission of the mechanical force of myocyte contraction [213].

1.4.1.1.2 Collagen biosynthesis and degradation

Under normal physiological conditions, collagen homeostasis involves an equilibrium between the deposition of newly synthesized collagen and the degradation of old collagen fibers. With a half-life of 80-120 days, collagen is highly stable protein with a slow turnover [219].Collagen is synthesized as a large precursor (preprocollagen), which is then transported to the rough endoplasmic reticulum (ER) where it undergoes cleavage and removal of its signal peptide by a signal peptidase, forming procollagen α chains. Thethree α chains are covalently linked by disulfide bonds and assembled together to form a triple helix. In the Golgi apparatus, the triple helices are packaged into vesicles and secreted into the extracellular space. In the interstitial space, the secreted procollagen undergoes further post-translational modifications prior to assembly into a supramolecular structure by removal of their C- and N- terminal extension propeptides, which keep collagen soluble, by procollagen C-proteinase and procollagen N-proteinase to form mature collagen. Mature collagens then self-assemble into collagen microfibrils, which can be further stabilized by the formation of covalent inter-fibrillar and intermolecular cross-links by lysyl oxidases (LOX) or by a reduction due to the formation of advanced glycation end-products (AGEs). The intermolecular cross-links between three collagen molecules is required for the physical and mechanical properties of collagen fibrils and the formation of a stable network. Matricellular proteins play a role for the integration of collagen fibrils into the ECM and ascorbic acid (vitamin C) is required for post-translational modification of procollagen molecules (Figure 7) [215, 218, 220, 221].

Members of the matrix metalloproteinase (MMP) family of zinc-dependent endopeptidases, also called matrixins, possess collagenolytic activity that is responsible for the degradation of collagen molecules. Almost all MMPs are synthesized by many cell types in the myocardium (myocytes, fibroblasts, endothelial cells, macrophages, and neutrophils) as inactive prepro-enzymes and secreted as inactive pro-MMPs that are activated by proteolytic cleavage. Of many proteinases, plasmin is considered the most potent physiological activator of MMPs. MMPs are divided into four groups. Group 1 MMPs are collagenases that catalyze for the first step in collagen degradation and includes MMP-1, MMP-8 and MMP-13, which are capable of cleaving type I, II, and III collagen fibers into characteristic ¼ and ¾ length fragments (telopeptides). Group 2 MMPs, the gelatinases, includes MMP-2 and MMP-9, and further degrade type I and III collagen fragments into amino acids and oligopeptides. In addition, both MMP-2 and MMP-9 are involved in the turnover of collagen type IV found in basement membranes. Group 3 MMPs, the stromelysins, includes MMP-3, MMP-10 and MMP-11, degrade proteoglycans, laminins, fibronectin and some types of collagen. Group 4 MMPs are the membrane-type MMPs, which activate other MMPs, process biologically active signaling molecules, and degrade many ECM structures. Procollagen molecules may also undergo intracellular degradation in lysosomes, the Golgi apparatus, or the ER, within minutes of synthesis [222]. Active MMPs are inhibited by a family of four endogenous TIMPs, which bind to the MMP catalytic domain and thereby block substrate binding. A tightly controlled balance between the function of MMPs and their inhibitory TIMPs is essential in maintaining ECM homeostasis (Figure 7) [91, 220, 223-226].

Autocrine and paracrine hormones such as Ang II, TGF-β, and aldosterone regulate collagen synthesis. Ang-II secreted from fibroblasts stimulates TGF-β and collagen I expression. ACE inhibitors reduce TGF-β, collagen deposition, and fibrosis. In addition, in response to Ang II, myocytes produce higher levels of cytokines and growth factors, leading to enhancement of fibroblast sensitivity to cytokines, and stimulating their proliferation [227]. Ang II also reduces collagen degradation by decreasing collagenase activity in adult rat and human cardiac fibroblasts, and by stimulating TIMP-1 secretion in rat cardiac endothelial cells [220].

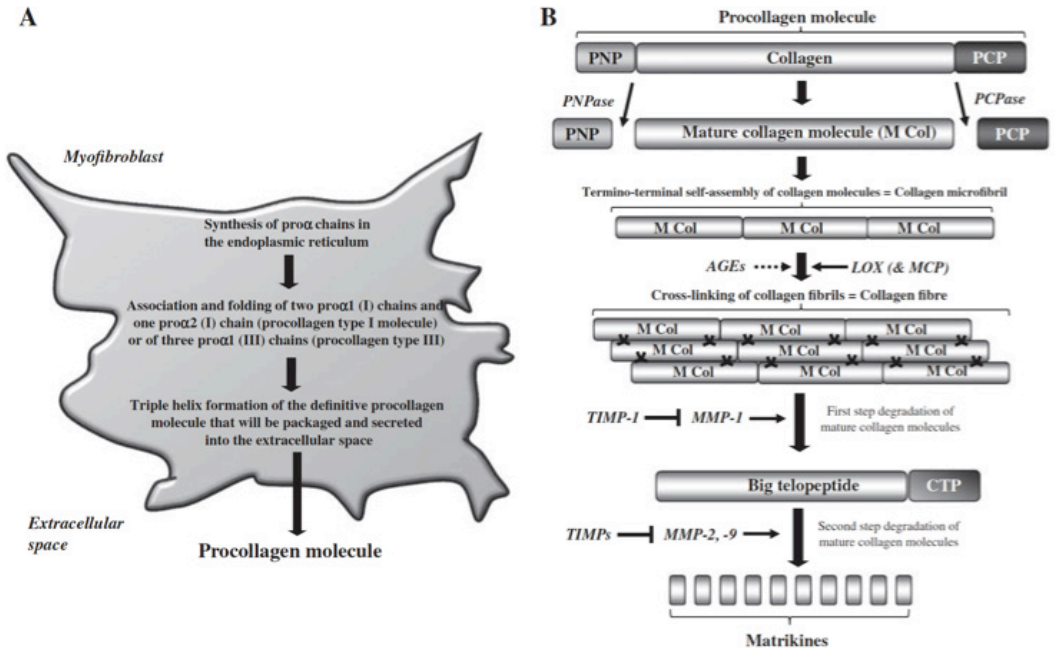

Figure 7. Collagen biosynthesis and degradation. (A) Synthesis of procollagen precursors in myofibroblasts. (B) Extracellular formation and degradation of collagen types I and III fibers. PNP, procollagen N-terminal propeptide; PCP, procollagen C-terminal propeptide; PNPase, procollagen N-terminal proteinase; PCPase, procollagen C-terminal proteinase; AGEs, advanced glycation end-products; LOX, lysyl oxidase; MCP, matricellular proteins; MMP, matrix metalloproteinase; TIMP, tissue inhibitors of MMPs; CTP, C-terminal telopeptide. The black symbols between collagen fibrils represent the covalent intra- and intermolecular cross-links, mostly LOX mediated (adapted from Heymans et al, 2015) [4].

1.4.1.2 Fibronectin (FN)

Fibronectin is an adhesive glycoprotein that is expressed by multiple cell types including cardiac fibroblasts, macrophages and endothelial cells [227, 228]. There are two forms of FN: plasma FN, the soluble form and cellular FN, the insoluble form that is abundant in the fibrillar matrices of most tissues. FN is formed of two subunits that are disulfide-bonded at their C-termini. These subunits are composed of types I, II, and III repeating domains [2]. There are 3 variants of FN mRNA, resulting from alternative splicing within the type III repeat region, referred to as extra

domain ED-A, ED-B, and IIICS [229]. FN binds to cells via integrin receptors. Syndecan receptors also bind FN, serving as co-receptors with integrins in cellular FN binding [2]. Polymerization of FN into the ECM is an essential step for the deposition of type I collagen and thrombospondin-1 [230]. FN also plays a role in cell adhesion and migration. In addition, it is involved in the cross-linking and stabilization of other ECM molecules. Furthermore, FN is implicated in cell-matrix signaling and mechanotransduction [221]. FN has been shown to be an *in vivo* substrate for both MMP-7 and MMP-9 [231, 232]. Following an MI, the EDA-FN variant is upregulated and co-operates with TGF-β in promoting the myofibroblast phenotype and enhancing the inflammatory response. In addition, EDA-FN stimulates monocyte migration and increases MMP production [215, 221].

1.4.2 ECM remodeling during heart diseases

As CFs have the ability to both secrete and degrade ECM proteins by modulating the expression of MMPs and TIMPs, CFs are considered the key modulator of ECM homeostasis [10]. In pathological conditions, such as cardiac hypertrophy and MI, fibroblasts are transdifferentiated into myofibroblasts, promoting ECM overexpansion, resulting in increased tissue stiffness and wall stress [214]. During normal and pathological conditions, the ECM is an extremely dynamic structural network that constantly undergoes remodeling mediated by matrix-degrading enzymes. Dysregulation of ECM homeostasis has been implicated in the development and progression of several pathologic conditions [2].

1.4.2.1 ECM remodeling following pressure overload

In response to pressure overload, cardiac hypertrophy serves initially to sustain cardiac output and normalize the increased wall stress. However, a persistent hypertrophic response leads to ventricular dilatation and, subsequently, cardiac dysfunction [91]. Animal models of pressure-overload-induced cardiac hypertrophy that mimic hypertension are characterized by deposition of collagen in the interstitium [233, 234]. Thus, fibrosis is considered as a hallmark of cardiac hypertrophy and heart failure and a determinant of cardiac function. Many animal studies of pressure overload have shown an increase in mRNA for collagen types I and III and TGF-β1 and significant collagen accumulation (interstitial fibrosis) following ligation of the transverse aorta [31, 235-237]. Moreover, fibrotic remodeling of the ECM is associated with increased wall stiffness and impaired diastolic function. Studies on hypertensive patients with cardiac hypertrophy reported fibrosis and impaired

diastolic function [238] associated with reduced plasma levels of MMP-1 [239], MMP-2, and MMP-9 [240] as well as elevated plasma levels of TIMP-1 [239]. In contrast, ventricular chamber dilatation and systolic dysfunction are associated with collagen fiber degradation [91]. In hypertensive patients with systolic heart failure, MMP-1 expression and the MMP-1: TIMP-1 ratio is increased in tissue and serum when compared with patients with diastolic heart failure [241].

1.4.2.2 ECM remodeling following MI

In response to MI, the myocardium undergoes a process of remodeling, which includes angiogenesis, myocyte hypertrophy, and fibroblast proliferation resulting in collagen deposition and alterations in ECM homeostasis [142]. Infarct healing is divided into three overlapping phases: inflammatory, proliferative, and maturation [242]. These phases are reviewed in Chapter 2. During all these phases, the composition of the ECM plays a pivotal role in the regulation of cell behavior [76]. Briefly, during the inflammatory phase, MMPs are activated within 10 min of coronary occlusion resulting in degradation of matrix proteins [74]. After depletion of latent collagenases, synthesis of new MMPs occurs, promoting fragmentation of ECM constituents and generation of low molecular weight fragments that possess proinflammatory properties. A fibrin-based provisional matrix is formed after the ECM is degraded [90]. This provisional matrix plays a hemostatic role, promotes leukocyte infiltration, and supports proliferation and migration of CFs [243]. Afterwards, an organized "second order" provisional matrix containing fibronectin and hyaluronan replaces this provisional matrix. Moreover, matricellular proteins are released and activate signaling pathways necessary for heart repair. Finally, wound maturation is accompanied by degradation of matricellular proteins and cross-linking of the deposited collagen to form stable scar. Excessive early degradation of the ECM and defective or delayed synthesis of newly formed ECM proteins may have a critical role in the pathogenesis of cardiac rupture [91]. An imbalance in collagen synthesis and degradation and other ECM constituents results in increased myocardial pressure, left ventricular dilatation, and heart failure. Moreover, secreted TGF-β promotes myocyte hypertrophy, decreased MMP production, and increased TIMP synthesis leading to increased collagen deposition (fibrosis) that in turn results in increased myocardial stiffness and alterations in the mechanical and electrical dynamics of heart function [227]. Several studies using genetically modified mouse models that study MI showed that targeted deletion of MMP-2 reduces the rate of LV rupture and impedes macrophage infiltration [244], MMP-9 deletion reduces LV dilatation and dysfunction and partially protects the heart from rupture

[245], and MMP-7 deletion improves myocardial conduction and post-MI survival [246]. In contrast, deleting TIMP-1, TIMP-2, or TIMP-3 results in altered in LV structure and function [80, 247, 248], while lack of TIMP-4 only increases the rate of LV rupture [249]. Overexpression of TIMPs has been shown to exert beneficial effects post-MI [250-252].

1.4.3 ECM Regulation by microRNA

MicroRNAs (miRNAs) are small non-protein-coding RNA molecules of 20-26 nucleotides in length. The human genome is estimated to encode more than 1000 miRNAs. They negatively regulate gene expression by affecting mRNA stability, resulting in its degradation, and/or by blocking protein translation [253]. Several miRNAs have key roles in promoting (miR-21, miR-34, miR-199b, miR-208) or inhibiting (miR-1, miR-26a, miR-29, miR-101, miR-122, miR-133/miR-30, miR-133a, miR-214) myocardial fibrosis (reviewed in [254, 255]). For example, miR-21 is highly expressed in cardiac fibroblasts and its level is upregulated in the failing heart. Thum *et al.* have shown that miR-21 promotes cardiac hypertrophy and fibrosis in a model of pressure overload [256]. Transfection of rat and mouse fibroblasts with synthetic miR-21 precursor molecules significantly increases the activation of the ERK-MAPK signaling pathway in response to the inhibition of the protein sprouty (Spry1) that is a potent inhibitor of profibrotic ERK-MAPK signaling in cardiac fibroblasts. Thus, miR-21 plays a critical role in the regulation of ERK-MAP activity in cardiac fibroblasts. Moreover, in response to pressure overload, knocking down miR-21 with a cholesterol-modified antagomir attenuates cardiac dysfunction, decreases ERK-MAPK activity, and prevents both hypertrophy and fibrosis [256]. In contrast, Patrick *et al.* have shown that neither genetic deletion nor locked-nucleic acid (LNA)-mediated knockdown of miR-21 in mice block cardiac remodeling in response to pressure overload or Ang-II administration [257]. Furthermore, the miR-29 family is downregulated after MI and it may act as a fibrosis regular by inhibiting the expression of several collagens and ECM proteins, thus contributing to scar formation and fibrosis. Suppressing miR-29 expression using anti-miRs *in vitro* and *in vivo* stimulates collagen expression. Conversely, overexpressing miR-29 in fibroblasts decreases collagen expression [258]. Similarly, Abonnenc *et al.* have shown that miR-29b is a potent regulator of ECM synthesis; it attenuates the cardiac fibroblast response to TGF-β and reduces collagen and MMP-2 secretion [259]. miR-29b inhibition,using antagomirs that silence the endogenous miR-29b, induces excess perivascular fibrosis following transverse aortic constriction. Conditioned medium from cardiac fibroblasts transfected with pre-

miR-29b lost the ability to support adhesion of rat ventricular myocytes [259]. Additionally, miR-133 is expressed primarily in cardiomyocytes, whereas miR-30 is expressed in both cardiac myocytes and cardiac fibroblasts. Both miR-30 and miR-133 are involved in the regulation of connective tissue growth factor (CTGF), a key profibrotic protein. Both miRNAs are downregulated in pathological left ventricular hypertrophy and are inversely correlated to the levels of CTGF, collagen production, and cardiac fibrosis. Knockdown of miR-30 and miR-133 in cultured cardiomyocytes and fibroblasts resulted in an increase in CTGF levels. Conversely, over-expression of these 2 miRNAs reduced CTGF levels and collagen synthesis. Thus, these 2 miRNAs regulate cardiac ECM remodeling [260]. Moreover, Abonnenc *et al.* reported that miR-30c levels decreased in mice following constriction of the transverse aorta [259]. These studies provide promising avenues in the development of diagnostic and therapeutic tools to regulate cardiac remodeling using miRNAs.

1.5 Mitogen-activated protein kinase-activated protein kinase 5 (MK5)

1.5.1 Overview

Cells have sophisticated mechanisms to receive signals through their surface receptors, transmit the information, and respond appropriately to any changes in the extracellular milieu. Signal transduction cascades often involve post-translational modification of proteins. Protein phosphorylation is an important post-translational modification. The human genome encodes 518 protein kinases capable of phosphorylating more than one third of all cellular proteins [261]. One major group of protein kinases are the mitogen-activated protein kinases (MAPKs), which regulate many signal transduction pathways and cellular processes such as growth, differentiation, apoptosis, motility and gene expression [262]. In cardiomyocytes, MAPK signaling is initiated by G-protein coupled receptors (GPCRs), receptor serine/threonine kinase receptors (e.g., TGF-β), receptortyrosine kinase receptors (e.g., IGF-1 receptors), cardiotrophin-1 (gp130 receptor), and by mechanical stretch [19]. Characterization of these signaling pathways represent an important step in the understanding of cellular signalling under physiological and pathological conditions.

In mammalian cells, MAPK pathways are divided into four conventional pathways: extracellular signal-regulated kinases 1 and 2 (ERK1/2), the c-JUN N-terminal kinases 1-3 (JNK1-3) or stress-activated protein kinases (SAPKα, β and γ), p38 MAPKs (p38 α, β, γ, and δ) and big MAPK (BMK/ERK5). There are also three atypical MAPK pathways: ERK3/4, ERK7/8, and nemo-like kinase (NLK) pathways. The classical MAPK pathway displays a characteristic hierarchical organization of a three-tiered cascade in which MAPK kinase kinases (MAPKKK, MAP3K, or MEKK) phosphorylate and activate MAPK kinases (MAPKK or MAP2K), which in turn phosphorylate and activate MAPKs. Atypical MAPK pathways appear to lack this three-tiered structure [263]and do not possess the canonical "T-X-Y" motif within their activation loop that is present in the conventional MAPKs. Both the conventional and the atypical MAPK pathways can phosphorylate non-protein kinase substrates as well as other downstream protein kinases referred to as MAPK-activated protein kinases (MAPKAPKs, MKs). The MAPKAPK family includes the p90 ribosomal-S6-kinases (RSK1-4), the MAPK-interacting kinases (MNK1 and 2), the mitogen-and-stress-activated kinases (MSK1 and 2), and the MAPKAP kinases MK2, MK3, and MK5/p38-regulated/activated protein kinase (PRAK). Among the MKs that can be activated by different conventional MAPKs, MK5/PRAK is the only MK that is phosphorylated by both the conventional

p38 MAPK and the atypical ERK3/4 pathways (Figure 8) (Reviewed in [9, 263, 264]). Herein we will focus on MAPKAPK-5 and it will be referred to as MK5.

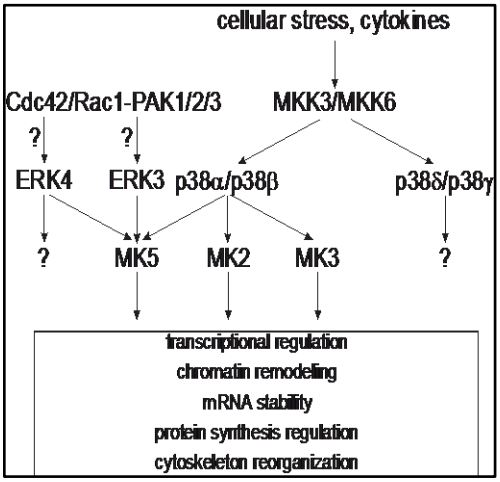

Figure 8. Schematic representation of the regulation of MKs and their potential physiological functions. Shown are the four p38 isoforms (α, β, γ, and δ) along with their interactions with MK2, MK3, and MK5. Also shown is the regulation of MK5 by the atypical MAP kinases ERK3 and ERK4 plus several biological functions of these signaling pathways. (Adapted from Cuenda and Rousseau, 2007)[7].

1.5.2 Identification of MK5

MK5 and its human homologue PRAK are serine/threonine kinases that were discovered simultaneously in 1998 by Ni *et al.* and New *et al.* respectively, based on homology with MK2 [265, 266].

1.5.3 MK5 Gene

The *Mapkapk5* gene is highly conserved in most vertebrates but is absent in *Caenorhabditis elegans* and *Drosophila* genomes [265, 267]. In humans, *Mapkapk5* is located on chromosome 12 whereas in mice it is on chromosome 5. The human *Mapkapk5* gene consists of 14 exons, however the number of exons varies between species [9].The human, rat and mouse *Mapkapk5* promotor

region is GC rich and lacks a canonical TATA box consensus sequence. Moreover, the *Mapkapk5* promotor region contains putative binding sites for several transcription factors (e.g., the cAMP-binding response element-binding protein, CREB), the composition of which differs in human compared to rat or mouse. However, in response to increased cAMP levels, MK5 transcript levels increase without changes in protein levels, suggesting a regulation at the level of translation [262].

1.5.4 MK5 mRNA

MK5 mRNA is expressed ubiquitously, with higher expression in the cardiac left ventricle, skeletal muscle, brain, pancreas, lung and kidneys [262, 265, 266]. MK5 transcripts and protein are also detected during murine embryogenesis [268, 269]. The human *Mapkapk5* gene encodes two known spliced transcripts of 471 and 473 amino acids whereas in mouse, mRNA for five MK5 splice variants (MK5.1-MK5.5) have been identified. These splice variants result from exon skipping and alternative splice site activation during pre-mRNA processing. Murine MK5.1 is the original full-length MK5 (14 exons) and the most abundant variant, followed by MK5.2. MK5.3 lacks exon 12 and, hence, regions within the C-terminal region of the protein, including the ERK3/ERK4 binding motif, are absent. MK5.4 and MK5.5 lack exons 2-6, encoding the kinase domain, making these variants kinase-dead. Both MK5.2 and MK5.5 lack 6 bases at the 3'-end of exon 12. Although the regulatory mechanism of MK5 mRNA splicing, their subcellular localization, and functions have not been identified, the 5 MK5 transcripts were detected in all mouse tissue examined. The relative abundance of the transcripts for the 5 mouse MK5 variants is tissue-specific and is altered in response to hypertrophy and during postnatal cardiac development, suggesting that these isoforms may have distinct roles in physiological processes [270].

1.5.5 MK5 protein

MK5 is well conserved with high sequence identity across many species. MK5 shows similarity in structural organization and 42% amino acid homology with MK2 and MK3. Their kinase catalytic domains are most similar to that of the calcium/calmodulin-dependent protein kinase (CAMK) superfamily [267]. Similar to MK2/3, MK5 consists of a 284 amino acid kinase domain flanked by a short N-terminal region butlacks the SH3 domain-binding motif present in MK2/3, and a C-terminal extension of 100 amino acids containing overlapping nuclear localization (NLS; Arg-Lys-Arg-Lys) and nuclear export signals (NES; Leu-Arg-Val-Ser-Leu-Arg-Pro-Leu-

His-Ser), a p38 MAPK-docking motif (D domain) that mediates the interaction with p38α and p38β and overlaps with the NLS, and an ERK3/4 binding domain. Threonine-182 in the MK5 activation loop is also conserved and is phosphorylated by p38α/β, ERK3, and ERK4. Moreover, serine-115, which is the phosphoacceptor site for protein kinase A (PKA) is conserved in all species examined to date (Figure 9) [265, 271].

Figure 9. Functional domains of MK5. The blue rectangle represents the MK5 catalytic domain (residues 22-304) in which Threonine-182 is the residue phosphorylated by p38, ERK3 and ERK4, and Serine-115 that is the phosphoacceptor site for protein kinase A (PKA). The green rectangle is the nuclear localization signal (NLS) overlapping with p38 docking site. The red rectangle is the nuclear export signal (NES), which overlaps with NLS. The ERK3/4 docking site is indicated (adapted from Kostenko et al, 2011) [9].

The interaction of MAPKs with their activators and substrates occurs via the common docking (CD) motif within the MAPKs and regions within the binding partner known as the docking motif (D domain), kinase-interacting motif (KIM), or reverse D motif (revD) (hydrophobic residues located N-terminal to the D-motif) ([272, 273] reviewed in [274, 275]). However, these interacting domains may actuallybe part of an extended recognition motif, referred to as the linear motif (LM), that is essential for specific interaction between MAPKs and their binding partners, including MK5 [275]. In contrast, the interaction of ERK3/4 with MK5 is mediated by a novel FRIEDE motif in loop L-16, which lies C terminal to the CD-motif in MK5 [276]

1.5.6 Subcellular localization and regulation of MK5 activity

Each of the MK5 variants (MK5.1-MK5.5) possesses both NLS and NES. Both endogenous and ectopically expressed MK5 is predominantly nuclear in unstimulated cells; however, MK5 shuttles continuously between the nucleus and cytoplasm. The subcellular localization of MK5 is regulated by: p38 MAPK, ERK3 and ERK4, PKA, and the dual-specificity phosphatase Cdc14A. Upon stimulation, MK5 translocates to the cytoplasm [265, 271, 277-284]. However, Dingar *et al.* showed that although MK5.1, MK5.2, and MK5.3 reside in the nucleus, MK5.4 and MK5.5 are in the cytoplasm when expressed in quiescent HEK293 cells [270]. Upon activation of the p38 MAPK pathway by anisomycin, MK5.1-MK5.3 are exported to cytoplasm whereas small amounts of MK5.4 and MK5.5 were transported to nucleus [270].

1.5.6.1 Regulation by p38 MAPK

Activation of p38 MAPK results in MK5 translocation [265, 271] and this translocation is inhibited by leptomycin B, an inhibitor of nuclear export [271]. Moreover, kinase-dead MK5 mutants still undergo nucleocytoplasmic translocation when p38 MAPK is activated [265, 271, 283]. Nuclear export of MK5 in response to p38 activation is regulated by p38 MAPK binding to MK5 and masking the NLS, thus blocking the binding of importins to the NLS, and by phosphorylation of threonine-182 by p38 MAPK, which activates or unmasks the NES due a conformational change in MK5. Replacing threonine-182 with a non-phosphorylatable residue or inhibiting p38α/β with SB203580 prevents the nuclear export of MK5 [265, 271]. p38 α and β have been shown to have different effects on MK5 translocation. p38α-MK5 complexes reside in the nucleus, whereas p38β-MK5 complexes are cytoplasmic [285]. The subcellular localization of p38-MK5 complexes is determined by two amino acid residues within the p38 isoforms (aspartate-145 and leucine-156 in p38α, glycine-145 and valine-156 in p38β). Furthermore, the different subcellular localizations of these complexes affects the inhibitory effect of MK5 on NIH3T3 cell proliferation, suggesting the subcellular localization of MK5 is an important determinant of its physiological function [285].

1.5.6.2 Regulation by ERK3 and ERK4

Co-expression of ERK3 or ERK4 with MK5 results in the translocation of MK5 to the cytosol [278, 279]. Nucleocytoplasmic translocation of MK5 upon binding to ERK3 or ERK4 does not require their kinase activity [279, 281, 286], nor the catalytic activity of MK5, or phosphorylation at

threonine-182 in the activation loop of MK5 [278], suggesting the formation of ERK3/4-MK5 complexes is responsible for MK5 translocation. However, the mechanism of MK5 translocation upon binding to ERK3 or ERK4 is remains unknown. ERK3 and ERK4 bind to MK5 through a region containing residues 383-393 and 460-465, respectively, in the C-terminal region of MK5 [276].

1.5.6.3 Regulation by PKA

PKA is a cAMP dependent protein kinase consisting of two catalytic (C) and two regulatory (R) subunits. When cAMP binds to the PKA regulatory subunits, it causes them to dissociate from the catalytic subunits, which are then free to phosphorylate substrates [287]. Forskolin, an adenylate cyclase activator, which activates the cAMP/PKA pathway, results in transient nuclear export of MK5, as does overexpression of the PKA catalytic subunit (PKA-C). This translocation requires the kinase activities of both PKA and MK5. In PKA-deficient cells, forskolin is unable to induce MK5 translocation [280, 284]. The phosphoacceptor site serine-115 in MK5 is required for translocation of MK5 from nucleus to cytoplasm in response to PKA activation. When this residue is replaced with an alanine residue, MK5 translocation in response to PKA activation is prevented. If serine-115 is replaced with a phosphomimetic aspartic acid residue (S115D) MK5 is present in the cytoplasm and nucleus of unstimulated cells [284]. The ability of PKA to induce MK5 translocation is lost in kinase-dead MK5 (T182A and K51E) [280].

1.5.6.4 Regulation by Cdc14A

Overexpression of the dual-specificity phosphatase Cdc14A results in nuclear export of MK5. MK5-Cdc14A binding is not dependent on the catalytic activity of Cdc14A. As Cdc14A binds with ERK3 and ERK4, Cdc14A may be involved in ERK3/ERK4-regulated nuclear export of MK5 [282].

1.5.7 Activation of MK5

There is controversy regarding the activation mechanisms of MK5. MK5 has been shown to be phosphorylated by many kinases including p38 MAPK, ERK3/4, PKA, and focal adhesion kinase (FAK) in *vitro* and *in vivo*[265, 266, 277, 278, 280, 288]. Analysis of *in vitro*-phosphorylated MK5 revealed that threonine-182 in its activation loop is essential for its activation [265]. Moreover, phosphorylation at serine-93, threonine-186, serine-212, serine-115, and threonine-214 have been

detected but are not required for MK5 activation [265, 284]. Moreover, Zheng *et al.* reported a role of Tip60, a member of the MYST family of histone acetyltransferases (HAT), in MK5 catalytic activation through acetylation of MK5 at lysine-364. Acetylation of MK5 by Tip60 is dependent on phosphorylation of both Tip60 and MK5 (at threonine-182) by p38 [289]. MK5 may also undergo ubiquitin-mediated proteosomal degradation, as in mouse embryonic fibroblasts (MEFs) and rabbit reticulocyte lysates, the presence of ubiquitinated and SUMOylated forms of MK5 were detected [290].

Several *in vitro* and *in vivo* studies show that phosphorylation of threonine-182 by p38 MAPKs is required for its catalytic activity. New *et al.* showed that MK5 could be phosphorylated *in vitro* by all four p38 isoforms (α, β, γ, δ) but only p38α and p38β are able to phosphorylate and activate MK5. Both p38α and p38β phosphorylate MK5 at threonine-182 *in vitro* and replacing threonine-182 by alanine results in a form of MK5 that is not activated by these 2 kinases. Stimulation of HeLa cells with pro-inflammatory cytokines, stress, or arsenite (stimulators of p38 MAPK) results in MK5 activation and phosphorylation of the 27-kDa heat shock protein (Hsp27), which are inhibited by the p38α/β inhibitor SB203580 [265]. Furthermore, mutations on the phosphorylation sites or the substrate docking motif on p38α or p38β inhibited TNF-stimulated activation of MK5 [291]. Co-immunoprecipitation studies reveal that p38 MAPK and MK5 form a stable complex when transfected into HEK 293T or NIH3T3 cells [285]. This interaction is abolished in p38 MAPK CD motif mutants and mutations of MK5 in the p38-docking site or NLS but not by modification of threonine-182 [271, 291]. These studies suggest a direct interaction between MK5 and p38 MAPK, forming a complex via binding of p38α/β to the D domain.

Although MK5 can be activated by p38α and p38β *in vitro* and *in vivo* through phosphorylation of threonine-182 within the activation loop of MK5, the physiological relevance of MK5 regulation by p38 MAPK *in vivo* is still under debate. In MEFs exposed to extracellular stress endogenous MK2 interacts with and stabilizes p38α and becomes activated. In contrast, MK5 did none of these [292]. Moreover, MK5-deficient mice are not resistant to endotoxic shock caused by lipopolysaccharide (strong activator of p38) and do not have the impaired cytokine production observed in MK2-deficient mice [292].

MK5 can be activated *in vivo* and *in vitro* by the catalytic subunit of PKA. Immunoprecipitated MK5 from cells treated with forskolin, an adenylate cyclase activator, showed

increased catalytic activity [280]. Phosphorylation of MK5 at serine-115 by PKA increases its kinase activity [280, 284, 293]. In HeLa cells, overexpressed MK5 and the PKA Cα subunit interact physically resulting in MK5 phosphorylation and activation. Furthermore, PKA mediated F-actin remodeling in PC12 cells is inhibited upon siRNA-mediated MK5 knockdown [280]. Kostenko *et al.* showed that PKA-MK5 mediated microfilament rearrangement requires Hsp27 phosphorylation by MK5 [293].

MK5 activity is also regulated by atypical MAPKs ERK3/ERK4 [277, 279]. ERK3 and ERK4 have been shown to phosphorylate MK5 on threonine-182 and increase its activation. A direct interaction between MK5 and ERK3, and not p38, has been shown in RAW 264.7 cells. MK5 endogenous activity was reduced by 25% in primary MEF cells derived from $ERK3^{+/-}$ mice and by 50% from $ERK3^{-/-}$ cells compared to $ERK3^{+/+}$ cells, with no change in its protein levels. ERK3 is not a stable protein, it requires the physical presence of MK5 for its stabilization [277]. $MK5^{-/-}$ MEF cells showed a reduction in ERK3 levels. Moreover, MK5 catalytic activity is essential for its phosphorylation at threonine-182 upon binding to ERK3. When co-expressed with ERK3, kinase-dead MK5 K51E cannot be phosphorylated at threonine-182, suggesting that ERK3 binding promotes the MK5 autophosphorylation, thus acting as a scaffolding protein [278]. However, ERK4 kinase activity is required for MK5 activation. Both ERK3 and ERK4 are phosphorylated by the activated MK5 and bind to the amino acid residues in the C-terminus of MK5. siRNA knockdown of ERK4 results in a reduction of MK5 activity [279]similar to that resulting from an ERK3 knockdown [277].

The atypical MAPKs ERK3/ERK4 contain an S-E-G motif instead of the conserved T-X-Y motif in the activation loop of conventional MAPK and they have a single phosphor-acceptor site, serine-189 in ERK3 and serine-186 in ERK4, within their activation loop. Phosphorylation on the S-E-G motif is essential for ERK3/4 to bind, activate, and translocation of MK5 *in vivo* and *in vitro*[281, 294]. Specifically, phosphorylation of the S-E-G motif is essential for the FRIEDE motif to be accessible to bind MK5. The substitution of isoleucine with lysine in the FRIEDE motif of ERK3 or ERK4 prevents MK5 docking, activation, and translocation [276]. Group 1 p21-activated kinases (PAKs), a principal effector of GTPases Rac and Cdc42 that are involved in cytoskeleton remodeling and cell migration, were identified as upstream activators of ERK3/4 and lead to downstream activation of MK5 [295, 296]. However, the physiological role of the PAK-ERK3/ERK4-MK5 pathway remains unknown.

Cdc14A, a serine/threonine phosphoprotein phosphatase, forms a complex with ERK3. In addition, cdc14A is able to dephosphorylate a C-terminal fragment of ERK3 following phosphorylation of the fragment by Cdk1 kinase. Similarly, Cdc14A binds to MK5 independent of its catalytic activity leading to the accumulation of MK5 within the cytoplasm [282, 297]. Furthermore, the dual specificity protein phosphatase 2 (DUSP2) dephosphorylates the serine residue in the S-E-G motif of both ERK3 and ERK4, resulting in reduction of their catalytic activity towards MK5 and thus indirectly regulates MK5 activity [298]. This suggests a role for phosphoprotein phosphatases such as Cdc12A and DUSP2 in negative regulation of ERK3/ERK4-MK5 signaling.

1.5.8 MK5 substrates

Several proteins can interact with and act as substrates for MK5. The first substrates identified for MK5 *in vitro* were glycogen synthetase, myosin heavy chain, and Hsp27 (Hsp25 in mice and rats). Only Hsp27 has been shown to be a substrate of MK5 *in vivo*. MK5 phosphorylates Hsp27 at serines-15, -78, and -82 *in vivo* and *in vitro* as MK2 and MK3 do [265]. A yeast two-hybrid screen of mouse and human brain cDNA libraries [299, 300], GST pull-down and co-immunoprecipitation assays, septin 8, a small cytoskeletal GTP-binding protein, has also been identified as an *invitro* substrate for MK5 [300]. MK5 phosphorylates septin 8 at serines-242 and -271 [300]. Yeast two-hybrid screening also identified septin 7 and kalirin-7 as ERK3 and MK5-interacting partners and substrates respectively [299]. Kalirin-7 is a brain-specific neuronal guanine exchange factor that activates Rho GTPases involved in actin polymerization [301]. Septin-interacting and -regulating Binder of Rho GTPases (Borgs) proteins (Borg1, 2, 3) have been demonstrated as direct substrates for ERK3 and MK5 *in vitro*. Septin 7 interacts with MK5 in the form of an ERK3/MK5/septin 7 ternary complex [299]. Numerous other possible substrates for MK5 have been described, including 14-3-3ε [302], DJ-1 [303], Hsp40 [304], Tip60 [289], FoxO1 [305], FoxO3a [306], $hTid_s$ [307], and Rheb [308].

1.5.9 Biological Functions of MK5

The lack of an obvious phenotype in $MK5^{-/-}$ mice hampers studies of the physiological functions of MK5. MK5 knockout mice were generated on a mixed 129/Ola × C57/B6 genetic background by targeting exons 6 (MK5-Δex6) [292] or 8 (MK5-Δex8) [309]. $MK5^{\Delta ex8/\Delta ex8}$ mice are healthy and fertile. $MK5^{\Delta ex6/\Delta ex6}$ mice show embryonic lethality with incomplete penetrance

resulting in only 50% of the expected number of MK5 embryos detectable after embryonic day E12. Moreover, the surviving mice fail to reproduce. $MK5^{+/\Delta e\times 6}$ mice are healthy [278]. As mentioned above, there are five known murine MK5 mRNA variants: MK5.2-5.5, in addition to the original MK5.1. The physiological roles of MK5.2-MK5.5 have not yet been identified. All the studies performed to-date have employed on the full length MK5.1. Although the biological functions of MK5 remain incompletely understood, some of the functions have started to be identified. Most of the studies have employed *in vitro* approaches and imply a role of MK5 in transcription, F-actin remodeling, cell migration and proliferation, tumor suppression, and autophagy. However, the *in vivo* functions of MK5 remain to be addressed especially in terminally differentiated cell systems such as heart.

1.5.9.1 MK5 and F-actin remodeling and cell migration

The unphosphorylated form of Hsp27 binds to the barbed, growing ends of actin filaments leading to their stabilization and inhibits further polymerization [310]. Phosphorylation of Hsp27 results in Hsp27 dissociation from actin, allowing actin polymerization and microfilament rearrangement [311, 312]. As MK5 can phosphorylate Hsp27 *in vitro*, so it may be involved in regulating F-actin remodeling. Overexpression of wild type MK5 in HeLa cells increased Hsp27 phosphorylation, F-actin production, and cell migration whereas MK5 T182A had no effect [302]. Furthermore, MK5 mediated F-actin remodeling is negatively regulated by 14-3-3ε (a member of 14-3-3 family of molecular scaffolds that regulate intracellular signaling). In HeLa cells, co-expression of 14-3-3ε with MK5 inhibits MK5, resulting in decreased Hsp27 phosphorylation, cell migration, and actin filament rearrangement. In addition, siRNA knockdown of endogenous 14-3-3ε results in MK5 and Hsp27 phosphorylation as well as cell migration and cytoskeletal remodeling [302]. Coexpression of MK5 with human tumorous imaginal $disc1_s$ ($hTid\text{-}1_s$), a member of the hsp40 family inhibits MK5 activity, Hsp27 phosphorylation and cell migration, whereas downregulation of its expression increases cell migration [307]. Similar findings were observed in PC12 and HeLa cells, where activation of PKA or ectopic expression of the PKA catalytic subunit results in MK5 phosphorylation and activation, and formation of actin-based filopodia, whereas knockdown of endogenous MK5 or Hsp27 or ectopic expression of a nonphosphorylatable Hsp27 (Ser-15,78,82-Ala) mutant in PC12 cells prevents forskolin-induced F-actin reorganization [280, 293]. Knockdown of insulin-like growth factor 2 binding protein (IGF2BP1) in osteosarcoma-derived U2OS cells leads

to MK5 activation, Hsp27 phosphorylation, increase in the abundance of ERK4, decrease in cell migration and loss of stress fibers; those effects were abolished upon MK5 knockdown [313]. In contrast, treatment of human umbilical vein endothelial cells (HUVECs) with VEGF induced the formation of actin stress fibers and cell migration via activation of focal adhesion kinase (FAK) and not Hsp27 phosphorylation; this response was lost upon knockdown of MK5 [314]. Hence, the role of MK5 as an Hsp27 kinase in regulating cytoskeletal rearrangement may depend upon the type of cells and the nature of the stimulus. Although MK5 can phosphorylate Hsp27 *in vitro*, there is some debateabout the contribution of MK5 to phosphorylate Hsp27 *in vivo* as in response to cellular stress, deletion of MK5 in MEFs did not prevent the phosphorylation of Hsp25 whereas MK2 deletion did [292]. However, the role of MK5 in cytoskeletal remodeling and migration has been demonstrated in many different cell systems.

1.5.9.2 MK5 and cell proliferation and malignant tumors

MK5 was shown to promote tumor suppression and oncogenic RAS-induced senescence [309]. In response to dimethylbenzanthracene (DMBA), a mutagen that causes skin tumors, MK5-deficient mice were more susceptible to skin carcinogenesis compared to wild-type mice. Moreover, MK5 was demonstrated to be necessary for RAS-induced senescence in primary mouse skin fibroblasts, MEFs, and primary human fibroblasts as it is lost upon deletion of MK5 or reintroducing of kinase dead MK5 mutant in MK5-deficient cells, whereas it is restored by reintroducing wild type MK5. In addition, the same group has demonstrated that in response to oncogenic RAS expression, MK5 phosphorylates p53 at serine-37 resulting in the activation of its transcription activity, the upregulation of cyclin-dependent protein kinase inhibitor $p21^{WAF1/CIP1}$, and reduced cell proliferation. These effects were abolished in MK5-deficient cells [309]. Also, Chen *et al.* have shown that activated MK5 may interfere with RAS-induced JNK activation, resulting in inhibition of proliferation [315]. Moreover, MK5 is activated in senescent cells and by oncogenic RAS [315] and senescence was enhanced by the ectopic expression of MK5 along with RAS [309]. In another study, in a mouse model expressing oncogenic N-rasG12D, MK5 deletion enhanced hematopoietic tumorigenesis and oncogenic RAS-induced cell proliferation, and abolished RAS-induced accumulation of senescence markers in a JNK-dependent manner [316]. These results suggest that MK5 may act as a tumor suppressor in multiple cell types, including fibroblasts. However, the role of MK5 in tumor suppression varies according to the genetic targeting of MK5, as deletion of exon

8 suggests that MK5 may function as a tumor suppressor [309]while deletion of exon 6 does not [317].

Kress *et al.* have described another mechanism for suppression of tumorigenesis by MK5 [306]. They have identified MK5 as a negative regulator of c-Myc expression. siRNA knockdown of MK5 in U2OS, cervical carcinoma, and colon carcinoma cells was associated with increased Myc protein levels, whereas ectopic expression of a constitutively active MK5 mutant in HeLa cells was associated with decreased Myc protein levels and suppressed cell proliferation in U2OS cells. MK5 negatively regulates Myc at the translational level by enhancing the expression of microRNA miR-34b and miR-34c that bind to the 3'UTR of Myc and inhibits its translation. Phosphorylation of the transcription factor FoxO3a at serine-215 *in vivo* by MK5 was found to upregulate miR-34b and miR-34c expression. Moreover, Myc protein forms a negative feedback loop by binding to the *Mapkapk5* promoter region and upregulating its expression. In colon carcinomas, this feedback loop was disrupted as MK5 expression was found to be downregulated while Myc expression was upregulated [306].

Two opposing functions of the p38/MK5 pathway in tumorigenesis were described: tumor suppression and tumor promotion. In the initiation and promotion stages of DMBA-induced skin carcinogenesis, MK5 suppressed tumors by mediating oncogene-induced senescence [309]. However, once the skin tumors are formed (progression stage), proangiogenic factors secreted by the tumor activate MK5 in the host endothelial cells and promote their migration towards tumors and mediate tumor angiogenesis that plays an important role in sustained tumor growth [314]. Skin tumors in $MK5^{-/-}$ mice have impaired angiogenesis and significantly increased apoptotic cells compared with wild-type mice. Furthermore, when skin tumors are transplanted into $MK5^{+/+}$, $MK5^{+/-}$ and $MK5^{-/-}$ mice, tumors formed in $MK5^{-/-}$ mice have a significantly reduced growth rate, fewer and thinner vessels, and increased apoptotic cells compared to $MK5^{+/+}$ and $MK5^{+/-}$ mice [314]. Hence, MK5 is required in the tumor microenvironment to induce angiogenesis and tumor growth.

1.5.9.3 MK5 and cell growth and metabolism

The serine/threonine protein kinase mammalian target of rapamycin (mTOR) acts as a regulator for cell growth and metabolism. mTOR comprises 2 complexes mTORC1 and mTORC2 [318]. The small G-protein Rheb (Ras homolog enriched in the brain) is a key regulator of mTORC1; in its GTP-bound state, it activates mTORC1. MK5 has been shown to bind and phosphorylate

Rheb, inhibiting the ability of Rheb to bind GTP, resulting in mTORC1 inactivation and decreased cell growth [308].

1.5.9.4 MK5 and Autophagy

Autophagy is a self-degradative process that plays a housekeeping role in elimination of intracellular pathogens and damaged organelles, and promotes cellular senescence. Defects in autophagy have been linked to cancer, diabetes, cardiovascular disease, and neurodegenerative diseases such as Alzheimer's disease (AD) [319]. A recent study demonstrated a role of MK5 in the regulation of β-amyloid receptor for advanced glycation end products (RAGE)-mediated autophagy in AD [320]. β-Amyloid peptide is a major pathological characteristic of AD [321]and it is one of the ligands that bind to RAGE [322] causing generation of reactive oxygen species, affecting cellular homeostasis [323]. MK5 has been shown to associate with the cytoplasmic domain of RAGE. In a mouse model of AD, the interaction between MK5 and RAGE was increased in the brain. Moreover, upon treatment with β-amyloid, which binds to RAGE, phosphorylation of MK5 at threonine-182 and the interaction between MK5 and RAGE both increased. In addition, knockdown of MK5 decreased RAGE-mediated formation of autophagosome via the mTORC1 signaling pathway [320].

1.5.9.5 MK5 and neurological function

The ERK3/MK5 pathway has been shown to regulate neuronal cytoskeleton and dendritic-spine formation [299]. In hippocampal neurons of MK5-deficient mice, there was impairment of dendritic spine formation. In addition, the ERK3/MK5 signaling pathway stimulates septin7-dependent dendrite development and spine formation in transfected primary hippocampal neurons [299]. Thus, the ERK3/MK5 signaling module may play a role in neural morphogenesis. In addition, in mice expressing a constitutive active mutant of MK5 (MK5 L337G), females displayed differences in anxiety behavior compared to controls whereas males did not [324].

Synaptophysin is a synaptic vesicle protein that is involved in synaptic functions such as exocytosis, synapse formation, and endocytosis of synaptic vesicles [325]. Septin 8 colocalizes with synaptophysin in primary cultured rat hippocampal neurons [326]. Septin 8, a small GTPase that is highly expressed in neurons and platelets, may participate in neurotransmitter release, secretion from platelets, and SNARE complex formation [326]. MK5 has been shown to bind to septin 8 *in vitro*

and *in vivo* and both proteins colocalize with synaptophysin in human neuroblastoma SK-N-DZ cells [300]. p38 MAPK is involved in SNARE-dependent exocytotic release of brain-derived neurotrophic factor from microglia [327]. Hence, MK5 may have a role in neurotransmitter release. Further studies are needed to prove this assumption and to unveil the involvement of MK5 in this process.

1.5.9.6 MK5 and cardiac function

Although the left ventricle shows the highest known expression level of MK5 mRNA [262], we know very little concerning the role of MK5 in the heart. In the heart, MK5 forms a stable complex with ERK3 but not with ERK4 or p38α. In heart lysates from control and hypertrophied hearts exposed to chronic pressure overload that activates p38, MK5 co-immunoprecipitates ERK3, but not ERK4 or p38α. Exogenously added GST-ERK3 or GST-p38 failed to pull-down endogenous MK5 [270]. In response to stresses (e.g., chronic pressure overload, ischemia, heart failure), Hsp27 becomes phosphorylated [328]which in turn plays a cardioprotective role [329-332]. MK5 is able to phosphorylate Hsp27 *in vitro* and MK5 is activated in response to elevated aortic pressure in retrograde perfusion of isolated rat hearts *ex vivo* [333]. Thus, MK5 may be involved in regulating the cardioprotective effects of Hsp27 during stress. However, the exact role of MK5 remains to be identified in the heart.

1.5.10 Pharmacological inhibitors of MK5

Recently, several MK5 inhibitors have been discovered that particularly inhibit MK5 activity, such as epigallocatechin gallate (EGCG) [334], flavokavain A [335], flavokavain B [335], immidazopyrazine derivatives [336], noroxoaconitine [337], SFV785 [338], and GLPG0259 [339, 340]. From those compounds, only GLPG0259 was tested in a clinical study in the treatment of rheumatoid arthritis [340]as it was shown to reduce the inflammation in a mouse model of collagen-induced arthritis [336]. Phase I clinical trials showed that single and repeated doses of GLPG0259 were safe and well tolerated in healthy subjects [339]. However, a phase II study revealed GLPG0259 lacked efficacy on patients with active rheumatoid arthritis [340].

2 Hypothesis and Objectives

2.1 Hypothesis

Activation of p38 MAPK in the heart is thought to play a role in cardiac remodeling. Acute activation of p38 in the adult mouse heart results in a rapid onset of lethal cardiomyopathy associated with pathological cardiomyocyte hypertrophy, interstitial fibrosis and contractile dysfunction within one week [330]. The mechanisms whereby this signaling pathway is involved in these effects are unknown. Furthermore, clinical trials of p38 inhibitors failed to make it to phase III due to a high incidence of side effects such as hepatotoxicity, skin rashes, dizziness, and use-dependent loss of efficacy [331-333]. Hence, it is important to further our understanding of the downstream targets of p38 in the heart in order to identify novel potential targets for therapeutic intervention. The MAPK-activated protein kinases (MKs)-2, -3, and -5 are MKs known to be activated by p38α and p38β. p38 may exertits physiological and/or pathological functions through the selective regulation of MK activity. However, although MK5 was originally identified as p38-regulated and activated kinase (PRAK), it is also activated by the atypical MAPKs ERK3 and ERK4. Moreover, although MK5 is highly expressed in the left ventricle of the heart, its role(s) in cardiac physiology and pathophysiology remain unknown. **The hypothesis of the current study is: MK5 signaling is involved in pathological remodeling in the heart.**

2.2 Objectives

The following objectives were pursued to test the hypothesis:

1- Determineif MK5 is involved in pathological cardiac remodeling induced by chronic pressure overload. These studies employed wild type and MK5 haplodeficient mice ($MK5^{+/-}$).

2- Determine if MK5 is involvedin pathological cardiac remodeling secondary to myocardial ischemia induced by ligation of the left anterior descending coronary artery. These studies employed wild type and MK5 haplodeficient mice ($MK5^{+/-}$).

3- Determine the expression and function of MK5 in ventricular cardiac myocytes and fibroblasts.

3 Article-1

Title: MK5 haplodeficiency attenuates hypertrophy and preserves diastolic function during remodeling induced by chronic pressure overload in the mouse heart.

This article was accepted for publication on 15th of April 2017 and published in *American Journal of Physiology, Heart and Circulatory Physiology* on 1st of July 2017.

Contribution of co-authors

S. A. Nawaito and D. Dingar contributed equally to this work.

Sherin Ali Nawaito: conceived**,** performed the experiments for 8 weeks pressure-overloaded mice, performed transfection of HEK293 cells, isolation of cardiomyocytes and cardiac fibroblasts, performed immunoblotting and qPCR experiments, analyzed the data, interpreted the results, prerformed statistical analysis, prepared the figures, drafted part of manuscript, edited and revised the nanuscript.

Dharmendra Dingar: performed the experiments for 2 weeks pressure-overloaded mice, analyzed the data, interpreted the results and prepared the figures.

Pramod Sahadevan: performed part of the immunoblotting experiments.

Bahira Hussein: assisted in 8 weeks-overloaded mice experiments.

Fatiha Sahmi: assisted in qPCR experiments.

Yanfen Shi: acquired and interpreted the echocardiography data.

Marc-Antoine Gillis: performed the pressure overload surgery in mice.

Matthias Gaestel: developer of the MK5 mice model.

Jean-Claude Tardif: supervised the echocardiography unit and approved the final version of the manuscript.

Bruce G. Allen: conceived and designed the experiments, analyzed the data, interpreted the results, edited the manuscript and approved the final version of the manuscript.

Am J Physiol Heart Circ Physiol 313: H46–H58, 2017.
First published April 21, 2017; doi:10.1152/ajpheart.00597.2016.

RESEARCH ARTICLE *Signaling and Stress Response*

MK5 haplodeficiency attenuates hypertrophy and preserves diastolic function during remodeling induced by chronic pressure overload in the mouse heart

Sherin Ali Nawaito,[1,2]* Dharmendra Dingar,[1,3]* Pramod Sahadevan,[1,3] Bahira Hussein,[1] Fatiha Sahmi,[1] Yanfen Shi,[1] Marc-Antoine Gillis,[1] Matthias Gaestel,[4] Jean-Claude Tardif,[1,5] and Bruce G. Allen[1,2,3,5]

[1]Montreal Heart Institute, Montréal, Québec, Canada; [2]Department of Physiology and Pharmacology, Université de Montréal, Montréal, Québec, Canada; [3]Department of Biochemistry and Molecular Medicine, Université de Montréal, Montréal, Québec, Canada; [4]Institute of Biochemistry, Hannover Medical School, Hannover, Germany; and [5]Department of Medicine, Université de Montréal, Montréal, Québec, Canada

Submitted 30 August 2016; accepted in final form 15 April 2017

* S. A. Nawaito and D. Dingar contributed equally to this work.

Address for reprint requests and other correspondence: B. G. Allen, Mon- treal Heart Institute, 5000 Belanger St., Montréal, Québec, Canada H1T 1C8 (e-mail: bruce.g.allen@umontreal.ca)

3.1 Abstract

MAPK-activated protein kinase-5 (MK5) is a protein serine/threonine kinase that is activated by p38 MAPK and the atypical MAPKs ERK3 and ERK4. The physiological function(s) of MK5 remains unknown. Here, we examined the effect of MK5 haplodeficiency on cardiac function and myocardial remodeling. At 12-wk of age, MK5 haplodeficient mice ($MK5^{+/-}$) were smaller than age-matched wild-type littermates ($MK5^{+/+}$), with similar diastolic function but reduced systolic function. Transverse aortic constriction (TAC) was used to induce a chronic pressure overload in 12-wk-old male $MK5^{+/-}$ and $MK5^{+/+}$ mice. Two weeks post-TAC, heart weight-to-tibia length ratios were similarly increased in $MK5^{+/-}$ and $MK5^{+/+}$ hearts as was the abundance of B-type natriuretic peptide and β-myosin heavy chain mRNA. Left ventricular ejection fraction was reduced in both $MK5^{+/+}$ and $MK5^{+/-}$ mice whereas regional peak systolic tissue velocities were reduced and isovolumetric relaxation time was prolonged in $MK5^{+/+}$hearts, but not in $MK5^{+/-}$ hearts. The TAC-induced increase in collagen type 1-α_1 mRNA observed in $MK5^{+/+}$ hearts was markedly attenuated in $MK5^{+/-}$ hearts. Eight weeks post-TAC, systolic function was equally impaired in $MK5^{+/+}$ and $MK5^{+/-}$ mice. In contrast, the increase in E wave deceleration rate and progression of hypertrophy observed in TAC-$MK5^{+/+}$ mice were attenuated in TAC-$MK5^{+/-}$ mice. MK5 immunoreactivity was detected in adult fibroblasts but not myocytes. $MK5^{+/+}$, $MK5^{+/-}$, and $MK5^{-/-}$ fibroblasts all expressed α-smooth muscle actin in culture. Hence, reduced MK5 expression in cardiac fibroblasts was associated with the attenuation of both hypertrophy and development of restrictive filling pattern during myocardial remodeling in response to chronic pressure overload.

Keywords:

MAPK-activated protein kinase-5; p38-regulated/activated protein kinase; cardiac remodeling; hypertrophy; fibroblast; pressure overload; p38 mitogen-activated protein kinase

New and Noteworthy

MAPK-activated protein kinase-5 (MK5)/p38-regulated/activated protein kinase is a protein serine/threonine kinase activated by p38 MAPK and/or atypical MAPKs ERK3/4. MK5 immunoreactivity was detected in adult ventricular fibroblasts but not myocytes. MK5 haplodefficiency attenuated the progression of hypertrophy, reduced collagen type 1 mRNA, and protected diastolic function in response to chronic pressure overload.

Glossary

ANP, atrial natriuretic peptide; BNP, B-type natriuretic peptides; BW, body weight; COL1A1, collagen type 1 alpha 1; DMSO, dimethylsulfoxide; DN, dominant negative; E, early diastolic transmitral filling velocity; EDT, early diastolic transmitral filling deceleration time; ED rate, early diastolic transmitral filling deceleration rate; Em, peak early diastolic tissue velocity; ERK3, extracellular signal-regulated kinase 3; ERK4, extracellular signal-regulated kinase 4; HW, heart weight; IVRT, isovolumetric relaxation time; LV, left ventricle; FS, Fractional shortening, LVEF, Left ventricular ejection fraction; LVM, left ventricular mass; MAP kinase, mitogen-activated protein kinase; MK2, MAP kinase-activated protein kinase-2; MK3, MAP kinase-activated protein kinase-3; MK5, MAP kinase-activated protein kinase-5; MKK3, MAP kinase kinase 3; MKK6, MAP kinase kinase 6; β-MHC, β-myosin heavy chain; MMP, matrix metalloproteinase; MPI, myocardial performance index; PRAK, p38-regulated/activated protein kinase; Sm, peak systolic tissue velocity; TAC, transverse aortic constriction; TDI, tissue Doppler imaging; TGF- β1, transforming growth factor beta 1; TGF-β3, transforming growth factor beta 3; TL, tibia length.

3.2 Introduction

When faced with a chronic hemodynamic overload, such as imposed by arterial hypertension or myocardial infarction, the heart undergoes a series of adaptive responses that includes molecular remodeling, hypertrophy, fibroblast recruitment and proliferation, interstitial fibrosis, and extracellular matrix remodeling. The purposes of these changes are to 1) generate additional sarcomeres so that the heart can generate additional force to compensate for the increased load, 2) structurally reinforce the myocardium, and 3) distribute contractile force throughout the myocardium. Cardiac hypertrophy, the increase in ventricular mass resulting from an increase in cardiomyocyte size, is the heart's adaptive response to an increase in hemodynamic load arising from either physiological factors, such as exercise, or pathological stress and represents the heart's attempt to maintain cardiac output. Exercise-induced, or physiological, hypertrophy is not associated with interstitial fibrosis and does not progress to heart failure. Chronic pressure overload, on the other hand, induces a compensatory hypertrophy that, if left unchecked, can progress to a decompensated hypertrophy, resulting in contractile dysfunction, arrhythmias, and ultimately heart failure. In contrast to physiological hypertrophy, pressure overload also induces interstitial fibrosis which, in turn, increases both the occurrence of ventricular tachyarrhythmias and the stiffness of myocardium, resulting in diastolic dysfunction (2, 20, 24).

Chronic pressure overload activates MAPKs, including p38 (13). Chronic activation of p38 induces interstitial fibrosis, but not hypertrophy (60). In contrast, acute activation of p38 results in the rapid induction of a severe cardiomyopathy that includes myocyte hypertrophy, interstitial fibrosis, and contractile dysfunction (51). There are four known isoforms of p38 (α, β, δ, and γ), with p38α and p38γ being the most abundant in the heart (9, 12). Downstream of p38α and p38β lie the MAPK-activated protein kinases (MKs): MK2, MK3, and MK5 (41). MK5, originally classified as a p38-regulated/activated protein kinase (PRAK) (32, 33), has been implicated in senescence upon activation of p38 by oncogenic Ras (52). In addition to p38, MK5 is phosphorylated by atypical MAPKs ERK3 and ERK4 (21, 46, 49). However, the physiological role of MK5, as well as its role in p38 and ERK3/4 signaling in vivo, remains unknown. Here, we used heterozygous mice that bear a null allele of MK5 ($MK5^{+/-}$) (50) to study the role of MK5 signaling in pressure overload-induced myocardial remodeling.

Compared with wild-type littermates, the development of a progressive hypertrophy was significantly attenuated in $MK5^{+/-}$ mice. The increase in collagen type 1 $-\alpha_1$ (COL1A1)mRNA levels induced by pressure overload was also reduced in $MK5^{+/-}$ mice. Whereas reduced MK5 expression preserved diastolic function, systolic, function was similarly impaired in both $MK5^{+/+}$ and $MK5^{+/-}$ mice during pressure overload. Interestingly, MK5 immunoreactivity was detected in fibroblasts but not myocytes, suggesting MK5 plays a role the response of cardiac fibroblasts to chronic pressure overload and the subsequent pathological remodeling.

3.3 Material and Methods

Materials

SDS-PAGE reagents, nitrocellulose, and Bradford protein assay reagents were from Bio-Rad Laboratories. Membrane grade Triton X-100, leupeptin, and PMSF were from Roche Molecular Biochemicals. Rabbit anti-collagen type I (no. 203002) was from MD Biosciences. Mouse anti-GAPDH (no. 4300) was from Ambion. Rabbit anti-MK-5 (no. D70A10) was from Cell Signaling Technology. Goat anti-caveolin-3 (no. SC7665) was from Santa Cruz Biotechnology. Rabbit anti-MK-5 phospho-Thr^{182} (no. ab138668) and mouse anti-cardiac troponin T (no. ab8295) were from Abcam Biotechnology Co. Horseradish peroxidase conjugated secondary antibodies were from Jackson ImmunoResearch Laboratories (West Grove, PA). All other reagents were of analytic grade or the best grade available. Primers for quantitative PCR were from Invitrogen. Lysates of human embryonic kidney-293 cells expressing MK5.1-V5 were prepared as previously described (11).

Knockout mice

The MK5 knockout mice used in these experiments have been previouslydescribed (50) and were on a mixed 129/Ola x C57BL background. Twelve- to thirteen-week old male $MK5^{+/+}$ and $MK5^{+/-}$ littermates were used in these experiments (n=18-26). $MK5^{-/-}$ mice show embryonic lethality with incomplete penetrance resulting in only ~ 50% of the expected number of $MK5^{-/-}$ embryos detectable after *embryonic day 12* (E12). Surviving $MK5^{-/-}$ mice fail to reproduce. $MK5^{+/-}$ mice are healthy. All animal experiments were approved by the local ethics committee and performed according to the guidelines of the Canadian Council on Animal Care.

Transverse aortic constriction

Baseline assessments of cardiac structure and function were performed by transthoracic echocardiography (see below). The following day, transverse aortic constriction (TAC) was done as previously described (38) in adult (12-13 wk) male mice anesthetized with isofluorane gas plus buprenorphine (0.05 mg/kg, intraperitoneal injection). A 7-0 silk suture was used to constrict the transverse aorta, between the left and right carotid arteries, around a 27-gauge piece of stainless steel tubing. The suture was knotted and the steel tube removed. The result was a constriction of the transverse aorta of ~ 60%. Sham-operated (sham) animals underwent the identical surgical procedure but the aorta was not constricted. The surgeon was blinded to

the genotype of the mice. Two- and eight-weeks after surgery, assessment by transthoracic echocardiography was repeated. The next day, mice were anesthetized with pentobarbital and *in vivo* cardiac function was assessed using a Millar Mikro-Tip pressure catheter via the right carotid artery. Mice were then euthanized, the hearts were removed, weighed, snap frozen in liquid nitrogen-chilled 2- methyl butane, and stored at -80 °C. Pentobarbital, rather than isoflurane, was always used before sacrifice as isofluorane activates p38 in the mouse heart (data not shown).

Transthoracic echocardiography and calculations

Transthoracic echocardiography was performed on mice, mildly sedated with isofluorane, 1 day before TAC and 1 day before death using a Vivid 7 Dimension ultrasound system (GE Healthcare Ultrasound, Horten, Norway) and i13L probe (10-14 MHz). The aortic arch was visualized in a modified parasternal long-axis view to assess flow at the site of constriction: peak velocity, peak and mean gradient were measured using sample volume enlarged pulsed wave Doppler (PW). The left ventricular (LV) M-mode spectrum was obtained in parasternal short-axis view at the level of papillary muscles. LV dimensions at both end cardiac diastole (LVDd) and systole (LVDs) were measured, the thickness of LV anterior wall (LVAW) and that of LV posterior wall (LVPW) at end cardiac diastole were also measured in this view. LV mass was calculated as follows: $(LVDd + LVAW + LVPW)^3 - (LVDd)^3) \times 1.055$ (29) indexed to body weight (BW). LV fractional shortening (FS) was calculated as follows: (LVDd – LVDs) / LVDd X 100%. To determine LV regional contractility, LV basal lateral and septal peak systolic velocities (S_m) were derived by tissue Doppler imaging (TDI). To study LV diastolic properties, pulsed-wave Doppler was used to evaluate transmitral flow in apical four-chamber view, and peak velocities during early filling (*E*) and atrial filling (*A*) were measured. Mitral annulus movement was recorded by TDI, velocities during early filling (E_m) and atrial filling (A_m) were measured for both lateral and septal annulus, and lateral and septal E/E_m were calculated. LV isovolumetric relaxation time (IVRT) was measured using sample volume enlarged pulsed-wave Doppler at the conjunction of LV inflow and outflow in apical five-chamber view and was corrected ($IVRT_c$) by the square root of R-R interval [IVRT/(RR)1/2] on simultaneously recorded ECG. The time intervals from the end of A_m to the beginning of E_m(b), and from the beginning to the end of Sm (a) were measured in both lateral and septal TDI, and the LV regional myocardial performance index (MPI) was calculated as (b−a)/a

X100% for both basal lateral and basal septal walls. The average of three consecutive cardiac cycles was used for each measurement. Special care was taken to obtain similar imaging planes during preoperative and predeath assessments for each animal. The echocardiographer was blinded to the genotype of the mice.

Histological analysis

Staining and collagen quantification were performed in the histology facility in the laboratory of Dr. Martin Sirois at the Montreal Heart Institute by personnel blinded to the treatment group of the sample. Hearts were embedded in Tissue-Tek OCT. compound (Sakura Finetek USA, Inc.), and transverse cryosections (8 μm) of the ventricles were prepared and stained with Masson's trichrome. Images were taken at X40 using an Olympus BX46 microscope. Collagen content was quantified using Image Pro Plus version 7 (Media Cybernetics) and expressed as a percentage of the surface area. Perivascular collagen was excluded from the measurements. Myocyte diameter was also determined in trichome-stained cryosections using Image Pro Plus.

RNA analysis

Total cellular RNA was isolated from transverse cryosections (14 μm) of the murine ventricular myocardium using RNeasy Micro kits (2-wk TAC, Qiagen) or whole murine ventricles using RNeasy Mini Kits (8-wk TAC, Qiagen) with minor modifications. For samples from the 2-wk TAC group, total RNA was extracted by vortexing 14-μm tissue sections in 300 μl TRIzol reagent (Sigma) for 30 s. After samples had been incubated at ambient temperature for 5 minutes, 60 μl chloroform was added, and samples were again vortexed and maintained at ambient temperature for an additional 2-3 min. After centrifugation for 15 min at 18,300 *g* and 4 °C, the upper aqueous phase was collected and diluted with an equal volume of 70% ethanol, and total RNA was purified on Qiagen columns according to the manufacturer's instructions. Finally, total RNA was eluted with 14 μl of distilled RNase-free water. cDNA synthesis was performed with 11 μl of the isolated total RNA in 20-μl reaction volumes as previouslydescribed (11). Hearts from the 8-wk TAC group were pulverized under liquid nitrogen using a mortar and pestle. Heart powder (20-25 mg) was weighed out and homogenized at room temperature in 300 μl RLT buffer containing 1% (vol/vol) 2-mercaptoethanol using a 2 ml Potter- Elvehjem homogenizer. The homogenate was supplemented with 590 μl RNase-free water and 10 μl proteinase K, vortexed, incubated at 55

°C for 10 min, then centrifuged for 3 min at 4000 rpm and 20 °C. The supernatant (≈ 900 μl) was transferred to a 1.5 ml tube, and RNA was precipitated by adding 0.5 volumes of 100% ethanol, and purified using RNeasy Mini Kits (Qiagen) according to the manufacturer's instructions. RNA was quantified using a NanoDrop ND-1000 spectrophotometer, and only samples having absorbance at 260 nm-to-280-nm ratio greater than 1.8 were used. cDNA synthesis was performed in a 20-μl reaction volume containing 1 μg of total RNA as previouslydescribed (11) Real-time quantitative PCRs reactions were performed as previously described (11). The primers used are shown in Table 1. The amplification efficiency for each primer pair was between 90 and 110%, and the threshold cycles values for all the genes examined in the present study were in the range of 18−25. All samples were normalized to GAPDH, which was amplified in parallel.

Preparation of murine cardiac lysates

Mice were euthanized. Hearts were rapidly removed, snap frozen, and pulverized under, liquid nitrogen. Powdered tissue was resuspended using a 2-ml Potter-Elvehjem tissue grinder (25–30 passes) in 1.2 ml of ice-cold lysis buffer composed 50 mM Tris (pH 7.5 at 4 °C), 20 mM β-glycerophosphate, 20 mM NaF, 5 mM EDTA, 10 mM EGTA, 1.0% Triton X-100, 1 mM Na_3VO_4, 1 μM microcystin LR, 5 mM DTT, 10 μg/ml leupeptin, 0.5 mM PMSF, and 10 mM benzamidine. Homogenates were then cleared of cellular debris by centrifugation for 30 min at 100,000 *g* (48,000 rpm) and 4 °C in a Beckman TLA-100.3 rotor. Finally, supernatants were collected, aliquoted, snap-frozen with liquid nitrogen, and stored at –80 °C. Protein concentrations were determined by micro Bradford assay as previously described (11).

Isolation of cardiac ventricular myocytes

Cardiac ventricular myocytes were isolated from 12-14-wk-old $MK5^{+/+}$ mice (36) and used immediately. Briefly, mice were anesthetized with intraperitoneal injection of a combination of sodium pentobarbital (0.55 mg/kg BW) and heparin (1.0 U/kg BW). Hearts were exposed via sternotomy, rapidly excised, and immersed in ice-cold Tyrode solutioncontaining: 140 mM NaCl, 5.5 mM KCl, 1 mM $MgCl_2$, 0.3 mM KH_2PO_4, 10 mM dextrose, 5 mM HEPES, 2 mM $CaCl_2$, adjusted to pH 7.5 at room temperature with NaOH. Hearts were mounted on an isolated heart perfusion system (Harvard Apparatus) via cannulation of the ascending aorta, and the coronary arteries were perfused at 6 ml/min with modified Tyrode solution (140 mM NaCl, 5.5 mM KCl, 1 mM $MgCl_2$, 0.3 mM NaH_2PO_4, 5

mM HEPES and 10 mM dextrose adjusted to pH 7.5 at room temperature with NaOH) containing 200 μM $CaCl_2$. After 3 minutes of perfusion, the buffer was changed to Ca^{2+}-free Tyrode solution, and perfusion continued for an additional 5 min. Hearts were then enzymatically digested by recirculation with Ca^{2+}-free Tyrode solution containing 0.5 mg/ml collagenase type II for ~ 25 min. When the myocardial tissue had softened, the LV was dissected away from the remainder of the heart and minced into small pieces in Kruftbrühe medium (20 mM KCl, 10 mM KH_2PO_4, 10 mM glucose, 40 mM mannitol, 70 mM L-glutamic acid, 10 mM β- hydroxybutyric acid, 20 mM taurine, 10 mM EGTA and 0.1% albumin; adjusted to pH 7.5 at room temperature with NaOH). To promote cell dissociation, the solution and tissue fragments were gently triturated using a transfer pipette and the suspension was filtered through a 200-μm nylon mesh. Cardiomyocytes were separated from noncardiomyocyte cells by centrifugation three times for 3 min each at 200 *g*. The supernatants from these washing steps were discarded and the final pellet, containing LV myocytes, was used for subsequent experiments. All solutions were constantly aerated with carbogen gas (95% O_2, 5% CO_2), and solutions and cells were maintained at 37 °C throughout the isolation process.

Isolation of cardiac ventricular fibroblasts

Cardiac ventricular fibroblasts were isolated from 12-14-wk-old $MK5^{+/+}$, $MK5^{+/-}$, and $MK5^{-/-}$ mice as previously described (23). Briefly, mice were anesthetized with an intraperitoneal injection of sodium pentobarbital (0.55 mg/kg BW). Hearts were excised and placed in sterile PBS containing 137 mM NaCl, 2.7 mM KCl, 4.2 mM $Na_2HPO_4 \cdot H_2O$, 1.8 mM KH_2PO_4, pH 7.4 at 37 °C. Once the atria were removed, the ventricular tissue was minced into small bits and subjected to a series of digestions in dissociation medium (116.4 mM NaCl, 23.4 mM HEPES, 0.94 mM $NaH_2PO_4.H_2O$, 5.4 mM KCl, 5.5 mM dextrose, 0.4 mM $MgSO_4$, 1 mM $CaCl_2$, 1 mg/ml BSA, 0.5 mg/ml collagenase type IA, 1 mg/ml trypsin, and 0.020 mg/ml pancreatin, pH 7.4). The digestion was aided by gentle agitation of the tissue on an orbital shaker maintained at 37 °C. The digest was centrifuged at 405 *g* for 5 min, and the resulting pellet suspend in 4 ml of medium M199 supplemented with 10% FBS and 2% penicillin-streptomycin, seeded into two 35-mm cell culture dishes, and incubated in a humidified incubator maintained at 37 °C under 5% CO_2. The medium was changed after 150 min to remove unattached cells and debris. Cultures from *passage* 2 were used for the experiments described here.

Immunoblotting

Heart, cardiomyocyte, and cardiac fibroblast lysates were separated by SDS-PAGE, and proteins were electrophoretically transferred to nitrocellulose membranes for 90 min at 50 V in CAPS buffer (10 mM CAPS-NaOH and 10% methanol, pH 11). Membranes were blocked for 2 h at room temperature in Tris-buffered saline (25 mM Tris-HCl and 150 mM NaCl (pH 7.5) at room temperature) containing 1% (vol/vol) Tween 20 (TBST) and 5% (wt/vol) nonfat dried milk (Carnation) and then incubated overnight at 5 °C with the indicated antibodies diluted 1:1,000 in TBST containing 1% (wt/vol) BSA. Filters were then washed three times in TBST and incubated with the appropriate horseradish peroxidase–conjugated secondary antibody (Jackson ImmunoResearch Laboratories) diluted 1:10,000 in TBST containing 5% (wt/vol) nonfat dried milk. Immunoreactive bands were visualized using Western Lightning Plus ECL reagent (PerkinElmer BioSignal., Montreal, QC, Canada) and Kodak BioMax Light film.

Statistical Analysis

The data shown are means ± SE. Two-way ANOVA followed by Bonferroni's multiple-comparison test was performed for statistical comparisons involving two variables (e.g., genotype and TAC) using GraphPad Prism version 6.0h for the Mac OSX (GraphPad Software, La Jolla, CA). For comparisons between two groups, two-tailed *t*-tests were used.*P* values of <0.05 was considered as significant.

3.4 Results

The objective of the present study was to determine the effect(s) of reduced MK5 expression on cardiac function and pathological cardiac remodeling induced by a chronic pressure overload using a genetic model of MK5 haploinsufficient mice (50). Figure 1 shows MK5 immunoreactivity was reduced in hearts from $MK5^{+/-}$ and $MK5^{-/-}$ mice compared with hearts from wild-type littermates. We have previously identified mRNA for four splice variants of MK5 (MK5.2- MK5.5) in the murine ventricular myocardium predicted to translate to proteins of lower molecular mass than MK5.1 (11). Here, immunoblot analysis reveals both a band at 48-kDa, similar to the predicted molecular mass of MK5, and another at 62-kDa (Fig. 1A). The 48-kDa band migrated on 10% acrylamide gels with an electrophoretic mobility similar to that of an MK5.1-V5 fusion protein (Fig. 1B) (11). Both 48- and 62-kDa bands were reduced by ~ 50% in $MK5^{+/-}$ hearts and much more so in hearts from $MK5^{-/-}$ mice (Fig. 1A). It should be noted here that the MK5-deficient mice were created by deleting exon 6 within the catalytic domain, but contain an intact promoter region. The observed reduced immunoreactivity is presumably a consequence of reduced stability. Examination of 12-wk-old male mice revealed that $MK5^{+/-}$ mice were smaller than $MK5^{+/+}$ mice ($MK5^{+/+}$: 25.9±0.5 g n=45; $MK5^{+/-}$; 24.1±0.4 g n=35, $p<0.05$), with similar heart rates, LV wall thickness, LVDs, and diastolic function but reduced LVDd ($MK5^{+/+}$: 4.12±0.05 mm n=45; $MK5^{+/-}$: 3.98±0.05 mm n=35, $p<0.05$) and systolic function [LV ejection fraction (EF) for $MK5^{+/+}$: 73.5±1.2% n=45 $MK5^{+/-}$: 69.0±1.1% n=35, $p<0.01$]. In addition, hearts from 12- wk-old $MK5^{+/-}$ mice have an increased (i.e., less favorable) MPI ($MK5^{+/+}$: 40.8±1.9% n=45; $MK5^{+/-}$: 50.9±2.5% n=35, $p<0.01$) due to an increase in isovolumetric contraction time ($MK5^{+/+}$: 14.0±1.0 ms n=41; $MK5^{+/-}$: 17.9±1.3 ms n=35, $p<0.05$; Table 2). Hence, at 12 wk of age, MK5 haploinsufficient mice show a modest reduction in systolic function.

Hypertrophic responses in $MK5^{+/-}$ mice after TAC

To determine the effects of reduced MK5 expression on cardiac remodeling, 12-wk-old male $MK5^{+/-}$ and $MK5^{+/+}$ littermate mice underwent TAC and were euthanized 2 or 8 wk post-surgery. Direct hemodynamic assessment using a Millar Mikro-Tip pressure catheter showed TAC induced increases in peak systolic arterial pressure and peak LV pressure that did not

differ significantly between TAC-MK5$^{+/+}$ and TAC-MK5$^{+/-}$ groups (Table 3, Fig. 2A) with an average overall increase in peak systolic arterial pressure of 45 mmHg. In addition, echocardiographic imaging of the aortic arch revealed comparable flow velocities at the site of constriction in TAC-MK5$^{+/+}$ and TAC-MK5$^{+/-}$ groups (Table 4). Two weeks post-TAC, heart weight to tibia length ratios (HW/TL) were increased by 20% in MK5$^{+/+}$ (from 73.7±3.4 mg/cm to 88.0±5.4 mg/cm,) and by 26% in MK5$^{+/-}$ mice (70.5±3.8 mg/cm to 89.0±5.1 mg/cm; Fig. 2B). The increased HW/TL ratios in MK5$^{+/+}$ and MK5$^{+/-}$ indicated the development of similar levels of hypertrophy in both groups. Left ventricular mass, determined from echocardiographic imaging, normalized to BW (LV mass/BW) confirmed similar levels of hypertrophy in TAC MK5$^{+/+}$ and TAC-MK5$^{+/-}$ hearts. In TAC-MK5$^{+/+}$ mice, the LV mass/BW increased by 48% (from 4.30±0.17 mg/g to 6.35±0.29 mg/g, $p<0.0001$), and by 34% in TAC-MK5$^{+/-}$ (from 4.31±0.14 mg/g to 5.79±0.20 mg/g, $p<0.001$; Fig. 2C). However, 8 wk post-TAC, HW/TL was increased by 55% in TAC-MK5$^{+/+}$ mice (from 86.2±3.1 mg/cm to 133.3±12.8 mg/cm, $p<0.0001$) and by 46 % in TAC-MK5$^{+/-}$ mice (72.5±2.5 mg/cm to 105.7±7.0 mg/cm, $p<0.01$). HW/TL was significantly lower in TAC-MK5$^{+/-}$ compared with TAC-MK5$^{+/+}$ mice (105.7±7 mg/cm versus 133.3±12.7 mg/cm, $p<0.05$; Fig. 2B). Similarly, echocardiography revealed that LV mass/BW in TAC-MK5$^{+/-}$ mice was significantly lower than TAC-MK5$^{+/+}$ mice (6.19±0.36 mg/g versus 7.43±0.60 mg/g respectively, $p<0.05$; Fig. 2C). The reduced hypertrophy in MK5 haplodeficient mice was also observed at the cellular level upon assessment of myocyte diameter in hearts 8 wk post-TAC (Fig. 2D). Furthermore, a plot of LV mass (from echocardiography, Table 4) versus LV pressure (from Millar, Table 3) yielded a slope of 0.46±0.15 mg/mmHg (n=10, r^2=0.54) for TAC-MK5$^{+/+}$ hearts and -0.15±0.07 mg/mmHg (n=11, r2=0.38) for TAC-MK5$^{+/-}$ hearts (not shown) eight weeks post-TAC indicated the manner 321 in which MK5$^{+/-}$ mice responded to a chronic increase in pressure was distinctly different from that of their wild-type littermates. Hence, although MK5 haploinsufficient mice initially developed LV hypertrophy to an extent similar to wild-type mice in response to chronic pressure overload, the progression of hypertrophy was attenuated in MK5$^{+/-}$ hearts.

Fetal gene expression in MK5$^{+/-}$ mice after TAC

Pathological LV hypertrophy is associated with molecular remodeling that includes the

reexpression of the cardiac fetal genes atrial and B-type natriuretic peptides (ANP, BNP) and β-myosin heavy chain (β-MHC) (3). Hence ANP, BNP, and β-MHC mRNA levels were quantified by quantatitive PCR 2 and 8 wk post-TAC. Chronic pressure overload increased β-MHC, ANP, and BNP mRNA levels in $MK5^{+/+}$ hearts; however, the increase in ANP mRNA in $MK5^{+/-}$ hearts failed to reach significance (Fig. 3). Two weeks post-TAC, ANP RNA levels in TAC-$MK5^{+/-}$ hearts were significantly lower than those in TAC-$MK5^{+/+}$ hearts ($p<0.05$, Fig. 3A). TAC increased β-MHC mRNA in both $MK5^{+/-}$ and $MK5^{+/+}$ hearts 2 wk post-TAC; however, β-MHC mRNA levels had returned to near sham levels by 8 wk post-TAC in $MK5^{+/-}$ hearts, whereas they remained elevated in $MK5^{+/+}$ hearts (Fig. 3C). Eight weeks post- TAC, β-MHC RNA levels in TAC-$MK5^{+/-}$ hearts were significantly lower than those in TAC $MK5^{+/+}$ hearts ($p<0.01$). There were no significant differences in ANP, BNP, and β-MHC mRNA levels between sham-$MK5^{+/-}$ and sham-$MK5^{+/+}$ hearts. Thus, although MK5 haploinsufficiency did not prevent molecular remodeling in response to pressure overload, the profile of fetal gene reexpression was altered.

Echocardiographic characterization of $MK5^{+/-}$ mice after TAC

Ventricular structure and function was assessed by echocardiography. LVDd was reduced in 12-wk-old $MK5^{+/-}$ mice (Table 2); although these differences did not reach significance in the 2 wk-TAC groups, in the 8 wk-TAC groups LVDd was significantly reduced in $MK5^{+/-}$ mice compared to $MK5^{+/+}$ mice in both sham and TAC groups (Table 4). In contrast, LVSd, which did not differ significantly between $MK5^{+/-}$ mice and $MK5^{+/+}$ littermates at 12 wk of age (Table 2), increased in response to pressure overload (Table 4); however, the increase in LVDs was significantly less in TAC $MK5^{+/-}$ mice than in TAC-$MK5^{+/+}$ mice 8 wk post-TAC (3.29±0.12 mm versus 3.67±0.23 mm, $p<0.05$). As mentioned above, at 12 wk of age, MK5 haplodeficient mice displayed a modest reduction in systolic function (Table 2); however, differences in LV EF or LV FS were not observed at 14 wk (Table 4, 2-wk sham) or 20 wk (Table 4, 8-wk sham) of age. LV FS and LV EF were similarly reduced in $MK5^{+/+}$ and $MK5^{+/-}$ mice following 2 and 8 wk of pressure overload (Table 4, Figure 4A). TDI was used to determine S_m and E_m of the basal segments of the interventricular septum and lateral LV wall. After 2 wk of pressure overload, lateral- and septal-S_m were significantly reduced in $MK5^{+/+}$ but not $MK5^{+/-}$ hearts (Table 4). Furthermore, IVRTs (Fig. 4B) were prolonged in TAC-$MK5^{+/+}$

but not TAC MK5$^{+/-}$ hearts. As observed in 12-wk-old mice (Table 2), at 2-wk post-TAC the MPI for MK5$^{+/-}$ mice was higher than that for the MK5$^{+/+}$ mice (Fig. 4D and Table 4). Hence, hearts from MK5$^{+/-}$ mice maintained diastolic function during chronic pressure overload compared with MK5$^{+/+}$ littermates. After 8 wk of chronic pressure overload, lateral S_m was significantly reduced in MK5$^{+/+}$ and MK5$^{+/-}$ hearts. Septal S_m was also reduced in MK5$^{+/+}$ and MK5$^{+/-}$ hearts, but the change failed to reach significance. Furthermore, 8-wk post-TAC, IVRTs in TAC mice did not differ significantly from those in sham-operated mice (Fig. 4B). Alternatively, the E wave deceleration rate, which was increased in TAC-MK5$^{+/+}$ mice at both 2 and 8 wk (Fig. 4C, Table 4), was significantly lower in TAC-MK5$^{+/-}$ than TAC-MK5$^{+/+}$ hearts 8 wk post-TAC (31.4±2.3 m/s2 versus 41.1±3.1 m/s2, $p<0.05$). There were no significant differences in MPI 8 wk post-TAC (Fig. 4D). Hence, in response to chronic pressure overload, both MK5$^{+/+}$ and MK5$^{+/-}$ mice developed a reduced systolic function whereas MK5$^{+/+}$ mice showed a more restrictive cardiac filling pattern in response to TAC.

Fibrosis in MK5$^{+/-}$ hearts following TAC

In addition to LV hypertrophy and molecular remodeling, chronic pressure overload induces interstitial fibrosis. Collagen type 1 accounts for ~ 85% of the total collagen content of the heart. Consequently, COL1A1 mRNA levels were measured by qPCR and found to increase as a result of pressure overload (Fig. 5A). Two weeks post-TAC the increase in COL1A1 mRNA was reduced by 50% in MK5$^{+/-}$ hearts compared with MK5$^{+/+}$ hearts. Eight weeks post-TAC, although variable, COL1A1 mRNA levels in TAC hearts appeared to be returning to levels similar to those in sham-operated mice. No significant difference was observed in COL1A1 mRNA levels between sham-MK5$^{+/+}$ and sham-MK5$^{+/-}$ hearts. Hence, collagen accumulation was examined in cryosections of the ventricular myocardium by Masson trichrome staining. Two (Data not shown) and eight (Fig. 5, B and C) weeks of pressure overload resulted in negligible increases in collagen deposition in TAC-MK5$^{+/+}$ and TAC-MK5$^{+/-}$ hearts. No genotype-dependent differences in collagen deposition were observed in sham hearts. After constriction of the transverse aorta, pressure in the right carotid artery is elevated (Table 3) (38) and perivascular fibrosis develops. After TAC, we observed fibrosis of the right carotid artery in MK5$^{+/+}$ but not MK5$^{+/-}$ mice (Data not shown).

Assessment of transforming growth factor-β expression in MK5$^{+/-}$ mice post-TAC

Members of the tissue growth factor (TGF)-β family are mediators of fibroblast activation, with TGF-β1 serving a major role in pathological fibrosis (see (25, 55)). TGF-β1 has also been shown to mediate cardiomyocyte hypertrophy (45). Furthermore, hypertrophy induced by aortic banding or phenylephrine infusion is associated with increased TGF-β1 mRNA (53, 56) as is myocardial infarction (54), genetically determined hypertrophy (43), and idiopathic hypertrophic cardiomyopathy (26). To determine if the induction of TGF-β expression in response to pressure overload is altered in MK5 haplodeficient mice, we assessed TGF-β1 and TGF-β3 mRNA levels by quantitative PCR in total RNA from sham and TAC hearts (Fig. 6). TGF-β1 and TGF-β3 mRNA levels showed only modest increases in both MK5$^{+/+}$ and MK5$^{+/-}$ hearts 2 wk post- TAC. By 8 wk postsurgery the TAC-induced increase in TGF-β3 mRNA had reached significance in MK5$^{+/+}$ hearts (Fig. 6B). However, in general there was no correlation between changes in the abundance of COL1A1 mRNA and changes in TGF-β mRNA.

Expression of MK5 in heart cells

MK5 immunoreactivity was detected in lysates prepared from whole mouse heart (Fig. 1, A and B). As the ability of a chronic pressure overload to both induce hypertrophy and increase COL1A1 mRNA levels was attenuated in hearts from MK5$^{+/-}$ mice, we sought to verify that MK5 is expressed in both ventricular myocytes and fibroblasts. Ventricular myocytes and fibroblasts were isolated from adult mouse hearts, lysates prepared and resolved by SDS-PAGE, and the presence of MK5 immunoreactivity determined by immunoblot analysis. Surprisingly, MK5 immunoreactivity was detected in fibroblasts but not in myocytes (Fig. 7A). We previously reported that 1 wk after surgery the abundance of MK5 mRNA in TAC and sham mouse ventricular myocardium did not differ significantly (11). Figure 7B shows that the abundance of MK5 immunoreactivity in hearts from either MK5$^{+/+}$ or MK5$^{+/-}$ mice was not affected by 8 wk of TAC. As mentioned above, the line of mice used in this study have roughly a 50% reduction in MK5, and MK5 is able to bind several other signaling proteins including p38, ERK3 and ERK4; hence, the phenotype may result from a reduction in activatable MK5 or a reduction in MK5 as a molecular scaffold. We attempted to determine if MK5 was activated during TAC using an anti-MK5 phospho-Thr^{182}, which reports on the

phosphorylation status of MK5 at the activating Thr residue. Unfortunately, the antibody revealed numerous nonspecific bands in heart lysates from sham and TAC hearts (not shown).

To determine if reduced levels of MK5 impaired the phenoconversion of fibroblasts into myofibroblasts, α-smooth muscle actin expression was examined. When ventricular fibroblasts were isolated from $MK5^{+/+}$, $MK5^{+/-}$, and $MK5^{-/-}$ mice, and maintained in culture for 6 days, no genotype-specific differences in the abundance of α-smooth muscle actin immunoreactivity were detected by immunoblot analysis (Fig. 7C). Hence, the cardiac phenotype observed in MK5 haplodeficient mice reflects the role of this protein serine/threonine kinase in modulating fibroblast function; however, MK5 is not required for fibroblast differentiation.

3.5 Discussion

In vitro and in vivo studies have suggested the involvement of MK5 downstream of p38 MAPK (31-33, 48, 52), although the biological role of MK5 remains unknown. We show here that 12-wk-old MK5 haploinsufficient mice were 6-7% smaller than age- and sex-matched wild-type littermates and showed normal LV diastolic function but reduced systolic LV function (4.5% decrease in EF). In response to chronic pressure overload, hearts from $MK5^{+/-}$ mice reexpressed fetal genes (e.g., ANP, BNP, β-MHC) and hypertrophied. However, the profile of fetal gene expression evoked by TAC differed from wild-type mice and hearts from $MK5^{+/-}$ mice showed significantly less hypertrophy 8 wk post-TAC than hearts from $MK5^{+/+}$ mice. Furthermore, the increase in COL1A1 mRNA induced by chronic pressure overload was attenuated in $MK5^{+/-}$ mice compared with $MK5^{+/+}$ littermates. Finally, whereas $MK5^{+/+}$ hearts developed a more restrictive filling pattern in response to TAC, $MK5^{+/-}$ hearts did not. These results suggest that MK5 could mediate the function of both ventricular fibroblasts and myocytes; however, MK5 immunoreactivity was detected in fibroblasts but not myocytes, suggesting a role for MK5 in paracrine regulation of myocyte function by fibroblasts. MK5 may mediate at least some of the pathological remodeling associated with p38 activation in the heart; however, MK5 is also regulated by, and remains one of the few known physiological substrate for, atypical MAPKs ERK3 and ERK4 (1, 21, 46, 49). In the murine heart, MK5 associates with ERK3, but not ERK4 or p38α (11). Several signaling pathways are activated in cardiac tissues in response to pressure overload, including MAPK pathways, calcineurin-nuclear factor of activated T cells (NFAT), and the phosphatidylinositol 3-kinase (PI3K)/protein kinase B (PKB) pathway (18). Seven distinct MAPK pathways have been identified in mammals: ERK1/2, ERK3/4, ERK5, ERK7, JNKs, p38 MAPKs (α, β, δ, and γ), and Nemo-like kinase (NLK) (8). Pressure overload activates p38α and p38β and causes the accumulation of p38γ in the nucleus (12, 57). Transfecting of neonatal myocytes with activated mutants of MAPKK 6b (MKK6b) or MKK3b, upstream activators of p38α and p38β, evokes changes characteristic of the hypertrophic phenotype and apoptosis, respectively (57). In the intact heart, the situation is more complicated. Chronic inhibition of p38 signaling, using cardiac-directed expression of dominant negative (DN)- p38α, DN-p38β, DN-MKK3, or DN-MKK6, facilitates cardiac hypertrophy and expression of fetal genes (ANP and BNP), but not

fibrosis, in response to pressure overload (6, 60) or infusion of ANG II, isoproterenol, or phenylephrine (6). In addition, cardiac-specific expression of constitutively active MKK3bE or MKK6bE results in cardiac fibrosis and both systolic and diastolic dysfunction, but not hypertrophy (28) in some cases but hypertrophy in others (14). Expression of an activated form of TGF-β-activated kinase (TAK1) in heart results in p38 activation associated with hypertrophy (59). Cardiac-specific $p38\alpha^{-/-}$ mice exhibit hypertrophy in response to aortic banding, but also show cardiac dysfunction and dilation accompanied by massive fibrosis and myocyte apoptosis (34). One explanation for the differences observed using in vivo models is that the chronic nature of the modification in p38 signaling used in these models may interfere with other aspects of intracellular signaling or induce compensatory mechanisms. The role of p38 in hypertrophy may depend upon the nature and/or duration of the hypertrophic stimulus (27, 34, 35) as the nature and intensity of the stimuli have been shown to alter which p38 isoforms become activated (37). Consistent with this, acute activation of p38α, induced by the conditional and myocyte-specific expression of MKK3bEE, in the adult mouse heart results in the rapid onset of a severe cardiomyopathy involving hypertrophy, interstitial fibrosis and impaired cardiac function (51). In addition, mice lacking the p38α/β target MK2 do not develop diabetic cardiomyopathy in a murine model of type 2 diabetes (42). Hence, inhibition of p38 would be a desirable pharmacological intervention in the treatment of cardiovascular disease. However, clinical trials of p38 inhibitors have revealed adverse effects including hepatotoxicity, skin rash and dizziness as well as loss of efficacy during chronic inhibition (30, 58). In addition, as the means whereby p38 mediates deleterious effects upon cardiac structure and function remains largely unknown, a better understanding of the roles and regulation of downstream targets of p38, including MK2/3 and MK5, is an important step towards both understanding the role of p38 signaling in cardiomyopathies and the development of more selective therapies.

Chronic pressure overload induces cardiac fibroblast proliferation, increased interstitial fibrosis, and remodeling of the extracellular matrix (10). Cardiac interstitial fibrosis can result from either enhanced collagen deposition or reduced degradation. Collagen type I and type III are the major components of the cardiac extracellular matrix with collagen type 1 comprising ~85% of total collagen in the heart and hence representing a major determinant for myocardial stiffness (4, 17). In $MK5^{+/-}$ hearts, there was a significant reduction in the ability of pressure

overload to increase COL1A1 mRNA synthesis and/or stability. TGF-β is a cytokine, expressed in both myocytes and fibroblasts, which acts upon receptors that are also expressed in both cell types. In ventricular myocytes, TGF-β induces molecular remodeling and hypertrophy (40) whereas in fibroblasts it induces proliferation, differentiation to myofibroblasts, and production of extracellular matrix proteins including collagen, fibronectin, and proteoglycans (39). TGF-β also reduces extracellular matrix breakdown by both inhibiting matrix metalloproteinase expression and by inducing the synthesis of matrix metalloproteinase inhibitors, such as plasminogen activator inhibitor-1 and tissue inhibitors of metalloproteinases (44). In rats, aortic banding evokes an increase in myocardial TGF-β mRNA (7, 53, 56) within 12 h of aortic banding that has decreased to near control levels within 2 wk (56). In the present study, where TGF-β mRNA was assessed after 2 and 8 wk of chronic pressure overload, no persistent increase in TGF-β1 mRNA was detected in TAC $MK5^{+/-}$ mice. Furthermore, the increase in TGF-β1 mRNA observed in rats after aortic banding occurred in cardiomyocytes but not nonmyocytes (7, 53) whereas we detected MK5 immunoreactivity in fibroblasts but not myocytes suggesting a role for MK5 in fibroblast function. The only significant difference in TGF-β mRNA levels observed in the present study was an increase in TGF-β3 mRNA in $MK5^{+/+}$, but not $MK5^{+/-}$, hearts 8 wk post-TAC. Very little is currently known regarding the role of TGF-β3 in cardiac remodeling; however, a TGF-β3 polymorphism is associated with changes LV geometry in hypertensive patients (19). β-Adrenergic receptor signaling has been implicated downstream of TGF-β1 and the catalytic subunit of PKA has been recently shown to phosphorylate MK5, resulting in its activation and translocation out of the nucleus (15, 22). However, as β1-adrenergic receptor blockade in mice overexpressing TGF-β1 is antihypertrophic but not antifibrotic (47), whereas MK5 haploinsufficiency attenuated the TAC- induced increase in COL1A1 mRNA it is unlikely that MK5 haploinsufficiency is preventing fibrosis by attenuating TGF-β1/β-adrenergic receptor signaling in the heart. Further study will be required to determine the exact role(s) MK5 plays in the fibrotic response induced by chronic pressure overload.

Potential Limitation

Although the line of mice used in this study hypertrophied in response to TAC, and COL1A1 mRNA was increased, they showed very little fibrosis. This may have been a characteristic of

their being on a mixed 129/Ola x C57BL background. Attempts to backcross onto a C57BL/6 background were not successful (Sylvain Meloche, Université de Montréal, Personal Communication). The genetic modification used to generate these mice reduced the total amount of MK5 protein, not just the amount of activatable MK5. As MK5 has been shown to form complexes with several signaling proteins, including p38 MAPK (32, 48), ERK3 (11, 46), ERK4 (1, 21), Cdc14A (16), kalirin-7 (5) and septins 7 and 8 (5) it is not clear at present if the cardiac phenotype we observed was a result of reduced MK5 activity per se or alterations in protein-protein interactions resulting from a reduction in MK5 as a molecular scaffold. Differences in systolic function in the form of reduced LV EF and LV FS observed in MK5 haplodeficient mice at 12 wk of age were not observed in the sham mice postsurgery but were observed in both the TAC-MK5$^{+/+}$ and TAC MK5$^{+/-}$ mice showed reduced systolic function when compared to their respective sham groups. As the sham groups had undergone major surgery, verification of these observations would require further study in the form of a longitudinal study to determine if this was an effect of aging versus surgery upon systolic function in the sham groups.

3.6 Conclusions

Here, we showed that MK5$^{+/-}$ mice have reduced EF at 12 wk of age. Although MK5$^{+/-}$ hearts hypertrophied in response to chronic pressure overload, the progression of hypertrophic growth was significantly attenuated 8 wk post-TAC. Two-weeks post-TAC, the increase in COL1A1 mRNA level was significantly lower in TAC-MK5$^{+/-}$ hearts compared with TAC-MK5$^{+/+}$ hearts. TAC-MK5$^{+/-}$ did not develop the restrictive filling pattern observed inTAC-MK5$^{+/+}$ hearts. In contrast, systolic function was similarly reduced in both TAC-MK5$^{+/+}$ and TAC-MK5$^{+/-}$ mice. That MK5 immunoreactivity was only detected in cardiac fibroblasts suggests that MK5 plays a role in the cardiac fibroblast response to chronic pressure overload and the reduced hypertrophy was a consequence of alterations in paracrine signaling or direct fibroblast-myocyte coupling. Our findings reveal a novel role for MK5 during the pathological cardiac remodeling induced by chronic pressure overload and suggest it may mediate some of the pathological effects of p38 activation. However, atypical MAPKs ERK3 and ERK4 also activate MK5 and the role of these kinases in cardiac pathophysiology remains to be determined.

Acknowledgements

We thank. Karine Bouthillier and Kim Levesque for animal care and breeding, and George Vaniotis for critical reading of the manuscript.

Grants

This work was supported by Canadian Institutes of Health Research Grant MOP-77791, Heart and Stroke Foundation of Canada Grant G-14-0006060, and the Montreal Heart Institute Foundation to (B.Allen). S.Nawaito was supported by the Faculty of Graduate and Postdoctoral Studies of the Université de Montreal and The Egyptian Supreme Council of Universities. B. Allen was a New Investigator of the Heart and Stroke Foundation of Canada and Senior Scholar of the Fondation de la Recherche en Santé du Québec. J. Tardif holds the Université de Montréal Pfizer endowed research chair in atherosclerosis.

Disclosures

No conflicts of interest, financial or otherwise, are declared by the author(s).

Author contributions

S.N., D.D., P.S., B.H., F.S., Y.S., and M.-A.G. performed experiments;S.N., D.D., P.S., Y.S., J.-C.T., and B.G.A. analyzed data; S.N., D.D., Y.S.,J.-C.T., and B.G.A. interpreted results of experiments; S.N., D.D., P.S., and B.G.A. prepared figures; S.N., D.D., and B.G.A. drafted manuscript; S.N.,D.D., M.G., and B.G.A. edited and revised manuscript; S.N., D.D., P.S., and B.G.A. approved final version of manuscript; B.G.A. conceived and designed research.

3.7 References

1. Aberg E, Perander M, Johansen B, Julien C, Meloche S, Keyse SM, and Seternes OM. Regulation of MAPK-activated protein kinase 5 activity and subcellular localization by the atypical MAPK ERK4/MAPK4. J Biol Chem 281: 35499-35510, 2006.

2. Adabag AS, Maron BJ, Appelbaum E, Harrigan CJ, Buros JL, Gibson CM, Lesser JR, Hanna CA, Udelson JE, Manning WJ, and Maron MS. Occurrence and frequency of arrhythmias in hypertrophic cardiomyopathy in relation to delayed enhancement on cardiovascular magnetic resonance. J Am Coll Cardiol 51: 1369-1374, 2008.

3. Akashi YJ, Springer J, Lainscak M, and Anker SD. Atrial natriuretic peptide and related peptides. Clin Chem Lab Med 45: 1259-1267, 2007.

4. Berg TJ, Snorgaard O, Faber J, Torjesen PA, Hildebrandt P, Mehlsen J, and Hanssen KF. Serum levels of advanced glycation end products are associated with left ventricular diastolic function in patients with type 1 diabetes. Diabetes Care 22: 1186-1190, 1999.

5. Brand F, Schumacher S, Kant S, Menon MB, Simon R, Turgeon B, Britsch S, Meloche S, Gaestel M, and Kotlyarov A. The extracellular signal-regulated kinase 3 (mitogen activated protein kinase 6 [MAPK6])-MAPK-activated protein kinase 5 signaling complex regulates septin function and dendrite morphology. Mol Cell Biol 32: 2467-2478, 2012.

6. Braz JC, Bueno OF, Liang Q, Wilkins BJ, Dai Y-S, Parsons S, Braunwart J, Glascock BJ, Klevistsky R, Kimball TF, Hewett TE, and Molkentin JD. Targeted inhibition of p38 MAPK promotes hypertrophic cardiomyopathy through upregulation of calcineurin-NFAT signaling. J Clin Invest 111: 1475-1486, 2003.

7. Calderone A, Takahashi N, Izzo NJ, Jr., Thaik CM, and Colucci WS. Pressure- and2 volume-induced left ventricular hypertrophies are associated with distinct myocyte phenotypes and differential induction of peptide growth factor mRNAs. Circulation 92: 2385-2390, 1995.

8. Coulombe P, and Meloche S. Atypical mitogen-activated protein kinases: structure, regulation and functions. Biochim Biophys Acta 1773: 1376-1387, 2007.

9. Court NW, dos Remedios CG, Cordell J, and Bogoyevitch MA. Cardiac expression and subcellular localization of the p38 mitogen-activated protein kinase member, stress-activated protein kinase-3 (SAPK3). J Mol Cell Cardiol 34: 413-426, 2002.

10. Creemers EE, and Pinto YM. Molecular mechanisms that control interstitial fibrosis in the

pressure-overloaded heart. Cardiovasc Res 89: 265-272, 2011.

11. Dingar D, Benoit MJ, Mamarbachi AM, Villeneuve LR, Gillis MA, Grandy S, Gaestel M, Fiset C, and Allen BG. Characterization of the expression and regulation of MK5 in the murine ventricular myocardium. Cell Signal 22: 1063–1075, 2010.

12. Dingar D, Merlen C, Grandy S, Gillis MA, Villeneuve LR, Mamarbachi AM, Fiset C,and Allen BG. Effect of pressure overload-induced hypertrophy on the expression and localization of p38 MAP kinase isoforms in the mouse heart. Cell Signal 22: 1634-1644, 2010.

13. Esposito G, Prasad SVN, Rapacciuolo A, Mao L, Koch WJ, and Rockman HA. Cardiac overexpression of a Gq inhibitor blocks induction of extracellular signal–regulated kinase and c-Jun NH2-terminal kinase activity in in vivo pressure overload. Circulation 103: 1453-1458, 2001.

14. Fernando P, Ding W, Pekalska B, Derepentigny Y, Kothary R, Kelly JF, and Megeney LA. Active kinase proteome screening reveals novel signal complexity in cardiomyopathy. Mol Cell Proteomics 4: 673-682, 2005.

15. Gerits N, Mikalsen T, Kostenko S, Shiryaev A, Johannessen M, and Moens U. Modulation of F-actin rearrangement by the cyclic AMP/cAMP-dependent protein kinase (PKA) pathway is mediated by MAPK-activated protein kinase 5 and requires PKA-induced nuclear export of MK5. J Biol Chem 282: 37232-37243, 2007.

16. Hansen CA, Bartek J, and Jensen S. A functional link between the human cell cycle regulatory phosphatase Cdc14A and the atypical mitogen-activated kinase Erk3. Cell Cycle 7: 325-334, 2008.

17. Heeneman S, Cleutjens JP, Faber BC, Creemers EE, van Suylen RJ, Lutgens E, Cleutjens KB, and Daemen MJ. The dynamic extracellular matrix: intervention strategies during heart failure and atherosclerosis. J Pathol 200: 516-525, 2003.

18. Heineke J, and Molkentin JD. Regulation of cardiac hypertrophy by intracellular signalling pathways. Nat Rev Mol Cell Biol 7: 589-600, 2006.

19. Hu BC, Li L, Sun RH, Gao PJ, Zhu DL, Wang JG, and Chu SL. The association between transforming growth factor beta3 polymorphisms and left ventricular structure in hypertensive subjects. Clin Chim Acta 411: 558-562, 2010.

20. Kai H, Kuwahara F, Tokuda K, and Imaizumi T. Diastolic dysfunction in hypertensive hearts: roles of perivascular inflammation and reactive myocardial fibrosis. Hypertens Res 28:

483-490, 2005.

21. Kant S, Schumacher S, Singh MK, Kispert A, Kotlyarov A, and Gaestel M. Characterization of the atypical MAPK ERK4 and its activation of the MAPK-activated protein kinase MK5. J Biol Chem 281: 35511-35519, 2006.

22. Kostenko S, Shiryaev A, Gerits N, Dumitriu G, Klenow H, Johannessen M, and6 Moens U. Serine residue 115 of MAPK-activated protein kinase MK5 is crucial for its PKA regulated nuclear export and biological function. Cell Mol Life Sci 68: 847-862, 2011.

23. Kumaran C, and Shivakumar K. Calcium- and superoxide anion-mediated mitogenic action of substance P on cardiac fibroblasts. Am J Physiol Heart Circ Physiol 282: H1855-1862, 2002.

24. Kuwahara F, Kai H, Tokuda K, Kai M, Takeshita A, Egashira K, and Imaizumi T. Transforming growth factor-beta function blocking prevents myocardial fibrosis and diastolic dysfunction in pressure-overloaded rats. Circulation 106: 130-135, 2002.

25. Leask A, and Abraham DJ. TGF-beta signaling and the fibrotic response. Faseb J 18: 816-827, 2004.

26. Li RK, Li G, Mickle DA, Weisel RD, Merante F, Luss H, Rao V, Christakis GT, and Williams WG. Overexpression of transforming growth factor-β1 and insulin-like growth factor-I in patients with idiopathic hypertrophic cardiomyopathy. Circulation 96: 874-881, 1997.

27. Liang Q, and Molkentin JD. Redefining the roles of p38 and JNK signaling in cardiac hypertrophy: dichotomy between cultured myocytes and animal models. J Mol Cell Cardiol 35: 1385-1394, 2003.

28. Liao P, Georgakopoulos D, Kovacs A, Zheng M, Lerner D, Pu H, Saffitz J, Chien K, Xiao RP, Kass DA, and Wang Y. The in vivo role of p38 MAP kinases in cardiac remodeling and restrictive cardiomyopathy. Proc Natl Acad Sci U S A 98: 12283-12288, 2001.

29. Liao Y, Ishikura F, Beppu S, Asakura M, Takashima S, Asanuma H, Sanada S, Kim6 J, Ogita H, Kuzuya T, Node K, Kitakaze M, and Hori M. Echocardiographic assessment of LV hypertrophy and function in aortic-banded mice: necropsy validation. Am J Physiol Heart Circ Physiol 282: H1703-H1708, 2002.

30. Marber MS, Rose B, and Wang Y. The p38 mitogen-activated protein kinase pathway-A potential target for intervention in infarction, hypertrophy, and heart failure. J Mol Cell Cardiol doi:10.1016/j.yjmcc.2010.1010.1021, 2010.

31. New L, Jiang Y, and Han J. Regulation of PRAK subcellular location by p38 MAP kinases. Mol Biol Cell 14: 2603-2616, 2003.

32. New L, Jiang Y, Zhao M, Liu K, Zhu W, Flood LJ, Kato Y, Parry GCN, and Han J.5 PRAK, a novel protein kinase regulated by the p38 MAP kinase. EMBO J 17: 3372-3384, 1998.

33. Ni H, Wang XS, Diener K, and Yao Z. MAPKAPK5, a novel mitogen-activated protein kinase (MAPK)-activated protein kinase, is a substrate of the extracellular-regulated kinase (ERK) and p38 kinase. Biochem Biophys Res Commun 243: 492-496, 1998.

34. Nishida K, Yamaguchi O, Hirotani S, Hikoso S, Higuchi Y, Watanabe T, Takeda T, Osuka S, Morita T, Kondoh G, Uno Y, Kashiwase K, Taniike M, Nakai A, Matsumura Y, Miyazaki J, Sudo T, Hongo K, Kusakari Y, Kurihara S, Chien KR, Takeda J, Hori M, and Otsu K. p38α mitogen-activated protein kinase plays a critical role in cardiomyocyte survival but not in cardiac hypertrophic growth in response to pressure overload. Mol Cell Biol 24: 10611- 10620, 2004.

35. Petrich BG, and Wang Y. Stress-activated MAP kinases in cardiac remodeling and heart failure: New insights from transgenic studies. Trends Cardiovasc Med 14: 50-55, 2004.

36. Quang KL, Maguy A, Qi XY, Naud P, Xiong F, Tadevosyan A, Shi YF, Chartier D, Tardif JC, Dobrev D, and Nattel S. Loss of cardiomyocyte integrin-linked kinase produces an arrhythmogenic cardiomyopathy in mice. Circ Arrhythm Electrophysiol 8: 921-932, 2015.

37. Remy G, Risco AM, Inesta-Vaquera FA, Gonzalez-Teran B, Sabio G, Davis RJ, and Cuenda A. Differential activation of p38MAPK isoforms by MKK6 and MKK3. Cell Signal 22: 660-667, 2010.

38. Rockman HA, Ross RS, Harris AN, Knowlton KU, Steinhelper ME, Field LJ, Ross J, Jr., and Chien KR. Segregation of atrial-specific and inducible expression of an atrial natriuretic 5 factor transgene in an in vivo murine model of cardiac hypertrophy. Proc Nat Acad Sci USA 88: 8277-8281, 1991.

39. Rosenkranz S. TGF-beta1 and angiotensin networking in cardiac remodeling. Cardiovasc Res 63: 423-432, 2004.

40. Rosenkranz S, Flesch M, Amann K, Haeuseler C, Kilter 679 H, Seeland U, Schluter KD, and Bohm M. Alterations of beta-adrenergic signaling and cardiac hypertrophy in transgenic mice overexpressing TGF-beta (1). Am J Physiol 283: H1253-H1262, 2002.

41. Roux PP, and Blenis J. ERK and p38 MAPK-activated protein kinases: a family of protein kinases with diverse biological functions. Microbiol Mol Biol Rev 68: 320-344, 2004.

42. Ruiz M, Coderre L, Lachance D, Houde V, Martel C, Legault JT, Gillis MA, Bouchard B, Daneault C, Carpentier AC, Gaestel M, Allen BG, and Rosiers CD. MK2 Deletion In Mice Prevents Diabetes-Induced Perturbations In Lipid Metabolism And Cardiac Dysfunction. Diabetes 65: 381-392, 2016.

43. Sakata Y. Tissue factors contributing to cardiac hypertrophy in cardiomyopathic hamsters (BIO14.6): involvement of transforming growth factor-beta 1 and tissue renin-angiotensin system in the progression of cardiac hypertrophy. Hokkaido Igaku Zasshi 68: 18-28, 1993.

44. Schiller M, Javelaud D, and Mauviel A. TGF-beta-induced SMAD signaling and gene regulation: consequences for extracellular matrix remodeling and wound healing. J Dermatol Sci 35: 83-92, 2004.

45. Schultz Jel J, Witt SA, Glascock BJ, Nieman ML, Reiser PJ, Nix SL, Kimball TR,and Doetschman T. TGF-beta1 mediates the hypertrophic cardiomyocyte growth induced by angiotensin II. J Clin Invest 109: 787-796, 2002.

46. Schumacher S, Laass K, Kant S, Shi Y, Visel A, Gruber AD, Kotlyarov A, and Gaestel M. Scaffolding by ERK3 regulates MK5 in development. EMBO J 23: 4770-4779, 2004.

47. Seeland U, Schaffer A, Selejan S, Hohl M, Reil JC, Muller P, Rosenkranz S, and Bohm M. Effects of AT1- and beta-adrenergic receptor antagonists on TGF-beta1-induced fibrosis in transgenic mice. Eur J Clin Invest 39: 851-985, 2009.

48. Seternes OM, Johansen B, Hegge B, Johannessen M, Keyse SM, and Moens U. Both binding and activation of p38 mitogen-activated protein kinase (MAPK) play essential roles in regulation of the nucleocytoplasmic distribution of MAPK-activated protein kinase 5 by cellular stress. Mol Cell Biol 22: 6931-6945, 2002.

49. Seternes OM, Mikalsen T, Johansen B, Michaelsen E, Armstrong CG, Morrice NA, Turgeon B, Meloche S, Moens U, and Keyse SM. Activation of MK5/PRAK by the atypical MAP kinase ERK3 defines a novel signal transduction pathway. EMBO J 23: 4780-4791, 2004.

50. Shi Y, Kotlyarov A, Laaβ K, Gruber AD, Butt E, Marcus K, Meyer HE, Friedrich A, Volk HD, and Gaestel M. Elimination of protein kinase MK5/PRAK activity by targeted homologous recombination.Mol Cell Biol 23: 7732-7741, 2003. 51. Streicher JM, Ren S, Herschman H, and Wang Y. MAPK-activated protein kinase-2 in cardiac hypertrophy and

cyclooxygenase-2 regulation in heart. Circ Res 106: 1434-1443, 2010.

52. Sun P, Yoshizuka N, New L, Moser BA, Li Y, Liao R, Xie C, Chen J, Deng Q, Yamout M, Dong MQ, Frangou CG, Yates JR, 3rd, Wright PE, and Han J. PRAK is essential for ras-Induced senescence and tumor suppression. Cell 128: 295-308, 2007.

53. Takahashi N, Calderone A, Izzo NJ, Jr., Maki TM, Marsh JD, and Colucci WS. Hypertrophic stimuli induce transforming growth factor-beta 1 expression in rat ventricular myocytes. J Clin Invest94: 1470-1476, 1994.

54. Thompson NL, 720 Bazoberry F, Speir EH, Casscells W, Ferrans VJ, Flanders KC, Kondaiah P, Geiser AG, and Sporn MB. Transforming growth factor beta-1 in acut myocardial infarction in rats. Growth Factors 1: 91-99, 1988.

55. Travers JG, Kamal FA, Robbins J, Yutzey KE, and Blaxall BC. Cardiac Fibrosis: The Fibroblast Awakens. Circ Res 118: 1021-1040, 2016.

56. Villarreal FJ, and Dillmann WH. Cardiac hypertrophy-induced changes in mRNA levels for TGF-beta 1, fibronectin, and collagen. Am J Physiol 262: H1861-H1866, 1992.

57. Wang Y, Huang S, Sah VP, Ross J, Jr., Brown JH, Han J, and Chien KR. Cardiac muscle cell hypertrophy and apoptosis induced by distinct members of the p38 mitogen-activated protein kinase family. J Biol Chem 273: 2161-2168, 1998.

58. Xing L. Clinical candidates of small molecule p38 MAPK inhibitors for inflammatory diseases. MAP Kinases 4: 24-30, 2015.

59. Zhang D, Gaussin V, Taffet GE, Belaguli NS, Yamada M, Schwartz RJ, Michael LH, A. OP, and Schneider MD. TAK1 is activated in the myocardium after pressure overload and is sufficient to provoke heart failure in transgenic mice. Nat Med 6: 556 - 563, 2000.

60. Zhang S, Weinheimer C, Courtois M, Kovacs A, Zhang CE, Cheng AM, Wang Y, and Muslin AJ. The role of the Grb2-p38 MAPK signaling pathway in cardiac hypertrophy and fibrosis. J Clin Invest 111: 833-841, 2003.

Figure Legends

Figure 1. MAPK-activated protein kinase-5 (MK5) immunoreactivity is reduced in $MK5^{+/-}$ and $MK5^{-/-}$ hearts. A: MK5 immunoreactive bands of 48- and 62-kDa were detected in heart lysates (25 μg/lane) from $MK5^{+/+}$ mice. The intensity of both bands was reduced in hearts from $MK5^{+/-}$ mice and virtually absent in hearts from $MK5^{-/-}$ mice. MK5* represents a novel splice variant of MK5, referred to herein as MK5.6. Numbers at the *right* indicate molecular mass (in kDa). B: An MK5 immunoreactive band of 50-kDa was detected in lysates (40 ng/lane) from human embryonic kidney-293 cells transfected with pIRES MK5.1-V5 (*lane a*) (11) whereas bands of 48 and 62 kDa were detected in heart lysates (100 μg/lane) from $MK5^{+/+}$ mice (*lane b*). Numbers at the *right* indicate the positions of the molecular mass marker proteins (in kDa).

Figure 2. Hypertrophy is attenuated in TAC-$MK5^{+/-}$ hearts subjected to transverse aortic constriction (TAC). Pressure overload was induced in $MK5^{+/-}$ and wild-type littermate controls ($MK5^{+/+}$) mice by TAC and mice were euthanized 2 and 8 wk postsurgery. Sham-operated (sham) animals underwent the identical surgical procedure; however, the aorta was not constricted. A-C: left ventricular (LV) maximum developed pressure (LV P_{max},; A), heart weight-to-ibia length ratio (HW/TL; B), and LV mass-to- body weight ratio (LV Mass/BW; C). Heart weight refers to the mass of the whole heart (minus atria) as determined gravimetrically. LV mass was determined by Echo. D: myocyte diameter 8 wk postsurgery was determined for 10 cells/heart. Data are expressed as means ± SE; n = 12-26 mice in A-C and n+ 9-11 mice in D. ****, $p < 0.0001$: ***, $p < 0.001$: **, $p < 0.01$: *, $p < 0.05$ by two-way ANOVA with Bonferroni's multiple comparison test.

Figure 3. The profile of fetal gene expression is altered in TAC $MK5^{+/-}$ hearts. Pressure overload was induced in $MK5^{+/-}$ and wild-type littermate control ($MK5^{+/+}$) mice by TAC, and mice were euthanized 2 and 8 wk postsurgery. Sham animals underwent the identical surgical procedure; however, the aorta was not constricted. Total RNA was isolated and the abundance of atrial natriuretic peptide (ANP; A), B-type natriuretic peptide (BNP; B), and β -myosin heavy chain (β-MHC; C) was quantified by quantitative PCR and normalized to GAPDH mRNA levels. Data are expressed as means ± SE; n= 8-18. ****, $p < 0.0001$: ***, $p < 0.001$: **, $p < 0.01$: *, $p < 0.05$ by two-way ANOVA with Bonferroni's multiple comparison test.

Figure 4. TAC $MK5^{+/-}$ hearts show a less restrictive filling pattern that TAC $MK5^{+/+}$ hearts. Pressure overload was induced in $MK5^{+/-}$ and $MK5^{+/+}$ mice by TAC. Two and eight weeks later, LV structure and function were assessed by echocardiographic imaging. A-D: LV fractional shortening (FS; A), isovolumetric relaxation time (IVRT; B), E wave deceleration rate (ED rate; C), and LV myocardial performance index (MPI; D). Data are expressed as means ± SE; n= 12-26 ***, $p < 0.001$: **, $p < 0.01$: *, $p < 0.05$ by two-way ANOVA with Bonferroni's multiple comparison test.

Figure 5. The TAC-induced increase in collagen type 1-α_1 (COL1A1) mRNA is attenuated in $MK5^{+/-}$ hearts. A: Two and eight weeks post-TAC, COL1A1 mRNA levels were measured by quantitative PCR and normalized to the amount of GAPDH mRNA. B: Transverse cryosections (8 μm) of the ventricular myocardium were stained with Masson's trichrome 8 wk post-TAC. C: collagen content was quantified. The original magnification was 40X. Data are expressed as means ± SE; n= 8-18. ****, $p < 0.0001$: **, $p < 0.01$ by two-way ANOVA with Bonferroni's multiple comparisons test.

Figure 6. Effect of TAC on transforming growth factor (TGF)-β1 and TGF-β3 mRNA. Total TGF-β1, (A) and TGF-β3 (B) mRNA levels were quantified by quantitative PCR and normalized to the amount of GAPDH mRNA in $MK5^{+/+}$ and $MK5^{+/-}$ hearts 2 and 8 wk post-TAC. Data are expressed as mean ± SE; n= 8-18. *, $p < 0.05$ by two way ANOVA with Bonferroni's multiple comparison test.

Figure 7. MK5 is expressed in fibroblasts but not myocytes: lack of MK5 does not affect fibroblast activation. A: Ventricular fibroblasts and myocytes were isolated from adult $MK5^{+/+}$ mouse heart. Lysates (25 μg/lane) were prepared, resolved by SDS-PAGE and transferred to nitrocellulose. MK5 immunoreactive bands of 48 and 62 kDa were detected in fibroblast lysates (*lane a*) whereas no immunoreactivity was detected in myocyte lysates (*lane b*). Collagen type I-immunoreactive bands of 150 and 200 kDa were detected in fibroblast lysates (*lane a*) whereas no immunoreactivity was detected in myocyte lysates (*lane b*). Membranes were reprobed for caveolin 3, troponin T and GAPDH. Caveolin 3 (20 kDa) and Troponin T (40 kDa) immunoreactivity was detected in myocyte lysates (*lane b*) whereas no

immunoreactivity was detected in fibroblast lysates (*lane a*). GAPDH immunoreactivity was used as a loading control. Numbers at the *right* indicate molecular mass (in kDa). These results are qualitatively similar to those obtained from three separate cell preparations. B: MK5-immunoreactive bands of 48 (MK5.1) and 62 kDa (MK5.6) in heart lysates (25 μg/lane) from 8-wk sham (S) and TAC (T) $MK5^{+/+}$ and $MK5^{+/-}$ mice. TAC did not alter MK5 immunoreactivity. GAPDH immunoreactivity was used as a loading control. Numbers at the *right* indicate molecular mass (in kDa). C: Cardiac fibroblasts were isolated from $MK5^{+/+}$, $MK5^{+/-}$, and $MK5^{-/-}$ mice, maintained in culture for 6 days, lysed, and α-smooth muscle actin (α-SMA) expression assessed by immunoblot analysis. GAPDH immunoreactivity was used as a loading control. The *top* image shows a representative immunoblot whereas *bottom* graph shows the means ± SE of two ($MK5^{+/-}$) or three ($MK5^{+/+}$, $MK5^{-/-}$) separate cell isolations. Means were not significantly different by one-way ANOVA with Bonferroni's multiple comparison test.

TABLE Primers used for quantitative PCR

Target	Primers
ANP	
Sense	5’-GTG CGG TGT CCA ACA CAG A-3’
Antisense	5’-TTC TAC CGG CAT CTT CTC CTC-3’
BNP	
Sense	5’-GTT TGG GCT GTA ACG CAC TGA-3’
Antisense	5’-GAA AGA GAC CCA GGC AGA GTC A-3’
β-MHC S	5’-AGG GTG GCA AAG TCA CTG CT-3’
Antisense	5’-CAT CAC CTG GTC CTC CTT CA-3’
TGF-β1 S	5’-TGC TAA TGG TGG ACC GCA A-3’
Antisense	5’-AGA TGT CTT TGG TTT TCT CAT AGA TGG-3’
TGF- β3 S	5’-AGA GAT CCA TAA ATT CGA CAT-3’
Antisense	5’-ACA CAT TGA AAC GAA AAA CCT-3’
COL1A1 S	5’-CTG ACG CAT GGC CAA GAA GAC A-3’
Antisense	5’- CGT GCC ATT GTG GCA GAT ACA GAT -3’
GAPDH S	5’-CTG CAC CAC CAA CTG CTT AGC-3’
Antisense	5’-ACT GTG GTC ATG AGC CCT TCC A-3’

ANP, atrial natriuretic peptide; BNP, B-type natriuretic peptides; β-MHC, beta-myosin heavy chain; TGF, transforming growth factor ; COL1A1, collagen type 1 α_1.

Table 1. Echocardiographic parameters of 12-wk-old $MK5^{+/+}$ and $MK5^{+/-}$ mice.

	$MK5^{+/+}$ (n=45)	$MK5^{+/-}$ (n=35)
R-R interval ,ms	149±2	148±2
LV dimensions and mass		
LVAWd, mm	0.737±0.014	0.723±0.014
LVPWd, mm	0.672±0.012	0.674±0.013
LVDd, mm	4.12±0.05	3.98±0.05†
LVDs, mm	2.59±0.06	2.64±0.05
LV mass, mg	105.1±2.7	98.5±3.1
LV mass / LVDd, mg/mm	25.45±0.54	24.62±0.62
BW,g	25.85±0.49	24.07±0.44†
LV mass/BW,mg/g	4.12±0.12	4.12±0.13
LV Systolic Function		
LVFS, %	37.55±0.98	33.82±0.91§
LVEF, %	73.5±1.2	69.0±1.1§
Lateral S_m , cm/s	2.387±0.090	2.279±0.091
Septal S_m, cm/s	2.519±0.089	2.384±0.089
IVCT,ms	14.0±1.0 (n=41	17.9±1.3†
Diastolic function		
E velocity, cm/s	72.4±2.1	75.1±2.0
E DT, msec	36.8±1.3	36.5±1.5
E D rate, m/s^2	20.81±0.95	21.8±1.1
Lateral E_m, cm/s	2.78±0.13	2.89±0.11
Lateral A_m,cm/s	2.53±0.11	2.40±0.14
Lateral E_m/A_m	1.13±0.06	1.27±0.07
Septal E_m cm/s	3.03±0.12	2.99±0.10
Septal A_m cm/s	2.65±0.10	2.71±0.16
Septal E_m/A_m	1.16±0.04	1.17±0.07
IVRT, ms	11.53±0.77	11.33±0.72
MPI		
Septal MPI, %	67.8±3.3	70.3±2.5
Lateral MPI, %	67.4±2.5	73.7±4.2
Global MPI, %	40.8±1.9	50.9±2.5§

Data are expressed as mean ± SE MK5, MAPK-activated protein kinase-5; LVAWd, left ventricular (LV) anterior wall end-diastolic thickness; LVPWd, LV posterior wall end- diastolic thickness; LVDd, LV end diastolic diameter; LVDs, LV end-systolic diameter; BW, body weight; LV FS, LV Fractional shortening; LV EF, LV ejection fraction; S_m, peak systolic tissue velocity; IVCT,

isovolumetric contraction time E, early diastolic transmitral filling velocity; EDT, early diastolic transmitral filling deceleration time; ED rate, early diastolic transmitral filling deceleration rate; E_m, peak early diastolic tissue velocity; A_m, peak late diastolic tissue velocity; IVRT, isovolumic relaxation time; MPI, myocardial performance index. †, $p<0.05$ for $MK5^{+/-}$ versus $MK5^{+/+}$: §, $p<0.01$ for $MK5^{+/-}$ versus $MK5^{+/+}$.

Table 2. Hemodynamic parameters for MK5$^{+/+}$ and MK5$^{+/-}$ mice after 2 and 8 wk of pressure overload.

	2 weeks				8 weeks			
	Sham		TAC		Sham		TAC	
	MK5$^{+/+}$ (n=7)	MK5$^{+/-}$ (n=6)	MK5$^{+/+}$ (n=9)	MK5$^{+/-}$ (n=6)	MK5$^{+/+}$ (n=13)	MK5$^{+/-}$ (n=9)	MK5$^{+/+}$ (n= 11)	MK5$^{+/-}$ (n=11)
BPmax (mmHg)	99.6±3.5	94.8±4.3	145±10‡	131±15ξ	81.3±3.1	83.9±3.7	130±10a	127±4‡
LVPmax (mmHg)	100±4	97.0±3.7	161±10a	146±17*	86.9±2,0	84.3±2.9	143±11a	138±4a
LVPmin (mmHg)	1.8±1.2	2.6±0.6	1.3±0.9	2.1±1.2	1.1±0.3	1±0.4	1.6±0.6	2.5±0.4
dP/dt_{max} (mmHg/s)	6598±540	6145±382	5993±792	5982±516	5924±229	5612±462	6478±482	6541±365
dP/dt_{min} (mmHg/s)	-5774±437	-5586±408	-6269±822	-6545±648	-6355±227	-6193±500	-7491±498	-7910±484ξ
LVEDP (mmHg)	8.4±1.4	8.3±1.2	8.3±1.9	9.4±2.7	5.2±0.4	3.7±0.7	5.9±0.9	7±0.6
CT (msec)	13.4±0.6	13.2±0.4	15.4±3.1	13.8±0.5	11.1±0.2	10.3±1.3	11.4±0.2	11.5±0.2
RT (msec)	46.7±0.9	45.8±1.1	41.7±5.2	47.3±1.5	40±0.7	40.6±0.4	41.3±0.3	40.9±0.8
Tau (msec)	9.1±0.4	8.9±0.5	8.2±0.9	9.2±0.5	6.1±0.2	6.1±0.3	6.1±0.6	6.8±0.4
HR (bpm)	354±18	356±19	305±41	334±18	455±11	464±18	458±12	447±11

Data are expressed as mean ± SE. Sham, sham operation; TAC, transverse aortic constriction; BP_{max}, maximum systolic blood pressure; LVP_{max}, LV maximum systolic pressure; LVP_{min}, LV minimum diastolic pressure; dP/dt_{max}, maximum rate of LV pressure increase during contraction; dP/dt_{min}, maximum rate of LV decline during relaxation; LVEDP, LV end-diastolic pressure; CT, contraction time; RT, relaxation time; *T*, time constant; HR, heart rate.. For statistical comparisons Two-way ANOVA followed by Bonferroni's multiple comparaison test was performed. ξ, $P<0.05$ vs Sham: *, $p<0.01$ vs Sham: ‡, $p<0.001$ vs Sham: a, $p<0.0001$ vs Sham.

Table 3. Echocardiographic parameters of $MK5^{+/+}$ and $MK5^{+/-}$ mice after 2 and 8 weeks of pressure overload.

	2 weeks				8 weeks			
	Sham		TAC		Sham		TAC	
	$MK5^{+/+}$ (n=19)	$MK5^{+/-}$ (n=18)	$MK5^{+/+}$ (n=26)	$MK5^{+/-}$ (n=20)	$MK5^{+/+}$ (n=13)	$MK5^{+/-}$ (n=12)	$MK5^{+/+}$ (n=12)	$MK5^{+/-}$ (n=14)
aortic peak velocity (cm/s)	98±5	99±4	357±12a	341±20a	89±4	82±3	362±10a	359±7a
R-R interval (ms)	150±5	137±4	142±6	137±4	149±3	141±5	130±6	123±5
Dimensions/Mass								
LVAWd (mm)	0.774±0.016	0.769±0.015	0.983±0.028a	0.935±0.029a	0.788±0.019	0.748±0.015	1.080±0.044a	1.066±0.037a
LVPWd (mm)	0.716±0.015	0.717±0.015	0.894±0.024a	0.854±0.029‡	0.727±0.012	0.726±0.012	0.994±0.034a	0.972±0.043a
LVDd (mm)	4.26±0.06	4.00±0.06	4.26±0.07	4.15±0.07	4.38±0.07	3.99±0.05†	4.72±0.15	4.32±0.07†
LVDs (mm)	2.66±0.06	2.45±0.07	3.01±0.10ξ	2.90±0.08ξ	2.90±0.08	2.60±0.07	3.67±0.23a	3.20±0.12*†
LV mass (mg)	119.8±4.3	107.3±4.0	165.4±8.2‡	145.9±6.0*	128.3±4.8	105.1±3.0	225±19a	189±14a
LV mass/LVDd (mg/mm)	28.0±0.8	26.7±0.8	38.5±1.5a	35.2±1.4‡	29.2±0.8	26.3±0.6	47±2.7a	43.5±2.6a
LV mass/BW (mg/g)	4.30±0.17	4.30±0.14	6.34±0.28a	5.80±0.20ξ	4.02±0.20	3.77±0.13	7.42±0.60a	6.19±0.36a†
systolic Function								
LVFS (%)	37.7±0.9	37.4±1.4	29.5±1.4‡	30.1±1.6*	33.8±1.4	35.0±1.1	23±2.3‡	26±2.1*
LVEF (%)	74.1±1.1	73.6±1.7	62.5±2.1*	63.3±2.5ξ	68.9±1.9	70.8±1.4	51.4±4.3‡	56.7±3.7*
Lateral Sm (cm/s)	2.54±0.09	2.38±0.14	1.97±0.11‡	2.09±0.10	2.18±0.10	2.31±0.10	1.56±0.10*	1.76±0.09ξ
Septal Sm (cm/s)	2.73±0.15	2.39±0.10	2.03±0.10a	2.53±0.15§	2.45±0.11	2.53±0.11	1.96±0.12	1.99±0.10
diastolic function								
E velocity (cm/s)	83.0±3.2	77.3±3.5	94.9±3.8	93.3±3.8ξ	88.7±3.8	84.3±2.8	103.0±4.4	100.2±4.4
E DT (msec)	34.0±1.5	39.7±2.0	32.5±2.0	34.1±1.5	32.3±1.5	31.8±1.1	26.0±1.4	33.0±1.7
E D rate (m/s^2)	25.0±1.2	20.1±1.2	33.0±2.7ξ	28.4±1.7ξ	27.6±0.5	26.7±0.9	41.1±3.1‡	31.4±2.3†
LV isovolumetric relaxation time								
IVRT (ms)	10.3±0.9	10.1±0.8	15.2±1.8*	10.8±1.0†	9.57±0.76	8.53±0.67	8.89±0.61	8.74±0.48
IVRTc (ms)	0.840±0.074	0.861±0.064	1.23±0.13ξ	0.915±0.071†	0.780±0.058	0.712±0.046	0.778±0.046	0.788±0.038

Myocardial performance index								
Septal MPI (%)	63.9±4.2	79.0±4.5	82.2±7.0*	67.9±4.4	56.1±2.2	61.8±3.8	60.4±3.2	69.8±6.4
Lateral MPI (%)	67.8±3.1	85.0±4.5	81.2±6.8	69.8±4.7	64.0±1.8	64.3±2.6	66.7±2.1	68.0±4.0
Global MPI (%)	35.9±2.9	50.8±4.7†	45.2±3.5	42.4±3.5	44.9±2.4	46.8±2.2	50.6±3.3	53.4±4.3

Data are expressed as mean ± SE. IVRTC, rate-corrected isovolumic relaxation time. ξ, $p<0.05$ vs Sham: *, $p<0.01$ vs Sham: ‡, $p<0.001$ vs Sham: a, $p<0.0001$ vs Sham: †, $p<0.05$ vs $MK5^{+/+}$: §, $p<0.01$ vs $MK5^{+/+}$.

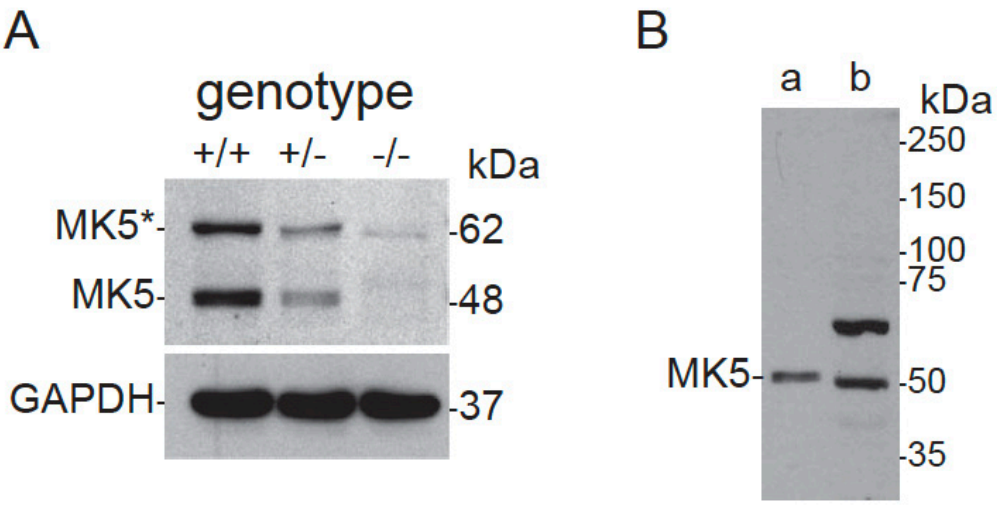
A
genotype
+/+ +/- -/-
kDa
MK5*
MK5
GAPDH
62
48
37
B
a b
kDa
250
150
100
75
MK5
50
35

Figure 1

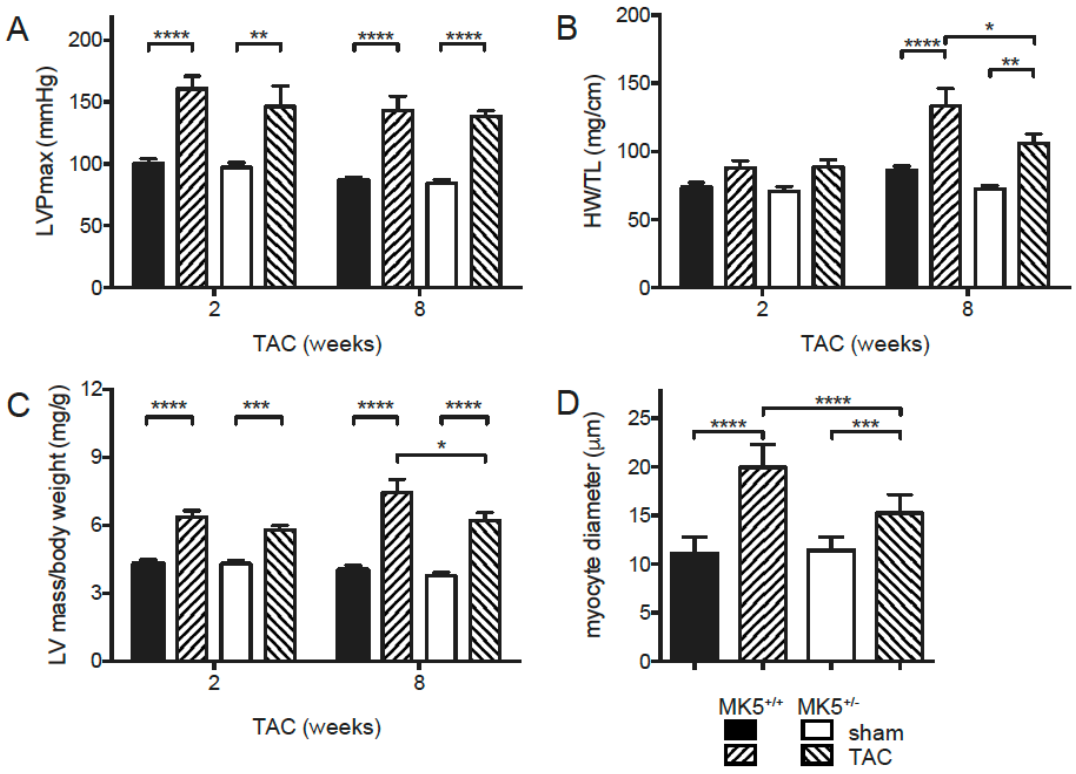
A
LVPmax (mmHg)
200
150
100
50
0
****
**
****
****
2
8
TAC (weeks)
B
HW/TL (mg/cm)
200
150
100
50
0
****
*
**
2
8
TAC (weeks)
C
LV mass/body weight (mg/g)
12
9
6
3
0
****
***
****
****
*
2
8
TAC (weeks)
D
myocyte diameter (μm)
25
20
15
10
5
0
****
****
***
MK5+/+
MK5+/-
sham
TAC

Figure 2

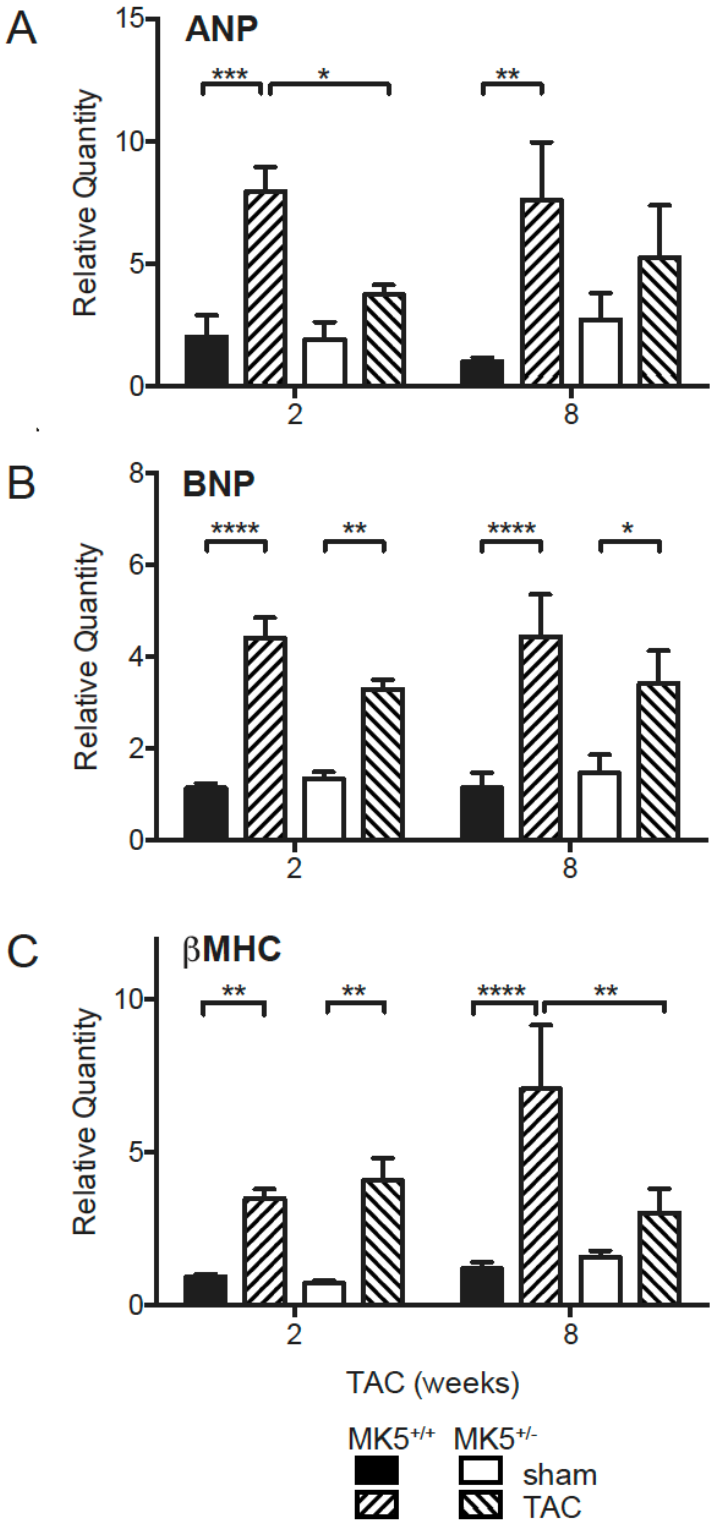
A
ANP
Relative Quantity
15
10
5
0
***
*
**
2
8
B
BNP
Relative Quantity
8
6
4
2
0
****
**
****
*
2
8
C
βMHC
Relative Quantity
10
5
0
**
**
****
**
2
8
TAC (weeks)
MK5+/+
MK5+/-
sham
TAC

Figure 3

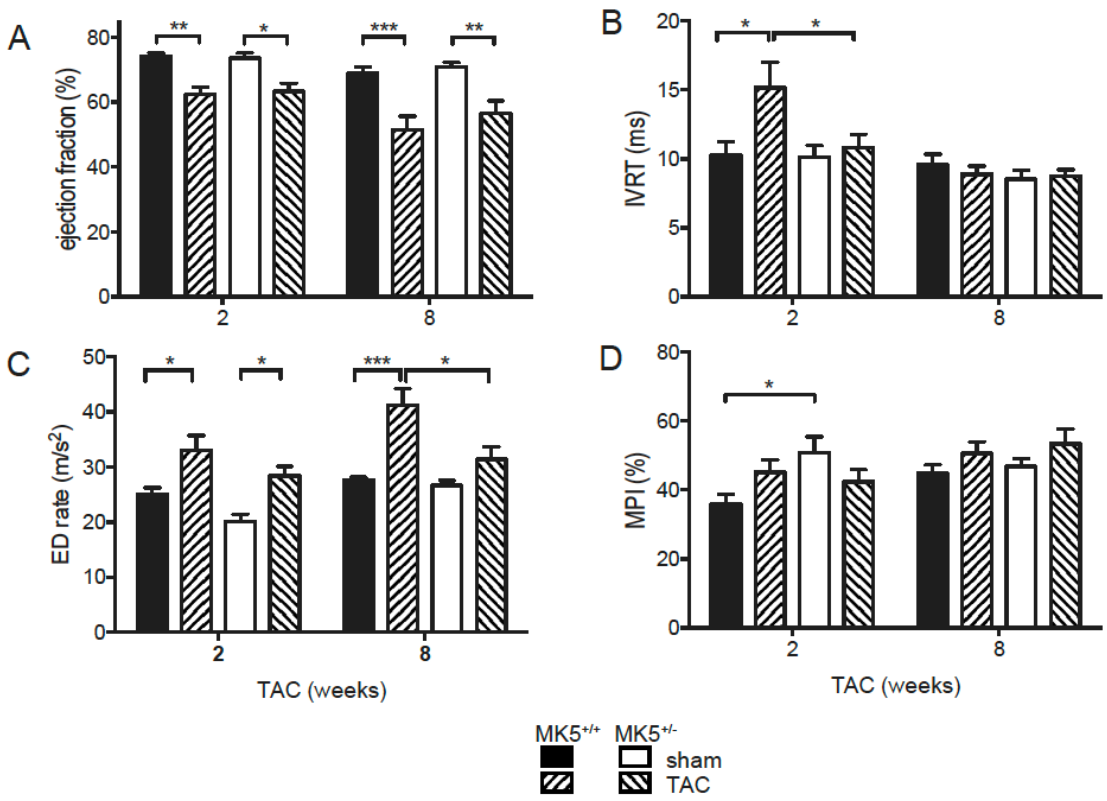
A
ejection fraction (%)
B
IVRT (ms)
C
ED rate (m/s²)
D
MPI (%)
TAC (weeks)
TAC (weeks)
MK5+/+
MK5+/-
sham
TAC

Figure 4

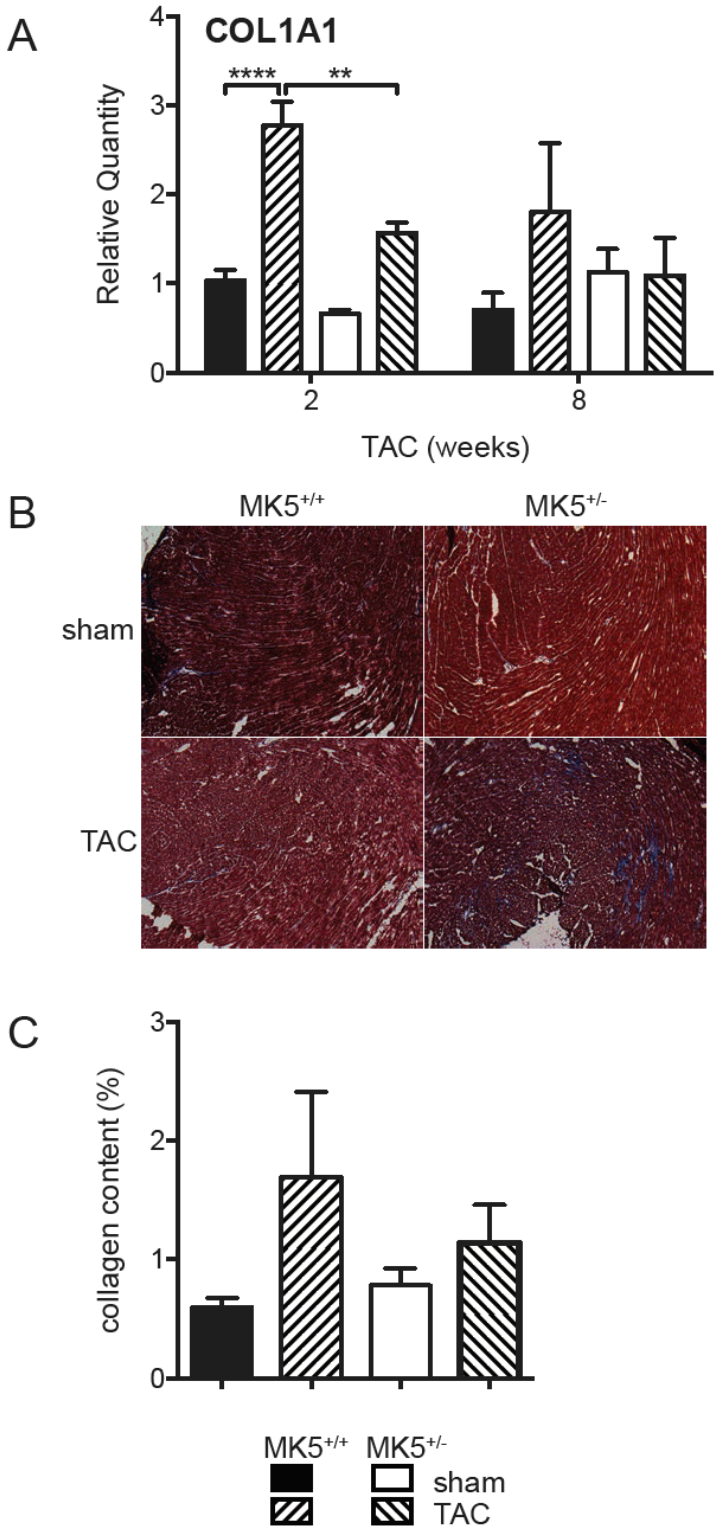
A
COL1A1
****
**
Relative Quantity
0
1
2
3
4
2
8
TAC (weeks)
B
MK5+/+
MK5+/-
sham
TAC
C
collagen content (%)
0
1
2
3
MK5+/+
MK5+/-
sham
TAC

Figure 5

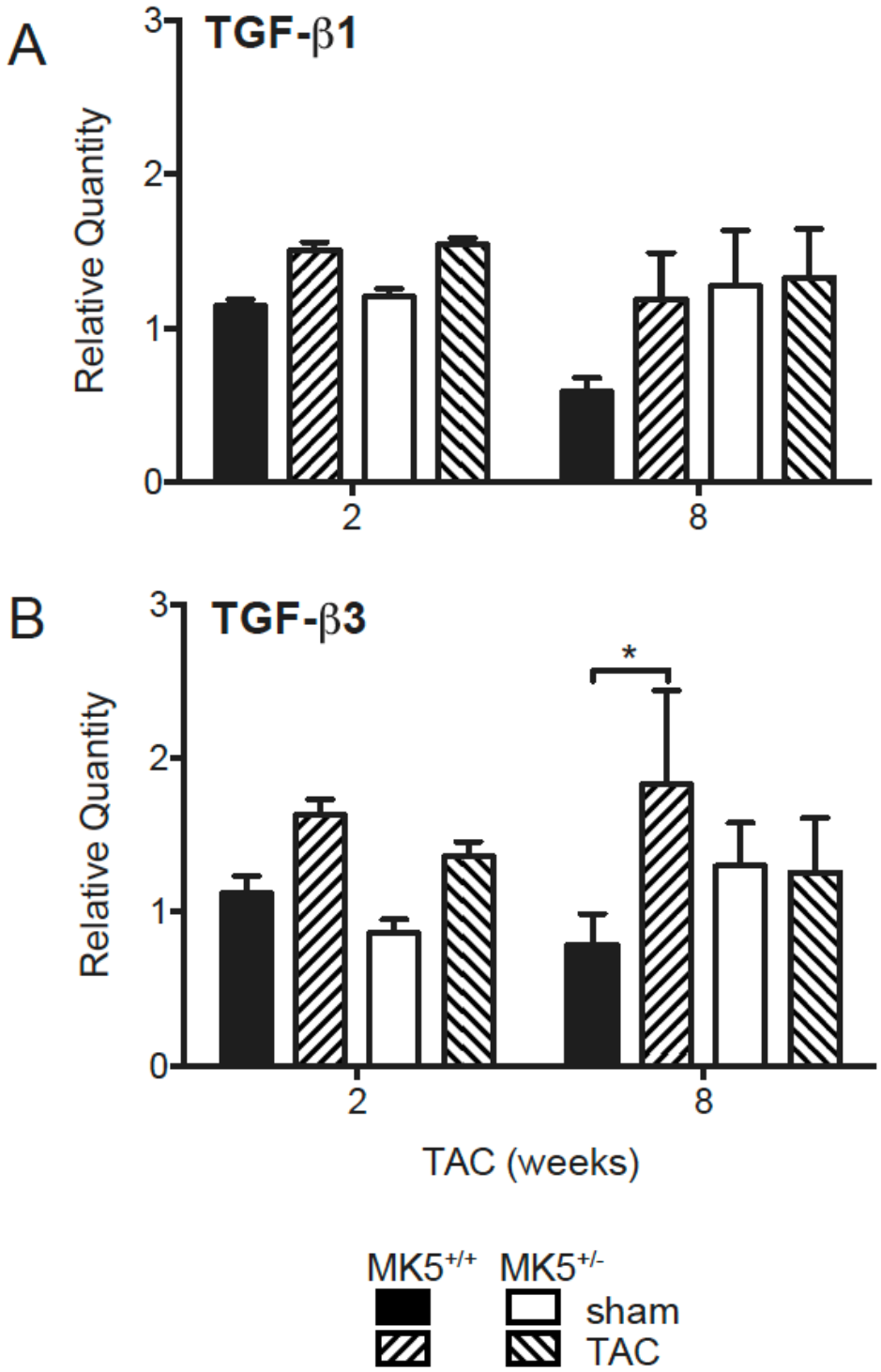
A
TGF-β1
Relative Quantity
3
2
1
0
2
8
B
TGF-β3
Relative Quantity
*
3
2
1
0
2
8
TAC (weeks)
MK5+/+
MK5+/-
sham
TAC

Figure 6

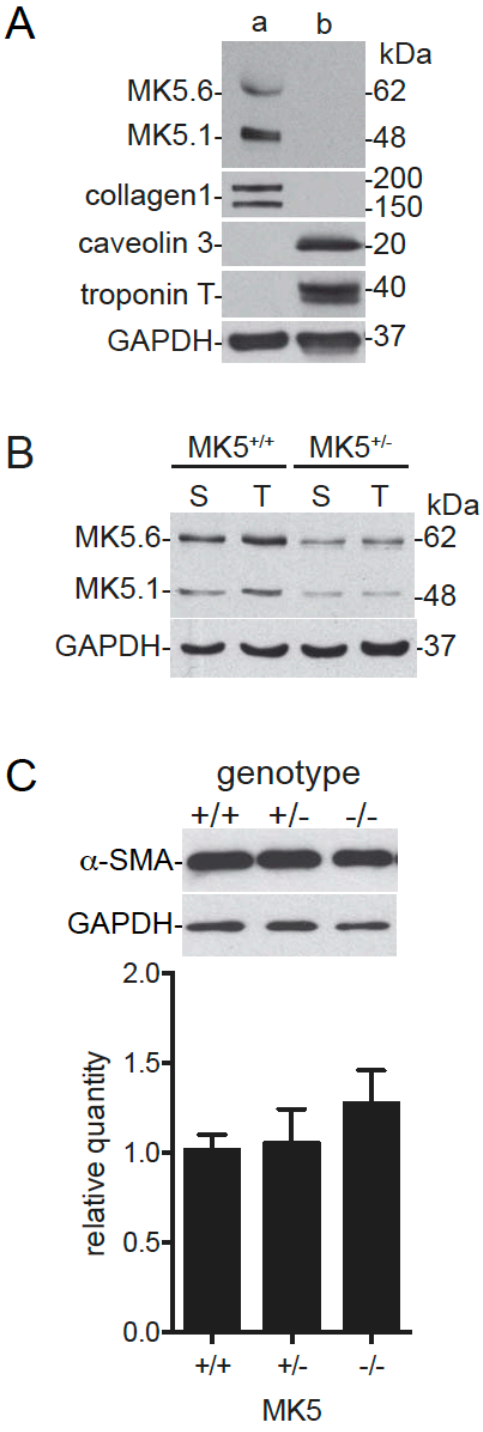
A
a
b
kDa
MK5.6-
MK5.1-
collagen1-
caveolin 3-
troponin T-
GAPDH-
-62
-48
-200
-150
-20
-40
-37
B
MK5+/+
MK5+/-
S
T
S
T
kDa
MK5.6-
MK5.1-
GAPDH-
-62
-48
-37
C
genotype
+/+
+/-
-/-
α-SMA-
GAPDH-
2.0
1.5
1.0
0.5
0.0
relative quantity
+/+
+/-
-/-
MK5

Figure 7

4 Article-2

Title: MK5 haplodeficiency decreases collagen deposition and scar size during post-myocardial infarction wound repair.

This article was submitted to *American Journal of Physiology, Heart and Circulatory Physiology* on 31st August 2017.

Contributions of co-authors

Sherin Ali Nawaito: conceived, designed and performed the all the experiments for the infarcted mice. Isolated and characterized MK5 deficient fibroblasts, quantified markers in immunohistochemistry analysis, performed migration and proliferation assay for the 3 genotypes of MK5 fibroblasts, analyzed the data, analyzed the magnetic resonnace imaging data, interpreted the results, performed stastistical analysis, prepared figures, wrote the first draft of the manuscript, edited and revised the manuscript.

Pramod Sahadevan: performed the migration assay for MK5 knockdown fibroblasts, analyzed the data, interpreted the results, prepared figures of the migration of MK5 knockdown fibroblasts and approved the final version of the manuscript.

Marie-Elaine Clavet-Lanthier: performed the histology for the infarcted mice and analyzed data.

Philippe Pouliot: performed the magnetic resonnance imaging for the mice.

Fatiha Sahmi: assisted in immunoblotting experiments.

Yanfen Shi: acquired and interpreted the echocardiography data.

Marc-Antoine Gillis: performed the ligation of coronary artery in mice as a model of myocardial infarction.

Frederic Lesage: supervised the cardiac magneticresonance unitand approved the final version of the manuscript.

Matthias Gaestel: developer of the MK5 mice model.

Martin G. Sirois: supervised the histology unitand approved the final version of the manuscript.

Angelo Calderone: provided expertise in cardiac fibrosis area and approved the final version of the manuscript.

Jean-Claude Tardif: supervised the echogardiography unitand appproved the final version of

the manuscript.

Bruce G. Allen: conceived and designed the experiments, analyzed the data, interpreted the results, edited the manuscript and approved the final version of the manuscript.

MK5 haplodeficiency decreases collagen deposition and scar size during post-myocardial infarction wound repair

Sherin Ali Nawaito[b,d], Pramod Sahadevan[a,d], Marie-Élaine Clavet-Lanthier[d], Philippe Pouliot[d], Fatiha Sahmi[d], Yanfen Shi[d], Marc-Antoine Gillis[d], Frederic Lesage[d,e], Matthias Gaestel[f], Martin G. Sirois[b,d], Angelo Calderone[b,d], Jean-Claude Tardif[c,d], and Bruce G. Allen[a,c,d]

From Departments of Biochemistry and Molecular Medicine[a], Pharmacology and Physiology[b], Medicine[c], Electrical Engineering[e], Université de Montréal, Montreal Heart Institute[d], and Institute of Biochemistry, Hannover Medical School, Hannover, Germany[f].

Address correspondence to:
Bruce G. Allen
Montreal Heart Institute
5000 Belanger St.
Montréal, Québec, Canada H1T 1C8.
Telephone: (514) 376-3330 (3591).
FAX: (514) 376-1355.
E-mail: bruce.g.allen@umontreal.ca

Running head: Role of MK5 in reparative fibrosis

4.1 Abstract

MK5 is a protein serine/threonine kinase activated by p38 MAPK and the atypical MAPKs ERK3 and ERK4. The present study examined the effect of MK5 haplodeficiency on reparative fibrosis following a myocardial infarction (MI). Twelve-week-old $MK5^{+/-}$ (n = 24) and wild-type littermate ($MK5^{+/+}$, n = 35) mice underwent ligation of the left anterior descending coronary artery (LADL). Surviving mice were sacrificed 8 or 21 days post-MI. Eight days post-MI, survival rates did not differ significantly between $MK5^{+/+}$ and $MK5^{+/-}$ mice, rupture of the LV wall being the primary cause of death; however, 21-days post-MI, survival was greater in $MK5^{+/+}$ mice than $MK5^{+/-}$ mice. Echocardiographic imaging revealed similar increases in LV end-diastolic diameter, myocardial performance index, and wall motion score index in LADL-$MK5^{+/+}$ and LADL-$MK5^{+/-}$ mice. Masson's trichrome staining revealed both decreased scar area and less collagen within the scar of LADL-$MK5^{+/-}$ hearts compared to LADL-$MK5^{+/+}$ hearts. Immunohistochemical analysis of mice experiencing heart rupture revealed increased MMP-9 immunoreactivity in the infarct border zone of LADL-$MK5^{+/-}$ hearts compared with LADL-$MK5^{+/+}$. While inflammatory cell infiltration was similar in LADL-$MK5^{+/+}$ and LADL-$MK5^{+/-}$ hearts, angiogenesis was more pronounced in the infarct border zone of LADL-$MK5^{+/-}$ mice compared with LADL-$MK5^{+/+}$ mice. Characterization of ventricular fibroblasts revealed reduced motility and proliferation in $MK5^{-/-}$ animals compared with both wild-type and haplodeficient mice. siRNA-mediated knockdown of MK5 in wild type fibroblasts also impaired motility. Hence, reduced MK5 expression alters fibroblast function and scar morphology but not mortality during the first week post-MI.

Keywords: MK5/PRAK, reparative fibrosis, myocardial infarction, fibroblast, p38 MAPK

New and Noteworthy

MK5/PRAK is a protein serine/threonine kinase activated by p38 MAPK and/or atypical MAPKs ERK3/4. MK5 haplodeficiency reduced scar area and scar collagen content post-myocardial infarction. Motility and proliferation were reduced in cultured MK5-null cardiac fibroblasts.

Glossary

a', atrial diastole; CO, cardiac output; CMRI, cardiac magnetic resonance imaging; DMEM, Dulbecco's modified Eagle's medium; ECM, extracellular matrix; E, transmitral flow peak velocity in early filling; EDT, early diastolic transmitral filling deceleration time; ED rate, early diastolic transmitral filling deceleration rate; e', early diastole; ERK3, extracellular signal-regulated kinase 3; ERK4, extracellular signal-regulated kinase 4; FAK, focal adhesion kinase; FBS, fetal bovine serum; IP, intraperitoneal; IVRT, isovolumic relaxation time; LGE, late gadolinium enhancement; LV, left ventricular; LVAWd, LV anterior wall end-diastolic thickness; LVPW, LV posterior wall end-diastolic thickness; LVD_d, LV dimension at end-diastole; LVD_s, LV dimension at end-systole; LAd_s, left atrium dimension at end cardiac systole; LADL, left anterior descending coronary artery ligation; LVOT, left ventricular outflow tract; LVFS, LV fractional shortening; LVEF, LV ejection fraction; LET, LV ejection time; LVM, LV mass; MI, myocardial infarction; MC_{CO}, time interval from mitral valve closure to opening; MAP kinase, mitogen-activated protein kinase; MK2, MAP kinase-activated protein kinase-2; MK3, MAP kinase-activated protein kinase-3; MK5, MAP kinase-activated protein kinase-5; $MK5^{+/+}$, MK5 wild type; $MK5^{+/-}$, heterozygous MK5-deficient; MK5-kDa, siRNA-mediated knock down of MK5; MPI_{global}, global myocardial performance index; M199, medium 199; MMP9, matrix metalloproteinase 9; PW, pulsed wave Doppler; PBS, phosphate buffered saline; PDGF, platelet derived growth factor; SV, stroke volume; S_L, mitral lateral annulus moving velocity in systole; S_S, mitral septal annulus moving velocity in systole; siRNA, small-interfering RNA; α-SMA; α-smooth muscle actin; VEGF, vascular endothelial growth factor; WISE, wall motion score index.

4.2 Introduction

Following myocardial infarction (MI), the infarcted tissue undergoes wound healing and accelerated deposition of extracellular matrix proteins (9). Fibroblasts are the main source of extracellular matrix (ECM) (34). Reparative fibrosis, a critical component of cardiac wound healing, consists of 3 phases: 1) the inflammatory phase (≈ 3-4 days in mice) in which inflammatory and immune cells digest and clear the damaged cells and the extracellular matrix, 2) the reparative and proliferative phase, which includes resolution of inflammation, (myo)fibroblast migration and proliferation, scar formation and angiogenesis; and 3) the maturation phase, which involves myofibroblast deactivation, cross-linking of the extracellular matrix and stabilization of the scar (>14 days in mice). Over time, interstitial fibrosis also occurs within the non-infarcted myocardium and is associated with increased myocardial stiffness. The adverse cardiac remodeling that occurs post-MI contributes to the impaired function and ischemic heart failure that develops following the initial ischemic event (50). In addition, excessive wound repair, which is characterized by marked interstitial cardiac fibrosis and myofibroblast proliferation, can contribute to the development of cardiac hypertrophy and heart failure (30). Moreover, a fatal acute complication following an MI is cardiac rupture due to improper cardiac healing (58). Numerous studies have shown that matrix metalloproteinases (MMPs) -2 and -9 play a pivotal role in cardiac rupture (17, 25, 27). Hence, appropriate wound healing following an MI involves the careful coordination of numerous processes.

The p38 MAPK pathway is activated during myocardial ischemia and reperfusion (5, 71). There are 4 known isoforms of p38 (α, β, δ, γ): all are expressed in the murine heart, with p38α and p38γ being the most abundant (14, 16). The MAP kinase-activated protein kinases (MKs) 2, 3, and 5 are phosphorylated and activated by p38α and p38β(57). MK5, also known as p38-regulated/activated protein kinase (PRAK), is also phosphorylated by atypical MAPKs ERK3 and ERK4 (33, 60, 61). MK5 transcripts are detected in heart tissue (15, 23, 46) and present in high abundance in the left ventricle (23). In MK5 haplodeficient mice, LV hypertrophy and the increase in collagen type 1-α_1 mRNA levels evoked by constriction of the transverse aorta are attenuated (44). Furthermore, MK5 immunoreactivity is detected in adult

murine cardiac fibroblasts, but not in myocytes (44). The present work was performed to examine the effect of reduced MK5 expression on the inflammatory, proliferative and reparative phases of reparative fibrosis, corresponding to 8 days following myocardial infarction as well as the maturation phase, corresponding to 21 days post-MI using MK5 haplodeficient ($MK5^{+/-}$) (63). Mortality did not differ over 7 days post-MI but was higher in MK5 haplodeficient mice over 21 days. Scar size and collagen content were significantly decreased in $MK5^{+/-}$ hearts. Motility and proliferation were reduced in ventricular fibroblasts isolated from $MK5^{-/-}$ hearts in comparison with fibroblasts from $MK5^{+/+}$ and $MK5^{+/-}$ hearts. Hence, MK5 plays an important role in regulating cardiac fibroblast function and reparative fibrosis.

4.3 Material and Methods

Mice

MK5 knockout mice employed in these studies have been described previously(63) and were produced by targeted disruption of exon 6 on a mixed 129/Ola x C57BL background. Twelve- to 13-week-old male wild-type and heterozygous littermate mice were used in this study. $MK5^{-/-}$ mice show embryonic lethality with incomplete penetrance resulting in 50% of the expected number of $MK5^{-/-}$ embryos detectable after day E12. Hence, it was difficult to get $MK5^{-/-}$ mice in sufficient numbers for surgical procedures. As a result, $MK5^{+/-}$ mice were used in these studies. However, $MK5^{-/-}$ mice were available in sufficient numbers to allow a limited number of experiments using MK5-null cardiac ventricular fibroblasts. All animal experiments were approved by the local ethics committee and performed according to the guidelines of the Canadian Council on Animal Care.

Myocardial infarction

Mice ($MK5^{+/+}$, 35; $MK5^{+/-}$, 24) were anesthetized with 2% isoflurane (in 100% oxygen, 1000 mL/min) and myocardial infarction was achieved by permanent ligation of the left anterior descending coronary artery at a level about 1 mm below the edge of the left atria using an 10-0 nylon suture. Sham operations were performed without ligating the coronary artery. Buprenorphine (0.1 mg/kg) was administered subcutaneously before as well as six and sixteen hours after surgery. The surgeon was blinded to the genotype of the mice. Cardiac structure and function were assessed by transthoracic echocardiography (see below) seven days post-MI on mice anesthetized using 2% isoflurane (in 100% oxygen, 1000 mL/min). Surviving mice were sacrificed eight or twenty-one days post-surgery.

Diagnosis of cardiac rupture

Necropsies were performed on all non-surviving mice. Death due to cardiac rupture was diagnosed by the presence of a blood clot around the heart and in the chest cavity and

perforation of the infarcted wall.

Cardiac Magnetic Resonance Imaging (CMRI)

Prior to surgery and eight days post-MI, late gadolinium enhancement (LGE) contrast-enhanced MRI was performed using a 30 cm 7T horizontal MR scanner (Agilent/Varian, Palo Alto, CA), on mice in a prone position, with a 12 cm inner diameter gradient coil insert, gradient strength 600 mT/m, rise-time 130 μs. A 4-channel receive-only surface coil positioned under the mouse was used in combination with a quadrature transmit/receive birdcage coil with an internal diameter of 69 mm (RAPID Biomedical, Germany). Anesthesia was maintained using 2.0-2.5% isoflurane in pure oxygen and body temperature was maintained at 37°C using a warm air fan (SA Instruments, Stony Brook, NY). ECGs were recorded via two metallic needles placed subcutaneously near the heart under the armpits. A pressure transducer for respiratory gating was placed under the abdomen near the sternum. The mice were positioned into the MRI after intraperitoneal (IP) injection of a 20 μL bolus of 1.0 mmol/kg Gd-DPTA (Gadovist, Bayer Schering Pharma). Shimming was performed using a combination of manual and automatic sequences to reach a linewidth of 150 Hz or less over the heart. Scouts images were obtained choosing heart short axis slices. LGE Cine-FLASH imaging, started 20 to 30 minutes after Gd injection, followed a technique validated by Protti (51, 52) (see also (65, 69)). Imaging was performed with simultaneous ECG triggering and respiration gating (double gating), while maintaining the steady-state (8, 59), with effective TRY equal to the RR-interval, TE = 1.1 ms, 16 cardiac time frames, FOV 30 x 30 mm, matrix size 128 x 128, slice thickness 1 mm, flip angle 40 degrees, 3 to 5 averages, 147 kHz acquisition bandwidth, 8 to 10 short axis slices covering the whole left ventricle from base to apex, for a 20-30 minute acquisition time.

Left ventricular mass (LVM) was estimated from the full stack of short-axis cine images by manually segmenting the left ventricle using freely available software Segment (Medviso, Sweden,(26)) http://segment.heiberg.se/. Infarct size was calculated from the late gadolinium images in Segment using the auto delineate (weighted method) function that was constrained by the endo and epicardial borders defined in the prior segmentation of LVM. The operator was blinded as to the genotype and treatment group of the mice.

Transthoracic echocardiography and calculations

Transthoracic echocardiography was performed using an i13L probe (10-14 MHz) and a Vivid 7 Dimension system (GE Healthcare Ultrasound, Horten, Norway) on mice sedated with 2% isoflurane for the duration of the procedure. Two-dimensional echocardiography was used to measure left ventricular outflow tract (LVOT) dimensions, visualize myocardial ischemia, and to evaluate wall motion and score as being: normal 1, hypokinesis 2, akinesis 3, dyskinesis 4, and aneurysmal 5. The wall motion score index (WMSI) was calculated as (sum of all scores / number of segments viewed) for 6-10 segments. The thickness of LV anterior and posterior wall at end diastole ($LVAW_d$, $LVPW_d$), LV dimension at end diastole and systole (LVD_d, LVD_s), and left atrial dimensions at end systole (LAD_s) were measured by M-mode echocardiography. LV mass was calculated using formula recommended by Liao Y *et al*. (40). LV fractional shortening and ejection fraction (FS, EF) were obtained by formulae within Vivid 7 system software. Trans mitral flow peak velocity in early filling (E), E wave deceleration time (53), deceleration rate (62), and the time interval from mitral valve closure to opening (MV_{CO}) were determined by pulsed wave Doppler (PW), as were velocity of systolic and diastolic (S, D) waves in both left lower and upper pulmonary venous flow. LVOT flow was obtained by PW, and traced to get stroke volume (SV) and cardiac output (CO). LV ejection time (LVET) was measured in LVOT flow. LV global myocardial performance index (MPI_{global}) was calculated as (MV_{CO}-LVET)/LVET X 100 %. Enlarged PW was used to measure isovolumetric relaxation time (IVRT). Mitral lateral and septal annulus moving velocity in systole (S_L, S_S), early and atrial diastole (e', a'), and time interval from ending of a' to beginning of e'(b), and from beginning to end of S_L / S_S (a) were measured by tissue Doppler imaging. LV regional MPI was calculated by (b-a)/a X 100 % for both lateral and septum. Average of three consecutive cardiac cycles was used for all measurements.

Histological analysis and immunostaining

Formalin-fixed hearts were dehydrated by treatment with solutions of increasing alcohol content (70%, 95%, and 100%), followed by xylene, and then embedded in paraffin. The

samples were then cut into 6 μm sections and mounted on charged slides. Each sample was tested for histomorphology and immunohistochemistry. Paraffin-embedded ventricle cross-sections were stained with Masson's trichrome. Collagen content was calculated and expressed as a percentage of the total left ventricular tissue area each section (20X magnification). The thickness of the infarcted wall and the percentage of left ventricular wall that was infarcted were measured (20X magnification). Cardiomyocyte diameter was measured in four different regions of the left ventricular wall at 100X magnification using Image Pro Plus version 7.0 (Media Cybernetics, Silver Spring, MD).

Prior to immunohistochemistry, citrate antigen retrieval and endogenous peroxidase blocking (3% hydrogen peroxide) were performed. Sections were then blocked by incubating in phosphate-buffered saline (PBS) containing 10% normal serum (same species as secondary antibody) for 20 minutes. Tissues were incubated with a commercially-available mouse monoclonal antibody against α-smooth muscle actin (α-SMA; Sigma, MO) or rabbit polyclonal antibodies against matrix metalloproteinase 9 (MMP9; Abcam, AB38898) or CD206 (anti-mannose receptor antibody, a macrophage marker; Abcam, AB64693), diluted in PBS containing 1% normal serum, overnight at 4°C in a humidified chamber. Primary antibodies were omitted for negative controls. After washing, sections were incubated with a biotinylated secondary antibody (Vector Labs, Burlingame, CA) for 30 minutes. Sections were then washed, incubated with streptavidin-HRP (Vector Labs) for 30 minutes and visualized using a DAB-peroxidase substrate solution (Vector Labs). Finally, the sections were counterstained with hematoxylin and mounted with Permount. The number of α-SMA-positive vessels located within non-infarcted myocardium and the infarct border zone was determined by manual counting. MMP9 and CD206 immunoreactivity in the scar and scar border zone was evaluated by color segmentation. All analyses were performed using Image Pro Plus version 7.0 (Media Cybernetics, Silver Spring, MD).

Isolation of myocardial fibroblasts

Cardiac fibroblasts were isolated from 12–14-week-old $MK5^{+/+}$, $MK5^{+/-}$, $MK5^{-/-}$ mice as described earlier (37). Briefly, mice were sacrificed by cervical dislocation. The heart was

excised and placed in sterile PBS (137 mM NaCl, 2.7 mM KCl, 4.2 mM $Na_2HPO_4 \cdot H_2O$, 1.8 mM KH_2PO_4, pH 7.4) at 37°C. The atria were removed, ventricular tissue macerated using scissors, and subjected to a series of digestions in dissociation medium (116.4 mM NaCl, 23.4 mM HEPES, 0.94 mM $NaH_2PO_4.H_2O$, 5.4 mM KCl, 5.5 mM dextrose, 0.4 mM $MgSO_4$, 1 mM $CaCl_2$, 1 mg/ml BSA, 0.5 mg/ml collagenase type IA, 1 mg/ml trypsin, and 0.020 mg/ml pancreatin, pH 7.4). Digestion was aided by gentle shaking on an orbital shaker maintained at 37°C. Digests were centrifuged at 1500 rpm for 5 minutes and the pellet was re-suspended in 4 ml of M199 media supplemented with 10% fetal bovine serum (FBS) and 2% penicillin/streptomycin. The cell suspension was plated into two 35 mm cell culture dishes and incubated in a humidified incubator at 37°C in a 5% CO_2 atmosphere. The medium was changed after 150 min to remove unattached cells and debris. Cultures from passages 2 were used.

Scratch-wound assay

Cardiac fibroblasts were seeded at 33 x 10^3 cells per ml and maintained in culture at 37°C in an atmosphere of 5% CO_2 until 80% confluent. Cells were then washed with 1X PBS and maintained in serum-free M199 media for 24 hours. On the day of the assay, scratches made using 100 µl pipette tips. Wells were then carefully washed with 1X PBS to remove detached cells, followed by the addition of 1 ml of serum-free M199 media alone (control), 1 ml of serum-free M199 media containing 1 µM angiotensin II, 1 ml of M199 containing 10% FBS, or 1 ml of M199 containing 10% FBS and 1 µM angiotensin II. At time zero, 6 and 24 hours, images were taken at 4X magnification using a Nikon inverted phase contrast microscope. 'Wound' areas were quantified using the ImageJ software version 1.49p and the percentage reduction in of wound area was calculated using the following formula: relative open wound area (%)=[wound area on the indicated time point/original wound area]×100.

MK5 knockdown

As MK5-deficient mice ($MK5^{+/-}$, $MK5^{-/-}$) experience a chronic reduction in MK5 levels, compensatory effects may have occurred. Hence, we also characterized fibroblasts from

$MK5^{+/+}$ mice following a knock down of MK5 using small inhibitory RNA (siRNA): referred to herein as MK5-kd. These experiments were performed using mice with the same genetic background. Cells ($8x10^4$/well) were seeded into 12-well plates. Twenty-four hours post sub-culture, the media was replaced with Opti-MEM containing Ambion Silencer-Select MK5 siRNA (5 pmol) (catalog number: 4390771 ID: s69588 and s69586) and Lipofectamine 2000 (2 µl) (Invitrogen) and cells incubated for 19 hours. Following a media change and an additional incubation in M199 media containing 10% FBS for 12 hours, and in serum-free M199 media for 12 additional hours. On the day of the assay, scratches were made in each well and the cells were incubated with or without angiotensin II in serum-free M199 for 24 hours. Images were captured at two different time zero and twenty-four hours later using an inverted microscope at 4X magnification. Scratch wound areas were quantified using the ImageJ software 1.49p and the percentage of wound area relative to the original wound were calculated as described above.

Proliferation assay

Fibroblast proliferation was determined using the CyQUANT Cell Proliferation Assay kit (Invitrogen) according to the manufacturer's protocol. Briefly, 1000 fibroblasts/well were plated in a 96-well plate. Cardiac fibroblasts were cultured for 24 hours in M199 media containing 10% FBS in the presence or absence of 1 µM angiotensin II. After treatment, the medium was removed by gently inverting the microplate. The plates were then stored frozen at -80°C for up to 4 weeks. At the time of processing, the plates were thawed at room temperature, and then 200 µl of CyQUANT dye/cell-lysis buffer was added to each well and plates were incubated for 2-5 minutes at room temperature in the dark. Fluorescence was measured using a BioTek Synergy 2 Microplate Reader (excitation λ=480 nm, emission λ=520 nm).

Statistical analysis

Statistical analysis was performed using GraphPad Prism version 6h for the Mac OSX (GraphPad Software, La Jolla, CA). Student's t-tests were employed for comparisons between

two groups. When comparing between more than two groups, one-way ANOVA followed by Tukey's multiple comparisons test was performed. Two-way ANOVA followed by Bonferroni's multiple comparisons test was used between more than two groups with two grouping variables. Survival rates were compared using Kaplan-Meier survival analysis (log-rank test). The correlation between infarct size and collagen content was tested by linear regression analysis. Values were shown as mean and SEM. A value of $P< 0.05$ was considered statistically significant.

4.4 Results

Survival rates of wild type and MK5 haploinsufficient mice after LAD ligation

We have shown previously that MK5 immunoreactivity is present in cardiac fibroblasts but not myocytes and that, compared to wild type littermates, MK5 haplodeficiency is associated with attenuation of both cardiac hypertrophy and the increase in collagen type 1-α1 mRNA induced by constriction of the transverse aorta (44). In light of this apparent effect of reduced MK5 levels on collagen expression, the present study was undertaken to determine the effects of MK5 haplodeficiency (63) on reparative fibrosis (scar formation) secondary to a myocardial infarction. There are three overlapping phases to post-ischemic cardiac repair wherein dead myocytes are replaced by a stable scar: (i) inflammation, (ii) proliferation/fibrosis, and (iii) maturation (21). Hence, myocardial infarctions were induced by ligation of the left anterior descending coronary artery and mice were examined eight and twenty-one days later. The cardiac phenotype of MK5 haplodeficient mice has been described (44). Reduced MK5 levels did not predispose mice to early post-operative mortality: six of thirty-five wild type mice died or were sacrificed within 24 hours of ligation whereas two of twenty-four MK5 haplodeficient mice died. There were no deaths in the sham-operated groups. Within the first seven days post-MI, corresponding to the inflammatory and scar formation phases of repair, survival rates for LADL-MK5$^{+/+}$ and LADL-MK5$^{+/-}$ mice were 62% (20 of 32 survived; excluding 3 mice that were euthanized within 24 hours of surgery as they were in distress) and 71% (17 of 24 survived), respectively (**Figure 1**). Postmortem examination showed that 60% of the premature deaths were due to rupture of the left ventricular wall, at the margin of the infarct, in wild type and MK5 haplodeficient mice with the incidence peaking 4-to-7 days after surgery. In MK5$^{+/-}$ mice, rupture was associated with large scars whereas MK5$^{+/+}$ mice with both large and medium-sized scars experienced rupture of the LV wall. In the 21-day cohorts, seven LADL-MK5+/+ mice (out of 16 surviving mice: 44% mortality in week 1) died within one-week post-MI and none died thereafter. In contrast, four LADL-MK5+/- mice (out of 9 surviving mice: 44%) died within one-week post-MI and two additional mice died thereafter (at day 9 and 11).

Echocardiographic characterization of cardiac structure and function following LAD ligation

Echocardiographic examination of LADL-MK5$^{+/+}$ and LADL-MK5$^{+/-}$ mice 7 days after surgery revealed that left ventricular systolic and diastolic diameters were similarly increased indicating left ventricular dilation (**Table 1**). Thinning of the left ventricular anterior wall reached significance in MK5$^{+/+}$ (sham; 0.786 ± 0.013 mm, LAD; 0.576 ± 0.041 mm, n = 20, $P< 0.05$) but not MK5$^{+/-}$ mice (sham; 0.784 ± 0.019 mm, LADL; 0.641 ± 0.049 mm, n = 17). Left ventricular ejection fraction was significantly reduced in both LADL-MK5$^{+/+}$ (sham; 76.1 ± 1.1%, LADL; 37.1 ± 4.0%, n = 20, $P< 0.0001$) and LADL-MK5$^{+/-}$ (sham; 72.7 ± 2.0%, LADL; 44.5 ± 5.5%, n = 17, $P< 0.01$) mice indicating systolic dysfunction. In addition, the wall motion score index (WMSI), an assessment of regional systolic function, was increased from a value of 1 in the sham groups to 1.86 ± 0.12 and 1.90 ± 0.15 in the LADL-MK5$^{+/+}$ and LADL-MK5$^{+/-}$ mice, respectively, indicating a similar extent of wall motion abnormality. E wave deceleration times were reduced and deceleration rates increased in both LADL-MK5$^{+/+}$ and LADL-MK5$^{+/-}$ mice indicating a restrictive filling pattern. Finally, myocardial performance index was increased to a similar extent in both LADL-MK5$^{+/+}$ and LADL-MK5$^{+/-}$ mice. These observations suggest that reduced expression of MK5 had neither detrimental nor beneficial effects on cardiac function after MI.

Tissue Morphology

Delayed enhancement cardiac magnetic resonance imaging (CMRI) using a gadolinium contrast agent provides a non-invasive means to visualize and quantify the infarcted area. Estimates of scar size obtained by CRMI eight days post-MI, and segmentation of the infarct areas using short axis images, suggested reduced infarct size in MK5$^{+/-}$ mice (**Figure 2**). Nine mice in each group were sacrificed eight days post-MI and their hearts were evaluated (**Figure 3A**). After left ventricular myocardial infarction, the infarcted myocardium undergoes accelerated extracellular matrix deposition (9) and a major component of the scar is collagen, which is critical for the formation of a stable scar. Hence, the collagen content in the scar was examined in paraffin-embedded short-axis sections of the ventricular myocardium by

Masson's trichrome staining (**Figure 3A**). LADL-MK5$^{+/-}$ hearts displayed significantly lower collagen content (stained blue) within the scar compared with LADL-MK5$^{+/+}$ hearts (**Figure 3B**). No genotype-dependent differences in collagen content were observed in sham hearts (not shown). Scar area was also reduced in MK5 haplodeficient mice (**Figure 3C**). After ligation, but prior to closing the incision, the surgeon (blinded with respect to genotype) classified the infarct zones according to size (small, medium, large). The distribution was similar in MK5$^{+/+}$ and MK5$^{+/-}$ hearts: 70% medium infarct, 20% large infarct and 10% small infarct (**Figure 3D**). Interestingly, when scar morphologies were examined in the same group of mice eight days post-MI, following Masson's trichrome staining, there were fewer mice in the medium and large categories and a shift towards smaller scar size compared to immediately post-surgery in MK5$^{+/-}$ mice whereas the distribution of scar size in MK5$^{+/+}$ hearts resembled the distribution of infarct area (**Figure 3E**). LV wall thickness across the scar did not differ significantly between LADL-MK5$^{+/+}$ and LADL-MK5$^{+/-}$ mice (**Figure 3F**): there was thinning of LV wall in both LADL-MK5$^{+/+}$ and LADL-MK5$^{+/-}$ mice compared to their respective sham operated mice. Cardiomyocyte diameter in the surviving myocardium was unaltered eight days post-MI (Data Not Shown).

Inflammatory cell infiltration

During post-MI healing, monocytes are recruited to the infarcted region where they differentiate into macrophages. Macrophages contribute to the healing process by: 1) phagocytosing dead cells and extracellular debris, 2) secreting growth factors and cytokines to regulate fibroblast function and angiogenesis, and 3) producing both matrix metalloproteinases (MMPs) and inhibitors of MMP activity (19). The presence of inflammatory cells in the scar was assessed by immunohistochemical staining for CD206 in both mice that died from scar within the first seven days post-MI and mice sacrificed eight days post-MI. CD206 immunoreactivity was similar in the scar border regions of LADL-MK5$^{+/+}$ and the LADL-MK5$^{+/-}$ mice that experienced scar rupture. However, there was a small, but not significant, reduction in CD206 immunoreactivity in the scar border regions in LADL-MK5$^{+/-}$ mice sacrificed on day eight compared with LADL-MK5$^{+/+}$ mice (**Figure 3G**).

MMP-9 immunoreactivity

Matrix metalloproteinases (MMPs), including MMP-9, play an important role in extracellular matrix remodeling and wound healing post-MI (17, 27, 55). We next assessed the presence of MMP-9 immunoreactivity in the scar border zone in both mice that experienced scar rupture within the first seven days post-MI and mice sacrificed 8-days post-MI. MMP-9 immunoreactivity was significantly increased in the scar border zone of LADL-MK5$^{+/-}$ hearts having undergone scar rupture (**Figure 3H**); however, no differences were observed between LADL-MK5$^{+/+}$ and LADL-MK5$^{+/-}$ hearts sacrificed 8-days after surgery. Moreover, there were significantly lower levels of MMP-9 immunoreactivity in both LADL-MK5$^{+/+}$ and LADL-MK5$^{+/-}$ hearts 8 days after surgery compared to those that experience scar rupture (**Figure 3H**).

Angiogenesis

Angiogenesis, an important step for the restoration of blood supply post-MI, was assessed by immunohistochemistry using an antibody directed against smooth muscle α-actin (α-SMA). No significant differences in the number of αSMA-positive vessels were observed in LV sections from sham-operated wild type and MK5 haplodeficient mice (**Figure 4A**) and in non-infarct areas in LADL-MK5$^{+/+}$ and LADL-MK5$^{+/-}$ hearts (**Figure 4B**). In contrast, αSMA-positive vessels were more abundant in the scar border zone in LADL-MK5$^{+/-}$ compared to LADL-MK5$^{+/+}$hearts (**Figure 4C**).

Motility is decreased in MK5-deficient fibroblasts

MK5 immunoreactivity is present in cardiac fibroblasts but not cardiomyocytes (44). As the scar area and collagen content (**Figure 3B,C**) were reduced in LADL-MK5$^{+/-}$ mice and fibroblasts are the main source of collagen, we next examined the effect of reduced MK5 expression on fibroblast function *in vitro*. Ventricular fibroblasts were isolated from the hearts of MK5$^{+/+}$, MK5$^{+/-}$, and MK5$^{-/-}$ mice. Migration was assessed by scratch-wound assay. Fibroblasts were grown to 80% confluency, 'wounds' created, and the cells incubated for an additional 24 hours with or without addition of serum and/or angiotensin II to the media.

Wound areas were measured morphometrically at time zero and after 6 and 24 hours. After 6 hours in culture, no significant differences in wound closure were observed between serum and/or angiotensin II stimulated cardiac fibroblasts compared to unstimulated cells. The percentage of wound closure was also comparable between genotypes after 6 hours (Data Not Shown) with one exception: in the presence of serum plus angiotensin II, $MK5^{+/-}$ fibroblasts showed significantly smaller open wound areas than $MK5^{-/-}$ fibroblasts ($MK5^{+/+}$: 92.0 ± 2.2%, $MK5^{+/-}$: 79.9 ± 9.0%, $MK5^{-/-}$: 97.3 ± 0.9%, $MK5^{+/-}$ versus $MK5^{-/-}$: $P < 0.05$, n=3). Furthermore, after 24 hours of culture in serum-free medium, open wound areas between cardiac fibroblasts from all three genotypes still did not differ significantly ($MK5^{+/+}$; 73.8 ± 4.7%, $MK5^{+/-}$; 76.7 ± 3.7%, $MK5^{-/-}$; 85.6 ± 0.1%, n=3; **Figure 5A,B**). However, after 24 hours, open wound areas in $MK5^{+/+}$ and $MK5^{+/-}$ fibroblasts treated with angiotensin II were reduced significantly in comparison with $MK5^{-/-}$ fibroblasts. After 24 hours of serum stimulation, the relative open wound areas were reduced to 20.7 ± 4.1% and 10.3 ± 8.6% for $MK5^{+/+}$ and $MK5^{+/-}$ fibroblasts whereas the open wound area for $MK5^{-/-}$ fibroblasts was 63.9 ± 14.1% (**Figure 5A,B**). Treatment with serum and angiotensin II for 24 hours produced results comparable to those observed with serum alone.

As a life-long reduction in MK-5 expression may have resulted in compensatory changes, we next examined the effects of an acute reduction in MK5 expression on fibroblast motility. Small interfering RNA was used to silence MK5 expression (MK5-kd). Immunoblotting indicated the siRNA-mediated knockdown using a single siRNA reduced the abundance of MK5 by 80-85% (**Figure 6A**). Knocking down MK5 in cardiac fibroblasts using siRNA decreased motility when treated with either serum or angiotensin II for 24 hours in comparison with fibroblasts transfected with a scrambled siRNA control (**Figure 6B**). Hence, either an acute or chronic depletion of MK5 markedly impairs cardiac fibroblast motility.

Proliferation is decreased in MK5-deficient fibroblasts

An essential component of the fibrotic response is an increase in fibroblast proliferation. To determine if deleting MK5 altered proliferation, ventricular fibroblasts isolated from $MK5^{+/+}$, $MK5^{+/-}$, and $MK5^{-/-}$ mice were incubated for 24 hours in media containing 10% serum and

then cell number was quantified using a fluorescent double-stranded DNA-binding dye, CyQUANT. $MK5^{-/-}$ fibroblasts showed a significantly lower rate of proliferation than did the wild-type fibroblasts (**Figure 7**). Haplodeficient fibroblasts showed a modest, but not significant, reduction.

4.5 Discussion

The findings in the present study demonstrate that eight days post-MI the survival rate for $MK5^{+/+}$ and $MK5^{+/-}$ mice did not differ significantly; however, mortality was higher in $MK5^{+/-}$ mice 21 days post-MI. Eight days post-MI, MK5 haplodeficient mice had smaller scars and Masson's trichrome staining indicated these scars contained less collagen. In fact, in $MK5^{+/-}$ mice there was a shift towards smaller scar size at sacrifice compared to the infarct size observed immediately following ligation. MMP-9 immunoreactivity, more abundant in the peri-infarct region of $MK5^{+/-}$ mice having experienced LV wall rupture, and inflammatory cell infiltration did not differ significantly eight days post-MI. αSMA-positive vessels were significantly more abundant in the scar border region of $MK5^{+/-}$ hearts. Fibroblast proliferation and migration plays an important role in wound healing and both were decreased in fibroblasts isolated from $MK5^{-/-}$ mice compared with fibroblasts from $MK5^{+/-}$ or $MK5^{+/+}$ mice. As MK5 immunoreactivity is present in cardiac fibroblasts and not in cardiomyocytes (44), these results imply a role for MK5 in regulating reparative fibrosis via alterations in fibroblast function.

There are three phases to post-MI tissue repair: inflammation, proliferation, and maturation. Myocardial infarction results in cell death, damage to the extracellular matrix, which in turn evoke a transient inflammatory response. Inflammation, in turn, plays a key role in the myocardial healing process (20). In response cytokine (i.e., TNF, IL-1β, IL-6) and chemokine release, mononuclear cells and neutrophils migrate into the infarcted myocardium, where cellular and ECM debris are removed by monocyte-derived macrophages. The inflammatory phase is also associated with a rapid activation of MMPs (47, 70). For tissue repair to proceed, the inflammatory response must end. An inflammatory response that is excessive or prolonged may result in left ventricular dilation and systolic dysfunction (20) or possibly enhanced cardiac rupture due to excessive MMP activity and ECM degradation (28, 32, 42, 49). Clinical studies have shown cardiac rupture to be associated with increased inflammatory cell infiltration and MMP-9 expression (31, 68). In the present study, the incidence of cardiac rupture as well as left ventricular dilation and reduced systolic function in MK5 haplodeficient mice seven days post-MI did not differ significantly from wild type mice, suggesting the inflammatory phase of tissue repair was not adversely affected by reduced

levels of MK5.

MMP-9 activity increases 3-5 days post-MI and then declines as the inflammatory phase of repair is resolved (3, 36). In the mice that died due to cardiac rupture, MK5 haplodeficiency was associated with increased MMP-9 immunoreactivity in the peri-infarct region, but no differences were observed in surviving mice 8-days post-MI. MMP-9 plays a significant role in both ECM remodeling and cardiac rupture following an MI (11, 17, 29). Inflammatory cells, including neutrophils and macrophages, have been implicated as a source of MMPs in cases of enhanced cardiac rupture (22, 49, 70) and M1 macrophages release MMP-9 (36, 43). However, cardiomyocytes also serve as a source of MMPs in the MI border zone (29). As there was no difference in macrophage infiltration between $MK5^{+/+}$ and $MK5^{+/-}$ mice, and MK5 immunoreactivity is not detected in adult mouse cardiomyocytes (44), fibroblasts may be responsible for the enhanced MMP9 production observed in the peri-infarct region of ruptured hearts.

In response to myocardial injury, fibroblasts become activated, differentiate into myofibroblast, and display increased proliferation, migration, and collagen production (7, 13). MAPK signaling plays a role in collagen production as well as migration, and proliferation of cardiac fibroblasts (13, 41, 48). Although its mechanism of activation is controversial (63) and its substrates are largely unknown, MK5 has been implicated in several important biological processes including transcription, cytoskeletal remodeling, migration, and tumorigenesis. As debris are cleared from the infarcted myocardium, the inflammatory response subsides and the proliferative phase of tissue repair begins. This process requires the proliferation and migration of fibroblasts as well as their phenoconversion to myofibroblasts. One week post-MI, MK5 haplodeficient mice had smaller infarcts containing less collagen, with similar rates of death through cardiac rupture, compared with wild-type littermates. Reduced MK5 expression does not prevent murine ventricular fibroblast activation to αSMA-expressing myofibroblasts *in vitro*(44). In contrast, we observed that MK5-deficiency reduced both the motility and proliferation of ventricular fibroblasts in culture relative to wild type or haplodeficient fibroblasts. Previous studies have shown that the ectopic expression of a constitutively active MK5 (MK5 L335G) inhibits proliferation in an U2OS osteosarcoma cell line (35) whereas ectopic expression of wild-type MK5 inhibits Ras-induced proliferation in BJ human fibroblasts (66), murine skin fibroblasts (66), and NIH3T3 cells (10, 39).

Furthermore, inhibition of proliferation in NIH3T3 requires nuclear localization of MK5 (39). The apparent discrepancy on proliferation may be related to differences in cell type or the means whereby MK5 signaling was manipulated experimentally. For example, MK5-deficient mice generated by targeting exon 6 versus exon 8 display phenotypic differences in tumor suppression even though both models involved deletions within the kinase catalytic domain (56, 63, 66).

Cell migration involves cytoskeletal rearrangement, the formation of membrane protrusions, and cell spreading. In its unphosphorylated state, the small heat-shock protein hsp27 sequesters globular actin and stabilizes filamentous actin (18). Phosphorylation of hsp27 at serines-15/-78/-82 causes hsp27 to dissociate from actin, permitting polymerization of cortical actin and microfilament rearrangement (4, 38). As MK5 can phosphorylate hsp27 at these sites (45) it may be involved in regulating cytoskeletal remodeling. There is, however, some debate about MK5 contributing to hsp27 phosphorylation *in vivo*, as phosphorylation of hsp25 (the rat and mouse homolog of hsp27) in response to cellular stress is unaffected by deletion of MK5 in murine embryonic fibroblasts (63). Alternatively, in other model systems, MK5 has been implicated in hsp27 phosphorylation and actin remodeling. Ectopic expression of MK5 in HeLa cells induces hsp27 phosphorylation and formation of actin stress fibers whereas MK5 T182A, a form of MK5 that cannot be activated, has no effect (12, 67). Migration is reduced in MK5-deficient endothelial cells (72). HeLa cells transfected with MK5 show increased migration whereas cells transfected with kinase-dead MK5 T182A do not (67). Transient transfection of HeLa cells with 14-3-3ξ, which inhibits MK5, inhibits migration induced by either TNF-α or ectopic expression of MK5 (67). Transfection of HeLa cells or human HaCaT keratinocytes with hTid-1_S, a member of the hsp40 family that inhibits MK5, inhibits TNF-α induced migration, whereas downregulation of endogenous hTid-1_S expression in HeLa cells increases both TNFα- and hypoxia-induced migration (12). In tumor-derived cell lines, knocking down IGF2BP1, which increases the abundance of MK5 activator ERK4, results in a decrease in cell migration that is rescued by knocking down MK5 (64). Similarly, VEGF induced migration in wild-type cells but not MK5-deficient mouse vascular endothelial cells or HUVECs (72). In transfected MDA-MB-231 and MCF-7 breast cancer cells, increasing ERK3 expression, an activator of MK5, increases cell motility (2). Hence, a role for MK5 in cytoskeletal remodeling and migration has been demonstrated in

several different cell systems; however, the actual role played by MK5 appears to vary depending upon the cellular model and, possibly, the cellular environment. In the present study, migration and proliferation were reduced in MK5-deficient fibroblast and following siRNA-mediated knockdown but not haplodeficient cells whereas differences in reparative fibrosis were observed in MK5 haplodeficient mice. These apparent disparate results may be related to the contextual differences between fibroblasts *in vivo* and those maintained in 2D culture on a rigid matrix.

Revascularization of the infarct zone is essential for scar formation and the successful healing of the myocardium. Within few hours of infarction, a rapid angiogenic response is activated that leads to the formation of new blood vessels in the infarct zone in order to provide oxygen and nutrients to mesenchymal cells in the healing infarct (21). Initially, the newly formed vessels have neither pericyte nor smooth muscle cell mural coat, resulting in hyperpermeable and proinflammatory vessels (21, 54). During the scar maturation phase, the infarct neovessels become coated with these mural cells in response to platelet-derived growth factor (50, 73). Defective vascular coating is associated with prolonged inflammatory extravasation and decreased collagen deposition in the healing infarct. Therefore, proper vessel maturation is required for the inhibition of granulation tissue formation, resolution of the inflammation post-MI, and the formation of stable scar (50). Eight days post-MI, there was no significant difference in the number of αSMA-positive vessels in the healthy myocardium of $MK5^{+/+}$ and $MK5^{+/-}$ hearts. In contrast, αSMA-positive vessels were more abundant in the peri-infarct zone in $MK5^{+/-}$ compared to $MK5^{+/+}$ hearts. Further studies will be required to determine if there exists a relationship between the smaller infarct size observed in the MK5 haplodeficient mice and the increased number of mature vessels.

Potential Limitations

The mice employed in the present study express lower amounts of MK5 at the protein level, not just the amount of activatable MK5. As MK5 has been shown to form complexes with several signaling proteins, including p38 MAP kinase (45, 61), ERK3 (15, 60), ERK4 (1, 33), Cdc14A (24), kalirin-7 (6) and septins 7 and 8 (6) it is not clear at present if the alterations in reparative fibrosis and fibroblast function we observed was a result of reduced

MK5 activity per se or alterations in protein-protein interactions resulting from a reduction in MK5 as a molecular scaffold. In addition, the mice used in this study are a pan-knockout and, considering the important role played by other cell types in post-MI repair of the myocardium, further studies should be undertaken using a fibroblast-targeted reduction in MK5 expression. In addition, MK5 haplodeficient mice showed alterations in wound repair whereas $MK5^{+/-}$ fibroblasts behaved similar to wild-type fibroblasts *in vitro* and only $MK5^{-/-}$ fibroblasts showed any marked alterations in motility or proliferation. This may be due to the absence of the many factors, such as stretch, a 3-dimensional extracellular matrix, or contact with other cell types, that these cells normally experience *in vivo*.

4.6 Conclusions

In conclusion, the present study shows that reduced MK5 was neither beneficial nor detrimental to viability, the extent of LV dilation, or systolic dysfunction eight days post-MI. In contrast, MK5 haplodeficiency resulted in increased neovascularization in the peri-infarct region and reduced scar size and scar collagen content. MK5-deficiency also resulted inimpaired proliferative and migratory responses in cultured ventricular fibroblasts. Our study discloses a novel role of MK5 in reparative fibrosis and cardiac fibroblast function.

Acknowledgements

Histological analysis was performed in the histology core facility in the laboratory of Dr. Martin Sirois at the Montreal Heart Institute. We thank Karine Bouthillier and Robert Parent for animal care and breeding and Dr. Dharmendra Dingar for his help in the proliferation analysis. This work was supported by grants from the Heart and Stroke Foundation of Canada, and Montreal Heart Institute Foundation (FICM) to BGA. SAN was supported by the Faculty of Graduate and Postdoctoral Studies of the Université de Montréal and The Egyptian Supreme Council of Universities. JCT holds the Canada Research Chair in translational and personalized medicine and the Université de Montréal Pfizer endowed research chair in atherosclerosis.

4.7 References

1. Aberg E, Perander M, Johansen B, Julien C, Meloche S, Keyse SM, and Seternes OM. Regulation of MAPK-activated protein kinase 5 activity and subcellular localization by the atypical MAPK ERK4/MAPK4. *J Biol Chem* 281: 35499-35510, 2006.

2. Al-Mahdi R, Babteen N, Thillai K, Holt M, Johansen B, Wetting HL, Seternes OM, and Wells CM. A novel role for atypical MAPK kinase ERK3 in regulating breast cancer cell morphology and migration. *Cell Adh Migr* 9: 483-494, 2015.

3. Anzai A, Anzai T, Nagai S, Maekawa Y, Naito K, Kaneko H, Sugano Y, Takahashi T, Abe H, Mochizuki S, Sano M, Yoshikawa T, Okada Y, Koyasu S, Ogawa S, and Fukuda K. Regulatory role of dendritic cells in postinfarction healing and left ventricular remodeling. *Circulation* 125: 1234-1245, 2012.

4. Benndorf R, Hayess K, Ryazantsev S, Wieske M, Behlke J, and Lutsch G. Phosphorylation and supramolecular organization of murine small heat shock protein HSP25 abolish its actin polymerization-inhibiting activity. *J Biol Chem* 269: 20780-20784, 1994.

5. Bogoyevitch MA, Gillespie-Brown J, Ketterman AJ, Fuller SJ, Ben-Levy R, Ashworth A, Marshall CJ, and Sugden PH. Stimulation of the stress-activated mitogen-activated protein kinase subfamilies in perfused heart. p38/RK mitogen-activated protein kinases and c-Jun N-terminal kinases are activated by ischemia/reperfusion. *Circ Res* 79: 162-173, 1996.

6. Brand F, Schumacher S, Kant S, Menon MB, Simon R, Turgeon B, Britsch S, Meloche S, Gaestel M, and Kotlyarov A. The extracellular signal-regulated kinase 3 (mitogen-activated protein kinase 6 [MAPK6])-MAPK-activated protein kinase 5 signaling complex regulates septin function and dendrite morphology. *Mol Cell Biol* 32: 2467-2478, 2012.

7. Burstein B, Libby E, Calderone A, and Nattel S. Differential behaviors of atrial versus ventricular fibroblasts: a potential role for platelet-derived growth factor in atrial-ventricular remodeling differences. *Circulation* 117: 1630-1641, 2008.

8. Cassidy PJ, Schneider JE, Grieve SM, Lygate C, Neubauer S, and Clarke K. Assessment of motion gating strategies for mouse magnetic resonance at high magnetic fields. *J Magn Reson Imaging* 19: 229-237, 2004.

9. Chang HY, Chi JT, Dudoit S, Bondre C, van de Rijn M, Botstein D, and Brown PO. Diversity, topographic differentiation, and positional memory in human fibroblasts. *Proc Natl Acad Sci U S A* 99: 12877-12882, 2002.

10. Chen G, Hitomi M, Han J, and Stacey DW. The p38 pathway provides negative feedback for Ras proliferative signaling. *J Biol Chem* 275: 38973-38980, 2000.

11. Chiao YA, Dai Q, Zhang J, Lin J, Lopez EF, Ahuja SS, Chou YM, Lindsey ML, and Jin YF. Multi-analyte profiling reveals matrix metalloproteinase-9 and monocyte chemotactic protein-1 as plasma biomarkers of cardiac aging. *Circ Cardiovasc Genet* 4: 455-462, 2011.

12. Choi JH, Choi DK, Sohn KC, Kwak SS, Suk J, Lim JS, Shin I, Kim SW, Lee JH, and Joe CO. Absence of a human DnaJ protein hTid-1S correlates with aberrant actin cytoskeleton organization in lesional psoriatic skin. *J Biol Chem* 287: 25954-25963, 2012.

13. Chung CC, Kao YH, Yao CJ, Lin YK, and Chen YJ. A Comparison of Left and Right Atrial Fibroblasts Reveals Different Collagen Production Activity and Stress-induced Mitogen-activated Protein Kinase Signaling in Rats. *Acta Physiol (Oxf)* 2016.

14. Court NW, dos Remedios CG, Cordell J, and Bogoyevitch MA. Cardiac expression and subcellular localization of the p38 mitogen-activated protein kinase member, stress-activated protein kinase-3 (SAPK3). *J Mol Cell Cardiol* 34: 413-426, 2002.

15. Dingar D, Benoit MJ, Mamarbachi AM, Villeneuve LR, Gillis MA, Grandy S, Gaestel M, Fiset C, and Allen BG. Characterization of the expression and regulation of MK5 in the murine ventricular myocardium. *Cell Signal* 22: 1063-1075, 2010.

16. Dingar D, Merlen C, Grandy S, Gillis MA, Villeneuve LR, Mamarbachi AM, Fiset C, and Allen BG. Effect of pressure overload-induced hypertrophy on the expression and localization of p38 MAP kinase isoforms in the mouse heart. *Cell Signal* 22: 1634-1644, 2010.

17. Ducharme A, Frantz S, Aikawa M, Rabkin E, Lindsey M, Rohde LE, Schoen FJ, Kelly RA, Werb Z, Libby P, and Lee RT. Targeted deletion of matrix metalloproteinase-9 attenuates left ventricular enlargement and collagen accumulation after experimental myocardial infarction. *J Clin Invest* 106: 55-62, 2000.

18. During RL, Gibson BG, Li W, Bishai EA, Sidhu GS, Landry J, and Southwick FS. Anthrax lethal toxin paralyzes actin-based motility by blocking Hsp27 phosphorylation. *EMBO J* 26: 2240-2250, 2007.

19. Frangogiannis NG. The immune system and cardiac repair. *Pharmacol Res* 58: 88-111, 2008.

20. Frangogiannis NG. The inflammatory response in myocardial injury, repair, and remodelling. *Nat Rev Cardiol* 11: 255-265, 2014.

21. Frangogiannis NG. Pathophysiology of Myocardial Infarction. *Compr Physiol* 5: 1841-1875, 2015.

22. Gao XM, Ming Z, Su Y, Fang L, Kiriazis H, Xu Q, Dart AM, and Du XJ. Infarct size and post-infarct inflammation determine the risk of cardiac rupture in mice. *Int J Cardiol* 143: 20-28, 2010.

23. Gerits N, Shiryaev A, Kostenko S, Klenow H, Shiryaeva O, Johannessen M, and Moens U. The transcriptional regulation and cell-specific expression of the MAPK-activated protein kinase MK5. *Cell Mol Biol Lett* 14: 548-574, 2009.

24. Hansen CA, Bartek J, and Jensen S. A functional link between the human cell cycle-regulatory phosphatase Cdc14A and the atypical mitogen-activated kinase Erk3. *Cell Cycle* 7: 325-334, 2008.

25. Hayashidani S, Tsutsui H, Ikeuchi M, Shiomi T, Matsusaka H, Kubota T, Imanaka-Yoshida K, Itoh T, and Takeshita A. Targeted deletion of MMP-2 attenuates early LV rupture and late remodeling after experimental myocardial infarction. *Am J Physiol Heart Circ Physiol* 285: H1229-1235, 2003.

26. Heiberg E, Sjogren J, Ugander M, Carlsson M, Engblom H, and Arheden H. Design and validation of Segment--freely available software for cardiovascular image analysis. *BMC Med Imaging* 10: 1, 2010.

27. Heymans S, Luttun A, Nuyens D, Theilmeier G, Creemers E, Moons L, Dyspersin GD, Cleutjens JP, Shipley M, Angellilo A, Levi M, Nube O, Baker A, Keshet E, Lupu F, Herbert JM, Smits JF, Shapiro SD, Baes M, Borgers M, Collen D, Daemen MJ, and Carmeliet P. Inhibition of plasminogen activators or matrix metalloproteinases prevents cardiac rupture but impairs therapeutic angiogenesis and causes cardiac failure. *Nat Med* 5: 1135-1142, 1999.

28. Hilfiker-Kleiner D, Shukla P, Klein G, Schaefer A, Stapel B, Hoch M, Muller W, Scherr M, Theilmeier G, Ernst M, Hilfiker A, and Drexler H. Continuous glycoprotein-130-mediated signal transducer and activator of transcription-3 activation promotes inflammation, left ventricular rupture, and adverse outcome in subacute myocardial infarction. *Circulation* 122: 145-155, 2010.

29. Inoue T, Ikeda M, Ide T, Fujino T, Matsuo Y, Arai S, Saku K, and Sunagawa K. Twinkle overexpression prevents cardiac rupture after myocardial infarction by alleviating impaired mitochondrial biogenesis. *Am J Physiol Heart Circ Physiol* 311: H509-519, 2016.

30. Ju H, Zhao S, Jassal DS, and Dixon IM. Effect of AT1 receptor blockade on cardiac collagen remodeling after myocardial infarction. *Cardiovasc Res* 35: 223-232, 1997.

31. Kameda K, Matsunaga T, Abe N, Fujiwara T, Hanada H, Fukui K, Fukuda I, Osanai T, and Okumura K. Increased pericardial fluid level of matrix metalloproteinase-9 activity in patients with acute myocardial infarction: possible role in the development of cardiac rupture. *Circ J* 70: 673-678, 2006.

32. Kandalam V, Basu R, Abraham T, Wang X, Awad A, Wang W, Lopaschuk GD, Maeda N, Oudit GY, and Kassiri Z. Early activation of matrix metalloproteinases underlies the exacerbated systolic and diastolic dysfunction in mice lacking TIMP3 following myocardial infarction. *Am J Physiol Heart Circ Physiol* 299: H1012-1023, 2010.

33. Kant S, Schumacher S, Singh MK, Kispert A, Kotlyarov A, and Gaestel M. Characterization of the atypical MAPK ERK4 and its activation of the MAPK-activated protein kinase MK5. *J Biol Chem* 281: 35511-35519, 2006.

34. Kendall RT, and Feghali-Bostwick CA. Fibroblasts in fibrosis: novel roles and mediators. *Front Pharmacol* 5: 123, 2014.

35. Kress TR, Cannell IG, Brenkman AB, Samans B, Gaestel M, Roepman P, Burgering BM, Bushell M, Rosenwald A, and Eilers M. The MK5/PRAK kinase and Myc form a negative feedback loop that is disrupted during colorectal tumorigenesis. *Mol Cell* 41: 445-457, 2011.

36. Kubota A, Hasegawa H, Tadokoro H, Hirose M, Kobara Y, Yamada-Inagawa T, Takemura G, Kobayashi Y, and Takano H. Deletion of CD28 Co-stimulatory Signals Exacerbates Left Ventricular Remodeling and Increases Cardiac Rupture After Myocardial Infarction. *Circ J* 80: 1971-1979, 2016.

37. Kumaran C, and Shivakumar K. Calcium- and superoxide anion-mediated mitogenic action of substance P on cardiac fibroblasts. *Am J Physiol Heart Circ Physiol* 282: H1855-1862, 2002.

38. Lavoie JN, Hickey E, Weber LA, and Landry J. Modulation of actin microfilament dynamics and fluid phase pinocytosis by phosphorylation of heat shock protein 27. *J Biol Chem* 268: 24210-24214, 1993.

39. Li Q, Zhang N, Zhang D, Wang Y, Lin T, Wang Y, Zhou H, Ye Z, Zhang F, Lin SC, and Han J. Determinants that control the distinct subcellular localization of p38α-PRAK and p38β-PRAK complexes. *J Biol Chem* 283: 11014-11023, 2008.

40. Liao Y, Ishikura F, Beppu S, Asakura M, Takashima S, Asanuma H, Sanada S, Kim J, Ogita H, Kuzuya T, Node K, Kitakaze M, and Hori M. Echocardiographic assessment of LV hypertrophy and function in aortic-banded mice: necropsy validation. *Am J Physiol Heart Circ Physiol* 282: H1703-1708, 2002.

41. Mitchell MD, Laird RE, Brown RD, and Long CS. IL-1β stimulates rat cardiac fibroblast migration via MAP kinase pathways. *Am J Physiol Heart Circ Physiol* 292: H1139-1147, 2007.

42. Monden Y, Kubota T, Tsutsumi T, Inoue T, Kawano S, Kawamura N, Ide T, Egashira K, Tsutsui H, and Sunagawa K. Soluble TNF receptors prevent apoptosis in infiltrating cells and promote ventricular rupture and remodeling after myocardial infarction. *Cardiovasc Res* 73: 794-805, 2007.

43. Murray PJ, Allen JE, Biswas SK, Fisher EA, Gilroy DW, Goerdt S, Gordon S, Hamilton JA, Ivashkiv LB, Lawrence T, Locati M, Mantovani A, Martinez FO, Mege JL, Mosser DM, Natoli G, Saeij JP, Schultze JL, Shirey KA, Sica A, Suttles J, Udalova I, van Ginderachter JA, Vogel SN, and Wynn TA. Macrophage activation and polarization: nomenclature and experimental guidelines. *Immunity* 41: 14-20, 2014.

44. Nawaito SA, Dingar D, Sahadevan P, Hussein B, Sahmi F, Shi Y, Gillis MA, Gaestel M, Tardif JC, and Allen BG. MK5 haplodeficiency attenuates hypertrophy and preserves diastolic function during remodeling induced by chronic pressure overload in the mouse heart. *Am J Physiol Heart Circ Physiol* 313: H46-H58, 2017.

45. New L, Jiang Y, Zhao M, Liu K, Zhu W, Flood LJ, Kato Y, Parry GC, and Han J. PRAK, a novel protein kinase regulated by the p38 MAP kinase. *EMBO J* 17: 3372-3384, 1998.

46. Ni H, Wang XS, Diener K, and Yao Z. MAPKAPK5, a novel mitogen-activated protein kinase (MAPK)-activated protein kinase, is a substrate of the extracellular-regulated kinase (ERK) and p38 kinase. *Biochem Biophys Res Commun* 243: 492-496, 1998.

47. Nian M, Lee P, Khaper N, and Liu P. Inflammatory cytokines and postmyocardial infarction remodeling. *Circ Res* 94: 1543-1553, 2004.

48. Pan Z, Zhao W, Zhang X, Wang B, Wang J, Sun X, Liu X, Feng S, Yang B, and Lu Y. Scutellarin alleviates interstitial fibrosis and cardiac dysfunction of infarct rats by inhibiting

TGFβ1 expression and activation of p38-MAPK and ERK1/2. *Br J Pharmacol* 162: 688-700, 2011.

49. Peng H, Xu J, Yang XP, Dai X, Peterson EL, Carretero OA, and Rhaleb NE. Thymosin-β4 prevents cardiac rupture and improves cardiac function in mice with myocardial infarction. *Am J Physiol Heart Circ Physiol* 307: H741-751, 2014.

50. Prabhu SD, and Frangogiannis NG. The Biological Basis for Cardiac Repair After Myocardial Infarction: From Inflammation to Fibrosis. *Circ Res* 119: 91-112, 2016.

51. Protti A, Dong X, Andia ME, Yu B, Dokukina K, Chaubey S, Phinikaridou A, Vizcay-Barrena G, Taupitz M, Botnar RM, and Shah AM. Assessment of inflammation with a very small iron-oxide particle in a murine model of reperfused myocardial infarction. *J Magn Reson Imaging* 39: 598-608, 2014.

52. Protti A, Sirker A, Shah AM, and Botnar R. Late gadolinium enhancement of acute myocardial infarction in mice at 7T: cine-FLASH versus inversion recovery. *J Magn Reson Imaging* 32: 878-886, 2010.

53. Quan TE, Cowper S, Wu SP, Bockenstedt LK, and Bucala R. Circulating fibrocytes: collagen-secreting cells of the peripheral blood. *Int J Biochem Cell Biol* 36: 598-606, 2004.

54. Ren G, Michael LH, Entman ML, and Frangogiannis NG. Morphological characteristics of the microvasculature in healing myocardial infarcts. *J Histochem Cytochem* 50: 71-79, 2002.

55. Rohde LE, Ducharme A, Arroyo LH, Aikawa M, Sukhova GH, Lopez-Anaya A, McClure KF, Mitchell PG, Libby P, and Lee RT. Matrix metalloproteinase inhibition attenuates early left ventricular enlargement after experimental myocardial infarction in mice. *Circulation* 99: 3063-3070, 1999.

56. Ronkina N, Johansen C, Bohlmann L, Lafera J, Menon MB, Tiedje C, Laass K, Turk BE, Iversen L, Kotlyarov A, and Gaestel M. Comparative Analysis of Two Gene-Targeting

Approaches Challenges the Tumor-Suppressive Role of the Protein Kinase MK5/PRAK. *PLoS One* 10: e0136138, 2015.

57. Roux PP, and Blenis J. ERK and p38 MAPK-Activated Protein Kinases: a Family of Protein Kinases with Diverse Biological Functions. *Microbiology and Molecular Biology Reviews* 68: 320-344, 2004.

58. Sane DC, Mozingo WS, and Becker RC. Cardiac rupture after myocardial infarction: new insights from murine models. *Cardiol Rev* 17: 293-299, 2009.

59. Schneider JE, Cassidy PJ, Lygate C, Tyler DJ, Wiesmann F, Grieve SM, Hulbert K, Clarke K, and Neubauer S. Fast, high-resolution in vivo cine magnetic resonance imaging in normal and failing mouse hearts on a vertical 11.7 T system. *J Magn Reson Imaging* 18: 691-701, 2003.

60. Schumacher S, Laass K, Kant S, Shi Y, Visel A, Gruber AD, Kotlyarov A, and Gaestel M. Scaffolding by ERK3 regulates MK5 in development. *EMBO J* 23: 4770-4779, 2004.

61. Seternes OM, Mikalsen T, Johansen B, Michaelsen E, Armstrong CG, Morrice NA, Turgeon B, Meloche S, Moens U, and Keyse SM. Activation of MK5/PRAK by the atypical MAP kinase ERK3 defines a novel signal transduction pathway. *EMBO J* 23: 4780-4791, 2004.

62. Shi Y, Denault AY, Couture P, Butnaru A, Carrier M, and Tardif JC. Biventricular diastolic filling patterns after coronary artery bypass graft surgery. *J Thorac Cardiovasc Surg* 131: 1080-1086, 2006.

63. Shi Y, Kotlyarov A, Laaβ K, Gruber AD, Butt E, Marcus K, Meyer HE, Friedrich A, Volk HD, and Gaestel M. Elimination of protein kinase MK5/PRAK activity by targeted homologous recombination. *Mol Cell Biol* 23: 7732-7741, 2003.

64. Stöhr N, Köhn M, Lederer M, Glass M, Reinke C, Singer RH, and Huttelmaier S. IGF2BP1 promotes cell migration by regulating MK5 and PTEN signaling. *Genes Dev* 26: 176-189, 2012.

65. Stuckey DJ, Carr CA, Camelliti P, Tyler DJ, Davies KE, and Clarke K. In vivo MRI characterization of progressive cardiac dysfunction in the mdx mouse model of muscular dystrophy. *PLoS One* 7: e28569, 2012.

66. Sun P, Yoshizuka N, New L, Moser BA, Li Y, Liao R, Xie C, Chen J, Deng Q, Yamout M, Dong MQ, Frangou CG, Yates JR, 3rd, Wright PE, and Han J. PRAK is essential for ras-induced senescence and tumor suppression. *Cell* 128: 295-308, 2007.

67. Tak H, Jang E, Kim SB, Park J, Suk J, Yoon YS, Ahn JK, Lee JH, and Joe CO. 14-3-3epsilon inhibits MK5-mediated cell migration by disrupting F-actin polymerization. *Cell Signal* 19: 2379-2387, 2007.

68. van den Borne SW, Cleutjens JP, Hanemaaijer R, Creemers EE, Smits JF, Daemen MJ, and Blankesteijn WM. Increased matrix metalloproteinase-8 and -9 activity in patients with infarct rupture after myocardial infarction. *Cardiovasc Pathol* 18: 37-43, 2009.

69. Vanhoutte L, Gerber BL, Gallez B, Po C, Magat J, Jean-Luc B, Feron O, and Moniotte S. High field magnetic resonance imaging of rodents in cardiovascular research. *Basic Res Cardiol* 111: 46, 2016.

70. Yang Y, Ma Y, Han W, Li J, Xiang Y, Liu F, Ma X, Zhang J, Fu Z, Su YD, Du XJ, and Gao XM. Age-related differences in postinfarct left ventricular rupture and remodeling. *Am J Physiol Heart Circ Physiol* 294: H1815-1822, 2008.

71. Yin T, Sandhu G, Wolfgang CD, Burrier A, Webb RL, Rigel DF, Hai T, and Whelan J. Tissue-specific pattern of stress kinase activation in ischemic/reperfused heart and kidney. *J Biol Chem* 272: 19943-19950, 1997.

72. Yoshizuka N, Chen RM, Xu Z, Liao R, Hong L, Hu WY, Yu G, Han J, Chen L, and Sun P. A novel function of p38-regulated/activated kinase in endothelial cell migration and tumor angiogenesis. *Mol Cell Biol* 32: 606-618, 2012.

73. Zymek P, Bujak M, Chatila K, Cieslak A, Thakker G, Entman ML, and Frangogiannis NG. The role of platelet-derived growth factor signaling in healing myocardial infarcts. *J Am Coll Cardiol* 48: 2315-2323, 2006.

Figure Legends

Figure 1. MK5$^{+/+}$ and MK5$^{+/-}$ mice demonstrated similar mortality rates one week after myocardial infarction. Kaplan-Meier survival curve for MK5$^{+/-}$ (dashed line, n = 24) and MK5$^{+/+}$ littermate mice (solid line, n = 35).

Figure 2. Short-axis end-diastolic cine-MR images from MK5$^{+/+}$ and MK5$^{+/-}$ mice eight days post-MI. Shown is a representative axial image series spanning the heart from base to apex of hearts from **(A)** MK5$^{+/+}$ and **(B)** MK5$^{+/-}$ mice eight days post-MI showing the normal myocardium **(a)** and scar region **(b)**. LV, left ventricle.

Figure 3. MK5 haplodeficient mice demonstrated similar cardiac function but reduced infarct size and collagen content one week after myocardial infarction. (A) Masson's trichrome staining of short-axis sections showing collagen deposition (blue) and healthy tissue (red) in the interventricular septum (IVS), left (LV) and right (RV) ventricular walls of sham and infarcted hearts in mice of both genotypes sacrificed eight days after myocardial infarction (MI). **(B)** Quantitative analysis of the collagen content in the infarct area of mice sacrificed eight days after MI. **P*< 0.05. Statistical analysis was by two-way, unpaired *t*-test. **(C)** Scar area determined from Masson's trichrome stained short axis sections. **P*< 0.05. Statistical analysis was by two-way, unpaired *t*-test. **(D)** Size distribution, expressed as percentage, of ischemic area (small, medium, large) as assessed by surgeon in MK5$^{+/+}$ and MK5$^{+/-}$ mice (n = 9 per group). **(E)** Size distribution, expressed as percentage, of scar area (small, medium, large) as assessed by histology in mice sacrificed eight post-MI in MK5$^{+/+}$ and MK5$^{+/-}$-LADL mice (n = 9; note, panels **D** and **E** are the same mice at two different time-points). **(F)** Left ventricular wall thickness for sham and LADL mice sacrificed eight days post-MI. ****P*< 0.001. Statistical analysis was by one-way ANOVA followed by Tukey's multiple comparisons test. (n = 9 per group). **(G)** Quantitative analysis of CD206 (an inflammatory cell marker) immunoreactivity-positive cells in the infarct border region of MK5$^{+/+}$ and MK5$^{+/-}$ mice that either died of heart rupture 5 days post-MI or were sacrificed 8 days post-MI. Immunoreactivity was evaluated by color segmentation and expressed as a percentage of the total field area. Statistical analysis was by two-way ANOVA followed by Bonferroni's multiple comparisons test (n = 3 - 6 per group). **(H)** Quantitative analysis of MMP-9

immunoreactivity in the infarct border region of $MK5^{+/+}$ and $MK5^{+/-}$ mice that either died of heart rupture 5 days post-MI or were sacrificed 8 days post-MI. $^{**}P< 0.01$; $^{****}P< 0.0001$. Immunoreactivity was evaluated by color segmentation and expressed as a percentage of the total field area. Statistical analysis was by two-way ANOVA followed by Bonferroni's multiple comparisons test (n = 3-6 per group). Results shown are mean ± SEM.

Figure 4. Angiogenesis is increased in the infarct border region of $MK5^{+/-}$ mice one week after myocardial infarction. Quantitative analysis of α-SMA-positive vessels in the **(A)** left ventricular myocardium of sham $MK5^{+/+}$ and $MK5^{+/-}$ mice, **(B)** healthy myocardium of $MK5^{+/+}$-LADL and $MK5^{+/-}$-LADL hearts, and **(C)** the infarct border region in both $MK5^{+/+}$-LADL and $MK5^{+/-}$-LADL hearts of mice sacrificed eight days post MI. $^{*}p < 0.05$ as determined by two-way, unpaired *t*-test (n = 6 - 9 per group). Results shown are mean ± SEM.

Figure 5. Migration is impaired in MK5-deficient ventricular fibroblasts.(A) Migration of cardiac fibroblasts isolated from the ventricular myocardium of $MK5^{+/+}$, $MK5^{+/-}$, and $MK5^{-/-}$ mice was assessed by scratch wound migration assay. After imposing the scratch, fibroblasts were cultured in media alone (control) or media supplemented with angiotensin II (Ang II, 1 μM), serum, or angiotensin II plus serum. Open wound areas were measured at times zero and 24 hours. **(B)** Open wound areas after 24 hours expressed as a percentage of the original wound area (time zero). $^{*}P< 0.05$; $^{***}P< 0.001$; $^{****}P< 0.0001$. Statistical analysis was by two-way ANOVA followed by Bonferroni's multiple comparisons test (n = 3, results shown for each genotype are mean ± SEM of assessments performed in fibroblasts isolated from 3 different mice).

Figure 6. siRNA-mediated knockdown of MK5 impairs fibroblast motility.(A) Immunoblot showing MK5 immunoreactive bands of 48-kDa (MK5) and 62-kDa (MK5*) in cardiac fibroblast lysates from two separate cell preparations (a, b) from $MK5^{+/+}$ mice transfected with either siRNA for MK5 (si) or a scrambled RNA sequence (sc). The intensity of both 48-kDa and 62-kDa bands was reduced upon knockdown using a single siRNA. Numbers at the *right* indicate the position of molecular mass markers (in kDa). MK5* represents a novel splice variant of MK5 (44). After probing for MK5 immunoreactivity, the membrane was stripped and reprobed for GAPDH immunoreactivity, which was used as a

loading control. **(B)** Cardiac fibroblasts were isolated from the ventricular myocardium of $MK5^{+/+}$ mice, split into two, transfected with either siRNA for MK5 (si) or a scrambled RNA sequence (sc), and motility was assessed by scratch wound assay. After imposing the scratch, fibroblasts were cultured in media alone (control) or media supplemented with angiotensin II (Ang II, 1 μM) or serum. Open wound areas were measured at times zero and 24 hours. **(C)** Open wound areas after 24 hours expressed as a percentage of the original wound area (time zero). **P*< 0.05; *****P*< 0.0001. Statistical analysis was by two-way ANOVA followed by Bonferroni's multiple comparisons test. (n = 3). Results shown for each genotype are mean ± SEM of assessments performed in fibroblasts isolated from 3 different mice).

Figure 7.Proliferative activity is impaired in MK5-deficientfibroblasts. Proliferative activity was assessed in cardiac fibroblasts isolated from the ventricular myocardium of $MK5^{+/+}$ and $MK5^{-/-}$ mice. Fibroblasts were incubated in media supplemented with 10% fetal bovine serum for 24 h. Cell number was then assessed using CyQUANT cell proliferation assays (n= 3-6 per group). Statistical analysis was by one-way ANOVA followed by Bonferroni's multiple comparisons test. (n = 3-6). Results shown for each genotype are mean ± SEM of assessments performed in fibroblasts isolated from '3-6' different mice).

Table 1. Echocardiographic parameters of $MK5^{+/+}$ and $MK5^{+/-}$ mice 1 week post-MI.

	Sham		LAD	
	$MK5^{+/+}$ (n=14)	$MK5^{+/-}$ (n=8)	$MK5^{+/+}$ (n=20)	$MK5^{+/-}$ (n=17)
R-R interval (ms)	117 ± 4	117 ± 3	125 ± 6	121 ± 4
dimensions/mass				
LVAWd, mm	0.786 ± 0.013	0.784 ± 0.019	0.576 ± 0.041‡	0.641 ± 0.049
LVPWd, mm	0.723 ± 0.011	0.725 ± 0.018	0.773 ± 0.029	0.783 ± 0.045
LVDd, mm	3.81 ± 0.07	4.00 ± 0.12	4.93 ± 0.12†	4.61 ± 0.17ξ
LVDs, mm	2.31 ± 0.06	2.53 ± 0.07	4.17 ± 0.18†	3.75 ± 0.26*
LV mass, mg	100 ± 3	110 ± 6	135 ± 6‡	127 ± 6
LV mass/LVDd, mg/mm	26.4 ± 0.5	27.3 ± 0.8	27.3 ± 1.1	27.8 ± 1.1
LVmass/BW, mg/g	3.88 ± 0.08	4.03 ± 0.19	5.44 ± 0.33‡	5.11 ± 0.30ξ
LVDd/BW, mm/g	0.147 ± 0.002	0.148 ± 0.003	0.198 ± 0.009†	0.186 ± 0.010ξ
systolic function				
LVFS, %	39.4 ± 0.9	36.5 ± 1.6	16.1 ± 2.0†	20.2 ± 3.0*
LVEF, %	76.1 ± 1.1	72.7 ± 2.0	37.5 ± 4.0†	44.5 ± 5.5*
Lateral Sm, cm/s	2.73 ± 0.09	2.66 ± 0.11	1.84 ± 0.12†	1.84 ± 0.13‡
Septal Sm, cm/s	2.91 ± 0.16	2.80 ± 0.12	2.18 ± 0.11‡	2.16 ± 0.15ξ
WMSI	1.000 ± 0.0	1.000 ± 0.0	1.86 ± 0.12	1.90 ± 0.15
diastolic function				
E velocity, cm/s	84.9 ± 3.0	86.0 ±3.6	83.2 ± 4.7	79.4 ± 3.8
E DT, msec	38.1 ± 1.9	39.9 ± 2.2	30.2 ± 1.5*	28.1 ± 1.3†
E D rate, m/s^2	22.4 ± 1.1	22.1 ± 1.4	28.2 ± 1.7ξ	28.6 ± 1.4*
S/D upper	0.534 ± 0.044	0.509 ± 0.020	0.421 ± 0.053	0.353 ± 0.067
S/D lower	1.84 ± 0.09	2.03 ± 0.32	1.97 ± 0.20	2.06 ± 0.16
LV isovolumetric relaxation time				
IVRT, ms	7.81 ± 0.67	7.91 ± 0.70	8.53 ± 0.99	7.84 ± 0.81
IVRTc	0.719 ± 0.059	0.730 ± 0.059	0.747 ± 0.065	0.706 ± 0.06
myocardial performance index				
Global MPI, %	42.9 ± 3.0	42.3 ± 3.3	63.3 ± 4.2*	79.3 ± 8.0*

LVAWd, LV anterior wall end-diastolic thickness; LVPWd, LV posterior wall end diastolic thickness; LVDd, Left ventricular end-diastolic diameter; LVDs, Left ventricular end-systolic diameter; FS, Fractional shortening, LVEF, Left ventricular ejection fraction; Sm, peak systolic tissue velocity; E, early diastolic transmitral filling velocity; EDT, early diastolic transmitral filling deceleration time; ED rate, early diastolic transmitral filling deceleration

rate; S/D, pulmonary venous systolic wave/ pulmonary venous early diastolic wave; IVRT, isovolumic relaxation time; IVRTc, rate-corrected isovolumic relaxation time; MPI, myocardial performance index; WMSI, wall motion score index.Data reported as mean ±SEM. ξ, $p<0.05$ vs Sham: *, $p<0.01$ versus Sham: ‡, $p<0.001$ versus Sham: †, $p<0.0001$ versus Sham.

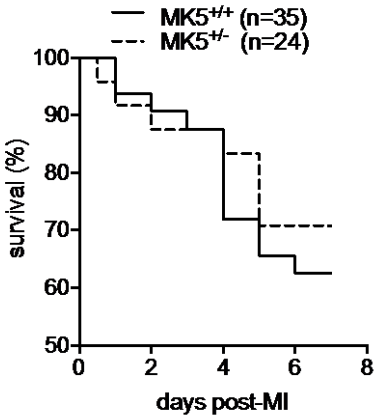

Figure 1

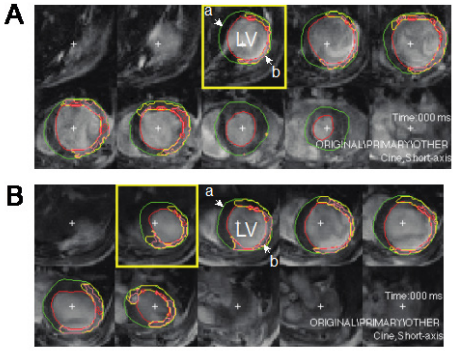

Figure 2

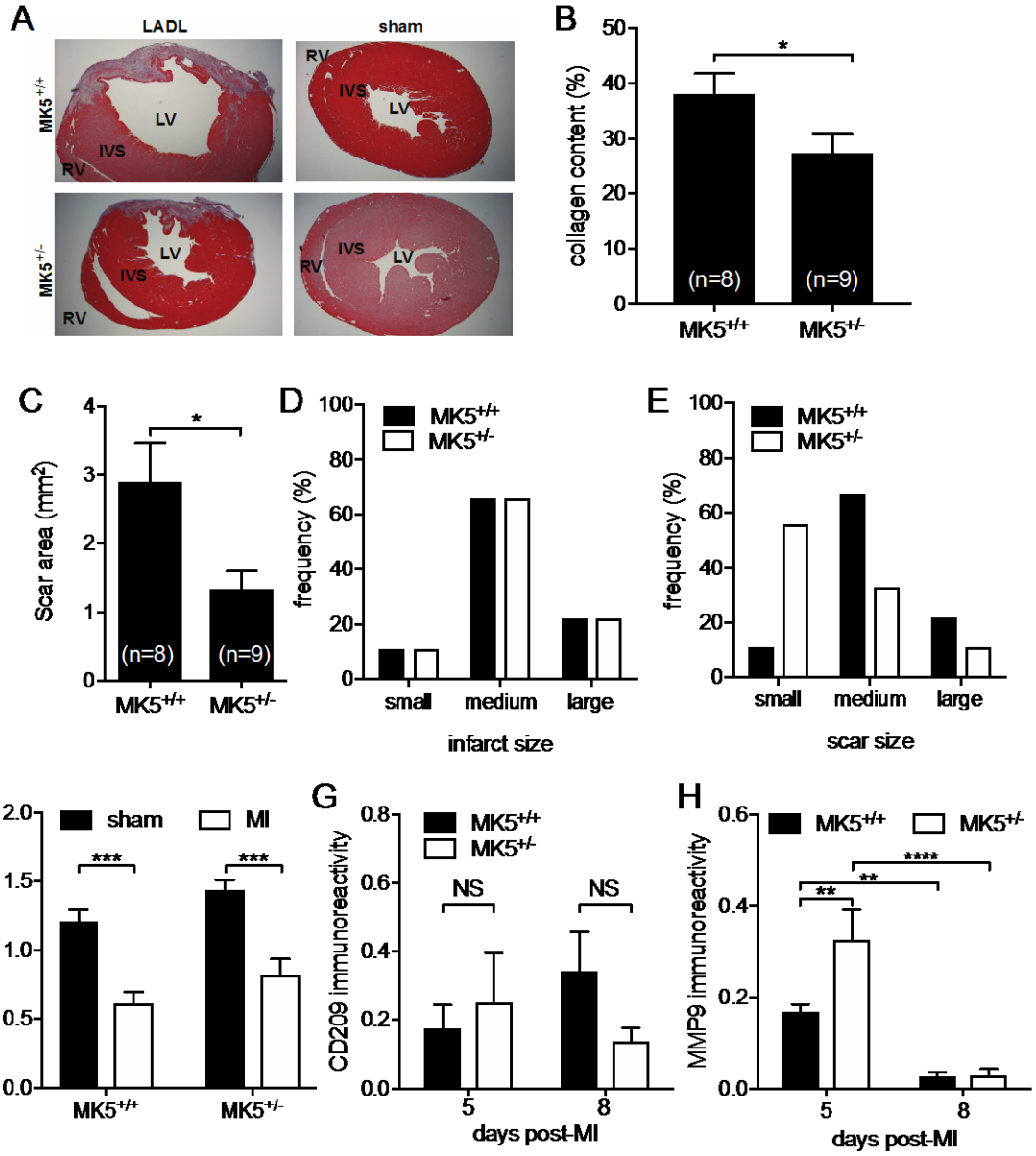
A
LADL
sham
MK5+/+
MK5+/-
LV
IVS
RV
B
collagen content (%)
(n=8)
(n=9)
MK5+/+
MK5+/-
C
Scar area (mm2)
D
frequency (%)
small
medium
large
infarct size
E
scar size
F
LV wall thickness (mm)
sham
MI
G
CD209 immunoreactivity
NS
days post-MI
H
MMP9 immunoreactivity

Figure 3

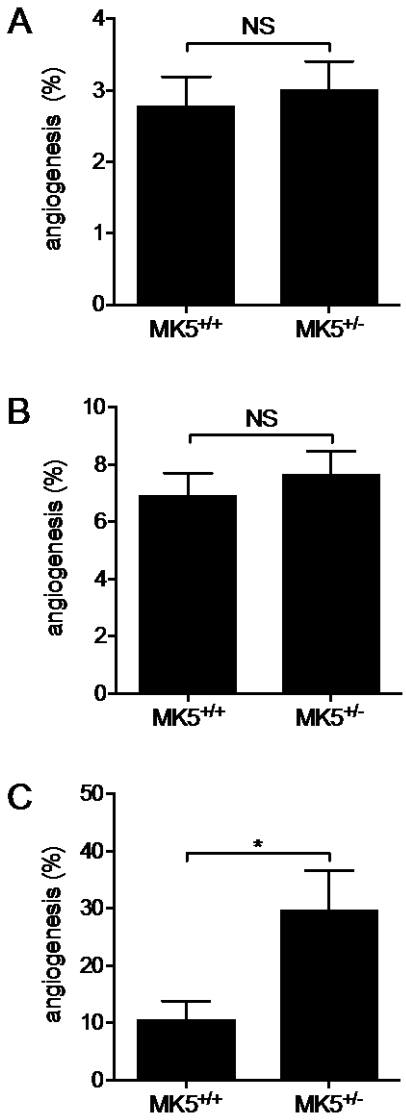
A
NS
angiogenesis (%)
4
3
2
1
0
MK5+/+
MK5+/-
B
NS
angiogenesis (%)
10
8
6
4
2
0
MK5+/+
MK5+/-
C
*
angiogenesis (%)
50
40
30
20
10
0
MK5+/+
MK5+/-

Figure 4

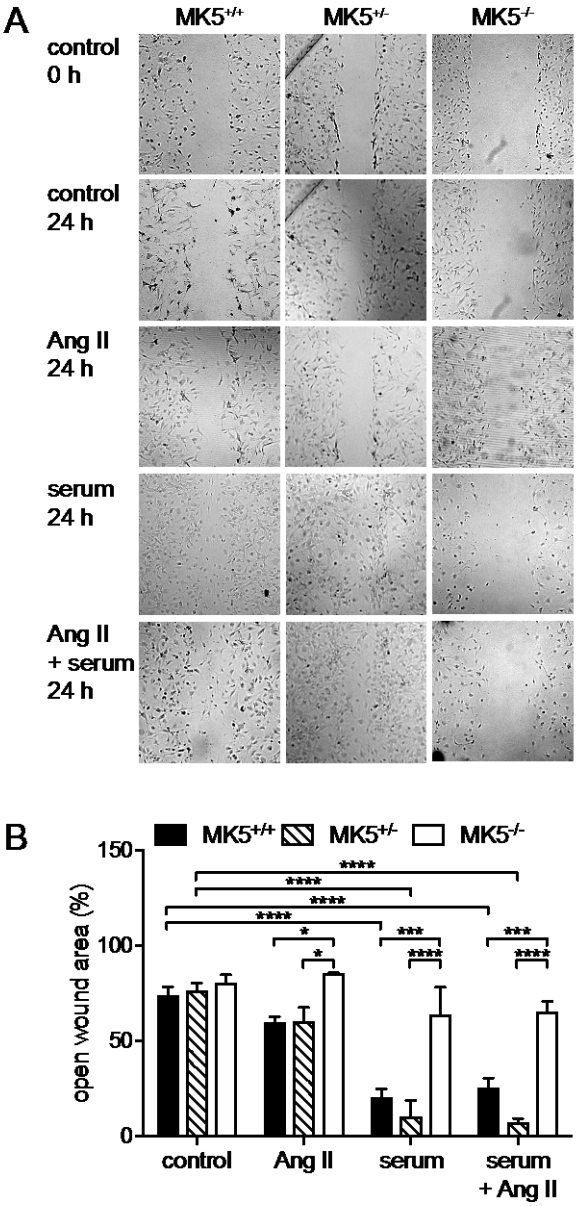
A
MK5+/+
MK5+/-
MK5-/-
control
0 h
control
24 h
Ang II
24 h
serum
24 h
Ang II
+ serum
24 h
B
MK5+/+
MK5+/-
MK5-/-
open wound area (%)
150
100
50
0
control
Ang II
serum
serum
+ Ang II

Figure 5

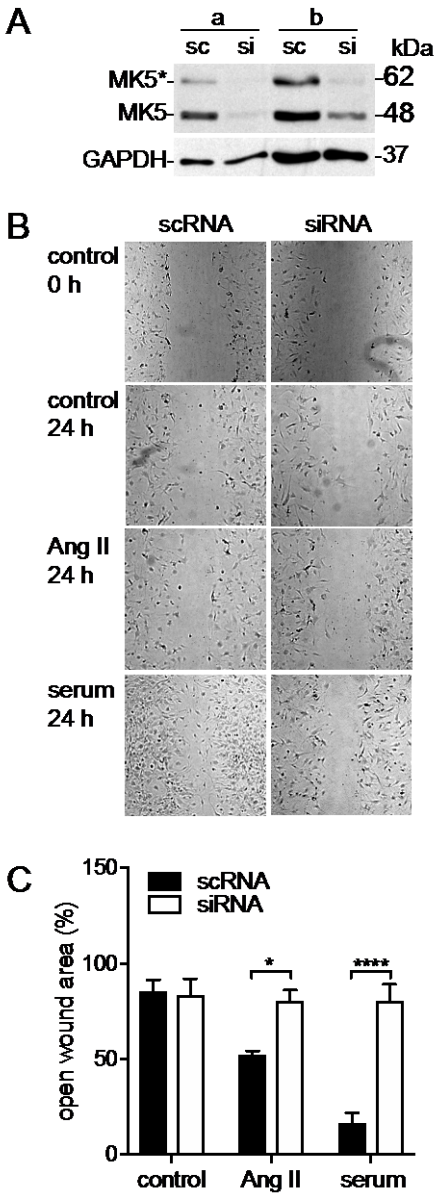
A
a
b
sc
si
sc
si
kDa
MK5*-
MK5-
GAPDH-
-62
-48
-37
B
scRNA
siRNA
control
0 h
control
24 h
Ang II
24 h
serum
24 h
C
scRNA
siRNA
open wound area (%)
150
100
50
0
*
****
control
Ang II
serum

Figure 6

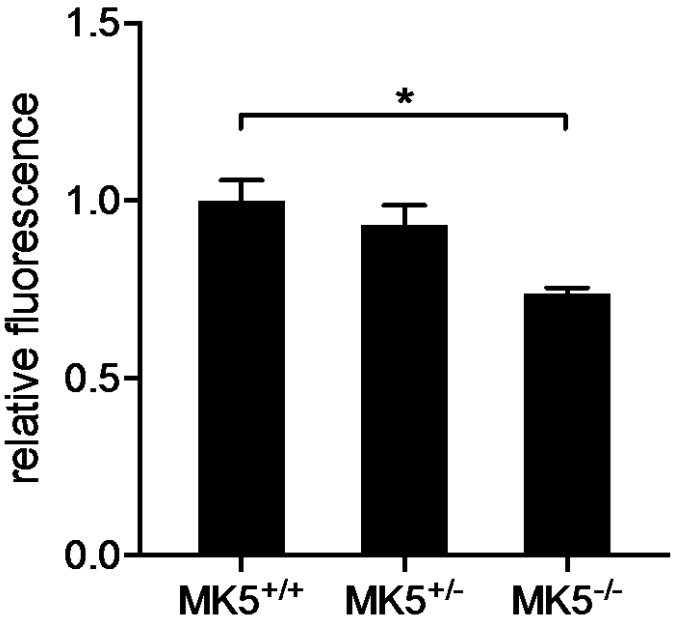

Figure 7

5 Article-3

Title: MK5 regulates collagen biosynthesis and extracellular matrix remodeling in murine ventricular cardiac fibroblasts.

This article is in preparation.

Contributions of co-autthors

S. A. Nawaito and P. Sahadevan contributed equally to this work.

Sherin Ali Nawaito: performed all the experiments of the knockout mice, RT2 profiler qPCR array, analyzed the data, interpreted the results, performed stastistical analysis, prepared figures, wrote the first draft of the manuscript, edited and revised the manuscript.

Pramod Sahadevan: performed all the experiments for MK5 knockdown, collagen gel contraction assay and immunoflorescence experiments, analyzed the data, interpreted the results, prepared figures and drafted part of the manuscript.

Fatiha Sahmi: assisted in immunoblotting experiments.

Matthias Gaestel: developer of the MK5 mice model.

Angelo Calderone: provided expertise in fibroblasts and approved the final version of the manuscript.

Bruce G. Allen: conceived and designed the experiments, analyzed the data, interpreted the results, edited the manuscript and approved the final version of the manuscript.

MK5 regulates collagen biosynthesis and extracellular matrix remodeling in cardiac ventricular fibroblasts

Sherin Ali Nawaito[b, d *], Pramod Sahadevan[a, d *], Fatiha Sahmi[d], Matthias Gaestel[e], Angelo Calderone[b, d], and Bruce G. Allen[a,b,c,d]

*These authors contributed equally

From Departments of Biochemistry and Molecular Medicine[a], Pharmacology and Physiology[b], Medicine[c], Université de Montréal and Montreal Heart Institute[d], and Institute of Biochemistry, Hannover Medical School, Hannover, Germany[e].

Address correspondence to:
Bruce G. Allen
Montreal Heart Institute
5000 Belanger St.
Montréal, Québec, Canada
H1T 1C8.
Telephone: (514) 376-3330 (3591).
FAX: (514) 376-1355.
E-mail: bruce.g.allen@umontreal.ca

Running head: Pro-fibrotic role of MK5

5.1 Abstract

mRNA for MK5, a protein serine and threonine kinase, activated by p38 MAPK and the atypical MAPKs ERK3 and ERK4, is detected a high levels in the left ventricular myocardium. However, little is understood of the physiological role of MK5 in the heart. The pressure overload-induced increase in collagen 1-α_1 mRNA is attenuated in hearts of MK5 haploinsufficient ($MK5^{+/-}$) mice whereas scar size and collagen content were reduced following a myocardial ischemia. In mice, MK5 immunoreactivity is detected in cardiac fibroblasts, but not myocytes; hence, the present study was to determine if MK5 has a role in ECM remodeling. Fibroblasts expressing lower levels of MK5 showed altered profiles mRNAs for proteins involved in ECM remodelling. In cultured $MK5^{-/-}$ fibroblasts, mRNAs for COL1A1, COL3A1, TGF-β3, Timp3, Snai1, SMAD6, and SMAD7 mRNA were increased significantly whereas those of thrombospondin 1, LTBP1, Hgf, and IL13 mRNA were decreased. mRNAs for MMPs 13, 8, 1a, and 3 as well as for IL1α & β, IL13ra2, IL4, IL10, CCL11, IFNγ and TNF showed modest, but not significant reductions. mRNA for VEGF showed modest, but not significant upregulation. Both MK5-deficient fibroblasts and those undergoing siRNA-mediated knockdown of MK5 (MK5-kd) secreted more soluble type 1 collagen and fibronectin than $MK5^{+/+}$ and $MK5^{+/-}$ fibroblasts. In addition, whereas collagen immunoreactivity was distributed throughout the cytosol of wild-type fibroblasts, it was perinuclear in $MK5^{-/-}$ fibroblasts. Finally, fibroblast contraction was decreased upon knocking down MK5. These results indicate that MK5 is involved in regulating the expression of proteins involved in remodelling of the extracellular matrix.

Keywords: MK5/PRAK, fibroblast, collagen biosynthesis, extracellular matrix remodelling, p38 MAPK

Glossary

β-ME, β-mercaptoethanol; Ang-II, angiotensin II; BSA, bovine serum albumin; CCL11, chemokine (C-C motif) ligand 11; CFs, cardiac fibroblasts; COL1A1, collagen type 1-α_1; COL3A1, collagen type 3-α_1; DTT, dithiothreitol; ECM, extracellular matrix; ER, endoplasmic reticulum; FBS, fetal bovine serum; FN, fibronectin; GAPDH, glyceraldehyde-3-phosphate dehydrogenase; Hgf, hepatocyte growth factor; IFNγ, interferon γ; IL13, interleukin 13; Itgb3, integrin beta 3; LAP, latency associated peptide; LTBP1, latent-transforming growth factor -binding protein 1; MAPK, mitogen-activated protein kinase; MCP, monocyte chemoattractant peptide; MK5, MAPK-activated protein kinase 5; $MK5^{+/-}$, MK5 haplodeficient; $MK5^{+/+}$, MK5 wild-type; $MK5^{-/-}$, MK5-deficient; MK5-kd, siRNA MK5; MMPs, matrix metalloproteinases; PBS, phosphate-buffered saline; PMSF, Phenylmethylsulfonyl fluoride; PRAK, p38-regulated/activated protein kinase; qPCR, quantitative polymerase chain reaction; siRNA, small inhibitory RNA; SDS-PAGE, sodium dodecyl sulphate-polyacrylamide gel electrophoresis; Stat1, signal transducer and activator of transcription 1;TAC, constriction of the transverse aorta; TCA, trichloroacetic acid; TGF-β, transforming growth factor β; Thbs1, thrombospondin; TIMPs, tissue inhibitor of metalloproteinases; Timp3, tissue inhibitor of metalloproteinase 3; TNFα, tumour necrosis factor α; TX-100, Triton X-100; VEGF, vascular endothelial growth factor.

5.2 Introduction

The cardiac extracellular matrix (ECM) is a highly active structural network that continuously undergoes remodeling under both normal and pathological conditions [1]. The ECM not only forms an organizational structural framework for cardiomyocytes but also distributes mechanical force throughout the myocardium, acts as an electrical barrier, transduces signals for cell-cell communication, serves as a reservoir for growth factors, and participates in biochemical signaling[2-5].Dysregulation of ECM homeostasis has been implicated in the development and progression of several pathological conditions[1].Cardiac fibrosis can be provoked by several stimuli[6-8], including angiotensin II (Ang-II)[9, 10]. Increased interstitial fibrosis is a result of changes in both the deposition and breakdown of ECM proteins, including collagen. Collagensare the most abundant and main structural constituents of the ECM, in which collagen type I and III constitute about 90% of all collagen in the heart [11]. As cardiac fibroblasts are the main cells responsible for secretion and degradation of ECM proteins, they are key modulator of ECM homeostasis [2].

Mitogen-activated protein kinase (MAPK) signaling has been shown to play a crucial role in collagen production and in the migration and proliferation of cardiac fibroblasts [12-14].p38 MAPK is activated in response to chronic pressure overload [15]and both acute and chronic activation of p38 induces interstitial fibrosis [16, 17]. Four p38 isoforms (α, β, δ, γ) have been identified, of which p38α and p38γ are the most abundant in the heart [18, 19]. MAP kinase-activated protein kinase 5 (MK5), originally named p38-Regulated/Activated Protein Kinase (PRAK) [20, 21], lies downstream of p38α and p38β [22]. In addition to p38α/β, the atypical MAPKs ERK3 and ERK4 activate MK5 [23-25]. MK5 is expressed in the heart [26] and its transcripts are in high abundance in left ventricular tissue [27]. However, MK5 immunoreactivity is detected in adult mousecardiac ventricular fibroblasts, but not in myocytes [28]. Following hemodynamic overload, the increase in collagen type 1-α_1 (COL1A1) mRNA levels is attenuated in MK5 haploinsufficient mice ($MK5^{+/-}$) [28]. Moreover, eight days post-myocardial infarction (MI), $MK5^{+/-}$ mice displayed a significant decrease in collagen content within the scar compared with $MK5^{+/+}$ mice (See chapter 4, figure 3A and B).This study was to determine if MK5 contributes to the regulation of ECM protein production by cardiac ventricular fibroblasts.

5.3 Materials and Methods

Materials

Rabbit anti-mouse type I collagen (#203002) was purchased from MD Bioproducts Inc. Mouse monoclonal fibronectin antibody (EP5) (# sc-8422) was purchased from Santa Cruz Biotechnology. Angiotensin II (# A9525), medium 199,fatty acid-free bovine serum albumin, pancreatin (# p3002-25G) and Fungizone were from Sigma-Aldrich, Fetal bovine serum (FBS) and trypsin were from Gibco Laboratories (Life Technologies Inc.).Penicillin-streptomycin solution was from Multicell. Collagenase type 1 (# LS004196) was from Worthington Biochem. Culture plates were from Sarstedt. The mouse fibrosis RT^2 profiler PCR array (PAMM-120Z) was from SABiosciences (QIAGEN Inc.). Primers and qPCR reagents were from Invitrogen. Angiotensin II was purchased from Sigma (# A9525). SDS-polyacrylamide gel electrophoresis reagents, nitrocellulose, and Bradford protein assay reagents were from Bio-Rad Laboratories. Triton X-100 (TX-100), leupeptin, and PMSF were from Roche Molecular Biochemicals.

Mice

The MK5-deficient mice employed in these studies have been described previously [28, 29] and were on a mixed 129/Ola x C57BL background. Twelve- to 13-week-old male wild type ($MK5^{+/+}$), heterozygote ($MK5^{+/-}$) and homozygote ($MK5^{-/-}$) littermate mice were used in this study. $MK5^{-/-}$ mice show embryonic lethality with incomplete penetrance resulting in only about 50% of the expected number of $MK5^{-/-}$ embryos detectable after day E12 (2-4 mice/month). However, $MK5^{-/-}$ mice were available in sufficient numbers to do experiments using MK5-null cardiac ventricular fibroblasts. All animal experiments were approved by the local ethics committee and performed according to the guidelines of the Canadian Council on Animal Care.

Isolation and culture of myocardial fibroblasts

Cardiac fibroblasts were isolated from 12–14 weeks-old $MK5^{+/+}$, $MK5^{+/-}$, $MK5^{-/-}$ mice as described earlier[30]. Briefly, mice were sacrificed by cervical dislocation. The heart was excised and placed in sterile PBS (137 mMNaCl, 2.7 mMKCl, 4.2 mM $Na_2HPO_4 \cdot H_2O$, 1.8

mM KH_2PO_4, pH 7.4) at 37°C. The atria were removed, ventricular tissue macerated using scissors, and subjected to a series of digestions in dissociation medium (116.4 mMNaCl, 23.4 mM HEPES, 0.94 mM NaH_2PO_4, 5.4 mMKCl, 5.5 mM dextrose, 0.4 mM $MgSO_4$, 1 mM $CaCl_2$, 1 mg/ml BSA, 0.5 mg/ml collagenase type IA, 1 mg/ml trypsin, and 0.020 mg/ml pancreatin, pH 7.4). Digestion was aided by gentle shaking on an orbital shaker maintained at 37°C. Digests were centrifuged at 1500 rpm for 5 minutes and the pellet was re-suspended in 4 ml of M199 media supplemented with 10% FBS and 2% penicillin/streptomycin. The cell suspension was plated into two 35 mm cell culture dishes and incubated in a humidified incubator at 37°C in a 5% CO_2 atmosphere. The medium was changed after 150 minutes to remove unattached cells and debris, and every 48 hoursthereafter. Cultures from passages 2 were used when 80% confluent. Cells were then washed with PBS and starved with serum-free M199 media for 24 hours prior to treatment with 1μM Ang-II for 6 and 24 hours.

MK5 knockdown

As $MK5^{+/-}$ and $MK5^{-/-}$ mice experience a chronic reduction in MK5 levels, compensatory effects may have occurred. Hence, we also characterized fibroblasts from $MK5^{+/+}$ mice following a knock down of MK5 using small inhibitory RNA (siRNA): referred to herein as MK5-kd. These experiments were performed using mice with the same genetic background. Cells ($8x10^4$/well) were seeded into 12-well plates. Twenty-four hours post sub-culture; the media was replaced with Opti-MEM containing Ambion Silencer-Select MK5 siRNA (5 pmol) (catalog number: 4390771 ID: s69588 and s69586) and Lipofectamine 2000 (2 μl) (Invitrogen) and cells incubated for 19 hours.Following a media change and an additional incubation in M199 media containing 10% FBS for 12 hours, and in serum-free M199 media for 12 additional hours.

RNA extraction and quantitative polymerase chain Reaction (qPCR)

Total RNA was extracted from passage 2 cardiac fibroblasts using RNeasy® Micro kits (Qiagen Inc.) following the manufacturer's instructions. First-strand cDNA was synthesized from 20 μl reaction volume containing 500 ngof RNA, 100ng of random primers, 1x First Strand buffer (50 mMTris-HCL pH 8.3, 75 mM KCL, 3 mM MgCl2), 0.5 mMdNTP, 10 mM

DTT, 40 U RNaseOUT recombinant ribonuclease inhibitor, and 200 U of M-MLV reverse transcriptaseusing the RT2 First Strand cDNA Synthesis Kit from (Invitrogen) according to the manufacturer's protocol. qPCR was performed using a MX3000P qPCR system (Stratagene). Each amplification reaction mixture (25 μl) contained 10 ngcDNA equivalent to reverse transcribed RNA, 300nM forward and reverse primers, 30 nM ROX, 12.5 μl platinum SYBR green mix (2x) (Invitrogen). qPCR reactions were: 1 cycle at 95°C for 10 min, 40 cycles at 95°C for 30 s, 60 °C for 1 min, and 1 cycle at 72 °C for 1 min, 55 °C for 30 s, and 95°C for 30 s. SYBR green fluorescence was measured at the end of the annealing and extension phases of each cycle. The specificity of each primer pair for the collagen 1A1 was verified using the dissociation curve. The amplification efficiency for each primer pair was determined from a standard curve of50–3.25 ng reverse transcribed RNA isolated from the heart after two-fold serialdilutions. The efficiency for each primer pair was between 90 and 110%. Samples were assayed in duplicate and the results were expressed relative to the internal control; Glyceraldehyde-3-phosphate dehydrogenase (GAPDH). The forward and reverse primers for collagen 1A1 are as follows: COL1-α_1 S: 5'-CTG ACG CAT GGC CAA GAA GAC A-3'. COL1-α_1 AS: 5'- CGT GCC ATT GTG GCA GAT ACA GAT -3'.

RT^2 Profiler PCR Array Transcriptomics

Total RNA was isolated from Ang-II-treated or untreated fibroblasts as described above. First-strand cDNA was synthesized from 500 ng RNA using the RT^2 First Strand kit and mRNA for proteins implicated in ECM remodeling were quantified using fibrosis pathway-targeted qPCR microarrays comprising 96-well plates pre-coated with the primers listed in Table 1 (QIAGEN PAMM-120Z). Each 96-well plate also contains primers for 5 housekeeping genes as well as positive and negative controls. qPCR was performed using an ABI StepOnePlus instrument according to the conditions describedby the array manufacturer. Data were analyzed using RT^2 profiler PCR Array Data Analysis software (Version 3.5; Qiagen Inc.) and normalized to internal controls. Changes were considered significant when $P< 0.05$.

Precipitation of proteins from conditioned culture medium

Media was collected from cultured fibroblasts and 1 ml of media was precipitated by adding

bovine serum albumin (BSA, 10 μg) and then adjusting to 10% (w/v) trichloroacetic acid (TCA) using a 100% TCA stock solution. The acidified medium was incubated on ice for 30 minutes and then centrifuged at 14,000 rpm and 4°C for 30 minutes. The supernatant was carefully aspirated and the pellet was resuspended in 30 μl of 1x SDS-PAGEsample buffer. Tris base (3 μl of 1 M stock) was added to neutralize the pH and then samples were heated for 90 seconds at 70°C, cooled, centrifuged at room temperature for 1 minute at 14,000 rpm, and loaded onto 6% acrylamide SDS-PAGE gels.

Immunoblotting

Fibroblasts were lysed in ice-cold LB1 lysis buffer comprising 50mM Tris-HCl, 20 mMβ-glycerophosphate, 20 mM NaF, 5 mM EDTA, 10 mM EGTA, 1.0% TX-100, 1mM $NaVO_4$, 1 μM microcystin LR, 5 mM DTT, 10 μg/ml leupeptin, 0.5 mM PMSF, and 10 mM benzamidine(pH 7.5 at 4°C). For immunoblotting, 1 ml of media was adjusted to 10% (w/v) trichloroacetic acid, incubated on ice for 30 minutes, centrifuged at 14,000 rpm and 4°C for 30 minutes, the supernatant removed by aspiration, the pellet resuspended in 30 μl of 1x SDS-PAGE sample buffer, and neutralized with 1 M Tris base. Precipitates were separated on 6% SDS-PAGE gels andthen transferred electrophoretically onto nitrocellulose membranes for 75 minutes at 70 volts in a buffer containing 25 mM Tris base, 192 mM glycine, 0.1% SDS and 5% methanol. Following the transfer, membranes were rinsed in PBS, fixed with 0.1% (v/v) glutaraldehyde[31], rinsed again with PBS, then blocked in 3% bovine serum albumin (BSA) in PBS overnight at 4°C on a clinical rotator. Membranes were incubated with the indicated primary antibodies diluted (collagen, 1:25,000; fibronectin, 1:1000) in TBST containing 1% (w/v) BSA for 1 hour at room temperature, washed once for 15 minutes in high salt solution (25 mM Tris base, 3 mM KCl, 500 mM NaCl, 1% (v/v) Tween 20 at pH 7.4) followed by 3 washes in TBST and then incubated with the appropriate horseradish peroxidase–conjugated secondary antibody (Jackson ImmunoResearch Laboratories, Inc., West Grove, PA, USA) diluted 1:10,000 in TBST containing 5% (w/v) non-fat dried milk. Immunoreactive bands were visualized using Western Lightning Plus ECL reagent (PerkinElmer BioSignal Inc., Montreal, Canada) and Kodak BioMax Light film. Band intensities were quantified with Bio-Rad Quantity One software.

Immunocytofluorescence

Cells were rinsed in PBST, fixed in 2% paraformaldehyde in PBS (1x) for 20 minutes, then permeabilized and blocked with PBST containing 0.2% Triton X-100 and 2% normal donkey serum. Cells were rinsed once with PBST and incubated overnight at 4°C with primary antibody for collagen I (1:100) in blocking solution. Cells were then washed three times with PBST, incubated in the dark for one hour with Alexa-Fluor-555 conjugated secondary antibody (1:500) and DAPI (1:1000) in PBST, rinsed three times with PBST, and mounted on glass slides using 15 ml of DABCO/glycerol. Images were acquired using a Zeiss LSM-512 confocal fluorescence microscope.

Collagen gel contraction assay

For a 24-well culture plate, 8.3 ml of cold collagen solution (3 mg/ml) was mixed gently with 1 ml of 10-fold concentrated cold MEM. The pH of the mixture was adjusted to 7.4 with 1M sterile NaOH and then the total volume was adjusted to 10 ml using distilled water. A 400µl aliquot of this collagen mixture was poured into each well of the plate. Plates were incubated at 37°C for 2 hours to allow the collagen to gel. A cell suspension containing $3.2x10^4$ cell/ml in M199 with 10% FCS was transferedinto each well and left for 2 hours for the cells to settle. Gel contraction was initiated (time zero) by detaching the edges of the collagen gels from the wall of the wells. To document collagen gel contraction, the gels were photographed using an inverted microscope at time zero and48 hours later.

Statistical analysis

Statistical analysis was performed using GraphPad Prism 6h for the Mac OS. Student's t-tests were employed for comparisons between two groups. When comparing between more than two groups, one-way ANOVA followed by Bonferroni multiple comparisons test was performed. Values shown are the mean and SEM. A value of $P<0.05$ was considered statistically significant.

5.4 Results

The profile of ECM mRNAs differed depending on fibroblast genotype

In MK5 haplodeficient mice the increase in collagen type 1-α_1 mRNA levels observed 2 weeks following TAC [28] was attenuated and scar size and collagen content following an MI were reduced (See Chapter 4, figure 3 A and B). As MK5 immunoreactivity is detected in cardiac fibroblasts, but not cardiomyocytes[28], we sought to study the role of MK5 in isolated cardiac ventricular fibroblasts. As fibroblasts are the primary source for proteins that form and degrade the ECM, we first examined the effects of reduced MK5 expression on the mRNA level for genes linked to ECM homeostasis by assessing using a fibrosis pathway-targeted qPCR microarray(QIAGEN PAMM-120Z). As primers for collagen type 1-α_1(Col1A1) were not included in the array, we examined is separately. Expression profilesdiffered depending on fibroblast genotype (Table 1-6). Surprisingly, of the genes examined, MK5-deficient fibroblasts showed significantly elevated evels of Col1A1 (Figure 1A), collagen type 3-α_1(Col3A1), Smad6, Smad7, tissue inhibitor of metalloproteinase 3 (Timp3), snail homologue 1 (Snai1) and transforming growth factor β3 (TGF-β3) mRNA (Figure 2A, Tables 1-3) as well as reduced levels of thrombospondin 1 (Thbs1), interleukin 13 (IL13), hepatocyte growth factor (Hgf), integrin beta 3 (Itgb3) and latent-TGF-β-binding protein 1 (LTBP1) mRNA compared to fibroblasts isolated from wild type mice(Figure 2B, Tables 2 and 3). In addition, themRNA for vascular endothelial growth factor (VEGF)(Figure 2A, Table 5) showed a modest, but not significant elevation whereas that of matrix metalloproteinases (MMPs) 13, 8, 1a and 3 showed modest, but not significant, reductions (Figure 2C, Table 1). On the otherhand,in the absence of MK5, the abundance of transcripts for several inflammatory cytokines and chemokines (IL1α, IL1β, IL13ra-2, IL10, IL4, IL13, chemokine (C-C motif) ligand 11 (CCL11), interferon γ (IFNγ), tumour necrosis factor α (TNFα)) was decreased (Figure 2D, table 4).

We next examined whether deleting MK5 altered the response of fibroblasts to the pro-fibrotic stimuli. Fibroblasts from wild type, MK5-haplodeficient, and MK5-deficient mice were treated with Ang-II for 6 or 24 hours and transcripts related to ECM remodelling examined as described above. In fibroblasts from wild type mice, Ang-II had no significant

effect on the abundance of Col1A1 mRNA (Figure 1A).However, 6 hours of Ang-II treatment significantly decreased the abundance of IL13 in $MK5^{+/+}$ fibroblasts. Hgf, IL13, Itgb3, LTBP1, and Thbs1 transcripts were reduced by treatment with Ang-II in $MK5^{-/-}$ fibroblasts whereas the Col3A1, Smad6, Smad7, TGF-β3, Timp3 and signal transducer and activator of transcription 1 (Stat1) were increased (Tables 1, 2, 4, and 5). After 24 hoursof treatment with Ang-II, Hgf and Itgb3 were significantly decreased in $MK5^{+/+}$ fibroblasts, whereas, Hgf, IL13, LTBP1, TGF-β1 and Thbs1 were significantly decreased in $MK5^{-/-}$ fibroblasts (Tables 1, 2, 4, and 5). Moreover, Col3A1 and Itgb3 were significantly increased in $MK5^{-/-}$ fibroblasts 24 hours of Ang-II treatment (Table 1). To determine if the effects on collagen 1-α_1 mRNA represented a compensatory effect to the live-long absence of MK5, we also assessed the effect of siRNA-mediated knock down of MK5 in cardiac fibroblasts on collagen mRNA expression and observed acute suppression of MK5 expression also increased the abundance of collagen 1-α_1 mRNA (Figure 1B), suggesting that reduced expression of MK5 affects transcription of *Col1a1* and/or the stability of the collagen 1-α_1 mRNAin mouse cardiac fibroblasts.

Reduced MK5 expression increases collagen secretion

To determine if the increases in collagen mRNA observed upon deletion of MK5 were of consequence at the protein level, we next examined the secretion of type 1 collagen by immunoblotting. Cardiac fibroblasts were isolated from mice of all three genotypes andincubated for 24 hours in media alone or media supplemented with Ang-II for 6 and 24-hours.Soluble type 1 collagen immunoreactivity was determined in the conditioned medium. As shown Panel A of Figure 3, collagen immunoreactivity was significantly increased in media from $MK5^{-/-}$ fibroblasts compared with media from $MK5^{+/+}$fibroblasts. In addition thesiRNA-mediated knock down of MK5 also increased the abundance of type 1collagen immunoreactivity in conditioned media, relative to fibrobalsts transfected with scrambled RNA (scRNA, Figure 3B). The presence of exogenous Ang-II in the media had no effect on the amount of type 1 collagen immunoreactivity secreted by either $MK5^{-/-}$ or MK5-kd

fibroblasts (Figure 3A,B). These observations suggest MK5 is involved in the biosynthesis and/or secretion of type 1 collagen in mouse cardiac fibroblasts.

Reduced MK5 expression increases fibronectinsecretion

Expression of fibronectin (Fn), a structural constituent of the ECM, is elevated throughout pathological remodeling after the myocardial infarction or pressure overload [32, 33]. During myocardial reparative fibrosis, a short-term induction of Fn may be beneficial because of its ability to promote proliferation of cardiac resident stem cells. We examined the effect of reduced MK5 expression on Fn secretion. In both $MK5^{-/-}$and MK5-kd fibroblasts, reduced MK5 expression significantly increased the amount of soluble fibronectin immunoreactivity in the conditioned media (Figure 4A,B). Incubation with Ang-II had no effect on the amount of soluble fibronectin immunoreactivity secreted by either $MK5^{-/-}$ or MK5-kd fibroblasts. These result indicates MK5 is involved in fibronectin biosynthesis or secretion in cardiac fibroblasts.

MK5 knockdownaltersthe subcellular distribution of type 1 collagen immunoreactivity

As the absence of MK5 increased the amount of soluble type 1 collagen immunoreactivity in conditioned media, we sought to determine if the absence of MK5 alters the subcellular distribution of type 1 collagen immunoreactivity. Confocal immunocytofluorescence microscopy revealed that in fibroblasts transfected with scrambled RNA (scRNA),type 1 immunoreactivity was diffusely distributed in the cytoplasm whereas it was condensed in the peri-nuclear region in MK5-kd fibroblasts (Figure 5A). Furthermore, the effect of reduced MK5 expression on collagen 1 distribution was similar when assessed in fibroblasts from passages 0 through 3 (Figure 5B,C).

MK5 knockdown reduces fibroblast contractility

During the process of wound repair following an MI, cardiac myofibroblasts contract to reduce the total scar area.As MK5 may be involved in remodelling of the actin cytoskeleton via phosphorylation of hsp27/25, we examined the effect of reduced MK5 expression on myofibroblast contraction using a collagen gel contraction assay system. As shown in Figure 6, fibroblasts transfected with scRNA produced greater reductions in the circumference of

collagen gels than fibroblasts transfected with siRNA targeting MK5 (MK5-kd). Hence, MK5-deficient myofibroblasts are less contractile.

5.5 Discussion

Cardiac fibroblasts constitute the largest cell population in the myocardium and contribute to multiple aspects of cardiac pathophysiology [34, 35]. One of the primary functions of CFs is to regulate the synthesis and breakdown of the ECM, a protein structure that provides structural and functional integrity to the heart. Myocardial injury can induce the differentiation and proliferation of CFs as well as the overproduction of ECM proteins[36]during the initial stage of the injury, all of which are expected to confer beneficial effects in the myocardial wound healing. However, prolonged fibroblast activation and the subsequent dysregulation of ECM homeostasis resulting in disproportionate stromal growth causes myocardial stiffness and compromise pump function[36, 37]. MK5 is a protein serine/threonine kinase activity present in cardiac ventricular fibroblasts but not myocytes. Following hemodynamic overload, the increase in collagen type 1-α_1 mRNA levels is attenuated in $MK5^{+/-}$ mice [28]. In addition, eight days post-MI, $MK5^{+/-}$ mice displayed a significant decrease in collagen content within the scar compared with $MK5^{+/+}$ mice. MK5-deficient fibroblasts also show reduced motility and proliferation. The present study was undertaken to examine further the role of MK5 in cardiac ventricular fibroblast function. In cultured fibroblasts, the abundance of mRNAs endoding proteins involved in ECM dynamics differed depending on fibroblast genotype. Moreover, type 1 collagen and fibronectin immunoreactivity was in significantly higher in conditioned media from $MK5^{-/-}$or MK5-kd fibroblasts compared to $MK5^{+/+}$or $MK5^{+/-}$ fibroblasts. Type 1 collagenimmunoreactivity was distributed diffusely in the cytoplasm of $MK5^{+/+}$ fibroblasts, whereas it was preinuclear in MK5-kd fibroblasts. In addition, in collagen gel contraction assays MK5-kd fibroblasts showed significantly lower contractility than $MK5^{+/+}$ fibroblasts. Hence, MK5 may be a regulator of ECM remodeling in the heart.

MK5 has been identified as a substrate of both p38α/β MAPKs and the atypical MAPKs ERK3 and ERK4[21, 23, 25, 38]. Although the exact biological role(s) of MK5 remain unknown, recent evidence indicates MK5 may be implicated in several cellular processes, such as cell proliferation and cancer, actin remodeling, cell migration, and apoptosis[39]. MK5 mRNA is expressed in the heart, and in high abundance in the left ventricle [27], but its role is just beginning to be understood. Recent studies from our laboratory have demonstrated that

the transverse aortic constriction (TAC)-induced increase in collagen 1-α_1mRNA observed in $MK5^{+/+}$ hearts was markedly attenuated in $MK5^{+/-}$ hearts [28]. Furthermore, $MK5^{+/-}$ heartsdeveloped smaller scars with less collagen following myocardial ischemia induced by ligation of the left anterior descending coronary artery (See chapter 4, figure 3 A, B and C). In contrast, Molkentin *et al*., have recently shown that fibroblast-directed deletion of p38α results in 100% mortality post-MI [40] whereas reduced MK5 expression does not (See chapter 4, figure 1). Hence, MK5 signalling may play a role in myocardial remodeling; however, this role may be distinct from that of p38α.

Myocardial injury triggers molecular and cellular changes in both the damaged and remote areas of the myocardium and causes widespread modifications in ventricular geometry. The inflammatory process is the first and a prerequisite associated with the repair of injured myocardium. Enhanced levels of pro-inflammatory cytokines such as TNFα, IL1, IL6, IL8, monocytechemoattractant peptide (MCP)-1/CCL2, IL-8/CXCL8 and macrophage inflammatory protein-1a /CCL3MCP1 are observed in the falling myocardium[41-44]. The initial inflammatory response is critical for cardiac repair but an inappropriate and persistent cardiac inflammation itself stimulates the maladaptive responses and therefore initiates adverse remodeling[45]. Although improper inflammatory response culminate to post-infarction remodeling and heart failure, many studies revealed that the anti-inflammatory therapy is detrimental in post-infarction repair due to impaired healing, scar thinning, and increased risk of ventricular rupture[46, 47]. Endothelial cells, resident cardiac mast cells, and vascular smooth muscle cells are the primary sources for these pro-inflammatory cytokines in the myocardium. During the inflammatory phase of post-injury healing, these cytokine and chemokine signals recruit and/or activate cardiac fibroblasts at the site of injury from the intra- and extra-cardiac sources. Activated fibroblasts transform into myofibroblasts, an additional source for a number of cytokines, which in turn assist to maintain the inflammatory response to injury[48]. In this study, we have demonstrated that the absence of MK5 reduces the mRNA abundance of inflammatory cytokines and chemokines such as IL13, IL1α, IL1β, IL1ra-2, IL10, IL4, CCL11, IFNγ, and TNFα in cultured fibroblasts; hence, MK5 may regulate the expression profile of inflammatory modulators during cardiac remodeling.

Cardiac fibroblasts are pleomorphic cells and their behavioural pattern depends on their microenvironment. Their response to cytokines as well as various mechanical and electrical parameters make them major players in cardiac remodeling [49-53]. In this study, the mRNA for ECM proteins and type 1 collagen immunoreactivity were examined. Surprisingly, COL1A1 (Figure 1A), COL3A1, TGF-β3, Timp3, Snai1, SMAD6, and SMAD7 transcripts were significantly increased in MK5-deficient fibroblasts (Figure 2A)whereas the level of TSP-1, Hgf, and LTBP1 mRNA was reduced (Figure 2B). Notably, the increase in the secretion of type 1 collagen paralleled that of*Col1a1* mRNA (Figure 3A). In contrast, *in vivo*, reduced MK5 expression attenuated the TAC-induced increase in*Col1a1* mRNA as well as the collagen content within the scar post-MI. In addition, motility and proliferation were significantly decreased in $MK5^{-/-}$ cardiac fibroblasts and/or MK5-kd fibroblasts in culture(See chapter 4, figure 5, 6 and 7). The explanation for these differences between *in vivo* and *in vitro* modelsmay lie in the artificial nature of a two-dimensional mono-culture system. *In vivo*, fibroblasts are constantly subjected to mechanical stretch and are responsive to various chemical stimuli whereas *in vitro*, the hard plastic surfaces andaltered cell-cell and/or cell-ECM contacts may affect both the fibroblast transcriptome and the signalling events upstream and downstream of MK5. It has been shown that the synthesis and remodeling of new ECM proteins deposited at the site of injury is regulated by the changes in mechanical tension. Regional differences such as changes in mechanical force may be involved in differential fibroblast differentiation and activation [54]. There is lack of knowledge about how fibroblasts sense their local and global environments and how they transduce these changes to modulate their phenotype.

TGF-β is a multifunctional growth factor involved in broad range of cellular processes such as proliferation, migration, differentiation, and apoptosis[55]. Following myocardial injury, enhance TGF-β expression, and associated modulation of its downstream effectors such as Smad2/3, have been commonly observed [56]. TGF-β signaling can affect fibroblast phenotype and gene expression and play an important role in the pathogenesis of cardiac remodeling and fibrosis[57]. Although TGF-β utilizes both Smad-dependent and -independent signaling pathways, the Smad3-dependent mechanism is implicated in the development of fibrosis[58, 59]. On the other hand, studies have provided new understanding of the inhibitory role of Smad6

and Smad7(inhibitory Smads), the structurally divergent Smad family members, in switching off TGF-β signaling by interfering with the activation of receptor-regulated Smads. TGF-β is secreted as an inactive latent peptide in with TGF-β non-covalently bound to the latency associated peptide (LAP). Proteolytic cleavage and separation of LAP from TGF-β makes it active and able to associate with its receptors[60]. Although protease-mediated liberation of active TGFβ is a poorly-understood process, thrombospondin (TSP)-1, a matricellular protein known to play a key role[61]. Other proteases such as plasmin, MMP-2 and MMP-9 are also identified to be involved in the activation of TGF-β [60, 62, 63]. LTBP-1, an extracellular multi-domain protein with numerous unique biological characters is expressed in heart, lung, spleen, kidney, and stomach. LTBP-1 plays multiple roles in TGF-β signalling, including the proper folding and secretion of the TGFβ precursor, as well as anchoring latent TGFβ to the ECM [64]. The actions of TGFβ on a specific cell type are affected by both the cytokines present and the differentiation state of the cells[65]. Although, TGF-β1 mRNA in fibroblasts from both $MK5^{+/-}$ and $MK5^{-/-}$ mice, this reduction did not reach significance. In contrast, transcript levels for TGF-β3 were increased in the absence of MK5 as were those of the inhibitory Smad6/7 mRNA. The abundance of mRNAs for TGFβ activators TSP-1 and LTBP1 were decreased. Taken together, these results suggest a role for MK5 in modulating TGF-β signalling in cardiac fibroblasts through regulating the expression levels of various key components of the pathway.

Collagens are initially produced as preprocollagens. In the endoplasmic reticulum the preprocollagen undergoes co- and post-translational modifications to form a triple-helical structure, procollagen. The procollagen is then transported to the Golgi complex, where it is packaged and secreted by exocytosis[66]. Procollagen has N- and C-propetides flanking the collagen domain that prohibit collagen fibril formation. Once, the propeptide domains are cleaved by procollagen peptidase, mature collagen moleculesare formed. Procollagen processing can take place in the extracellular space or late in the excretory pathway[67]. Once outside the cell, the mature collagen undergoes cross-linking to give rise to collagen fibrils and collagen fibers. In culture, MK5-deficient fibroblasts secreted more type 1 collagen; however, immunocytofluorescence studies indicated that reducing MK5 expression caused type 1 collagen immunoreactivity to be condensed around the nucleus whereas in $MK5^{+/+}$ fibroblasts

it was distributed throughout the cytoplasm. Such observation suggests that, MK5 is also involved in regulating intracellular collagen processing in cardiac fibroblasts.

The ability of fibroblasts to contract is thought to play a central role in the rearrangements of ECM that occur during the pathological fibrosis and wound healing. As MK5 has been implicated in maintaining and remodelling of the actin cytoskeleton in other cell types, through phosphorylation of the actin-capping protein hsp25/27, reduced MK5 expression may have an impact upon fibroblast contractility. The three-dimensional collagen gel culture system was used as an *in vitro* assay model of contraction. The present study revealed that MK5 knockdown decreased the collagen gel contraction by cardiac fibroblasts, suggesting that MK5 may be involved in the ability of cardiac fibroblasts to generate traction force during myocardial remodeling.

5.6 Conclusion

We have shown previously that reduced MK5 expression attenuates both the TAC-induced increase in collagen 1-α_1 mRNA and hypertrophy and decreases scar size and collagen content following an MI. In addition, cardiac fibroblasts isolated from $MK5^{-/-}$ mice demonstrated reduced proliferation and motility in comparison with those isolated from $MK5^{+/+}$ mice. The present study shows that reduced MK5 expression in cultured fibroblasts altered the abundance of transcripts encoding some, but not all, proteins involved in the formation and breakdown of the extracellular matrix. Type 1 collagen and fibronectin secretion were also significantly increased in both $MK5^{-/-}$ and MK5-kd fibroblasts compared with $MK5^{+/+}$, and $MK5^{+/-}$ fibroblasts. Furthermore, the absence of MK5 altered the subcellular distribution of intracellular collagen, causing to be condensed in the perinuclear region. However, the effects of MK5 were not restricted to ECM protein production as reduced MK5 expression impaired the ability of myofibroblasts to contract collagen gels. Hence, MK5 is involved in multiple aspects of fibroblast function and extracellularmatrix dynamics.

Acknowlegements

We thank Robert Parent for animal care and breeding. This work was supported bt grants from the Heart and Stroke Foundation of Canada, and Montreal Heart Institute Foundation (FICM) to BGA. SAN was supported by the Faculty of Graduate and Postdoctoral Studies of the Université de Montréal and the Egyptian Supreme Council of Universities.

5.7 References

1. Theocharis AD, Skandalis SS, Gialeli C and Karamanos NK. Extracellular matrix structure. *Adv Drug Deliv Rev*. 2016;97:4-27.

2. Krenning G, Zeisberg EM and Kalluri R. The origin of fibroblasts and mechanism of cardiac fibrosis. *J Cell Physiol*. 2010;225:631-7.

3. Valiente-Alandi I, Schafer AE and Blaxall BC. Extracellular matrix-mediated cellular communication in the heart. *J Mol Cell Cardiol*. 2016;91:228-37.

4. Chang CW, Dalgliesh AJ, Lopez JE and Griffiths LG. Cardiac extracellular matrix proteomics: Challenges, techniques, and clinical implications. *Proteomics Clin Appl*. 2016;10:39-50.

5. Talman V and Ruskoaho H. Cardiac fibrosis in myocardial infarction-from repair and remodeling to regeneration. *Cell Tissue Res*. 2016;365:563-81.

6. Liu C, Cao F, Tang QZ, Yan L, Dong YG, Zhu LH, Wang L, Bian ZY and Li H. Allicin protects against cardiac hypertrophy and fibrosis via attenuating reactive oxygen species-dependent signaling pathways. *J Nutr Biochem*. 2010;21:1238-50.

7. Bian Z, Cai J, Shen DF, Chen L, Yan L, Tang Q and Li H. Cellular repressor of E1A-stimulated genes attenuates cardiac hypertrophy and fibrosis. *J Cell Mol Med*. 2009;13:1302-13.

8. Matsui Y and Sadoshima J. Rapid upregulation of CTGF in cardiac myocytes by hypertrophic stimuli: implication for cardiac fibrosis and hypertrophy. *J Mol Cell Cardiol*. 2004;37:477-81.

9. Xu J, Lin SC, Chen J, Miao Y, Taffet GE, Entman ML and Wang Y. CCR2 mediates the uptake of bone marrow-derived fibroblast precursors in angiotensin II-induced cardiac fibrosis. *Am J Physiol Heart Circ Physiol*. 2011;301:H538-47.

10. Han YL, Li YL, Jia LX, Cheng JZ, Qi YF, Zhang HJ and Du J. Reciprocal interaction between macrophages and T cells stimulates IFN-gamma and MCP-1 production in Ang II-induced cardiac inflammation and fibrosis. *PLoS One*. 2012;7:e35506.

11. Shoulders MD and Raines RT. Collagen structure and stability. *Annu Rev Biochem*. 2009;78:929-58.

12. Chung CC, Kao YH, Yao CJ, Lin YK and Chen YJ. A Comparison of Left and Right Atrial Fibroblasts Reveals Different Collagen Production Activity and Stress-induced Mitogen-activated Protein Kinase Signaling in Rats. *Acta Physiol (Oxf)*. 2016.

13. Pan Z, Zhao W, Zhang X, Wang B, Wang J, Sun X, Liu X, Feng S, Yang B and Lu Y. Scutellarin alleviates interstitial fibrosis and cardiac dysfunction of infarct rats by inhibiting TGFbeta1 expression and activation of p38-MAPK and ERK1/2. *Br J Pharmacol*. 2011;162:688-700.

14. Mitchell MD, Laird RE, Brown RD and Long CS. IL-1beta stimulates rat cardiac fibroblast migration via MAP kinase pathways. *Am J Physiol Heart Circ Physiol*. 2007;292:H1139-47.

15. Esposito G, Prasad SV, Rapacciuolo A, Mao L, Koch WJ and Rockman HA. Cardiac overexpression of a G(q) inhibitor blocks induction of extracellular signal-regulated kinase and c-Jun NH(2)-terminal kinase activity in in vivo pressure overload. *Circulation*. 2001;103:1453-8.

16. Zhang S, Weinheimer C, Courtois M, Kovacs A, Zhang CE, Cheng AM, Wang Y and Muslin AJ. The role of the Grb2-p38 MAPK signaling pathway in cardiac hypertrophy and fibrosis. *J Clin Invest*. 2003;111:833-41.

17. Streicher JM, Ren S, Herschman H and Wang Y. MAPK-activated protein kinase-2 in cardiac hypertrophy and cyclooxygenase-2 regulation in heart. *Circ Res*. 2010;106:1434-43.

18. Court NW, dos Remedios CG, Cordell J and Bogoyevitch MA. Cardiac expression and subcellular localization of the p38 mitogen-activated protein kinase member, stress-activated protein kinase-3 (SAPK3). *J Mol Cell Cardiol*. 2002;34:413-26.

19. Dingar D, Merlen C, Grandy S, Gillis MA, Villeneuve LR, Mamarbachi AM, Fiset C and Allen BG. Effect of pressure overload-induced hypertrophy on the expression and localization of p38 MAP kinase isoforms in the mouse heart. *Cell Signal*. 2010;22:1634-44.

20. New L, Jiang Y, Zhao M, Liu K, Zhu W, Flood LJ, Kato Y, Parry GC and Han J. PRAK, a novel protein kinase regulated by the p38 MAP kinase. *EMBO J*. 1998;17:3372-84.

21. Ni H, Wang XS, Diener K and Yao Z. MAPKAPK5, a novel mitogen-activated protein kinase (MAPK)-activated protein kinase, is a substrate of the extracellular-regulated kinase (ERK) and p38 kinase. *Biochem Biophys Res Commun*. 1998;243:492-6.

22. Roux PP and Blenis J. ERK and p38 MAPK-Activated Protein Kinases: a Family of Protein Kinases with Diverse Biological Functions. *Microbiology and Molecular Biology Reviews*. 2004;68:320-344.

23. Kant S, Schumacher S, Singh MK, Kispert A, Kotlyarov A and Gaestel M. Characterization of the atypical MAPK ERK4 and its activation of the MAPK-activated protein kinase MK5. *J Biol Chem*. 2006;281:35511-9.

24. Schumacher S, Laass K, Kant S, Shi Y, Visel A, Gruber AD, Kotlyarov A and Gaestel M. Scaffolding by ERK3 regulates MK5 in development. *EMBO J*. 2004;23:4770-9.

25. Seternes OM, Mikalsen T, Johansen B, Michaelsen E, Armstrong CG, Morrice NA, Turgeon B, Meloche S, Moens U and Keyse SM. Activation of MK5/PRAK by the atypical MAP kinase ERK3 defines a novel signal transduction pathway. *EMBO J*. 2004;23:4780-91.

26. Dingar D, Benoit MJ, Mamarbachi AM, Villeneuve LR, Gillis MA, Grandy S, Gaestel M, Fiset C and Allen BG. Characterization of the expression and regulation of MK5 in the murine ventricular myocardium. *Cell Signal*. 2010;22:1063-75.

27. Gerits N, Shiryaev A, Kostenko S, Klenow H, Shiryaeva O, Johannessen M and Moens U. The transcriptional regulation and cell-specific expression of the MAPK-activated protein kinase MK5. *Cell Mol Biol Lett*. 2009;14:548-74.

28. Nawaito S, Dingar D, Sahadevan P, Hussein B, Sahmi F, Shi Y, Gillis MA, Gaestel M, Tardif JC and Allen BG. MK5 haplodefficiency attenuates hypertrophy and preserves diastolic function during remodeling induced by chronic pressure overload in the mouse heart. *Am J Physiol Heart Circ Physiol*. 2017:ajpheart 00597 2016.

29. Shi Y, Kotlyarov A, Laabeta K, Gruber AD, Butt E, Marcus K, Meyer HE, Friedrich A, Volk HD and Gaestel M. Elimination of protein kinase MK5/PRAK activity by targeted homologous recombination. *Mol Cell Biol*. 2003;23:7732-41.

30. Kumaran C and Shivakumar K. Calcium- and superoxide anion-mediated mitogenic action of substance P on cardiac fibroblasts. *Am J Physiol Heart Circ Physiol*. 2002;282:H1855-62.

31. Karey KP and Sirbasku DA. Glutaraldehyde fixation increases retention of low molecular weight proteins (growth factors) transferred to nylon membranes for western blot analysis. *Anal Biochem*. 1989;178:255-9.

32. Konstandin MH, Volkers M, Collins B, Quijada P, Quintana M, De La Torre A, Ormachea L, Din S, Gude N, Toko H and Sussman MA. Fibronectin contributes to pathological cardiac hypertrophy but not physiological growth. *Basic Res Cardiol*. 2013;108:375.

33. Konstandin MH, Toko H, Gastelum GM, Quijada P, De La Torre A, Quintana M, Collins B, Din S, Avitabile D, Volkers M, Gude N, Fassler R and Sussman MA. Fibronectin is essential for reparative cardiac progenitor cell response after myocardial infarction. *Circ Res*. 2013;113:115-25.

34. Adler CP, Ringlage WP and Bohm N. [DNA content and cell number in heart and liver of children. Comparable biochemical, cytophotometric and histological investigations (author's transl)]. *Pathol Res Pract*. 1981;172:25-41.

35. Camelliti P, Borg TK and Kohl P. Structural and functional characterisation of cardiac fibroblasts. *Cardiovasc Res*. 2005;65:40-51.

36. Weber KT, Sun Y, Bhattacharya SK, Ahokas RA and Gerling IC. Myofibroblast-mediated mechanisms of pathological remodelling of the heart. *Nat Rev Cardiol*. 2013;10:15-26.

37. Chen W and Frangogiannis NG. Fibroblasts in post-infarction inflammation and cardiac repair. *Biochim Biophys Acta*. 2013;1833:945-53.

38. Sun P, Yoshizuka N, New L, Moser BA, Li Y, Liao R, Xie C, Chen J, Deng Q, Yamout M, Dong MQ, Frangou CG, Yates JR, 3rd, Wright PE and Han J. PRAK is essential for ras-induced senescence and tumor suppression. *Cell*. 2007;128:295-308.

39. Sahadevan P and Allen BG. MK5: A novel regulator of cardiac fibroblast function? *IUBMB Life*. 2017;69:785-794.

40. Molkentin JD, Bugg D, Ghearing N, Dorn LE, Kim P, Sargent MA, Gunaje J, Otsu K and Davis J. Fibroblast-Specific Genetic Manipulation of p38 Mitogen-Activated Protein Kinase In Vivo Reveals Its Central Regulatory Role in Fibrosis. *Circulation*. 2017;136:549-561.

41. Adamopoulos S, Parissis JT and Kremastinos DT. A glossary of circulating cytokines in chronic heart failure. *Eur J Heart Fail*. 2001;3:517-26.

42. Torre-Amione G, Kapadia S, Lee J, Durand JB, Bies RD, Young JB and Mann DL. Tumor necrosis factor-alpha and tumor necrosis factor receptors in the failing human heart. *Circulation*. 1996;93:704-11.

43. Torre-Amione G, Kapadia S, Benedict C, Oral H, Young JB and Mann DL. Proinflammatory cytokine levels in patients with depressed left ventricular ejection fraction: a report from the Studies of Left Ventricular Dysfunction (SOLVD). *J Am Coll Cardiol*. 1996;27:1201-6.

44. Testa M, Yeh M, Lee P, Fanelli R, Loperfido F, Berman JW and LeJemtel TH. Circulating levels of cytokines and their endogenous modulators in patients with mild to severe congestive heart failure due to coronary artery disease or hypertension. *J Am Coll Cardiol*. 1996;28:964-71.

45. Mann DL. Inflammatory mediators and the failing heart: past, present, and the foreseeable future. *Circ Res*. 2002;91:988-98.

46. Hammerman H, Kloner RA, Hale S, Schoen FJ and Braunwald E. Dose-dependent effects of short-term methylprednisolone on myocardial infarct extent, scar formation, and ventricular function. *Circulation*. 1983;68:446-52.

47. Kloner RA, Fishbein MC, Lew H, Maroko PR and Braunwald E. Mummification of the infarcted myocardium by high dose corticosteroids. *Circulation*. 1978;57:56-63.

48. Baum J and Duffy HS. Fibroblasts and myofibroblasts: what are we talking about? *J Cardiovasc Pharmacol*. 2011;57:376-9.

49. Snider P, Standley KN, Wang J, Azhar M, Doetschman T and Conway SJ. Origin of cardiac fibroblasts and the role of periostin. *Circ Res*. 2009;105:934-47.

50. Hsieh AH, Tsai CM, Ma QJ, Lin T, Banes AJ, Villarreal FJ, Akeson WH and Sung KL. Time-dependent increases in type-III collagen gene expression in medical collateral ligament fibroblasts under cyclic strains. *J Orthop Res*. 2000;18:220-7.

51. Butt RP and Bishop JE. Mechanical load enhances the stimulatory effect of serum growth factors on cardiac fibroblast procollagen synthesis. *J Mol Cell Cardiol*. 1997;29:1141-51.

52. Carver W, Nagpal ML, Nachtigal M, Borg TK and Terracio L. Collagen expression in mechanically stimulated cardiac fibroblasts. *Circ Res*. 1991;69:116-22.

53. Chapman D, Weber KT and Eghbali M. Regulation of fibrillar collagen types I and III and basement membrane type IV collagen gene expression in pressure overloaded rat myocardium. *Circ Res*. 1990;67:787-94.

54. Guo C and Piacentini L. Type I collagen-induced MMP-2 activation coincides with up-regulation of membrane type 1-matrix metalloproteinase and TIMP-2 in cardiac fibroblasts. *J Biol Chem*. 2003;278:46699-708.

55. Schiller M, Javelaud D and Mauviel A. TGF-beta-induced SMAD signaling and gene regulation: consequences for extracellular matrix remodeling and wound healing. *J Dermatol Sci*. 2004;35:83-92.

56. Bujak M, Ren G, Kweon HJ, Dobaczewski M, Reddy A, Taffet G, Wang XF and Frangogiannis NG. Essential role of Smad3 in infarct healing and in the pathogenesis of cardiac remodeling. *Circulation*. 2007;116:2127-38.

57. Leask A and Abraham DJ. TGF-beta signaling and the fibrotic response. *FASEB J*. 2004;18:816-27.

58. Biernacka A, Dobaczewski M and Frangogiannis NG. TGF-beta signaling in fibrosis. *Growth Factors*. 2011;29:196-202.

59. Derynck R and Zhang YE. Smad-dependent and Smad-independent pathways in TGF-beta family signalling. *Nature*. 2003;425:577-84.

60. Annes JP, Munger JS and Rifkin DB. Making sense of latent TGFbeta activation. *J Cell Sci*. 2003;116:217-24.

61. Murphy-Ullrich JE and Poczatek M. Activation of latent TGF-beta by thrombospondin-1: mechanisms and physiology. *Cytokine Growth Factor Rev*. 2000;11:59-69.

62. Rifkin DB, Mazzieri R, Munger JS, Noguera I and Sung J. Proteolytic control of growth factor availability. *APMIS*. 1999;107:80-5.

63. Ignotz RA and Massague J. Transforming growth factor-beta stimulates the expression of fibronectin and collagen and their incorporation into the extracellular matrix. *J Biol Chem*. 1986;261:4337-45.

64. Robertson IB, Horiguchi M, Zilberberg L, Dabovic B, Hadjiolova K and Rifkin DB. Latent TGF-beta-binding proteins. *Matrix Biol*. 2015;47:44-53.

65. Letterio JJ and Roberts AB. Regulation of immune responses by TGF-beta. *Annu Rev Immunol*. 1998;16:137-61.

66. Bonfanti L, Mironov AA, Jr., Martinez-Menarguez JA, Martella O, Fusella A, Baldassarre M, Buccione R, Geuze HJ, Mironov AA and Luini A. Procollagen traverses the Golgi stack without leaving the lumen of cisternae: evidence for cisternal maturation. *Cell*. 1998;95:993-1003.

67. Canty EG, Lu Y, Meadows RS, Shaw MK, Holmes DF and Kadler KE. Coalignment of plasma membrane channels and protrusions (fibripositors) specifies the parallelism of tendon. *J Cell Biol*. 2004;165:553-63.

Figure Legends

Figure 1. Decreasing MK5 expression increases collagen 1-α_1 mRNA levels in cardiac fibroblasts. Using qPCR, collagen 1-α_1 and GAPDH mRNA were quantified in RNA isolated from **(A)** $MK5^{+/+}$, $MK5^{+/-}$, and $MK5^{-/-}$ fibroblasts following 24 hours treatment with or without 1 μM Ang-II and **(B)** $MK5^{+/+}$cardiac fibroblasts transiently transfected with MK5 siRNA or scrambled siRNA (scRNA). In both cases, after 12 hours of serum deprivation, cells were exposed to M199 without serum in the presence or absence of 1 μM Ang-II as for 24 hours. Collagen 1-α_1 mRNA was normalized to the amount of GAPDH mRNA. Data are presented as the mean ± SEM of four (A) or three to five (B) independent experiments. Each experiment was performed with fibroblasts isolated from a separate mouse. * $P< 0.05$. ** $P< 0.01$. **** $P< 0.001$.

Figure 2. Decreasing MK5 expression alters the mRNA abundance for several proteins involved in ECM turnover.(A-D) Transcripts for proteins involved in fibrosis were quantified in RNA isolated from $MK5^{+/+}$, $MK5^{+/-}$, and $MK5^{-/-}$ cardiac fibroblasts using pathway-targeted qPCR arrays. For each transcript, expression was normalized to $MK5^{+/+}$. Data are presented as the mean ± SEM of three independent experiments. Each experiment was performed with fibroblasts isolated from a separate mouse. *$P< 0.05$.

Figure 3. Decreasing MK5 expression increases type 1 collagen secretion.(A) Type 1 collagen immunoreactivity was measured by immunoblotting in conditioned media from cultured $MK5^{+/+}$, $MK5^{+/-}$, and $MK5^{-/-}$ fibroblasts pre-treated without or with 1 μM Ang II for 6 and 24 hours in serum-free medium. Cell number was used as the normalizer. **(B)**Cardiac fibroblasts were transiently transfected with MK5 siRNA or scrambled siRNA as described in the Methods followed by an additional incubation in M199 containing 10% FCS for 12 hours. After 12 hours of serum deprivation, the transfected cells were exposed to M199 without serum in the presence or absence of 1 μM Ang II for 24 hours. Type 1 collagen immunoreactivity was measured by immunoblotting in conditioned media. Cell number was used as the normalizer. Representative immunoblots are shown above the histograms. Values in the histograms show mean ± SEM of three independent experiments. Each experiment was performed with fibroblasts isolated from a separate mouse. * $P< 0.05$. siRNA; small interfering RNA; scRNA, scrambled RNA.

Figure 4. Decreasing MK5 expression increases fibronectin secretion. Fibronectin immunoreactivity was measured by immunoblotting in conditioned media from cultured $MK5^{+/+}$, $MK5^{+/-}$, and $MK5^{-/-}$ fibroblasts pre-treated without or with 1 μM Ang II for 6 and 24 hours in serum-free medium. Cell number was used as the normalizer. **(B)**Cardiac fibroblasts were transiently transfected with MK5 siRNA or scrambled siRNA as described in the Methods followed by an additional incubation in M199 containing 10% FCS for 12 hours. After 12 hours of serum deprivation, the transfected cells were exposed to M199 without serum in the presence or absence of 1 μM Ang II for 24 hours. Fibronectin immunoreactivity was measured by immunoblotting in conditioned media. Cell number was used as the normalizer. Representative immunoblots are shown above the histograms. Values in the histograms show mean ± SEM of three independent experiments. Each experiment was performed with fibroblasts isolated from a separate mouse. * $P< 0.05$. siRNA; small interfering RNA; scRNA, scrambled RNA.

Figure 5. MK5 deficiency alters the subcellular distribution of type 1 collagen immunoreactivity. The subcellular localization of collagen was determined in cardiac fibroblasts isolated from $MK5^{+/+}$ and $MK5^{-/-}$ mice by confocal immunocytofluorescence microscopy. Passage 2 fibroblasts at were fixed and decorated with antisera against type 1 collagen 1 followed by an Alexa 555-coupled anti-rabbit secondary antibody (1:500). Nuclei were visualized by staining with DAPI (1:1000). Whole cell images were acquired by differential interference contrast (DIC) microscopy.

Figure 6. Suppressing MK5 expression decreases myofibroblast contraction. Following transfection with scrambled RNA (scRNA) **(A)** or MK5-directed siRNA **(B)** passage 2 fibroblast suspensions (containing 3.2 x 10^4 cells) were plated on preformed collagen type 1 gels in 24-well plates (growth area: 200 mm^2). Two hours after plating, collagen gel contraction was initiated by detaching the gels from the side of the wells. Images shown were taken 48 hours later. **(C)** Gel contraction expressed as the ratio of gel circumference measured immediately after detachment and 48 hours later. Data are presented as the mean ± SEM of four independent experiments. Each experiment was performed with fibroblasts isolated from a separate mouse.

Table 1. RT2 Profiler PCR array analysis of mouse fibrosis in isolated cardiac fibroblasts: ECM & cell adhesion molecules

		Genotype		6h Ang-II treatment			24 h Ang-II treatment		
Gene	Name	$MK5^{+/-}$	$MK5^{-/-}$	$MK5^{+/+}$	$MK5^{+/-}$	$MK5^{-/-}$	$MK5^{+/+}$	$MK5^{+/-}$	$MK5^{-/-}$
ECM struc									
Col3a1	**Collagen, type III, alpha 1**	1.384 (0.069)	**1.693 (0.022)**	-1.815 (0.227)	1.460 (0.127)	**1.665 (0.035)**	-1.012 (0.839)	1.425 (0.054)	**2.027 (0.012)**
ECM remodeling									
Mmp1a	MMP 1a (interstitial collagenase)	-2.077 (0.098)	-1.163 (0.579)	-1.153 (0.748)	-1.825 (0.173)	-1.456 (0.298)	1.054 (0.931)	-1.484 (0.239)	-1.248 (0.549)
Mmp3	MMP 3	-1.445 (0.443)	-1.358 (0.415)	-1.145 (0.52)	-1.621 (0.348)	-1.480 (0.373)	-1.334 (0.641)	-1.486 (0.557)	-1.557 (0.376)
Mmp8	MMP 8	1.205 (0.624)	-1.494 (0.479)	-1.146 (0.760)	1.209 (0.598)	-1.408 (0.315)	-1.124 (0.664)	1.409 (0.439)	-1.250 (0.606)
Mmp13	MMP 13	-2.709 (0.056)	-1.864 (0.248)	-1.358 (0.485)	-2.456 (0.083)	-3.280 (0.11)	-1.225 (0.854)	-2.703 (0.236)	-2.921 (0.136)
Timp3	**Tissue inhibitor of metalloproteinase 3**	**2.211 (0.142)**	**2.286 (0.030)**	1.053 (0.84)	**2.351 (0.029)**	**1.924 (0.041)**	1.019 (0.812)	2.124 (0.105)	1.687 (0.116)
Cell Adhesion									
Itgb3	**Integrin beta 3**	**-4.773 (0.006)**	**-5.418 (0.005)**	1.355 (0.22)	**-4.979 (0.004)**	**-6.135 (0.004)**	**-3.748 (0.003)**	**-3.821 (0.016)**	**-5.848 (0.004)**

Data shown are expressed as the fold-regulation in mRNA abundance relative to $MK5^{+/+}$. p-values are indicated in parentheses. (n=3).

Table 2. RT2 Profiler PCR array analysis of mouse fibrosis in isolated cardiac fibroblasts: Signal transduction

		Genotype		6h Ang-II treatment			24 h Ang-II treatment		
Gene	Name	$MK5^{+/-}$	$MK5^{-/-}$	$MK5^{+/+}$	$MK5^{+/-}$	$MK5^{-/-}$	$MK5^{+/+}$	$MK5^{+/-}$	$MK5^{-/-}$
TGFβ family									
Ltbp1	**Latent transforming growth factor beta binding protein 1**	**-2.520 (0.020)**	**-3.050 (0.027)**	-1.128 (0.599)	**-2.522 (0.037)**	**-3.428 (0.030)**	-1.038 (0.955)	-2.354 (0.062)	**-3.029 (0.025)**
Smad6	**MAD homolog 6 (Drosophila)**	**4.726 (0.008)**	**10.381 (0.007)**	-1.041 (0.575)	**4.374 (0.023)**	**9.169 (0.004)**	3.503 (0.221)	3.842 (0.055)	3.405 (0.256)
Smad7	**MAD homolog 7 (Drosophila)**	**1.618 (0.206)**	**2.667 (0.032)**	1.249 (0.540)	1.819 (0.089)	**2.392 (0.024)**	1.579 (0.322)	1.562 (0.236)	1.513 (0.351)
Tgfb1	Transforming growth factor, beta 1	-1.687 (0.157)	-1.820 (0.076)	-1.108 (0.963)	-1.579 (0.200)	-1.885 (0.082)	-1.244 (0.383)	-1.722 (0.068)	**-2.207 (0.047)**
Tgfb3	**Transforming growth factor, beta 3**	**2.010 (0.074)**	**2.602 (0.013)**	1.616 (0.172)	**2.195 (0.014)**	**2.751 (0.013)**	1.209 (0.567)	**2.259 (0.036)**	1.677 (0.155)
Thbs1	**Thrombospondin 1**	**-1.287 (0.150)**	**-1.723 (0.028)**	1.221 (0.243)	-1.144 (0.402)	**-1.597 (0.040)**	-1.198 (0.890)	-1.310 (0.216)	**-2.260 (0.011)**

Transcription factors									
Stat1	Signal transducer and activator of transcription 1	1.167 (0.199)	1.646 (0.056)	-1.333 (0.305)	1.453 (0.209)	**1.886 (0.021)**	-1.399 (0.667)	1.240 (0.233)	1.434 (0.222)

Data shown are expressed as the fold-regulation in mRNA abundance relative to $MK5^{+/+}$. p-values are indicated in parentheses. (n=3).

Table 3. RT2 Profiler PCR array analysis of mouse fibrosis in isolated cardiac fibroblasts: Pro and anti-fibrotic

Pro-Fib		Genotype		6h Ang-II treatment			24 h Ang-II treatment		
Gene	Name	$MK5^{+/-}$	$MK5^{-/-}$	$MK5^{+/+}$	$MK5^{+/-}$	$MK5^{-/-}$	$MK5^{+/+}$	$MK5^{+/-}$	$MK5^{-/-}$
Il13	**Interleukin 13**	**-2.789 (0.022)**	**-5.623 (0.017)**	**-1.934 (0.049)**	**-5.080 (0.009)**	**-7.057 (0.013)**	**-1.994** (0.134)	**-2.999** (0.112)	**-3.452 (0.032)**
Snai 1	**Snail homolog 1 (Drosophila)**	2.764 (0.230)	**4.485 (0.042)**	1.703 (0.777)	2.835 (0.221)	3.989 (0.092)	1.776 (0.406)	2.995 (0.220)	2.892 (0.254)
Anti-Fib									
Hgf	**Hepatocyte growth factor**	**-3.542 (0.004)**	**-2.562 (0.031)**	-1.445 (0.148)	**-2.728 (0.009)**	**-2.655 (0.040)**	**-2.166 (0.008)**	**-2.978 (0.004)**	**-3.051 (0.020)**

Data shown are expressed as the fold-regulation in mRNA abundance relative to $MK5^{+/+}$. p-values are indicated in parentheses. (n=3).

Table 4. RT2 Profiler PCR array analysis of mouse fibrosis in isolated cardiac fibroblasts: Inflammatory cytokines and chemokines

		Genotype		6h Ang-II treatment			24 h Ang-II treatment		
Gene	Name	$MK5^{+/-}$	$MK5^{-/-}$	$MK5^{+/+}$	$MK5^{+/-}$	$MK5^{-/-}$	$MK5^{+/+}$	$MK5^{+/-}$	$MK5^{-/-}$
Ccl11	Chemokine (C-C motif) ligand 11	-1.128 (0.513)	-2.274 (0.338)	-1.378 (0.917)	-1.379 (0.436)	-1.539 (0.467)	-2.375 (0.515)	-1.322 (0.474)	-1.502 (0.442)
Ifng	Interferon gamma	-1.218 (0.499)	-2.882 (0.249)	-1.303 (0.567)	-1.360 (0.444)	-1.493 (0.422)	1.006 (0.732)	1.494 (0.439)	-1.392 (0.538)
Il1a	Interleukin 1 alpha	-1.394 (0.456)	-1.087 (0.751)	-1.205 (0.795)	-1.673 (0.171)	-1.337 (0.367)	-1.189 (0.423)	-1.010 (0.636)	-1.497 (0.417)
Il1b	Interleukin 1 beta	-1.737 (0.232)	-1.892 (0.253)	-1.366 (0.256)	-1.738 (0.114)	-1.533 (0.325)	-1.565 (0.139)	1.212 (0.546)	-1.686 (0.222)
Il4	Interleukin 4	-1.606 (0.118)	-1.266 (0.482)	-1.163 (0.566)	-1.809 (0.106)	-1.552 (0.636)	-1.570 (0.114)	-1.169 (0.822)	-1.213 (0.641)
Il10	Interleukin 10	-1.269 (0.551)	-2.049 (0.403)	-1.417 (0.481)	-1.291 (0.566)	-2.318 (0.373)	-1.430 (0.537)	-1.000 (0.695)	-1.305 (0.513)
Il13	**Interleukin 13**	**-2.789 (0.022)**	**-5.623 (0.017)**	**-1.934 (0.049)**	**-5.080 (0.009)**	**-7.057 (0.013)**	-1.994 (0.134)	-2.999 (0.112)	**-3.452 (0.032)**
Il13ra2	Interleukin 13 receptor, alpha 2	-1.332 (0.463)	-2.097 (0.363)	1.279 (0.936)	-1.001 (0.598)	-2.219 (0.373)	-1.518 (0.929)	1.061 (0.793)	-1.781 (0.401)
Ilk	**Integrin linked kinase**	**1.352 (0.034)**	-1.559 (0.762)	1.002 (0.954)	1.323 (0.112)	1.452 (0.085)	1.474 (0.122)	1.234 (0.195)	1.312 (0.208)
Tnf	Tumor necrosis factor	1.133 (0.721)	-1.572 (0.303)	-1.146 (0.643)	-1.307 (0.440)	-2.025 (0.203)	-1.202 (0.291)	1.362 (0.581)	1.424 (0.734)

Data shown are expressed as the fold-regulation in mRNA abundance relative to $MK5^{+/+}$. p-values are indicated in parentheses. (n=3).

Table 5. RT2 Profiler PCR array analysis of mouse fibrosis in isolated cardiac fibroblasts: Growth factors

		Genotype		6h Ang-II treatment			24 h Ang-II treatment		
Gene	Name	$MK5^{+/-}$	$MK5^{-/-}$	$MK5^{+/+}$	$MK5^{+/-}$	$MK5^{-/-}$	$MK5^{+/+}$	$MK5^{+/-}$	$MK5^{-/-}$
Hgf	**Hepatocyte growth factor**	**-3.542 (0.004)**	**-2.562 (0.031)**	-1.445 (0.148)	**-2.728 (0.009)**	**-2.655 (0.040)**	**-2.166 (0.008)**	**-2.978 (0.004)**	**-3.051 (0.020)**
Vegfa	Vascular endothelial growth factor A	1.819 (0.137)	1.892 (0.057)	-1.001 (0.893)	**2.151 (0.042)**	1.716 (0.101)	1.060 (0.914)	2.038 (0.128)	-1.464 (0.742)

Data shown are expressed as the fold-regulation in mRNA abundance relative to $MK5^{+/+}$. p-values are indicated in parentheses. (n=3).

Table 6. RT2 Profiler PCR array analysis of mouse fibrosis in isolated cardiac fibroblasts: Epithelial-to-Mesenchymal Transition (EMT)

		Genotype		6h Ang-II treatment			24 h Ang-II treatment		
Gene	Name	$MK5^{+/-}$	$MK5^{-/-}$	$MK5^{+/+}$	$MK5^{+/-}$	$MK5^{-/-}$	$MK5^{+/+}$	$MK5^{+/-}$	$MK5^{-/-}$
Col3a1	**Collagen, type III, alpha 1**	**1.384 (0.069)**	**1.693 (0.022)**	-1.815 (0.227)	1.460 (0.127)	**1.665 (0.035)**	-1.012 (0.839)	1.425 (0.054)	**2.027 (0.012)**
Mmp3	Matrix metallopeptidase 3	-1.445 (0.443)	-1.358 (0.415)	-1.145 (0.52)	-1.621 (0.348)	-1.480 (0.373)	-1.334 (0.641)	-1.486 (0.557)	-1.557 (0.376)
Snai 1	**Snail homolog 1 (Drosophila)**	**2.764 (0.230)**	**4.485 (0.042)**	1.703 (0.777)	2.835 (0.221)	3.989 (0.092)	1.776 (0.406)	2.995 (0.22)	2.892 (0.254)
Tgfb1	Transforming growth factor, beta 1	-1.687 (0.157)	-1.820 (0.076)	-1.108 (0.963)	-1.579 (0.2)	-1.885 (0.082)	-1.244 (0.383)	-1.722 (0.068)	**-2.207 (0.047)**
Tgfb3	**Transforming growth factor, beta 3**	**2.010 (0.074)**	**2.602 (0.013)**	1.616 (0.172)	**2.195 (0.014)**	**2.751 (0.013)**	1.209 (0.567)	**2.259 (0.036)**	1.677 (0.155)

Data shown are expressed as the fold-regulation in mRNA abundance relative to $MK5^{+/+}$. p-values are indicated in parentheses. (n=3).

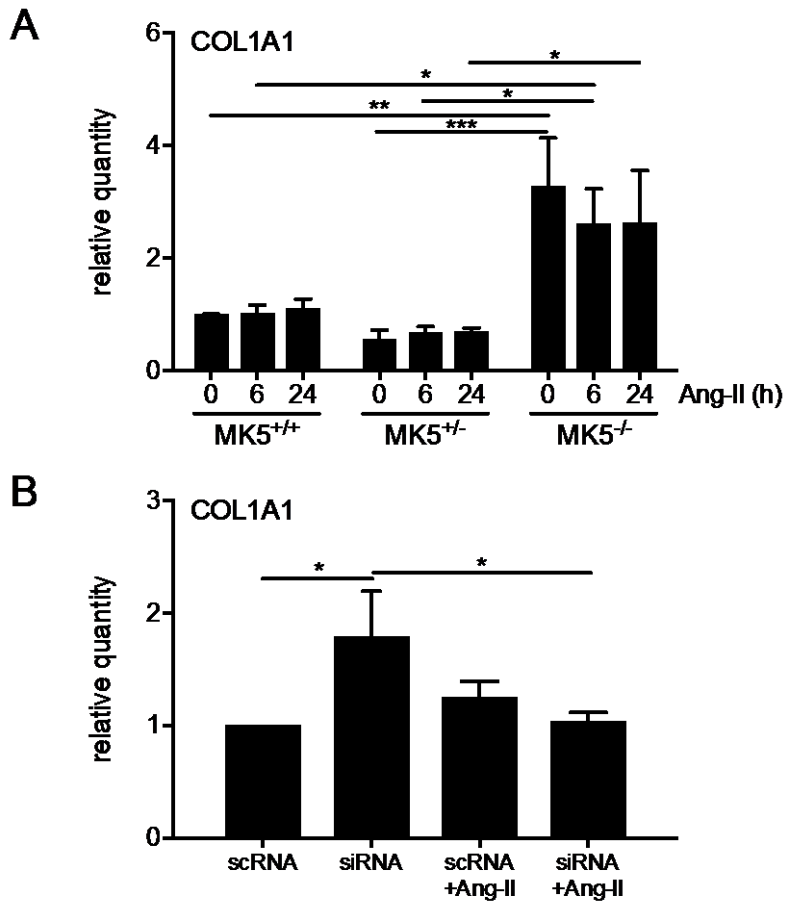
A
COL1A1
relative quantity
6
4
2
0
*
*
*
**
***
0 6 24 0 6 24 0 6 24
Ang-II (h)
MK5+/+
MK5+/-
MK5-/-
B
COL1A1
relative quantity
3
2
1
0
*
*
scRNA
siRNA
scRNA +Ang-II
siRNA +Ang-II

Figure 1

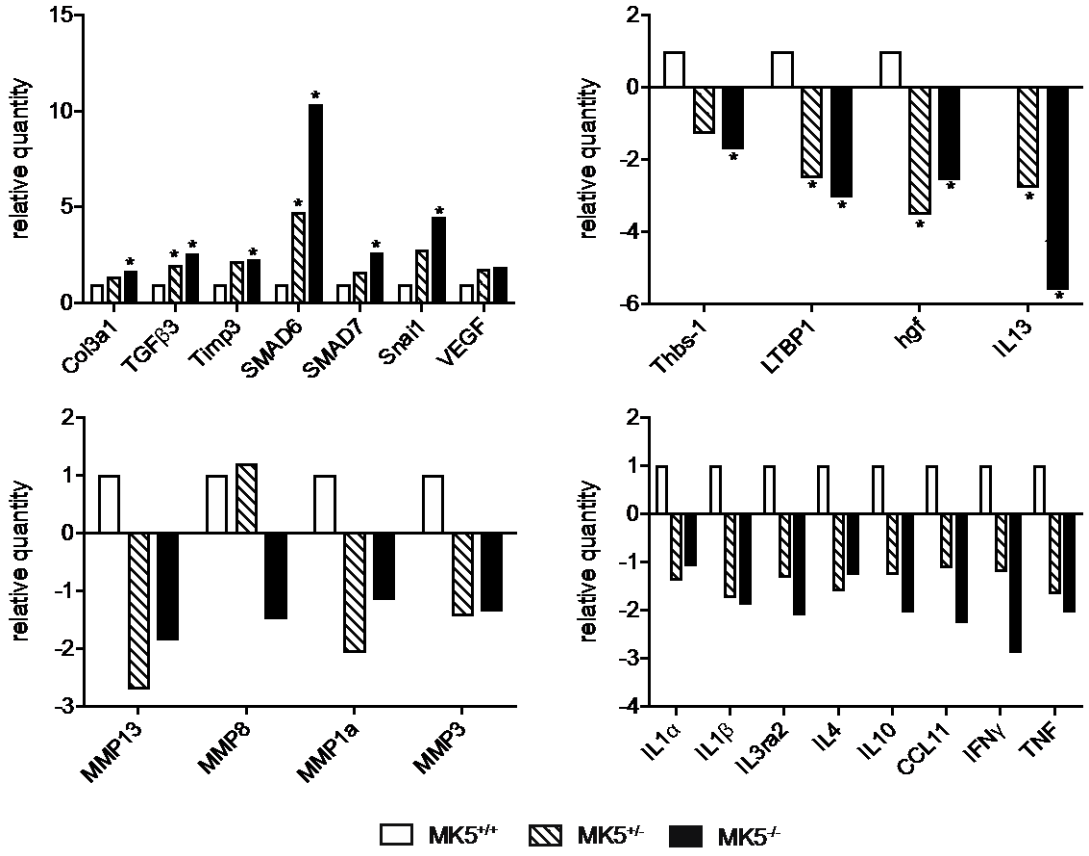
relative quantity
Col3a1
TGFβ3
Timp3
SMAD6
SMAD7
Snail1
VEGF
Thbs-1
LTBP1
hgf
IL13
MMP13
MMP8
MMP1a
MMP3
IL1α
IL1β
IL3ra2
IL4
IL10
CCL11
IFNγ
TNF
MK5+/+
MK5+/-
MK5-/-

Figure 2

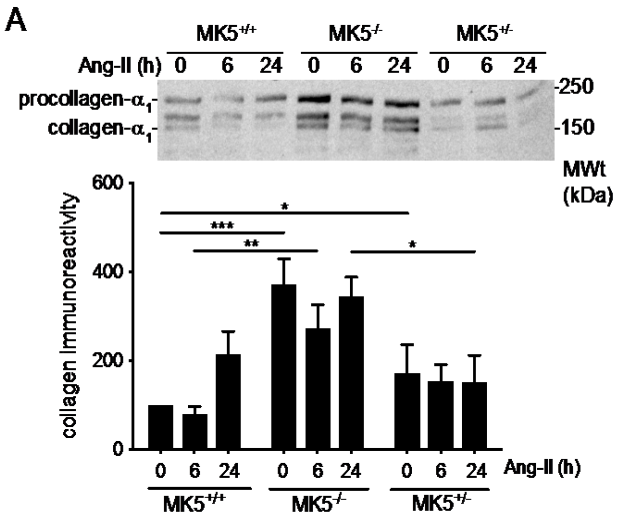
A
MK5+/+
MK5-/-
MK5+/-
Ang-II (h) 0 6 24 0 6 24 0 6 24
procollagen-α1
collagen-α1
250
150
MWt (kDa)
collagen Immunoreactivity
600
400
200
0
*
***
**
*
0 6 24 0 6 24 0 6 24 Ang-II (h)
MK5+/+
MK5-/-
MK5+/-

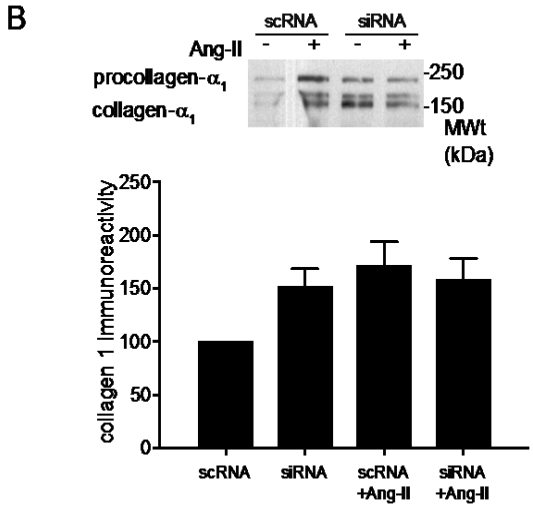
B
scRNA
siRNA
Ang-II - + - +
procollagen-α1
collagen-α1
250
150
MWt (kDa)
collagen 1 Immunoreactivity
250
200
150
100
50
0
scRNA
siRNA
scRNA +Ang-II
siRNA +Ang-II

Figure 3

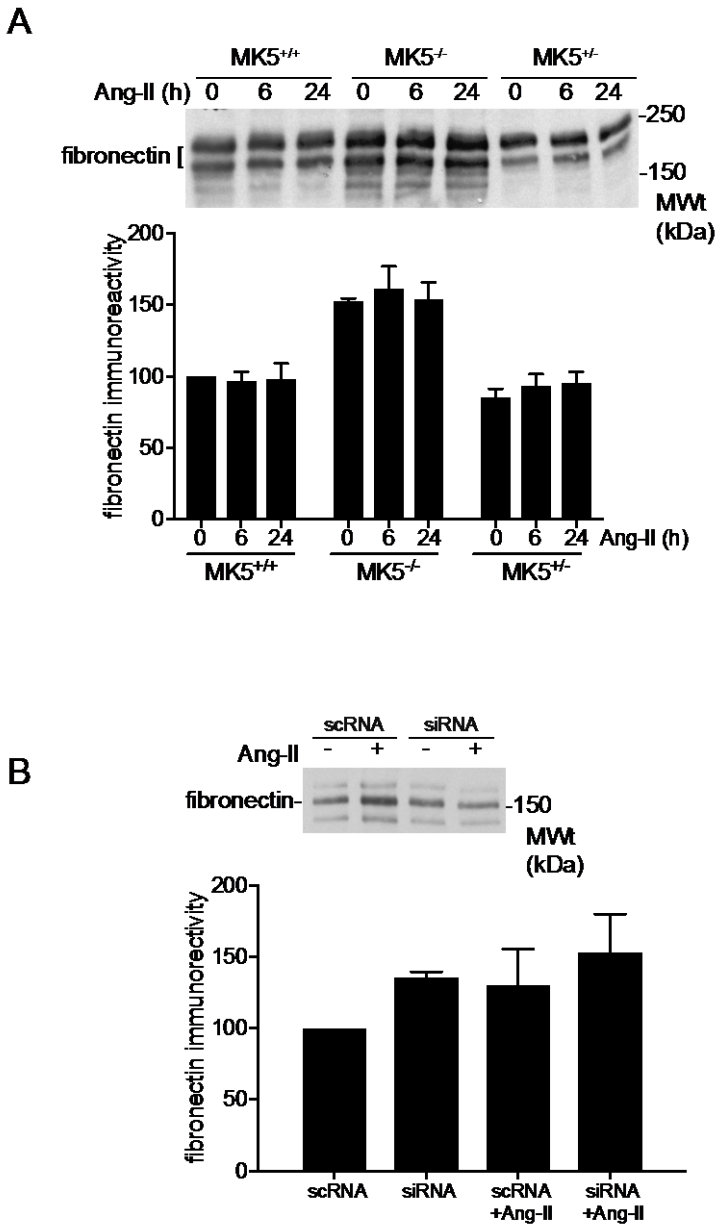
A
MK5+/+
MK5-/-
MK5+/-
Ang-II (h) 0 6 24 0 6 24 0 6 24
fibronectin [
-250
-150
MWt
(kDa)
fibronectin immunoreactivity
200
150
100
50
0
0 6 24 0 6 24 0 6 24 Ang-II (h)
MK5+/+
MK5-/-
MK5+/-
B
scRNA
siRNA
Ang-II - + - +
fibronectin-
-150
MWt
(kDa)
fibronectin immunoreactivity
200
150
100
50
0
scRNA
siRNA
scRNA +Ang-II
siRNA +Ang-II

Figure 4

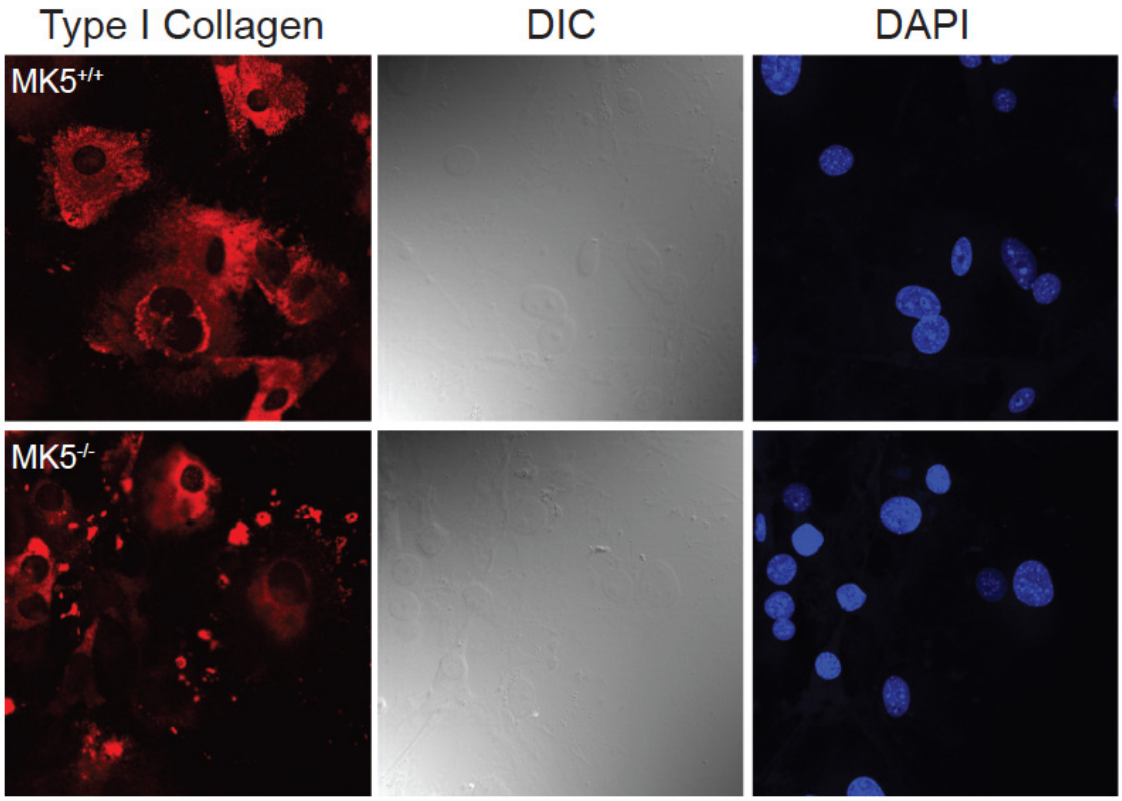

Figure 5

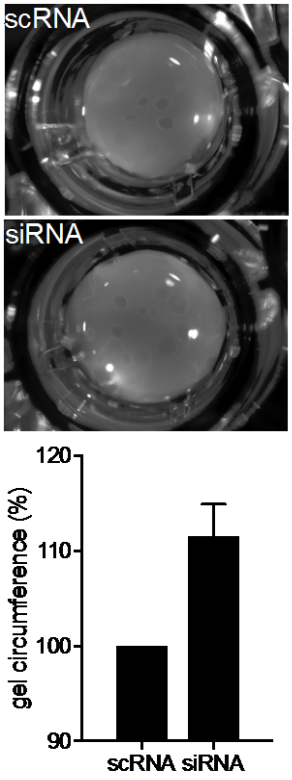

Figure 6

Discussion

In *vitro and in vivo* studies have shown MK5 to be phosphorylated and activated by p38α/β MAPK, ERK3/4, PKA, and focal adhesion kinase (FAK). However, the biological functions of MK5 remain incompletely understood. Studies that have employed *in vitro* and ectopically expressed MK5 have suggested a role of MK5 in cytoskeletal remodelling, cell migration and proliferation, tumour suppression, and autophagy. However, the *in vivo* functions of MK5 remain to be addressed, especially in terminally differentiated cell systems such as the heart. In fact, apart from demonstrations of MK5 expression at the mRNA and protein levels, nothing is known about its role in the heart. Hence, we explored its functions using *in vivo* models of both chronic pressure overload and myocardial infarction. In addition, we examined the mechanisms whereby MK5 may regulate extracellular matrix remodelling. The line of MK5 knockout mice employed in these studies was generated on a mixed 129/Ola × C57/B6 genetic background by targeted disruption of exon 6 (MK5-Δex6). $MK5^{-/-}$ mice show embryonic lethality with incomplete penetrance, resulting in only 50% of the expected number of $MK5^{-/-}$ embryos detectable after day E12. Moreover, the surviving $MK5^{-/-}$ mice fail to reproduce. $MK5^{+/-}$ mice are healthy. Thus, as it was difficult to obtain sufficient numbers of $MK5^{-/-}$ for surgical procedures, $MK5^{+/-}$ mice were used in our *in vivo* studies. However, we were able to use $MK5^{-/-}$ mice to isolate MK5-null cardiac ventricular fibroblasts for a limited number of *in vitro* experiments. Here we show that twelve-week-old $MK5^{+/-}$ mice were smaller than age-matched $MK5^{+/+}$ mice and they have normal left ventricular diastolic function but a modest reduction in left ventricular systolic function. In response to chronic pressure overload induced by constriction of the transverse aorta, the profile of fetal gene re-expression (e.g., ANP, BNP, β-MHC) in $MK5^{+/-}$ mice differed from $MK5^{+/+}$ mice. Following 8 weeks of pressure overload, hearts and ventricular cardiomyocytes from $MK5^{+/-}$ mice showed significantly less hypertrophy than $MK5^{+/+}$ littermates. Moreover, the ability of pressure overload to increase collagen 1-α_1 mRNA was significantly attenuated in $MK5^{+/-}$ mice relative to $MK5^{+/+}$ mice. Hence, MK5 haploinsufficiency alters myocardial remodeling when subjected to hemodynamic overload. Interestingly, MK5 immunoreactivity was detected in cardiac fibroblasts but not cardiomyocytes. Hence, MK5 may be involved in the cardiac

fibroblast response to chronic pressure overload and the reduced hypertrophy observed in $MK5^{+/-}$ hearts may be due to the involvement of MK5 in paracrine signaling between fibroblasts and cardiomyocytes or direct fibroblast-cardiomyocyte coupling. Furthermore, following myocardial infarction induced by permanent ligation of the left anterior descending coronary artery, mortality did not differ significantly between $MK5^{+/+}$ and $MK5^{+/-}$ mice the first 7 days post-MI but was higher in $MK5^{+/-}$ mice over 21 days. One-week post-MI, $MK5^{+/-}$ hearts had a significantly smaller scar, containing less collagen, compared to their $MK5^{+/+}$ littermates. In addition, the abundance of αSMA-positive vessels was higher in the peri-infarct region of $MK5^{+/-}$ hearts. Moreover, the abundance of MMP-9 immunoreactivity was significantly increased in the peri-infarct region of $MK5^{+/-}$ mice having experienced LV wall rupture.Cultured cardiac ventricular fibroblasts isolated from $MK5^{-/-}$ mice showed reduce migration and proliferation compared to those isolated from $MK5^{+/+}$ and $MK5^{+/-}$ mice. Taken together, these results suggest a role for MK5 in the regulation of cardiac fibroblast function. Fibroblasts contribute to many aspects of pathophysiological remodeling in the heart, including secretion of ECM proteins: here we show that decreased MK5 expression altered the profile of mRNAs encoding proteins involved in ECM remodeling. Moreover, $MK5^{-/-}$ and MK5-kd fibroblasts secreted more soluble collagen and fibronectin compared with $MK5^{+/+}$ and $MK5^{+/-}$ fibroblasts whereas the subcellular distribution of type 1 collagen immunoreactivity was diffused in the cytoplasm of $MK5^{+/+}$ fibroblasts but condensed in the perinuclear region of $MK5^{-/-}$ fibroblasts. In addition, knocking down MK5 impaired myofibroblast contraction. Hence, MK5 may be a regulator of cardiac fibroblast function, thus affecting ECM remodeling. In summary, we have now shown: 1) MK5 plays an important role in cardiac remodeling induced by pressure overload or by myocardial infarction, 2) MK5 plays a crucial role in cardiac fibroblast function, and 3) MK5 regulates transcript levels for several proteins involved in ECM turnover as well as collagen and fibronectin secretion in cardiac fibroblasts.

MK5 lies downstream of p38α/β, ERK3, and ERK4. Its physiological role in the heart has not been yet explored. Herein we determined if MK5 is involved in pathological cardiac remodeling following chronic pressure overload and myocardial infarction. Chronic pressure overload induces cardiac fibroblast proliferation, increased interstitial fibrosis, and ECM

remodeling [341]. Cardiac interstitial fibrosis can result from alteration of both the synthesis and degradation of collagen with net result of collagen accumulation and deposition. Cardiac interstitial fibrosis is the main determinant of diastolic dysfunction in heart diseases. Fibrosis can be either reactive or reparative. Reparative fibrosis (scar formation) is an important physiological process occurs in response to death of cardiomyocytes following myocardial infarction to preserve cardiac structural integrity, whereas reactive fibrosis is a pathological response that occurs in non-infarcted remote myocardial area or in response to chronic pressure overload resulting in ventricular dysfunction and myocardial stiffness [142, 143]. Type I and type III collagens are the major components of the cardiac ECM. Collagen type I represents approximately 85% of total collagen in the heart, thus it is a major determinant of myocardial stiffness [342, 343]. Here we show that reduced MK5 attenuates the ability of chronic pressure overload to induce a progressive hypertrophy, increase collagen 1-α_1 mRNA expression, and protect diastolic function. However, in response to myocardial ischemia, reduced MK5 expression resulted in smaller scars and less collagen content within these scars, as detected by Masson's trichrome staining, and more abundant α-SMA-positive vessels. Interestingly, MK5 immunoreactivity was detected in fibroblasts but not cardiomyocytes. These results indicate that MK5 is involved in both the manner in which the myocardium remodels when faced with a chronic hemodynamic overload and reparative fibrosis following myocardial injury via alterations in fibroblast function. The decreased hypertrophy observed in $MK5^{+/-}$ hearts may be a result of direct fibroblast-myocyte coupling or paracrine signalling between fibroblasts and cardiomyocytes. Hence, although MK5 may represent a potential anti-fibrotic and anti-hypertrophic treatment in pressure-overloaded heart, MK5 inhibitors would be contraindicated following a myocardial infarction. However, it remains to be determined if the effects of reduced MK5 expression on cardiac remodeling were due to a reduction of MK5 activity or to a decrease in the MK5 cellular content. This can be resolved by using mice engineered to express an inactive form of MK5, thus assessing the involvement of MK5 catalytic activity in cardiac remodeling.

Fibroblasts are the main source of collagen in the heart. Upon activation, they become myofibroblasts that express α-SMA and secrete collagen. The reduction or absence of MK5 did not affect fibroblast activation. TGF-β, a cytokine expressed in both myocytes and

fibroblasts, induces molecular remodeling and hypertrophy in ventricular myocytes [344], whereas in fibroblasts it induces proliferation, activation into myofibroblasts, and increased ECM production of proteins, including collagen, fibronectin, and proteoglycans [345]. In addition, TGF-β inhibits the expression of MMPs and induces the expression of protease inhibitors such as plasminogen activator inhibitor-1 (PAI-1) and tissue inhibitors of metalloproteinases (TIMPs), thus reducing ECM breakdown [346]. Within twelve hours of aortic constriction, there is an increase in rat myocardial TGF-β mRNA [236, 347, 348] which returns to near control levels within two weeks [236]. β-Adrenergic receptor signaling is implicated downstream of TGF-β1 and the catalytic subunit of PKA, which is activated by β-adrenergic receptors, phosphorylates, activates, and translocates MK5 [280, 284]. Blocking β1-adrenergic receptors in mice overexpressing TGF-β1 is antihypertrophic but not antifibrotic [349]. Herein, the ability of pressure overload to induce the expression TGFβ1 was not affected by reduced MK5 expression. In conclusion, although the chronic pressure overload induced increase in collagen 1-α_1 mRNA was markedly attenuated in MK5 haplodeficient mice, TGF-β1 expression was unaffected, suggesting that TGF-β1/β-adrenergic receptor signaling may not be involved in the fibrotic response to pressure overload in the heart. On the other hand, the increase in TGF-β3 mRNA was maintained in $MK5^{+/+}$ but not in $MK5^{+/-}$ hearts eight weeks post-TAC. Thus, TGF-β3 signaling may be involved in the reduced hypertrophic growth observed in MK5 haplodeficient mice eight weeks post-TAC.

The involvement of MK5 in cytoskeletal remodelling, migration [302, 307, 313, 314, 350] and proliferation [285, 306, 309, 315] is controversial. The apparent discrepancy concerning the role of MK5 in proliferation and migration may result from differences in cell type or model, cellular environment, and the means whereby MK5 signaling was manipulated experimentally. Herein we show that MK5 immunoreactivity is detected in fibroblasts and not myocytes. Both migration and proliferation were reduced in MK5-deficient and MK5-kd fibroblasts, but not in haplodeficient fibroblasts. Moreover, knocking down MK5 impaired myofibroblast contraction. Similarly, loss of p38α in murine embryonic fibroblasts inhibited collagen gel contraction but increased proliferation [351]. The differences observed between p38α-deficient and MK5-deficient fibroblasts suggest they may play distinct roles in regulating fibroblast function.

The regulation of MK5 activity by upstream kinases is currently controversial. p38 MAPK, ERK3/4, and PKA have been shown to phosphorylate and activate MK5 *in vitro* and *in vivo*. MK5 was originally described as a p38 substrate, as its cellular localization and activation depended on p38 activity [265]. Of the four p38 isoforms, MK5 is phosphorylated and activated by p38α and p38β. p38 pathway is considered as a stress response signalling pathway. Acute activation of endogenous p38 in the adult murine heart resulted in hypertrophy, fibrosis, contractile dysfunction, and fatal cardiomyopathy within one week [352]. Our findings reveal a novel role for MK5 during the pathological cardiac remodelling induced by chronic pressure overload and myocardial infarction and suggest it may mediate some of the pathological effects of p38 activation. However, atypical MAPKs ERK3 and ERK4 also activate MK5 and the role of these kinases in cardiac pathophysiology remains to be determined. In lysates from control and pressure overloaded murine hearts, MK5 coimmunoprecipitate with ERK3, but not ERK4 or p38α, and this ERK3-MK5 complex was stable regardless of p38 activity [270]. Moreover, Both $MK5^{+/-}$ and $ERK3^{+/-}$ hearts developed hypertrophy in response to two or three weeks of pressure overload respectively. MK5 and ERK3 immunoreactivity was detected in fibroblasts but not in myocytes. In contrast, un-published data from our laboratory showed that ERK4 immunoreactivity was detectd in myocytes. ERK4-null mice increased collagen expression in response to pressure overload. Hence, in the heart, ERK4 may not be involved in regulating MK5 in cardiac cells. MK5 may be downstream of ERK3 and ERK3-MK5 signalling may be involved in cardiac extracellular matrix remodeling following hemodynamic overload or myocardial injury. However, we do not know if the ERK3-MK5 complex is a simple heterodimer or includes other endogenous proteins. It is also possible that p38 may regulate the ERK3-MK5 complex. In cultured, non-cardiac cells, group 1 PAKs have been shown to bind, phosphorylate and activate ERK3/4-MK5 [295, 296]. PAK1-deficiency resulted in increased hypertrophic growth after seven days of isoproterenol infusion [353]. In contrast, in response to chronic pressure overload the progression of hypertrophy was attenuated in MK5 haplodeficient mice. This suggests that PAK1 may not be upstream of ERK3/4-MK5 in adult ventricular fibroblasts.

p38α is required for stimulus-induced myofibroblast activation. Loss of p38α *in vitro* (from MEFs) and *in vivo* (from adult cardiac fibroblasts) blocks TGFβ and Ang-II induced

myofibroblast activation[351]. Herein, reduced MK5 expression *in vitro* does not prevent murine ventricular fibroblasts from activation into α-SMA-expressing myofibroblasts and does not block TGF-β expression induced by chronic pressure overload. These results suggest that the effect of p38 deletion on myofibroblast activation in response to profibrotic stimuli is not through a TGF-β-p38/MK5 signalling pathway in cardiac fibroblasts and other downstream pathways are required for myofibroblast activation. In response to myocardial infarction, a cardiac fibroblast-specific p38α deletion was 100% lethal [351] whereas, survival rates of $MK5^{+/-}$ infarcted heart did not differ significantly eight days post-MI compared to wild type littermates, but was higher 21 days post-MI. Reducing MK5 or p38α expression does not result in the same phenotype in cardiac fibroblasts. The observed differences may result, in part, from the mouse model we used is heterozygous for a functional knockout of MK5 and not a complete knockout. However, in response to ischemia/reperfusion injury (I/R), mice having p38α loss had 50% lethality, with significant reduction in ventricular scar area [351]. Our results showed that following MI, $MK5^{+/-}$ hearts had smaller scar size and less collagen content within the scar. Moreover, in a model of chronic fibrotic injury induced by Ang-II infusion, myofibroblast-specific loss of p38α blocked cardiac hypertrophy and reduced cardiac fibrosis [351]. Herein, we demonstrated that MK5 haplodeficiency attenuated the ability of TAC-induced pressure overload to induce hypertrophy. One interpretation of these data is that p38 may regulate MK5 in the heart depending on the nature and the intensity of the stimulus, and the cell type it acts upon.

MAPK signaling plays a critical role in collagen secretion, and cardiac fibroblasts proliferation and migration [132, 354]. Knocking out MK5 altered the subcellular distribution of intracellular collagen immunoreactivity. Whereas type 1 collagen immunoreactivity was diffuse in fibroblasts treated with scrambled RNA, it was condensed in the perinuclear region following siRNA-mediated knock down of MK5, suggesting an effect on collagen biosynthesis or trafficking. Inhibition of p38 activity decreases collagen secretion in rat left atrial fibroblasts [355]. The p38 signalling pathway mediates VEGF production in vascular smooth muscle cells [356]. p38 inhibition increased VEGF production in both left and right atrial fibroblasts [355]. As VEGF stimulates angiogenesis, MK5 haplodefficiencymay stimulated angiogenesis by attenuating p38 signalling and thus increasing VEGF production following an

MI. Also, the VEGF-induced cytoskeletal reorganization mediated through p38/MK5/FAK activation was lost upon MK5 knockdown [314]. Hence, the role of MK5 in the regulation of cytoskeletal remodelling may depend upon the nature of the stimulus and the cellular context.

Fibroblasts are largely responsible for remodeling of the ECM. As MK5 immunoreactivity is found in fibroblasts but not in cardiomyocytes, and the ability of TAC to increase collagen 1-α_1 mRNA is attenuated hearts from $MK5^{+/-}$ mice compared $MK5^{+/+}$ mice, we examined type 1 collagen mRNA and immunoreactivity as well as mRNA levels encoding other proteins involved in ECM remodeling from cultured $MK5^{+/+}$, $MK5^{+/-}$, and $MK5^{-/-}$ fibroblasts. MK5 knock-out or knock-down resulted in alteration in the level of mRNA encoding many proteins involved in ECM remodeling. In addition, secretion of type 1 collagen was increased in MK5-deficient cultured fibroblasts. Surprisingly, $MK5^{-/-}$ fibroblasts showed significantly increased COL1A1, COL3A1, TGF-β3, SMAD6, and SMAD7 mRNA as well as reduced levels of Timp3, thrombospondin 1, and LTBP1 mRNA. mRNAs for MMPs 13, 8, 1a, and 3 also showed modest, but not significant reductions. One explanation for the observed discrepancy between the *in vivo* model of reparative and interstitial fibrosis and the *in vitro* model of cultured fibroblasts may be related to the contextual differences between fibroblasts *in vivo* and those maintained in 2D culture on a rigid matrix. Continuous mechanical stress induced by constant contraction and relaxation of the surrounding viable myocardium results preferential alignment of the myofibroblasts within the human myocardial scar [92]. Moreover, changes in tension affects the synthesis and remodeling of ECM at the site of injury [357]. Hence, the lack of cyclical stretch experienced by fibroblasts cultured on a rigid matrix may have an effect on MK5 signalling and the functional consequences of MK5 deletion. Another possibility is that cultured fibroblasts lose their paracrine signals and coupling with the surrounding cells found *in vivo*. Finally, the identification of a nodal role for MK5 in transducing signals within the fibroblasts suggests MK5 may serve as a target for the development of anti-fibrotic and anti-hypertrophic therapies. However, the timing of anti-fibrotic therapies is critical in order to maintain the initial wound healing phase.

Conclusion

This present study reveals a novel role for MK5 1) during the pathological cardiac remodeling induced by chronic pressure overload, 2) in reparative fibrosis following myocardial infarction, 3) in cardiac fibroblast function, and 4) in collagen biosynthesis and extracellular matrix remodeling. We have shown that at twelve weeks of age, $MK5^{+/-}$ mice have modest reduction in systolic function. The increase in collagen1-α_1 mRNA observed two weeks after constriction of the transverse aorta (TAC) was attenuated in $MK5^{+/-}$ hearts and the progression of hypertrophy was significantly reduced eight weeks post-TAC in $MK5^{+/-}$ hearts. $MK5^{+/-}$ mice show preserved diastolic function following two and eight weeks of pressure overload. The reduction in collagen mRNA level in $MK5^{+/-}$ two weeks post-TAC was not related to TGFβ mRNA synthesis. As MK5 immunoreactivity was detected in cardiac fibroblasts but not cardiomyocytes, the cardiac phenotype results may have originated from MK5-dependent changes in fibroblast function.

Furthermore, we have shown that both $MK5^{+/+}$ and $MK5^{+/-}$ mice have similar extent of LV dilatation, systolic dysfunction and viability eight days post-MI. Reduced MK5 resulted in a reduction in collagen content within the scar and scar size. MK5 haplodeficiency increased neovascularization in peri-infarct region. Both proliferative and migratory responses were impaired in cultured ventricular $MK5^{-/-}$ fibroblasts. Hence, MK5 plays a role in reparative fibrosis.

Finally, we have shown that deleting MK5 increased both the abundance of collagen1-α_1 mRNA and secretion of type 1 collagen. The profile of mRNAs encoding proteins involved in ECM remodeling as well as the subcellular distribution of intracellular collagen were also altered in the absence of MK5 as was the ability of myofibroblasts to contract on collagen gels. Taken together, these findings indicate a role for MK5 in several key aspects of fibroblast function.

Original contribution to the literature

1. MK5 immunoreactivity is detected in cardiac fibroblasts and not cardiomyocytes
2. MK5 is involved in the progression of hypertrophic growth and the increase in collagen expression induced by chronic pressure overload.
3. MK5 haplodeficiency preserves diastolic function when faced to hemodynamic overload.
4. Demonstration of a novel splice variant of MK5 in the heart (MK5.6).
5. MK5 haplodeficiency altered the profile of fetal gene re-expression but did not prevent molecular remodeling in response to pressure overload.
6. MK5 is involved in reparative fibrosis following myocardial infarction.
7. MK5 haplodeficiency increased angiogenesis in peri-infarct zone.
8. MK5 haplodeficiency decreases the collagen content within the scar and the scar size.
9. MK5-null fibroblasts have impaired proliferation and motility.
10. MK5 is involved in collagen biosynthesis or trafficking and in ECM remodeling.
11. The absence of MK5 alters the subcellular distribution of intracellular collagen immunoreactivity.
12. The absence of MK5 altered the profile of mRNA levels encoding proteins involved in ECM remodeling.

References

1. Rienks M, Papageorgiou AP, Frangogiannis NG and Heymans S. Myocardial extracellular matrix: an ever-changing and diverse entity. *Circ Res*. 2014;114:872-88.
2. Theocharis AD, Skandalis SS, Gialeli C and Karamanos NK. Extracellular matrix structure. *Adv Drug Deliv Rev*. 2016;97:4-27.
3. Shinde AV and Frangogiannis NG. Fibroblasts in myocardial infarction: a role in inflammation and repair. *J Mol Cell Cardiol*. 2014;70:74-82.
4. Heymans S, Gonzalez A, Pizard A, Papageorgiou AP, Lopez-Andres N, Jaisser F, Thum T, Zannad F and Diez J. Searching for new mechanisms of myocardial fibrosis with diagnostic and/or therapeutic potential. *Eur J Heart Fail*. 2015;17:764-71.
5. Kendall RT and Feghali-Bostwick CA. Fibroblasts in fibrosis: novel roles and mediators. *Front Pharmacol*. 2014;5:123.
6. Frangogiannis NG. Pathophysiology of Myocardial Infarction. *Compr Physiol*. 2015;5:1841-75.
7. Cuenda A and Rousseau S. p38 MAP-kinases pathway regulation, function and role in human diseases. *Biochim Biophys Acta*. 2007;1773:1358-75.
8. Bernardo BC, Weeks KL, Pretorius L and McMullen JR. Molecular distinction between physiological and pathological cardiac hypertrophy: experimental findings and therapeutic strategies. *Pharmacol Ther*. 2010;128:191-227.
9. Kostenko S, Dumitriu G, Laegreid KJ and Moens U. Physiological roles of mitogen-activated-protein-kinase-activated p38-regulated/activated protein kinase. *World J Biol Chem*. 2011;2:73-89.
10. Krenning G, Zeisberg EM and Kalluri R. The origin of fibroblasts and mechanism of cardiac fibrosis. *J Cell Physiol*. 2010;225:631-7.
11. Nag AC. Study of non-muscle cells of the adult mammalian heart: a fine structural analysis and distribution. *Cytobios*. 1980;28:41-61.
12. Estigoy CB, Pontén F, Odeberg J, Herbert B, Guilhaus M, Charleston M, Ho JWK, Cameron D and dos Remedios CG. Intercalated discs: multiple proteins perform multiple functions in non-failing and failing human hearts. *Biophysical Reviews*. 2009;1:43.
13. Hoshijima M. Mechanical stress-strain sensors embedded in cardiac cytoskeleton: Z disk, titin, and associated structures. *Am J Physiol Heart Circ Physiol*. 2006;290:H1313-25.
14. Knoll R, Hoshijima M and Chien K. Cardiac mechanotransduction and implications for heart disease. *J Mol Med (Berl)*. 2003;81:750-6.
15. Lazzeroni D, Rimoldi O and Camici PG. From Left Ventricular Hypertrophy to Dysfunction and Failure. *Circ J*. 2016;80:555-64.
16. Lorell BH and Carabello BA. Left ventricular hypertrophy: pathogenesis, detection, and prognosis. *Circulation*. 2000;102:470-9.
17. Kamo T, Akazawa H and Komuro I. Cardiac nonmyocytes in the hub of cardiac hypertrophy. *Circ Res*. 2015;117:89-98.
18. Olah A, Nemeth BT, Matyas C, Hidi L, Lux A, Ruppert M, Kellermayer D, Sayour AA, Szabo L, Torok M, Meltzer A, Geller L, Merkely B and Radovits T. Physiological and pathological left ventricular hypertrophy of comparable degree is associated with

characteristic differences of in vivo hemodynamics. *Am J Physiol Heart Circ Physiol*. 2016;310:H587-97.
19. Heineke J and Molkentin JD. Regulation of cardiac hypertrophy by intracellular signalling pathways. *Nat Rev Mol Cell Biol*. 2006;7:589-600.
20. Grossman W, Jones D and McLaurin LP. Wall stress and patterns of hypertrophy in the human left ventricle. *J Clin Invest*. 1975;56:56-64.
21. Maillet M, van Berlo JH and Molkentin JD. Molecular basis of physiological heart growth: fundamental concepts and new players. *Nat Rev Mol Cell Biol*. 2013;14:38-48.
22. Carbone A, D'Andrea A, Riegler L, Scarafile R, Pezzullo E, Martone F, America R, Liccardo B, Galderisi M, Bossone E and Calabro R. Cardiac damage in athlete's heart: When the "supernormal" heart fails! *World J Cardiol*. 2017;9:470-480.
23. Jin H, Yang R, Li W, Lu H, Ryan AM, Ogasawara AK, Van Peborgh J and Paoni NF. Effects of exercise training on cardiac function, gene expression, and apoptosis in rats. *Am J Physiol Heart Circ Physiol*. 2000;279:H2994-3002.
24. La Gerche A, Burns AT, Mooney DJ, Inder WJ, Taylor AJ, Bogaert J, Macisaac AI, Heidbuchel H and Prior DL. Exercise-induced right ventricular dysfunction and structural remodelling in endurance athletes. *Eur Heart J*. 2012;33:998-1006.
25. Galderisi M, Cardim N, D'Andrea A, Bruder O, Cosyns B, Davin L, Donal E, Edvardsen T, Freitas A, Habib G, Kitsiou A, Plein S, Petersen SE, Popescu BA, Schroeder S, Burgstahler C and Lancellotti P. The multi-modality cardiac imaging approach to the Athlete's heart: an expert consensus of the European Association of Cardiovascular Imaging. *Eur Heart J Cardiovasc Imaging*. 2015;16:353.
26. Benito B, Gay-Jordi G, Serrano-Mollar A, Guasch E, Shi Y, Tardif JC, Brugada J, Nattel S and Mont L. Cardiac arrhythmogenic remodeling in a rat model of long-term intensive exercise training. *Circulation*. 2011;123:13-22.
27. Shiojima I, Sato K, Izumiya Y, Schiekofer S, Ito M, Liao R, Colucci WS and Walsh K. Disruption of coordinated cardiac hypertrophy and angiogenesis contributes to the transition to heart failure. *J Clin Invest*. 2005;115:2108-18.
28. Cox EJ and Marsh SA. A systematic review of fetal genes as biomarkers of cardiac hypertrophy in rodent models of diabetes. *PLoS One*. 2014;9:e92903.
29. Franco V, Chen YF, Oparil S, Feng JA, Wang D, Hage F and Perry G. Atrial natriuretic peptide dose-dependently inhibits pressure overload-induced cardiac remodeling. *Hypertension*. 2004;44:746-50.
30. Rosenkranz AC, Hood SG, Woods RL, Dusting GJ and Ritchie RH. B-type natriuretic peptide prevents acute hypertrophic responses in the diabetic rat heart: importance of cyclic GMP. *Diabetes*. 2003;52:2389-95.
31. Wang D, Oparil S, Feng JA, Li P, Perry G, Chen LB, Dai M, John SW and Chen YF. Effects of pressure overload on extracellular matrix expression in the heart of the atrial natriuretic peptide-null mouse. *Hypertension*. 2003;42:88-95.
32. Krenz M and Robbins J. Impact of beta-myosin heavy chain expression on cardiac function during stress. *J Am Coll Cardiol*. 2004;44:2390-7.
33. Dorn GW, 2nd and Brown JH. Gq signaling in cardiac adaptation and maladaptation. *Trends Cardiovasc Med*. 1999;9:26-34.
34. Robitaille C, Dai S and Waters C. Ischemic heart disease prevalence and incidence in Canada. *Canadian Journal of Cardiology*. 2014;30:S75-S76.

35. Sheet-Populations SF. International cardiovascular disease statistics. *American Heart Association*. 2004.
36. Cheitlin MD, McAllister HA and de Castro CM. Myocardial infarction without atherosclerosis. *JAMA*. 1975;231:951-9.
37. van Nieuwenhoven FA and Turner NA. The role of cardiac fibroblasts in the transition from inflammation to fibrosis following myocardial infarction. *Vascul Pharmacol*. 2013;58:182-8.
38. Frangogiannis NG. The immune system and cardiac repair. *Pharmacol Res*. 2008;58:88-111.
39. Chen W and Frangogiannis NG. Fibroblasts in post-infarction inflammation and cardiac repair. *Biochim Biophys Acta*. 2013;1833:945-53.
40. Sutton MG and Sharpe N. Left ventricular remodeling after myocardial infarction: pathophysiology and therapy. *Circulation*. 2000;101:2981-8.
41. Kong P, Christia P and Frangogiannis NG. The pathogenesis of cardiac fibrosis. *Cell Mol Life Sci*. 2014;71:549-74.
42. Prabhu SD and Frangogiannis NG. The Biological Basis for Cardiac Repair After Myocardial Infarction: From Inflammation to Fibrosis. *Circ Res*. 2016;119:91-112.
43. Baines CP, Kaiser RA, Purcell NH, Blair NS, Osinska H, Hambleton MA, Brunskill EW, Sayen MR, Gottlieb RA, Dorn GW, Robbins J and Molkentin JD. Loss of cyclophilin D reveals a critical role for mitochondrial permeability transition in cell death. *Nature*. 2005;434:658-62.
44. Reimer KA, Lowe JE, Rasmussen MM and Jennings RB. The wavefront phenomenon of ischemic cell death. 1. Myocardial infarct size vs duration of coronary occlusion in dogs. *Circulation*. 1977;56:786-94.
45. Burke AP and Virmani R. Pathophysiology of acute myocardial infarction. *Med Clin North Am*. 2007;91:553-72; ix.
46. Ong SB and Gustafsson AB. New roles for mitochondria in cell death in the reperfused myocardium. *Cardiovasc Res*. 2012;94:190-6.
47. Matsui Y, Takagi H, Qu X, Abdellatif M, Sakoda H, Asano T, Levine B and Sadoshima J. Distinct roles of autophagy in the heart during ischemia and reperfusion: roles of AMP-activated protein kinase and Beclin 1 in mediating autophagy. *Circ Res*. 2007;100:914-22.
48. Kanamori H, Takemura G, Goto K, Maruyama R, Ono K, Nagao K, Tsujimoto A, Ogino A, Takeyama T, Kawaguchi T, Watanabe T, Kawasaki M, Fujiwara T, Fujiwara H, Seishima M and Minatoguchi S. Autophagy limits acute myocardial infarction induced by permanent coronary artery occlusion. *Am J Physiol Heart Circ Physiol*. 2011;300:H2261-71.
49. Lavandero S, Troncoso R, Rothermel BA, Martinet W, Sadoshima J and Hill JA. Cardiovascular autophagy: concepts, controversies, and perspectives. *Autophagy*. 2013;9:1455-66.
50. Bianchi ME. DAMPs, PAMPs and alarmins: all we need to know about danger. *J Leukoc Biol*. 2007;81:1-5.
51. Chan JK, Roth J, Oppenheim JJ, Tracey KJ, Vogl T, Feldmann M, Horwood N and Nanchahal J. Alarmins: awaiting a clinical response. *J Clin Invest*. 2012;122:2711-9.
52. Frangogiannis NG. The inflammatory response in myocardial injury, repair, and remodelling. *Nat Rev Cardiol*. 2014;11:255-65.

53. Andrassy M, Volz HC, Igwe JC, Funke B, Eichberger SN, Kaya Z, Buss S, Autschbach F, Pleger ST, Lukic IK, Bea F, Hardt SE, Humpert PM, Bianchi ME, Mairbaurl H, Nawroth PP, Remppis A, Katus HA and Bierhaus A. High-mobility group box-1 in ischemia-reperfusion injury of the heart. *Circulation*. 2008;117:3216-26.
54. Ghigo A, Franco I, Morello F and Hirsch E. Myocyte signalling in leucocyte recruitment to the heart. *Cardiovasc Res*. 2014;102:270-80.
55. Dreyer WJ, Michael LH, Nguyen T, Smith CW, Anderson DC, Entman ML and Rossen RD. Kinetics of C5a release in cardiac lymph of dogs experiencing coronary artery ischemia-reperfusion injury. *Circ Res*. 1992;71:1518-24.
56. Frangogiannis NG. Regulation of the inflammatory response in cardiac repair. *Circ Res*. 2012;110:159-73.
57. Newton K and Dixit VM. Signaling in innate immunity and inflammation. *Cold Spring Harb Perspect Biol*. 2012;4.
58. Hartupee J and Mann DL. Role of inflammatory cells in fibroblast activation. *J Mol Cell Cardiol*. 2016;93:143-8.
59. Gwechenberger M, Mendoza LH, Youker KA, Frangogiannis NG, Smith CW, Michael LH and Entman ML. Cardiac myocytes produce interleukin-6 in culture and in viable border zone of reperfused infarctions. *Circulation*. 1999;99:546-51.
60. Tian J, Guo X, Liu XM, Liu L, Weng QF, Dong SJ, Knowlton AA, Yuan WJ and Lin L. Extracellular HSP60 induces inflammation through activating and up-regulating TLRs in cardiomyocytes. *Cardiovasc Res*. 2013;98:391-401.
61. Frangogiannis NG. The reparative function of cardiomyocytes in the infarcted myocardium. *Cell Metab*. 2015;21:797-8.
62. Lorchner H, Poling J, Gajawada P, Hou Y, Polyakova V, Kostin S, Adrian-Segarra JM, Boettger T, Wietelmann A, Warnecke H, Richter M, Kubin T and Braun T. Myocardial healing requires Reg3beta-dependent accumulation of macrophages in the ischemic heart. *Nat Med*. 2015;21:353-62.
63. Bujak M, Dobaczewski M, Gonzalez-Quesada C, Xia Y, Leucker T, Zymek P, Veeranna V, Tager AM, Luster AD and Frangogiannis NG. Induction of the CXC chemokine interferon-gamma-inducible protein 10 regulates the reparative response following myocardial infarction. *Circ Res*. 2009;105:973-83.
64. Frangogiannis NG, Mendoza LH, Lewallen M, Michael LH, Smith CW and Entman ML. Induction and suppression of interferon-inducible protein 10 in reperfused myocardial infarcts may regulate angiogenesis. *FASEB J*. 2001;15:1428-30.
65. Souders CA, Bowers SL and Baudino TA. Cardiac fibroblast: the renaissance cell. *Circ Res*. 2009;105:1164-76.
66. Zhang X, Azhar G, Nagano K and Wei JY. Differential vulnerability to oxidative stress in rat cardiac myocytes versus fibroblasts. *J Am Coll Cardiol*. 2001;38:2055-62.
67. Nakaya M, Watari K, Tajima M, Nakaya T, Matsuda S, Ohara H, Nishihara H, Yamaguchi H, Hashimoto A, Nishida M, Nagasaka A, Horii Y, Ono H, Iribe G, Inoue R, Tsuda M, Inoue K, Tanaka A, Kuroda M, Nagata S and Kurose H. Cardiac myofibroblast engulfment of dead cells facilitates recovery after myocardial infarction. *J Clin Invest*. 2017;127:383-401.
68. Humeres C, Vivar R, Boza P, Munoz C, Bolivar S, Anfossi R, Osorio JM, Olivares-Silva F, Garcia L and Diaz-Araya G. Cardiac fibroblast cytokine profiles induced by

proinflammatory or profibrotic stimuli promote monocyte recruitment and modulate macrophage M1/M2 balance in vitro. *J Mol Cell Cardiol*. 2016.
69. Saxena A, Chen W, Su Y, Rai V, Uche OU, Li N and Frangogiannis NG. IL-1 induces proinflammatory leukocyte infiltration and regulates fibroblast phenotype in the infarcted myocardium. *J Immunol*. 2013;191:4838-48.
70. Gersch C, Dewald O, Zoerlein M, Michael LH, Entman ML and Frangogiannis NG. Mast cells and macrophages in normal C57/BL/6 mice. *Histochem Cell Biol*. 2002;118:41-9.
71. Darden AG, Forbes RD, Darden PM and Guttmann RD. The effects of genetics and age on expression of MHC class II and CD4 antigens on rat cardiac interstitial dendritic cells. *Cell Immunol*. 1990;126:322-30.
72. Frangogiannis NG, Lindsey ML, Michael LH, Youker KA, Bressler RB, Mendoza LH, Spengler RN, Smith CW and Entman ML. Resident cardiac mast cells degranulate and release preformed TNF-alpha, initiating the cytokine cascade in experimental canine myocardial ischemia/reperfusion. *Circulation*. 1998;98:699-710.
73. Zouggari Y, Ait-Oufella H, Bonnin P, Simon T, Sage AP, Guerin C, Vilar J, Caligiuri G, Tsiantoulas D, Laurans L, Dumeau E, Kotti S, Bruneval P, Charo IF, Binder CJ, Danchin N, Tedgui A, Tedder TF, Silvestre JS and Mallat Z. B lymphocytes trigger monocyte mobilization and impair heart function after acute myocardial infarction. *Nat Med*. 2013;19:1273-80.
74. Etoh T, Joffs C, Deschamps AM, Davis J, Dowdy K, Hendrick J, Baicu S, Mukherjee R, Manhaini M and Spinale FG. Myocardial and interstitial matrix metalloproteinase activity after acute myocardial infarction in pigs. *Am J Physiol Heart Circ Physiol*. 2001;281:H987-94.
75. Adair-Kirk TL and Senior RM. Fragments of extracellular matrix as mediators of inflammation. *Int J Biochem Cell Biol*. 2008;40:1101-10.
76. Dobaczewski M, Gonzalez-Quesada C and Frangogiannis NG. The extracellular matrix as a modulator of the inflammatory and reparative response following myocardial infarction. *J Mol Cell Cardiol*. 2010;48:504-11.
77. Frangogiannis NG, Smith CW and Entman ML. The inflammatory response in myocardial infarction. *Cardiovasc Res*. 2002;53:31-47.
78. Monden Y, Kubota T, Tsutsumi T, Inoue T, Kawano S, Kawamura N, Ide T, Egashira K, Tsutsui H and Sunagawa K. Soluble TNF receptors prevent apoptosis in infiltrating cells and promote ventricular rupture and remodeling after myocardial infarction. *Cardiovasc Res*. 2007;73:794-805.
79. Hilfiker-Kleiner D, Shukla P, Klein G, Schaefer A, Stapel B, Hoch M, Muller W, Scherr M, Theilmeier G, Ernst M, Hilfiker A and Drexler H. Continuous glycoprotein-130-mediated signal transducer and activator of transcription-3 activation promotes inflammation, left ventricular rupture, and adverse outcome in subacute myocardial infarction. *Circulation*. 2010;122:145-55.
80. Kandalam V, Basu R, Abraham T, Wang X, Awad A, Wang W, Lopaschuk GD, Maeda N, Oudit GY and Kassiri Z. Early activation of matrix metalloproteinases underlies the exacerbated systolic and diastolic dysfunction in mice lacking TIMP3 following myocardial infarction. *Am J Physiol Heart Circ Physiol*. 2010;299:H1012-23.
81. Matsui Y, Ikesue M, Danzaki K, Morimoto J, Sato M, Tanaka S, Kojima T, Tsutsui H and Uede T. Syndecan-4 prevents cardiac rupture and dysfunction after myocardial infarction. *Circ Res*. 2011;108:1328-39.

82. Faxon DP, Gibbons RJ, Chronos NA, Gurbel PA, Sheehan F and Investigators H-M. The effect of blockade of the CD11/CD18 integrin receptor on infarct size in patients with acute myocardial infarction treated with direct angioplasty: the results of the HALT-MI study. *J Am Coll Cardiol*. 2002;40:1199-204.
83. Seropian IM, Toldo S, Van Tassell BW and Abbate A. Anti-inflammatory strategies for ventricular remodeling following ST-segment elevation acute myocardial infarction. *J Am Coll Cardiol*. 2014;63:1593-603.
84. Armstrong PW, Granger CB, Adams PX, Hamm C, Holmes D, Jr., O'Neill WW, Todaro TG, Vahanian A and Van de Werf F. Pexelizumab for acute ST-elevation myocardial infarction in patients undergoing primary percutaneous coronary intervention: a randomized controlled trial. *JAMA*. 2007;297:43-51.
85. Horckmans M, Ring L, Duchene J, Santovito D, Schloss MJ, Drechsler M, Weber C, Soehnlein O and Steffens S. Neutrophils orchestrate post-myocardial infarction healing by polarizing macrophages towards a reparative phenotype. *Eur Heart J*. 2016.
86. Soehnlein O and Lindbom L. Phagocyte partnership during the onset and resolution of inflammation. *Nat Rev Immunol*. 2010;10:427-39.
87. Bujak M and Frangogiannis NG. The role of TGF-beta signaling in myocardial infarction and cardiac remodeling. *Cardiovasc Res*. 2007;74:184-95.
88. Ren G, Michael LH, Entman ML and Frangogiannis NG. Morphological characteristics of the microvasculature in healing myocardial infarcts. *J Histochem Cytochem*. 2002;50:71-9.
89. Zymek P, Bujak M, Chatila K, Cieslak A, Thakker G, Entman ML and Frangogiannis NG. The role of platelet-derived growth factor signaling in healing myocardial infarcts. *J Am Coll Cardiol*. 2006;48:2315-23.
90. Dobaczewski M, Bujak M, Zymek P, Ren G, Entman ML and Frangogiannis NG. Extracellular matrix remodeling in canine and mouse myocardial infarcts. *Cell Tissue Res*. 2006;324:475-88.
91. Frangogiannis NG. Matricellular proteins in cardiac adaptation and disease. *Physiol Rev*. 2012;92:635-88.
92. Willems IE, Havenith MG, De Mey JG and Daemen MJ. The alpha-smooth muscle actin-positive cells in healing human myocardial scars. *Am J Pathol*. 1994;145:868-75.
93. Frangogiannis NG, Michael LH and Entman ML. Myofibroblasts in reperfused myocardial infarcts express the embryonic form of smooth muscle myosin heavy chain (SMemb). *Cardiovasc Res*. 2000;48:89-100.
94. Turner NA and Porter KE. Function and fate of myofibroblasts after myocardial infarction. *Fibrogenesis Tissue Repair*. 2013;6:5.
95. Porter KE and Turner NA. Cardiac fibroblasts: at the heart of myocardial remodeling. *Pharmacol Ther*. 2009;123:255-78.
96. Hinz B. Formation and function of the myofibroblast during tissue repair. *J Invest Dermatol*. 2007;127:526-37.
97. Hinz B. The myofibroblast: paradigm for a mechanically active cell. *J Biomech*. 2010;43:146-55.
98. Hinz B, Phan SH, Thannickal VJ, Galli A, Bochaton-Piallat ML and Gabbiani G. The myofibroblast: one function, multiple origins. *Am J Pathol*. 2007;170:1807-16.
99. Chistiakov DA, Orekhov AN and Bobryshev YV. The role of cardiac fibroblasts in post-myocardial heart tissue repair. *Exp Mol Pathol*. 2016;101:231-240.

100. Yano T, Miura T, Ikeda Y, Matsuda E, Saito K, Miki T, Kobayashi H, Nishino Y, Ohtani S and Shimamoto K. Intracardiac fibroblasts, but not bone marrow derived cells, are the origin of myofibroblasts in myocardial infarct repair. *Cardiovasc Pathol*. 2005;14:241-6.
101. Zeisberg EM, Tarnavski O, Zeisberg M, Dorfman AL, McMullen JR, Gustafsson E, Chandraker A, Yuan X, Pu WT, Roberts AB, Neilson EG, Sayegh MH, Izumo S and Kalluri R. Endothelial-to-mesenchymal transition contributes to cardiac fibrosis. *Nat Med*. 2007;13:952-61.
102. Mollmann H, Nef HM, Kostin S, von Kalle C, Pilz I, Weber M, Schaper J, Hamm CW and Elsasser A. Bone marrow-derived cells contribute to infarct remodelling. *Cardiovasc Res*. 2006;71:661-71.
103. Kanisicak O, Khalil H, Ivey MJ, Karch J, Maliken BD, Correll RN, Brody MJ, SC JL, Aronow BJ, Tallquist MD and Molkentin JD. Genetic lineage tracing defines myofibroblast origin and function in the injured heart. *Nat Commun*. 2016;7:12260.
104. Murphy-Ullrich JE and Poczatek M. Activation of latent TGF-beta by thrombospondin-1: mechanisms and physiology. *Cytokine Growth Factor Rev*. 2000;11:59-69.
105. Rifkin DB, Mazzieri R, Munger JS, Noguera I and Sung J. Proteolytic control of growth factor availability. *APMIS*. 1999;107:80-5.
106. Wipff PJ and Hinz B. Integrins and the activation of latent transforming growth factor beta1 - an intimate relationship. *Eur J Cell Biol*. 2008;87:601-15.
107. Shi Y and Massague J. Mechanisms of TGF-beta signaling from cell membrane to the nucleus. *Cell*. 2003;113:685-700.
108. Jimenez SA and Derk CT. Following the molecular pathways toward an understanding of the pathogenesis of systemic sclerosis. *Ann Intern Med*. 2004;140:37-50.
109. Chacko BM, Qin B, Correia JJ, Lam SS, de Caestecker MP and Lin K. The L3 loop and C-terminal phosphorylation jointly define Smad protein trimerization. *Nat Struct Biol*. 2001;8:248-53.
110. Correia JJ, Chacko BM, Lam SS and Lin K. Sedimentation studies reveal a direct role of phosphorylation in Smad3:Smad4 homo- and hetero-trimerization. *Biochemistry*. 2001;40:1473-82.
111. Kawabata M, Inoue H, Hanyu A, Imamura T and Miyazono K. Smad proteins exist as monomers in vivo and undergo homo- and hetero-oligomerization upon activation by serine/threonine kinase receptors. *EMBO J*. 1998;17:4056-65.
112. Yan X, Liu Z and Chen Y. Regulation of TGF-beta signaling by Smad7. *Acta Biochim Biophys Sin (Shanghai)*. 2009;41:263-72.
113. Dobaczewski M, Bujak M, Li N, Gonzalez-Quesada C, Mendoza LH, Wang XF and Frangogiannis NG. Smad3 signaling critically regulates fibroblast phenotype and function in healing myocardial infarction. *Circ Res*. 2010;107:418-28.
114. Small EM, Thatcher JE, Sutherland LB, Kinoshita H, Gerard RD, Richardson JA, Dimaio JM, Sadek H, Kuwahara K and Olson EN. Myocardin-related transcription factor-a controls myofibroblast activation and fibrosis in response to myocardial infarction. *Circ Res*. 2010;107:294-304.
115. Sousa AM, Liu T, Guevara O, Stevens J, Fanburg BL, Gaestel M, Toksoz D and Kayyali US. Smooth muscle alpha-actin expression and myofibroblast differentiation by TGFbeta are dependent upon MK2. *J Cell Biochem*. 2007;100:1581-92.
116. Hashimoto S, Gon Y, Takeshita I, Matsumoto K, Maruoka S and Horie T. Transforming growth Factor-beta1 induces phenotypic modulation of human lung fibroblasts

to myofibroblast through a c-Jun-NH2-terminal kinase-dependent pathway. *Am J Respir Crit Care Med*. 2001;163:152-7.
117. Knowlton AA, Connelly CM, Romo GM, Mamuya W, Apstein CS and Brecher P. Rapid expression of fibronectin in the rabbit heart after myocardial infarction with and without reperfusion. *J Clin Invest*. 1992;89:1060-8.
118. Dobaczewski M, de Haan JJ and Frangogiannis NG. The extracellular matrix modulates fibroblast phenotype and function in the infarcted myocardium. *J Cardiovasc Transl Res*. 2012;5:837-47.
119. Arslan F, Smeets MB, Riem Vis PW, Karper JC, Quax PH, Bongartz LG, Peters JH, Hoefer IE, Doevendans PA, Pasterkamp G and de Kleijn DP. Lack of fibronectin-EDA promotes survival and prevents adverse remodeling and heart function deterioration after myocardial infarction. *Circ Res*. 2011;108:582-92.
120. Serini G, Bochaton-Piallat ML, Ropraz P, Geinoz A, Borsi L, Zardi L and Gabbiani G. The fibronectin domain ED-A is crucial for myofibroblastic phenotype induction by transforming growth factor-beta1. *J Cell Biol*. 1998;142:873-81.
121. Naugle JE, Olson ER, Zhang X, Mase SE, Pilati CF, Maron MB, Folkesson HG, Horne WI, Doane KJ and Meszaros JG. Type VI collagen induces cardiac myofibroblast differentiation: implications for postinfarction remodeling. *Am J Physiol Heart Circ Physiol*. 2006;290:H323-30.
122. Zhao XH, Laschinger C, Arora P, Szaszi K, Kapus A and McCulloch CA. Force activates smooth muscle alpha-actin promoter activity through the Rho signaling pathway. *J Cell Sci*. 2007;120:1801-9.
123. Wang J, Chen H, Seth A and McCulloch CA. Mechanical force regulation of myofibroblast differentiation in cardiac fibroblasts. *Am J Physiol Heart Circ Physiol*. 2003;285:H1871-81.
124. Wang J, Fan J, Laschinger C, Arora PD, Kapus A, Seth A and McCulloch CA. Smooth muscle actin determines mechanical force-induced p38 activation. *J Biol Chem*. 2005;280:7273-84.
125. Booz GW and Baker KM. Molecular signalling mechanisms controlling growth and function of cardiac fibroblasts. *Cardiovasc Res*. 1995;30:537-43.
126. McEwan PE, Gray GA, Sherry L, Webb DJ and Kenyon CJ. Differential effects of angiotensin II on cardiac cell proliferation and intramyocardial perivascular fibrosis in vivo. *Circulation*. 1998;98:2765-73.
127. Stockand JD and Meszaros JG. Aldosterone stimulates proliferation of cardiac fibroblasts by activating Ki-RasA and MAPK1/2 signaling. *Am J Physiol Heart Circ Physiol*. 2003;284:H176-84.
128. Zhao W, Zhao T, Huang V, Chen Y, Ahokas RA and Sun Y. Platelet-derived growth factor involvement in myocardial remodeling following infarction. *J Mol Cell Cardiol*. 2011;51:830-8.
129. Zhao XY, Zhao LY, Zheng QS, Su JL, Guan H, Shang FJ, Niu XL, He YP and Lu XL. Chymase induces profibrotic response via transforming growth factor-beta 1/Smad activation in rat cardiac fibroblasts. *Mol Cell Biochem*. 2008;310:159-66.
130. McLarty JL, Melendez GC, Brower GL, Janicki JS and Levick SP. Tryptase/Protease-activated receptor 2 interactions induce selective mitogen-activated protein kinase signaling and collagen synthesis by cardiac fibroblasts. *Hypertension*. 2011;58:264-70.

131. Blomer N, Pachel C, Hofmann U, Nordbeck P, Bauer W, Mathes D, Frey A, Bayer B, Vogel B, Ertl G, Bauersachs J and Frantz S. 5-Lipoxygenase facilitates healing after myocardial infarction. *Basic Res Cardiol*. 2013;108:367.
132. Mitchell MD, Laird RE, Brown RD and Long CS. IL-1beta stimulates rat cardiac fibroblast migration via MAP kinase pathways. *Am J Physiol Heart Circ Physiol*. 2007;292:H1139-47.
133. Frangogiannis NG, Dewald O, Xia Y, Ren G, Haudek S, Leucker T, Kraemer D, Taffet G, Rollins BJ and Entman ML. Critical role of monocyte chemoattractant protein-1/CC chemokine ligand 2 in the pathogenesis of ischemic cardiomyopathy. *Circulation*. 2007;115:584-92.
134. Virag JI and Murry CE. Myofibroblast and endothelial cell proliferation during murine myocardial infarct repair. *Am J Pathol*. 2003;163:2433-40.
135. van den Borne SW, Diez J, Blankesteijn WM, Verjans J, Hofstra L and Narula J. Myocardial remodeling after infarction: the role of myofibroblasts. *Nat Rev Cardiol*. 2010;7:30-7.
136. Cleutjens JP, Verluyten MJ, Smiths JF and Daemen MJ. Collagen remodeling after myocardial infarction in the rat heart. *Am J Pathol*. 1995;147:325-38.
137. Squires CE, Escobar GP, Payne JF, Leonardi RA, Goshorn DK, Sheats NJ, Mains IM, Mingoia JT, Flack EC and Lindsey ML. Altered fibroblast function following myocardial infarction. *J Mol Cell Cardiol*. 2005;39:699-707.
138. Xie Y, Chen J, Han P, Yang P, Hou J and Kang YJ. Immunohistochemical detection of differentially localized up-regulation of lysyl oxidase and down-regulation of matrix metalloproteinase-1 in rhesus monkey model of chronic myocardial infarction. *Exp Biol Med (Maywood)*. 2012;237:853-9.
139. Zimmerman SD, Thomas DP, Velleman SG, Li X, Hansen TR and McCormick RJ. Time course of collagen and decorin changes in rat cardiac and skeletal muscle post-MI. *Am J Physiol Heart Circ Physiol*. 2001;281:H1816-22.
140. Takemura G, Ohno M, Hayakawa Y, Misao J, Kanoh M, Ohno A, Uno Y, Minatoguchi S, Fujiwara T and Fujiwara H. Role of apoptosis in the disappearance of infiltrated and proliferated interstitial cells after myocardial infarction. *Circ Res*. 1998;82:1130-8.
141. Melchior-Becker A, Dai G, Ding Z, Schafer L, Schrader J, Young MF and Fischer JW. Deficiency of biglycan causes cardiac fibroblasts to differentiate into a myofibroblast phenotype. *J Biol Chem*. 2011;286:17365-75.
142. Manabe I, Shindo T and Nagai R. Gene expression in fibroblasts and fibrosis: involvement in cardiac hypertrophy. *Circ Res*. 2002;91:1103-13.
143. Weber KT, Pick R, Jalil JE, Janicki JS and Carroll EP. Patterns of myocardial fibrosis. *J Mol Cell Cardiol*. 1989;21 Suppl 5:121-31.
144. Sun Y. Myocardial repair/remodelling following infarction: roles of local factors. *Cardiovasc Res*. 2009;81:482-90.
145. Swynghedauw B. Molecular mechanisms of myocardial remodeling. *Physiol Rev*. 1999;79:215-62.
146. Sabbah HN, Sharov VG, Lesch M and Goldstein S. Progression of heart failure: a role for interstitial fibrosis. *Mol Cell Biochem*. 1995;147:29-34.
147. Wynn TA. Cellular and molecular mechanisms of fibrosis. *J Pathol*. 2008;214:199-210.

148. Kentish JC. The effects of inorganic phosphate and creatine phosphate on force production in skinned muscles from rat ventricle. *J Physiol*. 1986;370:585-604.
149. Solaro RJ, Lee JA, Kentish JC and Allen DG. Effects of acidosis on ventricular muscle from adult and neonatal rats. *Circ Res*. 1988;63:779-87.
150. Steenbergen C, Hill ML and Jennings RB. Volume regulation and plasma membrane injury in aerobic, anaerobic, and ischemic myocardium in vitro. Effects of osmotic cell swelling on plasma membrane integrity. *Circ Res*. 1985;57:864-75.
151. Kubler W and Spieckermann PG. Regulation of glycolysis in the ischemic and the anoxic myocardium. *J Mol Cell Cardiol*. 1970;1:351-77.
152. Kleber AG. Resting membrane potential, extracellular potassium activity, and intracellular sodium activity during acute global ischemia in isolated perfused guinea pig hearts. *Circ Res*. 1983;52:442-50.
153. Yang Y, Ma Y, Han W, Li J, Xiang Y, Liu F, Ma X, Zhang J, Fu Z, Su YD, Du XJ and Gao XM. Age-related differences in postinfarct left ventricular rupture and remodeling. *Am J Physiol Heart Circ Physiol*. 2008;294:H1815-22.
154. Reddy SG and Roberts WC. Frequency of rupture of the left ventricular free wall or ventricular septum among necropsy cases of fatal acute myocardial infarction since introduction of coronary care units. *Am J Cardiol*. 1989;63:906-11.
155. Gao XM, White DA, Dart AM and Du XJ. Post-infarct cardiac rupture: recent insights on pathogenesis and therapeutic interventions. *Pharmacol Ther*. 2012;134:156-79.
156. Vanhoutte D, Schellings M, Pinto Y and Heymans S. Relevance of matrix metalloproteinases and their inhibitors after myocardial infarction: a temporal and spatial window. *Cardiovasc Res*. 2006;69:604-13.
157. Cochain C, Auvynet C, Poupel L, Vilar J, Dumeau E, Richart A, Recalde A, Zouggari Y, Yin KY, Bruneval P, Renault G, Marchiol C, Bonnin P, Levy B, Bonecchi R, Locati M, Combadiere C and Silvestre JS. The chemokine decoy receptor D6 prevents excessive inflammation and adverse ventricular remodeling after myocardial infarction. *Arterioscler Thromb Vasc Biol*. 2012;32:2206-13.
158. Hayashidani S, Tsutsui H, Ikeuchi M, Shiomi T, Matsusaka H, Kubota T, Imanaka-Yoshida K, Itoh T and Takeshita A. Targeted deletion of MMP-2 attenuates early LV rupture and late remodeling after experimental myocardial infarction. *Am J Physiol Heart Circ Physiol*. 2003;285:H1229-35.
159. Picard MH, Wilkins GT, Gillam LD, Thomas JD and Weyman AE. Immediate regional endocardial surface expansion following coronary occlusion in the canine left ventricle: disproportionate effects of anterior versus inferior ischemia. *Am Heart J*. 1991;121:753-62.
160. Pierard LA, Albert A, Gilis F, Sprynger M, Carlier J and Kulbertus HE. Hemodynamic profile of patients with acute myocardial infarction at risk of infarct expansion. *Am J Cardiol*. 1987;60:5-9.
161. Christia P, Bujak M, Gonzalez-Quesada C, Chen W, Dobaczewski M, Reddy A and Frangogiannis NG. Systematic characterization of myocardial inflammation, repair, and remodeling in a mouse model of reperfused myocardial infarction. *J Histochem Cytochem*. 2013;61:555-70.
162. Dorfman TA and Aqel R. Regional pericarditis: a review of the pericardial manifestations of acute myocardial infarction. *Clin Cardiol*. 2009;32:115-20.
163. Widimsky P and Gregor P. Pericardial involvement during the course of myocardial infarction. A long-term clinical and echocardiographic study. *Chest*. 1995;108:89-93.

164. Fukuda K, Davies SS, Nakajima T, Ong BH, Kupershmidt S, Fessel J, Amarnath V, Anderson ME, Boyden PA, Viswanathan PC, Roberts LJ, 2nd and Balser JR. Oxidative mediated lipid peroxidation recapitulates proarrhythmic effects on cardiac sodium channels. *Circ Res*. 2005;97:1262-9.
165. Lajiness JD and Conway SJ. Origin, development, and differentiation of cardiac fibroblasts. *J Mol Cell Cardiol*. 2014;70:2-8.
166. Banerjee I, Fuseler JW, Price RL, Borg TK and Baudino TA. Determination of cell types and numbers during cardiac development in the neonatal and adult rat and mouse. *Am J Physiol Heart Circ Physiol*. 2007;293:H1883-91.
167. Ongstad E and Kohl P. Fibroblast-myocyte coupling in the heart: Potential relevance for therapeutic interventions. *J Mol Cell Cardiol*. 2016;91:238-46.
168. De Maziere AM, van Ginneken AC, Wilders R, Jongsma HJ and Bouman LN. Spatial and functional relationship between myocytes and fibroblasts in the rabbit sinoatrial node. *J Mol Cell Cardiol*. 1992;24:567-78.
169. Lajiness JD and Conway SJ. The dynamic role of cardiac fibroblasts in development and disease. *J Cardiovasc Transl Res*. 2012;5:739-48.
170. Beguin PC, Gosselin H, Mamarbachi M and Calderone A. Nestin expression is lost in ventricular fibroblasts during postnatal development of the rat heart and re-expressed in scar myofibroblasts. *J Cell Physiol*. 2012;227:813-20.
171. Mikawa T and Gourdie RG. Pericardial mesoderm generates a population of coronary smooth muscle cells migrating into the heart along with ingrowth of the epicardial organ. *Dev Biol*. 1996;174:221-32.
172. Gittenberger-de Groot AC, Vrancken Peeters MP, Mentink MM, Gourdie RG and Poelmann RE. Epicardium-derived cells contribute a novel population to the myocardial wall and the atrioventricular cushions. *Circ Res*. 1998;82:1043-52.
173. Norris RA, Borg TK, Butcher JT, Baudino TA, Banerjee I and Markwald RR. Neonatal and adult cardiovascular pathophysiological remodeling and repair: developmental role of periostin. *Ann N Y Acad Sci*. 2008;1123:30-40.
174. Manner J, Perez-Pomares JM, Macias D and Munoz-Chapuli R. The origin, formation and developmental significance of the epicardium: a review. *Cells Tissues Organs*. 2001;169:89-103.
175. Ng YY, Huang TP, Yang WC, Chen ZP, Yang AH, Mu W, Nikolic-Paterson DJ, Atkins RC and Lan HY. Tubular epithelial-myofibroblast transdifferentiation in progressive tubulointerstitial fibrosis in 5/6 nephrectomized rats. *Kidney Int*. 1998;54:864-76.
176. Piera-Velazquez S, Li Z and Jimenez SA. Role of endothelial-mesenchymal transition (EndoMT) in the pathogenesis of fibrotic disorders. *Am J Pathol*. 2011;179:1074-80.
177. Hung C, Linn G, Chow YH, Kobayashi A, Mittelsteadt K, Altemeier WA, Gharib SA, Schnapp LM and Duffield JS. Role of lung pericytes and resident fibroblasts in the pathogenesis of pulmonary fibrosis. *Am J Respir Crit Care Med*. 2013;188:820-30.
178. Quan TE, Cowper S, Wu SP, Bockenstedt LK and Bucala R. Circulating fibrocytes: collagen-secreting cells of the peripheral blood. *Int J Biochem Cell Biol*. 2004;36:598-606.
179. Yoshida T and Owens GK. Molecular determinants of vascular smooth muscle cell diversity. *Circ Res*. 2005;96:280-91.
180. Chang HY, Chi JT, Dudoit S, Bondre C, van de Rijn M, Botstein D and Brown PO. Diversity, topographic differentiation, and positional memory in human fibroblasts. *Proc Natl Acad Sci U S A*. 2002;99:12877-82.

181. Moore-Morris T, Guimaraes-Camboa N, Banerjee I, Zambon AC, Kisseleva T, Velayoudon A, Stallcup WB, Gu Y, Dalton ND, Cedenilla M, Gomez-Amaro R, Zhou B, Brenner DA, Peterson KL, Chen J and Evans SM. Resident fibroblast lineages mediate pressure overload-induced cardiac fibrosis. *J Clin Invest*. 2014;124:2921-34.
182. Catalucci D, Latronico MV, Ellingsen O and Condorelli G. Physiological myocardial hypertrophy: how and why? *Front Biosci*. 2008;13:312-24.
183. Holmes JW, Borg TK and Covell JW. Structure and mechanics of healing myocardial infarcts. *Annu Rev Biomed Eng*. 2005;7:223-53.
184. Zhao L and Eghbali-Webb M. Release of pro- and anti-angiogenic factors by human cardiac fibroblasts: effects on DNA synthesis and protection under hypoxia in human endothelial cells. *Biochim Biophys Acta*. 2001;1538:273-82.
185. Bix G and Iozzo RV. Matrix revolutions: "tails" of basement-membrane components with angiostatic functions. *Trends Cell Biol*. 2005;15:52-60.
186. Hamano Y, Zeisberg M, Sugimoto H, Lively JC, Maeshima Y, Yang C, Hynes RO, Werb Z, Sudhakar A and Kalluri R. Physiological levels of tumstatin, a fragment of collagen IV alpha3 chain, are generated by MMP-9 proteolysis and suppress angiogenesis via alphaV beta3 integrin. *Cancer Cell*. 2003;3:589-601.
187. Liu H, Chen B and Lilly B. Fibroblasts potentiate blood vessel formation partially through secreted factor TIMP-1. *Angiogenesis*. 2008;11:223-34.
188. Ieda M, Tsuchihashi T, Ivey KN, Ross RS, Hong TT, Shaw RM and Srivastava D. Cardiac fibroblasts regulate myocardial proliferation through beta1 integrin signaling. *Dev Cell*. 2009;16:233-44.
189. Bergmann O, Bhardwaj RD, Bernard S, Zdunek S, Barnabe-Heider F, Walsh S, Zupicich J, Alkass K, Buchholz BA, Druid H, Jovinge S and Frisen J. Evidence for cardiomyocyte renewal in humans. *Science*. 2009;324:98-102.
190. Kuhn B, del Monte F, Hajjar RJ, Chang YS, Lebeche D, Arab S and Keating MT. Periostin induces proliferation of differentiated cardiomyocytes and promotes cardiac repair. *Nat Med*. 2007;13:962-9.
191. Engel FB, Schebesta M, Duong MT, Lu G, Ren S, Madwed JB, Jiang H, Wang Y and Keating MT. p38 MAP kinase inhibition enables proliferation of adult mammalian cardiomyocytes. *Genes Dev*. 2005;19:1175-87.
192. Rohr S. Role of gap junctions in the propagation of the cardiac action potential. *Cardiovasc Res*. 2004;62:309-22.
193. Li GR, Sun HY, Chen JB, Zhou Y, Tse HF and Lau CP. Characterization of multiple ion channels in cultured human cardiac fibroblasts. *PLoS One*. 2009;4:e7307.
194. Isenberg G, Kazanski V, Kondratev D, Gallitelli MF, Kiseleva I and Kamkin A. Differential effects of stretch and compression on membrane currents and [Na+]c in ventricular myocytes. *Prog Biophys Mol Biol*. 2003;82:43-56.
195. Kamkin A, Kiseleva I, Isenberg G, Wagner KD, Gunther J, Theres H and Scholz H. Cardiac fibroblasts and the mechano-electric feedback mechanism in healthy and diseased hearts. *Prog Biophys Mol Biol*. 2003;82:111-20.
196. Zhou B, von Gise A, Ma Q, Hu YW and Pu WT. Genetic fate mapping demonstrates contribution of epicardium-derived cells to the annulus fibrosis of the mammalian heart. *Dev Biol*. 2010;338:251-61.
197. Kohl P and Camelliti P. Fibroblast-myocyte connections in the heart. *Heart Rhythm*. 2012;9:461-4.

198. He K, Shi X, Zhang X, Dang S, Ma X, Liu F, Xu M, Lv Z, Han D, Fang X and Zhang Y. Long-distance intercellular connectivity between cardiomyocytes and cardiofibroblasts mediated by membrane nanotubes. *Cardiovasc Res*. 2011;92:39-47.
199. Veeraraghavan R, Lin J, Hoeker GS, Keener JP, Gourdie RG and Poelzing S. Sodium channels in the Cx43 gap junction perinexus may constitute a cardiac ephapse: an experimental and modeling study. *Pflugers Arch*. 2015;467:2093-105.
200. Goshima K. Formation of nexuses and electrotonic transmission between myocardial and FL cells in monolayer culture. *Exp Cell Res*. 1970;63:124-30.
201. Chacar S, Fares N, Bois P and Faivre JF. Basic Signaling in Cardiac Fibroblasts. *J Cell Physiol*. 2017;232:725-730.
202. MacKenna D, Summerour SR and Villarreal FJ. Role of mechanical factors in modulating cardiac fibroblast function and extracellular matrix synthesis. *Cardiovasc Res*. 2000;46:257-63.
203. Hynes RO. Integrins: a family of cell surface receptors. *Cell*. 1987;48:549-54.
204. Manso AM, Kang SM and Ross RS. Integrins, focal adhesions, and cardiac fibroblasts. *J Investig Med*. 2009;57:856-60.
205. Zou Y, Akazawa H, Qin Y, Sano M, Takano H, Minamino T, Makita N, Iwanaga K, Zhu W, Kudoh S, Toko H, Tamura K, Kihara M, Nagai T, Fukamizu A, Umemura S, Iiri T, Fujita T and Komuro I. Mechanical stress activates angiotensin II type 1 receptor without the involvement of angiotensin II. *Nat Cell Biol*. 2004;6:499-506.
206. Pedersen SF and Nilius B. Transient receptor potential channels in mechanosensing and cell volume regulation. *Methods Enzymol*. 2007;428:183-207.
207. Weber KT. Fibrosis in hypertensive heart disease: focus on cardiac fibroblasts. *J Hypertens*. 2004;22:47-50.
208. Turner NA, Das A, O'Regan DJ, Ball SG and Porter KE. Human cardiac fibroblasts express ICAM-1, E-selectin and CXC chemokines in response to proinflammatory cytokine stimulation. *Int J Biochem Cell Biol*. 2011;43:1450-8.
209. Banerjee I, Fuseler JW, Intwala AR and Baudino TA. IL-6 loss causes ventricular dysfunction, fibrosis, reduced capillary density, and dramatically alters the cell populations of the developing and adult heart. *Am J Physiol Heart Circ Physiol*. 2009;296:H1694-704.
210. Gurtner GC, Werner S, Barrandon Y and Longaker MT. Wound repair and regeneration. *Nature*. 2008;453:314-21.
211. Leask A. TGFbeta, cardiac fibroblasts, and the fibrotic response. *Cardiovasc Res*. 2007;74:207-12.
212. Barnard JA, Lyons RM and Moses HL. The cell biology of transforming growth factor beta. *Biochim Biophys Acta*. 1990;1032:79-87.
213. Valiente-Alandi I, Schafer AE and Blaxall BC. Extracellular matrix-mediated cellular communication in the heart. *J Mol Cell Cardiol*. 2016;91:228-37.
214. Chang CW, Dalgliesh AJ, Lopez JE and Griffiths LG. Cardiac extracellular matrix proteomics: Challenges, techniques, and clinical implications. *Proteomics Clin Appl*. 2016;10:39-50.
215. Talman V and Ruskoaho H. Cardiac fibrosis in myocardial infarction-from repair and remodeling to regeneration. *Cell Tissue Res*. 2016;365:563-81.
216. Shoulders MD and Raines RT. Collagen structure and stability. *Annu Rev Biochem*. 2009;78:929-58.

217. Kadler KE, Holmes DF, Trotter JA and Chapman JA. Collagen fibril formation. *Biochem J*. 1996;316 (Pt 1):1-11.
218. Gelse K, Poschl E and Aigner T. Collagens--structure, function, and biosynthesis. *Adv Drug Deliv Rev*. 2003;55:1531-46.
219. Shirwany A and Weber KT. Extracellular matrix remodeling in hypertensive heart disease. *J Am Coll Cardiol*. 2006;48:97-8.
220. Gonzalez A, Lopez B, Querejeta R and Diez J. Regulation of myocardial fibrillar collagen by angiotensin II. A role in hypertensive heart disease? *J Mol Cell Cardiol*. 2002;34:1585-93.
221. Jourdan-Lesaux C, Zhang J and Lindsey ML. Extracellular matrix roles during cardiac repair. *Life Sci*. 2010;87:391-400.
222. McAnulty RJ and Laurent GJ. Collagen synthesis and degradation in vivo. Evidence for rapid rates of collagen turnover with extensive degradation of newly synthesized collagen in tissues of the adult rat. *Coll Relat Res*. 1987;7:93-104.
223. Fields GB. Interstitial collagen catabolism. *J Biol Chem*. 2013;288:8785-93.
224. Nagase H and Woessner JF, Jr. Matrix metalloproteinases. *J Biol Chem*. 1999;274:21491-4.
225. Phatharajaree W, Phrommintikul A and Chattipakorn N. Matrix metalloproteinases and myocardial infarction. *Can J Cardiol*. 2007;23:727-33.
226. Fan D, Takawale A, Lee J and Kassiri Z. Cardiac fibroblasts, fibrosis and extracellular matrix remodeling in heart disease. *Fibrogenesis Tissue Repair*. 2012;5:15.
227. Bowers SL, Banerjee I and Baudino TA. The extracellular matrix: at the center of it all. *J Mol Cell Cardiol*. 2010;48:474-82.
228. Ma Y, de Castro Bras LE, Toba H, Iyer RP, Hall ME, Winniford MD, Lange RA, Tyagi SC and Lindsey ML. Myofibroblasts and the extracellular matrix network in post-myocardial infarction cardiac remodeling. *Pflugers Arch*. 2014;466:1113-27.
229. Kumazaki T, Mitsui Y, Hamada K, Sumida H and Nishiyama M. Detection of alternative splicing of fibronectin mRNA in a single cell. *J Cell Sci*. 1999;112 (Pt 10):1449-53.
230. Sottile J and Hocking DC. Fibronectin polymerization regulates the composition and stability of extracellular matrix fibrils and cell-matrix adhesions. *Mol Biol Cell*. 2002;13:3546-59.
231. Chiao YA, Zamilpa R, Lopez EF, Dai Q, Escobar GP, Hakala K, Weintraub ST and Lindsey ML. In vivo matrix metalloproteinase-7 substrates identified in the left ventricle post-myocardial infarction using proteomics. *J Proteome Res*. 2010;9:2649-57.
232. Zamilpa R, Lopez EF, Chiao YA, Dai Q, Escobar GP, Hakala K, Weintraub ST and Lindsey ML. Proteomic analysis identifies in vivo candidate matrix metalloproteinase-9 substrates in the left ventricle post-myocardial infarction. *Proteomics*. 2010;10:2214-23.
233. Gaasch WH and Zile MR. Left ventricular diastolic dysfunction and diastolic heart failure. *Annu Rev Med*. 2004;55:373-94.
234. McCurdy S, Baicu CF, Heymans S and Bradshaw AD. Cardiac extracellular matrix remodeling: fibrillar collagens and Secreted Protein Acidic and Rich in Cysteine (SPARC). *J Mol Cell Cardiol*. 2010;48:544-9.
235. Chapman D, Weber KT and Eghbali M. Regulation of fibrillar collagen types I and III and basement membrane type IV collagen gene expression in pressure overloaded rat myocardium. *Circ Res*. 1990;67:787-94.

236. Villarreal FJ and Dillmann WH. Cardiac hypertrophy-induced changes in mRNA levels for TGF-beta 1, fibronectin, and collagen. *Am J Physiol*. 1992;262:H1861-6.
237. Bradshaw AD, Baicu CF, Rentz TJ, Van Laer AO, Boggs J, Lacy JM and Zile MR. Pressure overload-induced alterations in fibrillar collagen content and myocardial diastolic function: role of secreted protein acidic and rich in cysteine (SPARC) in post-synthetic procollagen processing. *Circulation*. 2009;119:269-80.
238. Lindsay MM, Maxwell P and Dunn FG. TIMP-1: a marker of left ventricular diastolic dysfunction and fibrosis in hypertension. *Hypertension*. 2002;40:136-41.
239. Laviades C, Varo N, Fernandez J, Mayor G, Gil MJ, Monreal I and Diez J. Abnormalities of the extracellular degradation of collagen type I in essential hypertension. *Circulation*. 1998;98:535-40.
240. Zervoudaki A, Economou E, Stefanadis C, Pitsavos C, Tsioufis K, Aggeli C, Vasiliadou K, Toutouza M and Toutouzas P. Plasma levels of active extracellular matrix metalloproteinases 2 and 9 in patients with essential hypertension before and after antihypertensive treatment. *J Hum Hypertens*. 2003;17:119-24.
241. Lopez B, Gonzalez A, Querejeta R, Larman M and Diez J. Alterations in the pattern of collagen deposition may contribute to the deterioration of systolic function in hypertensive patients with heart failure. *J Am Coll Cardiol*. 2006;48:89-96.
242. Frangogiannis NG. Chemokines in the ischemic myocardium: from inflammation to fibrosis. *Inflamm Res*. 2004;53:585-95.
243. Corbett SA and Schwarzbauer JE. Fibronectin-fibrin cross-linking: a regulator of cell behavior. *Trends Cardiovasc Med*. 1998;8:357-62.
244. Matsumura S, Iwanaga S, Mochizuki S, Okamoto H, Ogawa S and Okada Y. Targeted deletion or pharmacological inhibition of MMP-2 prevents cardiac rupture after myocardial infarction in mice. *J Clin Invest*. 2005;115:599-609.
245. Heymans S, Luttun A, Nuyens D, Theilmeier G, Creemers E, Moons L, Dyspersin GD, Cleutjens JP, Shipley M, Angellilo A, Levi M, Nube O, Baker A, Keshet E, Lupu F, Herbert JM, Smits JF, Shapiro SD, Baes M, Borgers M, Collen D, Daemen MJ and Carmeliet P. Inhibition of plasminogen activators or matrix metalloproteinases prevents cardiac rupture but impairs therapeutic angiogenesis and causes cardiac failure. *Nat Med*. 1999;5:1135-42.
246. Lindsey ML, Escobar GP, Mukherjee R, Goshorn DK, Sheats NJ, Bruce JA, Mains IM, Hendrick JK, Hewett KW, Gourdie RG, Matrisian LM and Spinale FG. Matrix metalloproteinase-7 affects connexin-43 levels, electrical conduction, and survival after myocardial infarction. *Circulation*. 2006;113:2919-28.
247. Creemers EE, Davis JN, Parkhurst AM, Leenders P, Dowdy KB, Hapke E, Hauet AM, Escobar PG, Cleutjens JP, Smits JF, Daemen MJ, Zile MR and Spinale FG. Deficiency of TIMP-1 exacerbates LV remodeling after myocardial infarction in mice. *Am J Physiol Heart Circ Physiol*. 2003;284:H364-71.
248. Kandalam V, Basu R, Abraham T, Wang X, Soloway PD, Jaworski DM, Oudit GY and Kassiri Z. TIMP2 deficiency accelerates adverse post-myocardial infarction remodeling because of enhanced MT1-MMP activity despite lack of MMP2 activation. *Circ Res*. 2010;106:796-808.
249. Koskivirta I, Kassiri Z, Rahkonen O, Kiviranta R, Oudit GY, McKee TD, Kyto V, Saraste A, Jokinen E, Liu PP, Vuorio E and Khokha R. Mice with tissue inhibitor of metalloproteinases 4 (Timp4) deletion succumb to induced myocardial infarction but not to cardiac pressure overload. *J Biol Chem*. 2010;285:24487-93.

250. Glass C and Singla DK. Overexpression of TIMP-1 in embryonic stem cells attenuates adverse cardiac remodeling following myocardial infarction. *Cell Transplant*. 2012;21:1931-44.
251. Ramani R, Nilles K, Gibson G, Burkhead B, Mathier M, McNamara D and McTiernan CF. Tissue inhibitor of metalloproteinase-2 gene delivery ameliorates postinfarction cardiac remodeling. *Clin Transl Sci*. 2011;4:24-31.
252. Takawale A, Zhang P, Azad A, Wang W, Wang X, Murray AG and Kassiri Z. Myocardial overexpression of TIMP3 following myocardial infarction exerts beneficial effects through promoting angiogenesis and suppressing early proteolysis. *Am J Physiol Heart Circ Physiol*. 2017:ajpheart 00108 2017.
253. Porrello ER. microRNAs in cardiac development and regeneration. *Clin Sci (Lond)*. 2013;125:151-66.
254. Thum T. Noncoding RNAs and myocardial fibrosis. *Nat Rev Cardiol*. 2014;11:655-63.
255. Piccoli MT, Bar C and Thum T. Non-coding RNAs as modulators of the cardiac fibroblast phenotype. *J Mol Cell Cardiol*. 2016;92:75-81.
256. Thum T, Gross C, Fiedler J, Fischer T, Kissler S, Bussen M, Galuppo P, Just S, Rottbauer W, Frantz S, Castoldi M, Soutschek J, Koteliansky V, Rosenwald A, Basson MA, Licht JD, Pena JT, Rouhanifard SH, Muckenthaler MU, Tuschl T, Martin GR, Bauersachs J and Engelhardt S. MicroRNA-21 contributes to myocardial disease by stimulating MAP kinase signalling in fibroblasts. *Nature*. 2008;456:980-4.
257. Patrick DM, Montgomery RL, Qi X, Obad S, Kauppinen S, Hill JA, van Rooij E and Olson EN. Stress-dependent cardiac remodeling occurs in the absence of microRNA-21 in mice. *J Clin Invest*. 2010;120:3912-6.
258. van Rooij E, Sutherland LB, Thatcher JE, DiMaio JM, Naseem RH, Marshall WS, Hill JA and Olson EN. Dysregulation of microRNAs after myocardial infarction reveals a role of miR-29 in cardiac fibrosis. *Proc Natl Acad Sci U S A*. 2008;105:13027-32.
259. Abonnenc M, Nabeebaccus AA, Mayr U, Barallobre-Barreiro J, Dong X, Cuello F, Sur S, Drozdov I, Langley SR, Lu R, Stathopoulou K, Didangelos A, Yin X, Zimmermann WH, Shah AM, Zampetaki A and Mayr M. Extracellular matrix secretion by cardiac fibroblasts: role of microRNA-29b and microRNA-30c. *Circ Res*. 2013;113:1138-47.
260. Duisters RF, Tijsen AJ, Schroen B, Leenders JJ, Lentink V, van der Made I, Herias V, van Leeuwen RE, Schellings MW, Barenbrug P, Maessen JG, Heymans S, Pinto YM and Creemers EE. miR-133 and miR-30 regulate connective tissue growth factor: implications for a role of microRNAs in myocardial matrix remodeling. *Circ Res*. 2009;104:170-8, 6p following 178.
261. Cuadrado A and Nebreda AR. Mechanisms and functions of p38 MAPK signalling. *Biochem J*. 2010;429:403-17.
262. Gerits N, Shiryaev A, Kostenko S, Klenow H, Shiryaeva O, Johannessen M and Moens U. The transcriptional regulation and cell-specific expression of the MAPK-activated protein kinase MK5. *Cell Mol Biol Lett*. 2009;14:548-74.
263. Moens U, Kostenko S and Sveinbjornsson B. The Role of Mitogen-Activated Protein Kinase-Activated Protein Kinases (MAPKAPKs) in Inflammation. *Genes (Basel)*. 2013;4:101-33.
264. Cargnello M and Roux PP. Activation and function of the MAPKs and their substrates, the MAPK-activated protein kinases. *Microbiol Mol Biol Rev*. 2011;75:50-83.

265. New L, Jiang Y, Zhao M, Liu K, Zhu W, Flood LJ, Kato Y, Parry GC and Han J. PRAK, a novel protein kinase regulated by the p38 MAP kinase. *EMBO J*. 1998;17:3372-84.
266. Ni H, Wang XS, Diener K and Yao Z. MAPKAPK5, a novel mitogen-activated protein kinase (MAPK)-activated protein kinase, is a substrate of the extracellular-regulated kinase (ERK) and p38 kinase. *Biochem Biophys Res Commun*. 1998;243:492-6.
267. Gaestel M. MAPKAP kinases - MKs - two's company, three's a crowd. *Nat Rev Mol Cell Biol*. 2006;7:120-30.
268. Natale DR, Paliga AJ, Beier F, D'Souza SJ and Watson AJ. p38 MAPK signaling during murine preimplantation development. *Dev Biol*. 2004;268:76-88.
269. Ewen K, Jackson A, Wilhelm D and Koopman P. A male-specific role for p38 mitogen-activated protein kinase in germ cell sex differentiation in mice. *Biol Reprod*. 2010;83:1005-14.
270. Dingar D, Benoit MJ, Mamarbachi AM, Villeneuve LR, Gillis MA, Grandy S, Gaestel M, Fiset C and Allen BG. Characterization of the expression and regulation of MK5 in the murine ventricular myocardium. *Cell Signal*. 2010;22:1063-75.
271. Seternes OM, Johansen B, Hegge B, Johannessen M, Keyse SM and Moens U. Both binding and activation of p38 mitogen-activated protein kinase (MAPK) play essential roles in regulation of the nucleocytoplasmic distribution of MAPK-activated protein kinase 5 by cellular stress. *Mol Cell Biol*. 2002;22:6931-45.
272. Tanoue T, Adachi M, Moriguchi T and Nishida E. A conserved docking motif in MAP kinases common to substrates, activators and regulators. *Nat Cell Biol*. 2000;2:110-6.
273. Garai A, Zeke A, Gogl G, Toro I, Fordos F, Blankenburg H, Barkai T, Varga J, Alexa A, Emig D, Albrecht M and Remenyi A. Specificity of linear motifs that bind to a common mitogen-activated protein kinase docking groove. *Sci Signal*. 2012;5:ra74.
274. Gaestel M. Specificity of signaling from MAPKs to MAPKAPKs: kinases' tango nuevo. *Front Biosci*. 2008;13:6050-9.
275. Gaestel M. MAPK-Activated Protein Kinases (MKs): Novel Insights and Challenges. *Front Cell Dev Biol*. 2015;3:88.
276. Aberg E, Torgersen KM, Johansen B, Keyse SM, Perander M and Seternes OM. Docking of PRAK/MK5 to the atypical MAPKs ERK3 and ERK4 defines a novel MAPK interaction motif. *J Biol Chem*. 2009;284:19392-401.
277. Seternes OM, Mikalsen T, Johansen B, Michaelsen E, Armstrong CG, Morrice NA, Turgeon B, Meloche S, Moens U and Keyse SM. Activation of MK5/PRAK by the atypical MAP kinase ERK3 defines a novel signal transduction pathway. *EMBO J*. 2004;23:4780-91.
278. Schumacher S, Laass K, Kant S, Shi Y, Visel A, Gruber AD, Kotlyarov A and Gaestel M. Scaffolding by ERK3 regulates MK5 in development. *EMBO J*. 2004;23:4770-9.
279. Kant S, Schumacher S, Singh MK, Kispert A, Kotlyarov A and Gaestel M. Characterization of the atypical MAPK ERK4 and its activation of the MAPK-activated protein kinase MK5. *J Biol Chem*. 2006;281:35511-9.
280. Gerits N, Mikalsen T, Kostenko S, Shiryaev A, Johannessen M and Moens U. Modulation of F-actin rearrangement by the cyclic AMP/cAMP-dependent protein kinase (PKA) pathway is mediated by MAPK-activated protein kinase 5 and requires PKA-induced nuclear export of MK5. *J Biol Chem*. 2007;282:37232-43.
281. Deleris P, Rousseau J, Coulombe P, Rodier G, Tanguay PL and Meloche S. Activation loop phosphorylation of the atypical MAP kinases ERK3 and ERK4 is required for binding, activation and cytoplasmic relocalization of MK5. *J Cell Physiol*. 2008;217:778-88.

282. Hansen CA, Bartek J and Jensen S. A functional link between the human cell cycle-regulatory phosphatase Cdc14A and the atypical mitogen-activated kinase Erk3. *Cell Cycle*. 2008;7:325-34.
283. Gong X, Ming X, Deng P and Jiang Y. Mechanisms regulating the nuclear translocation of p38 MAP kinase. *J Cell Biochem*. 2010;110:1420-9.
284. Kostenko S, Shiryaev A, Gerits N, Dumitriu G, Klenow H, Johannessen M and Moens U. Serine residue 115 of MAPK-activated protein kinase MK5 is crucial for its PKA-regulated nuclear export and biological function. *Cell Mol Life Sci*. 2011;68:847-62.
285. Li Q, Zhang N, Zhang D, Wang Y, Lin T, Wang Y, Zhou H, Ye Z, Zhang F, Lin SC and Han J. Determinants that control the distinct subcellular localization of p38alpha-PRAK and p38beta-PRAK complexes. *J Biol Chem*. 2008;283:11014-23.
286. Aberg E, Perander M, Johansen B, Julien C, Meloche S, Keyse SM and Seternes OM. Regulation of MAPK-activated protein kinase 5 activity and subcellular localization by the atypical MAPK ERK4/MAPK4. *J Biol Chem*. 2006;281:35499-510.
287. Skalhegg BS and Tasken K. Specificity in the cAMP/PKA signaling pathway. Differential expression,regulation, and subcellular localization of subunits of PKA. *Front Biosci*. 2000;5:D678-93.
288. Dwyer SF and Gelman IH. Cross-Phosphorylation and Interaction between Src/FAK and MAPKAP5/PRAK in Early Focal Adhesions Controls Cell Motility. *J Cancer Biol Res*. 2014;2.
289. Zheng H, Seit-Nebi A, Han X, Aslanian A, Tat J, Liao R, Yates JR, 3rd and Sun P. A posttranslational modification cascade involving p38, Tip60, and PRAK mediates oncogene-induced senescence. *Mol Cell*. 2013;50:699-710.
290. Del Rincon SV, Rogers J, Widschwendter M, Sun D, Sieburg HB and Spruck C. Development and validation of a method for profiling post-translational modification activities using protein microarrays. *PLoS One*. 2010;5:e11332.
291. New L, Jiang Y and Han J. Regulation of PRAK subcellular location by p38 MAP kinases. *Mol Biol Cell*. 2003;14:2603-16.
292. Shi Y, Kotlyarov A, Laabeta K, Gruber AD, Butt E, Marcus K, Meyer HE, Friedrich A, Volk HD and Gaestel M. Elimination of protein kinase MK5/PRAK activity by targeted homologous recombination. *Mol Cell Biol*. 2003;23:7732-41.
293. Kostenko S, Johannessen M and Moens U. PKA-induced F-actin rearrangement requires phosphorylation of Hsp27 by the MAPKAP kinase MK5. *Cell Signal*. 2009;21:712-8.
294. Perander M, Aberg E, Johansen B, Dreyer B, Guldvik IJ, Outzen H, Keyse SM and Seternes OM. The Ser(186) phospho-acceptor site within ERK4 is essential for its ability to interact with and activate PRAK/MK5. *Biochem J*. 2008;411:613-22.
295. Deleris P, Trost M, Topisirovic I, Tanguay PL, Borden KL, Thibault P and Meloche S. Activation loop phosphorylation of ERK3/ERK4 by group I p21-activated kinases (PAKs) defines a novel PAK-ERK3/4-MAPK-activated protein kinase 5 signaling pathway. *J Biol Chem*. 2011;286:6470-8.
296. De la Mota-Peynado A, Chernoff J and Beeser A. Identification of the atypical MAPK Erk3 as a novel substrate for p21-activated kinase (Pak) activity. *J Biol Chem*. 2011;286:13603-11.
297. Tanguay PL, Rodier G and Meloche S. C-terminal domain phosphorylation of ERK3 controlled by Cdk1 and Cdc14 regulates its stability in mitosis. *Biochem J*. 2010;428:103-11.

298. Perander M, Al-Mahdi R, Jensen TC, Nunn JA, Kildalsen H, Johansen B, Gabrielsen M, Keyse SM and Seternes OM. Regulation of atypical MAP kinases ERK3 and ERK4 by the phosphatase DUSP2. *Sci Rep*. 2017;7:43471.
299. Brand F, Schumacher S, Kant S, Menon MB, Simon R, Turgeon B, Britsch S, Meloche S, Gaestel M and Kotlyarov A. The extracellular signal-regulated kinase 3 (mitogen-activated protein kinase 6 [MAPK6])-MAPK-activated protein kinase 5 signaling complex regulates septin function and dendrite morphology. *Mol Cell Biol*. 2012;32:2467-78.
300. Shiryaev A, Kostenko S, Dumitriu G and Moens U. Septin 8 is an interaction partner and in vitro substrate of MK5. *World J Biol Chem*. 2012;3:98-109.
301. Xie Z, Srivastava DP, Photowala H, Kai L, Cahill ME, Woolfrey KM, Shum CY, Surmeier DJ and Penzes P. Kalirin-7 controls activity-dependent structural and functional plasticity of dendritic spines. *Neuron*. 2007;56:640-56.
302. Tak H, Jang E, Kim SB, Park J, Suk J, Yoon YS, Ahn JK, Lee JH and Joe CO. 14-3-3epsilon inhibits MK5-mediated cell migration by disrupting F-actin polymerization. *Cell Signal*. 2007;19:2379-87.
303. Tang J, Liu J, Li X, Zhong Y, Zhong T, Liu Y, Wang JH and Jiang Y. PRAK interacts with DJ-1 and prevents oxidative stress-induced cell death. *Oxid Med Cell Longev*. 2014;2014:735618.
304. Kostenko S, Jensen KL and Moens U. Phosphorylation of heat shock protein 40 (Hsp40/DnaJB1) by mitogen-activated protein kinase-activated protein kinase 5 (MK5/PRAK). *Int J Biochem Cell Biol*. 2014;47:29-37.
305. Chow KT, Timblin GA, McWhirter SM and Schlissel MS. MK5 activates Rag transcription via Foxo1 in developing B cells. *J Exp Med*. 2013;210:1621-34.
306. Kress TR, Cannell IG, Brenkman AB, Samans B, Gaestel M, Roepman P, Burgering BM, Bushell M, Rosenwald A and Eilers M. The MK5/PRAK kinase and Myc form a negative feedback loop that is disrupted during colorectal tumorigenesis. *Mol Cell*. 2011;41:445-57.
307. Choi JH, Choi DK, Sohn KC, Kwak SS, Suk J, Lim JS, Shin I, Kim SW, Lee JH and Joe CO. Absence of a human DnaJ protein hTid-1S correlates with aberrant actin cytoskeleton organization in lesional psoriatic skin. *J Biol Chem*. 2012;287:25954-63.
308. Zheng M, Wang YH, Wu XN, Wu SQ, Lu BJ, Dong MQ, Zhang H, Sun P, Lin SC, Guan KL and Han J. Inactivation of Rheb by PRAK-mediated phosphorylation is essential for energy-depletion-induced suppression of mTORC1. *Nat Cell Biol*. 2011;13:263-72.
309. Sun P, Yoshizuka N, New L, Moser BA, Li Y, Liao R, Xie C, Chen J, Deng Q, Yamout M, Dong MQ, Frangou CG, Yates JR, 3rd, Wright PE and Han J. PRAK is essential for ras-induced senescence and tumor suppression. *Cell*. 2007;128:295-308.
310. During RL, Gibson BG, Li W, Bishai EA, Sidhu GS, Landry J and Southwick FS. Anthrax lethal toxin paralyzes actin-based motility by blocking Hsp27 phosphorylation. *EMBO J*. 2007;26:2240-50.
311. Benndorf R, Hayess K, Ryazantsev S, Wieske M, Behlke J and Lutsch G. Phosphorylation and supramolecular organization of murine small heat shock protein HSP25 abolish its actin polymerization-inhibiting activity. *J Biol Chem*. 1994;269:20780-4.
312. Lavoie JN, Hickey E, Weber LA and Landry J. Modulation of actin microfilament dynamics and fluid phase pinocytosis by phosphorylation of heat shock protein 27. *J Biol Chem*. 1993;268:24210-4.

313. Stohr N, Kohn M, Lederer M, Glass M, Reinke C, Singer RH and Huttelmaier S. IGF2BP1 promotes cell migration by regulating MK5 and PTEN signaling. *Genes Dev*. 2012;26:176-89.
314. Yoshizuka N, Chen RM, Xu Z, Liao R, Hong L, Hu WY, Yu G, Han J, Chen L and Sun P. A novel function of p38-regulated/activated kinase in endothelial cell migration and tumor angiogenesis. *Mol Cell Biol*. 2012;32:606-18.
315. Chen G, Hitomi M, Han J and Stacey DW. The p38 pathway provides negative feedback for Ras proliferative signaling. *J Biol Chem*. 2000;275:38973-80.
316. Yoshizuka N, Lai M, Liao R, Cook R, Xiao C, Han J and Sun P. PRAK suppresses oncogenic ras-induced hematopoietic cancer development by antagonizing the JNK pathway. *Mol Cancer Res*. 2012;10:810-20.
317. Ronkina N, Johansen C, Bohlmann L, Lafera J, Menon MB, Tiedje C, Laass K, Turk BE, Iversen L, Kotlyarov A and Gaestel M. Comparative Analysis of Two Gene-Targeting Approaches Challenges the Tumor-Suppressive Role of the Protein Kinase MK5/PRAK. *PLoS One*. 2015;10:e0136138.
318. Wullschleger S, Loewith R and Hall MN. TOR signaling in growth and metabolism. *Cell*. 2006;124:471-84.
319. Glick D, Barth S and Macleod KF. Autophagy: cellular and molecular mechanisms. *J Pathol*. 2010;221:3-12.
320. Kim Y, Kim C, Son SM, Song H, Hong HS, Han SH and Mook-Jung I. The novel RAGE interactor PRAK is associated with autophagy signaling in Alzheimer's disease pathogenesis. *Mol Neurodegener*. 2016;11:4.
321. Skaper SD. Alzheimer's disease and amyloid: culprit or coincidence? *Int Rev Neurobiol*. 2012;102:277-316.
322. Yan SD, Chen X, Fu J, Chen M, Zhu H, Roher A, Slattery T, Zhao L, Nagashima M, Morser J, Migheli A, Nawroth P, Stern D and Schmidt AM. RAGE and amyloid-beta peptide neurotoxicity in Alzheimer's disease. *Nature*. 1996;382:685-91.
323. Wautier MP, Chappey O, Corda S, Stern DM, Schmidt AM and Wautier JL. Activation of NADPH oxidase by AGE links oxidant stress to altered gene expression via RAGE. *Am J Physiol Endocrinol Metab*. 2001;280:E685-94.
324. Gerits N, Van Belle W and Moens U. Transgenic mice expressing constitutive active MAPKAPK5 display gender-dependent differences in exploration and activity. *Behav Brain Funct*. 2007;3:58.
325. Kwon SE and Chapman ER. Synaptophysin regulates the kinetics of synaptic vesicle endocytosis in central neurons. *Neuron*. 2011;70:847-54.
326. Ito H, Atsuzawa K, Morishita R, Usuda N, Sudo K, Iwamoto I, Mizutani K, Katoh-Semba R, Nozawa Y, Asano T and Nagata K. Sept8 controls the binding of vesicle-associated membrane protein 2 to synaptophysin. *J Neurochem*. 2009;108:867-80.
327. Trang T, Beggs S, Wan X and Salter MW. P2X4-receptor-mediated synthesis and release of brain-derived neurotrophic factor in microglia is dependent on calcium and p38-mitogen-activated protein kinase activation. *J Neurosci*. 2009;29:3518-28.
328. Dingar D, Merlen C, Grandy S, Gillis MA, Villeneuve LR, Mamarbachi AM, Fiset C and Allen BG. Effect of pressure overload-induced hypertrophy on the expression and localization of p38 MAP kinase isoforms in the mouse heart. *Cell Signal*. 2010;22:1634-44.

329. Brundel BJ, Shiroshita-Takeshita A, Qi X, Yeh YH, Chartier D, van Gelder IC, Henning RH, Kampinga HH and Nattel S. Induction of heat shock response protects the heart against atrial fibrillation. *Circ Res*. 2006;99:1394-402.
330. Sakamoto M, Minamino T, Toko H, Kayama Y, Zou Y, Sano M, Takaki E, Aoyagi T, Tojo K, Tajima N, Nakai A, Aburatani H and Komuro I. Upregulation of heat shock transcription factor 1 plays a critical role in adaptive cardiac hypertrophy. *Circ Res*. 2006;99:1411-8.
331. Sakabe M, Shiroshita-Takeshita A, Maguy A, Brundel BJ, Fujiki A, Inoue H and Nattel S. Effects of a heat shock protein inducer on the atrial fibrillation substrate caused by acute atrial ischaemia. *Cardiovasc Res*. 2008;78:63-70.
332. Ghayour-Mobarhan M, Saber H and Ferns GA. The potential role of heat shock protein 27 in cardiovascular disease. *Clin Chim Acta*. 2012;413:15-24.
333. Boivin B, Khairallah M, Cartier R and Allen BG. Characterization of hsp27 kinases activated by elevated aortic pressure in heart. *Mol Cell Biochem*. 2012;371:31-42.
334. Bain J, McLauchlan H, Elliott M and Cohen P. The specificities of protein kinase inhibitors: an update. *Biochem J*. 2003;371:199-204.
335. Folmer F, Blasius R, Morceau F, Tabudravu J, Dicato M, Jaspars M and Diederich M. Inhibition of TNFalpha-induced activation of nuclear factor kappaB by kava (Piper methysticum) derivatives. *Biochem Pharmacol*. 2006;71:1206-18.
336. Andrews MJ, Clase JA, Bar G, Tricarico G, Edwards PJ, Brys R, Chambers M, Schmidt W, MacLeod A, Hirst K, Allen V, Birault V, Le J, Harris J, Self A, Nash K and Dixon G. Discovery of a series of imidazopyrazine small molecule inhibitors of the kinase MAPKAPK5, that show activity using in vitro and in vivo models of rheumatoid arthritis. *Bioorg Med Chem Lett*. 2012;22:2266-70.
337. Kostenko S, Khan MT, Sylte I and Moens U. The diterpenoid alkaloid noroxoaconitine is a Mapkap kinase 5 (MK5/PRAK) inhibitor. *Cell Mol Life Sci*. 2011;68:289-301.
338. Anwar A, Hosoya T, Leong KM, Onogi H, Okuno Y, Hiramatsu T, Koyama H, Suzuki M, Hagiwara M and Garcia-Blanco MA. The kinase inhibitor SFV785 dislocates dengue virus envelope protein from the replication complex and blocks virus assembly. *PLoS One*. 2011;6:e23246.
339. Namour F, Vanhoutte FP, Beetens J, Blockhuys S, De Weer M and Wigerinck P. Pharmacokinetics, safety, and tolerability of GLPG0259, a mitogen-activated protein kinase-activated protein kinase 5 (MAPKAPK5) inhibitor, given as single and multiple doses to healthy male subjects. *Drugs R D*. 2012;12:141-63.
340. Westhovens R, Keyser FD, Rekalov D, Nasonov EL, Beetens J, Van der Aa A, Wigerinck P, Namour F, Vanhoutte F and Durez P. Oral administration of GLPG0259, an inhibitor of MAPKAPK5, a new target for the treatment of rheumatoid arthritis: a phase II, randomised, double-blind, placebo-controlled, multicentre trial. *Ann Rheum Dis*. 2013;72:741-4.
341. Creemers EE and Pinto YM. Molecular mechanisms that control interstitial fibrosis in the pressure-overloaded heart. *Cardiovasc Res*. 2011;89:265-72.
342. Berg TJ, Snorgaard O, Faber J, Torjesen PA, Hildebrandt P, Mehlsen J and Hanssen KF. Serum levels of advanced glycation end products are associated with left ventricular diastolic function in patients with type 1 diabetes. *Diabetes Care*. 1999;22:1186-90.

343. Heeneman S, Cleutjens JP, Faber BC, Creemers EE, van Suylen RJ, Lutgens E, Cleutjens KB and Daemen MJ. The dynamic extracellular matrix: intervention strategies during heart failure and atherosclerosis. *J Pathol*. 2003;200:516-25.
344. Rosenkranz S, Flesch M, Amann K, Haeuseler C, Kilter H, Seeland U, Schluter KD and Bohm M. Alterations of beta-adrenergic signaling and cardiac hypertrophy in transgenic mice overexpressing TGF-beta(1). *Am J Physiol Heart Circ Physiol*. 2002;283:H1253-62.
345. Rosenkranz S. TGF-beta1 and angiotensin networking in cardiac remodeling. *Cardiovasc Res*. 2004;63:423-32.
346. Schiller M, Javelaud D and Mauviel A. TGF-beta-induced SMAD signaling and gene regulation: consequences for extracellular matrix remodeling and wound healing. *J Dermatol Sci*. 2004;35:83-92.
347. Calderone A, Takahashi N, Izzo NJ, Jr., Thaik CM and Colucci WS. Pressure- and volume-induced left ventricular hypertrophies are associated with distinct myocyte phenotypes and differential induction of peptide growth factor mRNAs. *Circulation*. 1995;92:2385-90.
348. Takahashi N, Calderone A, Izzo NJ, Jr., Maki TM, Marsh JD and Colucci WS. Hypertrophic stimuli induce transforming growth factor-beta 1 expression in rat ventricular myocytes. *J Clin Invest*. 1994;94:1470-6.
349. Seeland U, Schaffer A, Selejan S, Hohl M, Reil JC, Muller P, Rosenkranz S and Bohm M. Effects of AT1- and beta-adrenergic receptor antagonists on TGF-beta1-induced fibrosis in transgenic mice. *Eur J Clin Invest*. 2009;39:851-9.
350. Al-Mahdi R, Babteen N, Thillai K, Holt M, Johansen B, Wetting HL, Seternes OM and Wells CM. A novel role for atypical MAPK kinase ERK3 in regulating breast cancer cell morphology and migration. *Cell Adh Migr*. 2015;9:483-94.
351. Molkentin JD, Bugg D, Ghearing N, Dorn LE, Kim P, Sargent MA, Gunaje J, Otsu K and Davis J. Fibroblast-Specific Genetic Manipulation of p38 Mitogen-Activated Protein Kinase In Vivo Reveals Its Central Regulatory Role in Fibrosis. *Circulation*. 2017;136:549-561.
352. Streicher JM, Ren S, Herschman H and Wang Y. MAPK-activated protein kinase-2 in cardiac hypertrophy and cyclooxygenase-2 regulation in heart. *Circ Res*. 2010;106:1434-43.
353. Taglieri DM, Monasky MM, Knezevic I, Sheehan KA, Lei M, Wang X, Chernoff J, Wolska BM, Ke Y and Solaro RJ. Ablation of p21-activated kinase-1 in mice promotes isoproterenol-induced cardiac hypertrophy in association with activation of Erk1/2 and inhibition of protein phosphatase 2A. *J Mol Cell Cardiol*. 2011;51:988-96.
354. Pan Z, Zhao W, Zhang X, Wang B, Wang J, Sun X, Liu X, Feng S, Yang B and Lu Y. Scutellarin alleviates interstitial fibrosis and cardiac dysfunction of infarct rats by inhibiting TGFbeta1 expression and activation of p38-MAPK and ERK1/2. *Br J Pharmacol*. 2011;162:688-700.
355. Chung CC, Kao YH, Yao CJ, Lin YK and Chen YJ. A Comparison of Left and Right Atrial Fibroblasts Reveals Different Collagen Production Activity and Stress-induced Mitogen-activated Protein Kinase Signaling in Rats. *Acta Physiol (Oxf)*. 2016.
356. Demyanets S, Kaun C, Rychli K, Pfaffenberger S, Kastl SP, Hohensinner PJ, Rega G, Katsaros KM, Afonyushkin T, Bochkov VN, Paireder M, Huk I, Maurer G, Huber K and Wojta J. Oncostatin M-enhanced vascular endothelial growth factor expression in human vascular smooth muscle cells involves PI3K-, p38 MAPK-, Erk1/2- and STAT1/STAT3-dependent pathways and is attenuated by interferon-gamma. *Basic Res Cardiol*. 2011;106:217-31.

357. Guo C and Piacentini L. Type I collagen-induced MMP-2 activation coincides with up-regulation of membrane type 1-matrix metalloproteinase and TIMP-2 in cardiac fibroblasts. *J Biol Chem*. 2003;278:46699-708.